Long waves in water over a visco-elastic muddy seabed

by

Erell-Isis Garnier

Ingénieur de l'École Polytechnique (2009)

Submitted to the Department of Mechanical Engineering
in partial fulfillment of the requirements for the degree of

Master of Science in Mechanical Engineering

at the

MASSACHUSETTS INSTITUTE OF TECHNOLOGY

June 2011

Author .....
Department of Mechanical Engineering
February 16, 2011

Certified by .....
Chiang C. Mei
Ford Professor of Engineering Emeritus
Thesis Supervisor

Accepted by .....
David Hardt
Professor of Mechanical Engineering
Chairman, Committee on Graduate Students

Long waves in water over a visco-elastic muddy seabed

by

Erell-Isis Garnier

Submitted to the Department of Mechanical Engineering
on February 16, 2011, in partial fulfillment of the
requirements for the degree of
Master of Science in Mechanical Engineering

Abstract

The propagation of surface waves over a flat muddy seabed are studied. Mud is first considered as a Newtonian fluid. Water and mud equations are derived in order to obtain governing equation for surface and interface waves. By the method of multiple scales, nonlinear evolution equations are derived for the harmonic amplitudes. These equations are numerically solved for a finite number of harmonics to show the behavior of surface and interface motions. A drift current in mud is found at the second order, meaning that surface waves induce mud motion. Equation governing the total wave energy variation is derived and used to verify the accuracy of numerical solutions.

The model is extended to viscoelastic mud, using the results of four experiments carried on different types of muds. These muds range from very elastic to rather viscous, allowing us to compare the differences in behavior. Surface and interface variations, mud drift current and energy variations are plotted and compared to the results with Newtonian muds.

A sloping muddy seabed is then considered. Mud is modeled as viscoelastic to avoid a constant static current that would happen with Newtonian mud. By the method of multiple scales and by introducing a space-dependent wavenumber, mud drift current and energy variation equations are derived again, taking into account the effect of the slope. An analytic study of the surface variations demonstrates that surface and interface waves, as well as drift current, exponentially decay to reach a zero value at the shore.

Thesis Supervisor: Chiang C. Mei
Title: Ford Professor of Engineering Emeritus

Acknowledgments

This thesis has drawn upon the support and insights of many. First, I would like to thank my advisor, Professor Chiang C. Mei for all his support and guidance throughout these years at MIT. I have learned so much writing this thesis and have always felt extremely lucky to work with such an expert in ocean waves. Professor Mei is not only an excellent professor and scientist, but also an extremely kind and understanding person. Thank you for making so much of your time available for me, for your enthusiasm and your words of motivations. I would also like to thank my advisor's wife, Caroline, for her kindness and generosity, and for gathering the research group around delicious meals.

None of this would have been possible without the unconditional support of my family. I would like to thank my parents for their love and understanding throughout my education and especially during those last years of long-distance. I would never have been so far without them. I also want to thank my dear brothers, Dimitri and Gildas, whom I have always admired so much. They showed me the way and I will always be grateful for that.

I would like to thank the admirable people I have met at MIT. I have discovered amazing personalities that I always want to keep in my life. In particular, I want to name my roommates Geoffrey and Yves and my friends Damien and Cristina for sharing with me the everyday MIT life. Last but not least, I want to thank Grégoire for his love and support, even with the challenge of long distance.

I am thankful to École Polytechnique for my education as an engineer in France. I realize how much this background helped me at MIT.

I would like to acknowledge with gratitude the financial support of the US office of Naval Research, in the context of the MURI (Mechanisms of Fluid-Mud Interactions Under Waves) program under grant number N00014-06-1-0718.

Contents

List of Figures

List of Tables

Chapter 1

Introduction

1.1 Background and motivation

It is well known that fluid mud at the bottom of the oceans contribute, sometimes considerably, to waves attenuation. Moreover, its motion modifies the seabed, affects the wave climate and shapes the coastline in the long run. This is why the problem of wave-mud interaction has attract some attention in the last few decades.

The rheological properties of fluid mud is highly complex, depending on geological origins, mineral composition and salinity in seawater. Various models have been used in past theories.

Dalrymple and Liu used a simple Newtonian model in their linearized theory of infinitesimal waves ([7]) which predicts the damping mechanism for a wide range wave depth and mud depths. Sakakiyama and Bijker also used this model ([19]) to examine the mass transport phenomena in the mud layer. More recently, the Newtonian model was also used by Liu and Chan in 2006 ([14]) for weakly nonlinear long waves over a thin mud layer in a shallow sea, all for a horizontal seabed.

In steady motion mud is known to behave as a plastic material. In 1993, Jiang and Leblond([13]) used the Bingham-plastic stress/strain relation to numerically model mudslides and generated waves. This model has also been used by Mei & Liu in 1987 ([4]) to study the slow motion of mud slide on mountain slopes, and the damping of long waves. This particular case was extended by Liu and Chan in 2006 and 2008 ([14] and [5]), who considered both periodic waves and solitary waves, again over a horizontal seabed. Extension to the Herschel-Bulkel model was made in 1998 by Huang and Garcia ([9]) to determine a mud flow down a slope. Mainly for modeling a seabed dominated by a mixture of mud and sand, the poro-elastic ([20]) and the

visco-elastic-plastic models have also be applied ([18], [17], [1]).

More recent experiments have shown however that under oscillatory waves fluid mud is better modeled as a viscoelastic material. The simplest model with just two parameters were used by MacPherson ([3], and [2]). However experiments by Jiang and Mehta ([11]) and Huang and Huhe ([10]) using field samples, shows that the constitutive coefficients of these simple models depends on oscillation frequency, hence they are not really material properties but are properties of the motion itself. In 2009, Mei and al. ([15]) proposed that real mud under dynamical conditions must be described by the generalized model of visco-elasticity. In particular the relation between stress and strain is a high-order differential equation with coefficient that depends only on mineral composition but not on frequency. The generalized model was used by Mei et al to predict short and long waves damping over a muddy seabed.

In 1998, Wen & Liu ([21])have given an overview of fluid-mud models and the ranges of their applicability based on soil properties.

Bottom mud effects become more important near the shore, when water depth is considered to be shallow. In this case, the wave system is better described by Boussinesq-type wave equations (e.g. [16]).

1.2 Thesis outline

The first part of this thesis focuses on a simplified case (chapter 2). We study surface waves over a flat muddy seabed, and the mud is modeled as a Newtonian fluid. We first consider that non-linearity is stronger than dispersion, in order to show the effect of non-linearity without dispersion at the first order. We then derive water equations by expanding the potential in power series as done in [6], chapter 12. Kinematic and dynamic boundary conditions are used to obtain differential equations for the surface and interface. We then derive mud equations, such as momentum, continuity and boundary condition. Mud and water results are written at the first and second order for the harmonic amplitudes, by the method of multiple scales. Finally, results are combined in order to obtain a governing differential equation for the surface and interface at the first order. At the second order, a drift current is calculated in mud, meaning that surface waves induce mud horizontal motion. Finally, an equation governing the total wave energy variation is derived.

The system for an infinite number of harmonics is truncated to a finite number n of harmonics so that it can be solved numerically. Results are plotted for different

values of non-linearity and dispersion, in order to compare the effects of this parameters. Different mud layer depths are also compared. The analytic expression for the evolution of the wave energy is then used to verify the numerical simulations run for 10 harmonics.

The model is then expanded to viscoelastic muds (chapter 3). We make use of experimental results from Jiang & Mehta ([11]), Huhe & Huang ([10], [12]), and from Professor Dalrymlpe and PhD candidate Khatoon Melick from the department of civil engineering of Johns Hopkins University. The characteristics of those four muds are studied and the complex viscosity is plotted. Some of these muds are more elastic than the others, allowing us to study a panel of different behaviors. The harmonic amplitudes, mud drift current and energy variation are derived in this new setting. The attenuation rate is analytically found and its dependency on the water depth, wavelength, mud depth and harmonic number is studied. As before, the system for infinite number of harmonics is truncated to 10 harmonics in order to numerically solve the equations. The results are plotted and compared between the different types of muds and the Newtonian case from chapter 2.

The same process is then followed in a case where dispersion is comparable to non-linearity - corresponding to Boussinesq class (chapter 4). The governing equations are again derived at the first order, which is now the order at which both dispersion and non-linearity come into play. Drift current is not studied because appearing at a low order and thus negligible compared to other motions. Governing equations are found for surface and interface harmonics. A new term in the differential equation - due to dispersion - is highlighted. The system is truncated and the results are plotted for a finite number of harmonics. The analytic expression for the evolution of the wave energy is again used to verify the the numerical simulations run for 10 harmonics. The model is then extended to viscoelastic mud again (chapter 5), and the differences are once again compared.

The model is then extended from a flat to a sloping muddy seabed (chapter 6). We first study the case where non-linearity is stronger than dispersion. The case of a Newtonian mud is not studied, because pure real viscosity would involve a constant flow down the slope even in the static case that would invalidate our hypotheses. Thus, the calculations are directly carried for viscoelastic mud. The equations are once again derived. An analytic study of the surface harmonics at the shore, where the water depth is close to zero, show that surface and interface harmonics, as well as mud drift current, exponentially decay to zero. The equations are again truncated, and the results plotted and compared to the flat seabed case.

Finally, the same sloping viscoelastic muddy seabed is considered in a case where dispersion is comparable to non-linearity (chapter 7). The surface and interface equations are once again derived in this case. The results are plotted and compared to other chapters.

Chapter 2

Horizontal bottom, shallow Newtonian mud

2.1 Introduction

In this chapter, we focus on the case of a thin layer of mud on a horizontal seabed, as shown in figure 2-1.

2.1.1 Dimensional equations in water

In this thesis, all dimensional quantities will be written with primes $'$.

The water is supposed to be ideal and irrotational, so we introduce the potential ϕ' such as the velocity in water is $\vec{v}' = \vec{\nabla}.\phi'$. We define the x'-axis to be the propagation direction and z'-axis vertical, such that $z' = 0$ at the mean free surface. We call ζ' the free surface and η' the interface between mud and water. (as shown on figure 2-1). We denote by $\bar{h}$ the water depth, and as a consequence the interface between mud and water corresponds to $z' = -\bar{h} + \eta'$. The potential is thus governed by the Laplace equation:

$$\frac{\partial^2 \phi'}{\partial x'^2} + \frac{\partial^2 \phi'}{\partial z'^2} = 0, \quad for - \bar{h} + \eta'(x,t) < z' < \zeta'(x,t) \tag{2.1.1.1}$$

The potential ϕ' obeys the kinematic and dynamic boundary conditions at the free surface:

$$\frac{\partial \zeta'}{\partial t} + \frac{\partial \phi'}{\partial x'}\frac{\partial \zeta'}{\partial x'} = \frac{\partial \phi'}{\partial z'}, \quad z' = \zeta'(x',t') \tag{2.1.1.2}$$

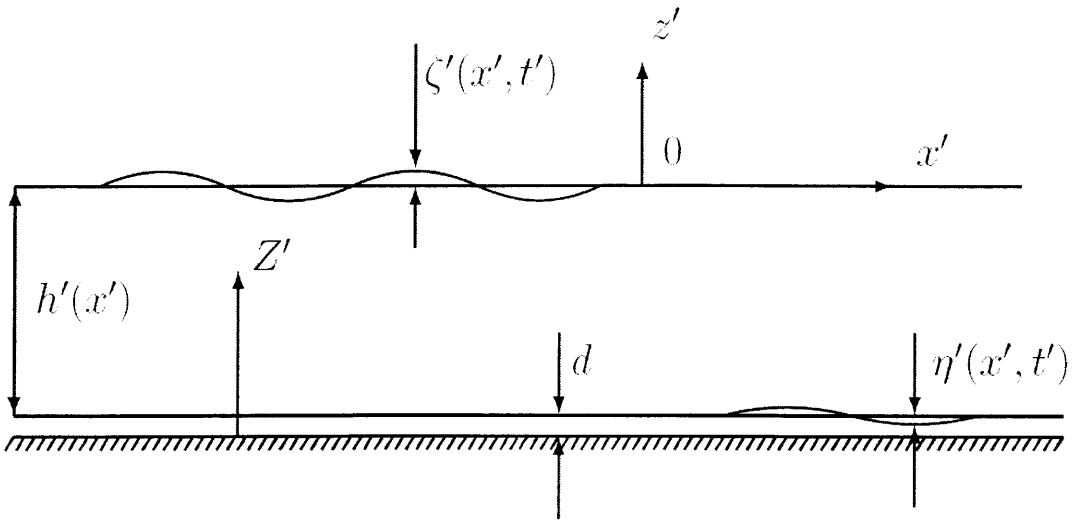

Figure 2-1: Definition sketch. d is the mud layer depth measured vertically.

$$\frac{\partial \phi'}{\partial t'} + g\zeta' + \frac{1}{2}\left[\left(\frac{\partial \phi'}{\partial x'}\right)^2 + \left(\frac{\partial \phi'}{\partial z'}\right)^2\right] = 0, \quad z' = \zeta'(x',t') \tag{2.1.1.3}$$

and it also obeys the kinematic boundary condition at the interface:

$$\phi'_{z'} = \frac{\partial \eta'}{\partial t'} + \frac{\partial \eta'}{\partial x'}\frac{\partial \phi'}{\partial x'}, \quad z' = -\bar{h} + \eta'(x',t') \tag{2.1.1.4}$$

From Bernoulli equation, we also deduce the total pressure p' in water (sum of the static and the dynamic pressures, respectively p'_s and p'_d) as a function of the potential:

$$p' = -\rho_W \left(\frac{\partial \phi'}{\partial t'} + \frac{1}{2}\left(\frac{\partial \phi'}{\partial x'}\right)^2 + gz'\right) \tag{2.1.1.5}$$

2.1.2 Dimensional equations in mud

In the mud, we use a different vertical axis measured from the rigid bed such that $Z' = z' - \bar{h} - d$. This way we get $Z' = 0$ at the bottom of the mud layer and $Z' = d + \eta'$ at the interface. The motion in the mud layer obeys the Navier-Stokes equation for an incompressible fluid. We write U' and V' respectively the horizontal and the vertical component of the mud velocity, P' the mud pressure and τ'_{ij} is the viscoelastic stress tensor. The momentum conservation equation projected on the horizontal axis is:

$$\rho_M \left(\frac{\partial U'}{\partial t'} + U'\frac{\partial U'}{\partial x'} + V'\frac{\partial U'}{\partial Z'}\right) = -\frac{\partial P'}{\partial Z'} + \left(\frac{\partial \tau'_{xZ}}{\partial Z'} + \frac{\partial \tau'_{xx}}{\partial x'}\right) \tag{2.1.2.1}$$

$\kappa = k\bar{h}$		ω' (rad/s) [T(s)]		
		1/3 [18]	1/2 [12]	1 [6]
$\bar{h}$	1 m	0.106	0.159	0.31
	2 m	0.15	0.225	0.45
	5 m	0.238	0.357	0.71
	5 m	0.33	0.5	1

Table 2.1: Values of κ for different ω and water depths $\bar{h}$

and on the vertical axis:

$$\rho_M \left(\frac{\partial V'}{\partial t'} + U' \frac{\partial V'}{\partial x'} + V' \frac{\partial V'}{\partial Z'} \right) = -\frac{\partial P'}{\partial Z'} + \left(\frac{\partial \tau'_{ZZ}}{\partial Z'} + \frac{\partial \tau'_{xZ}}{\partial x'} \right) \tag{2.1.2.2}$$

The mud motion also obeys the conservation equation:

$$\frac{\partial U'}{\partial x'} + \frac{\partial V'}{\partial Z'} = 0 \tag{2.1.2.3}$$

The kinematic boundary condition at the interface between mud and water also implies:

$$\frac{\partial \eta'}{\partial t'} = V' - \frac{\partial \eta'}{\partial x'} U', \quad Z = d + \eta \tag{2.1.2.4}$$

2.2 Scaling

We only consider long waves with small amplitude on the free surface. With k the typical wavenumber and A the typical surface wave amplitude, let us define the following ratios:

$$\boxed{\kappa = k\bar{h}}, \quad \boxed{\epsilon = \frac{A}{\bar{h}}} \tag{2.2.0.5}$$

where κ and ϵ respectively represent dispersion and non-linearity parameters.

Table 2.1 gives some sample values of κ in the ω' and $\bar{h}$-ranges that we consider: $1/3 < \omega' < 1$ and $1\text{m} < \bar{h} < 10\text{m}$. From this table, we deduce that κ can vary between 0.1 and 1. However, as the aim of this study is to focus on long waves, we will always choose values of $\bar{h}$ and ω' such as κ is smaller than 0.4. Thus, the κ-range that we will consider in this thesis is: $0.1 < \kappa < 0.4$.

Table 2.2 gives values of ϵ with respect to the water depth $\bar{h}$ and the wave amplitude A. We deduce from this table the following range for ϵ: $0.01 < \epsilon < 0.6$. Since we only aim at studying small non-linearity, we will always choose values of d and $\bar{h}$ such

$\epsilon = \frac{A}{\bar{h}}$		A (cm)			
		10	20	40	60
$\bar{h}$	1 m	0.1	0.2	0.4	0.6
	2 m	0.05	0.1	0.2	0.3
	5 m	0.02	0.04	0.08	0.12
	10 m	0.01	0.02	0.04	0.06

Table 2.2: Values of ϵ for different A and water depths $\bar{h}$

as $\epsilon < 0.4$. Thus, the ϵ-range that we will consider in this thesis is: $0.01 < \epsilon < 0.4$.

We deduced from tables 2.1 and 2.2 the ranges we want to consider for κ and ϵ: $0.1 < \kappa < 0.4$ and $0.01 < \epsilon < 0.4$. As a consequence, there are two cases to take into account:

- The cases where $\epsilon = O(\kappa)$, that is to say where non-linearity is more important than dispersion ;
- The cases where $\epsilon = O(\kappa^2)$, i.e., dispersion is comparable to nonlinearity (Boussinesq class).

Chapters 4 and 5 are devoted to the case $\epsilon = O(\kappa^2)$.

In this chapter and the following, we limit our study to the case $\epsilon = O(\kappa)$:

$$\boxed{O(\kappa) = O(\epsilon)} \tag{2.2.0.6}$$

We also assume the mud layer thickness d to be very small compared to the water depth $\bar{h}$. We choose the ratio κ_d to be between the values 0.05 and 0.2, and thus to be of order κ:

$$\boxed{\kappa_d = \frac{d}{\bar{h}} = O(\kappa)} \tag{2.2.0.7}$$

2.2.1 Non-dimensional variables in water

Based on the basic equations derived in section 2.1, we decide to introduce the following dimensionless variables in water:

$$\begin{array}{lll} x = kx' & z = \frac{z'}{\bar{h}} & t = k(g\bar{h})^{1/2}t' \\ p = \frac{p'}{\rho_W g A} & u = \frac{1}{\epsilon\sqrt{g\bar{h}}}u' & v = \frac{\kappa}{\epsilon\sqrt{g\bar{h}}}v' \\ \zeta = \frac{\zeta'}{A} & \phi = \phi'\left[\frac{A}{k\bar{h}}(g\bar{h})^{1/2}\right]^{-1} & \end{array} \tag{2.2.1.1}$$

2.2.2 Estimation of $O\left(\frac{\eta'}{\zeta'}\right)$

Let us deduce from the previous statements how large the ratio between the surface and the interface variations can be. For that, let us use the governing equation in water and in mud.

In water, the mass conservation principle for long waves becomes at the leading order:

$$\begin{aligned} \frac{\partial u'}{\partial x'} + \frac{\partial v'}{\partial z'} &= 0 \\ \frac{\partial \zeta'}{\partial t'} &= O(v') \end{aligned} \tag{2.2.2.1}$$

Using the non-dimensional variables we just defined, we find:

$$\begin{aligned} O(v') &= \kappa O(u') \\ &= k\sqrt{g\bar{h}}O(\zeta') \end{aligned} \tag{2.2.2.2}$$

In mud, we logically adopt the following non-dimensional variables:

$$x = kx' \quad Z = \frac{z'}{d} \quad t = k(g\bar{h})^{1/2}t' \tag{2.2.2.3}$$

As a consequence, the kinematic boundary condition at the interface at the leading order

$$\frac{\partial \eta'}{\partial t'} = V' \tag{2.2.2.4}$$

gives in non-dimensional variables:

$$k\sqrt{g\bar{h}}O(\eta') = O(V') \tag{2.2.2.5}$$

Still in mud, mass conservation gives:

$$\frac{\partial U'}{\partial x'} + \frac{\partial V'}{\partial z'} = 0 \tag{2.2.2.6}$$

From this equation we deduce a relationship between $O(U')$ and $O(V')$:

$$\begin{aligned} O(V') &= kdO(U') \\ &= \frac{d}{\bar{h}}k\bar{h}O(U') \\ &= \frac{d}{\bar{h}}\kappa O(U') \\ &= \kappa_d \kappa O(U') \end{aligned} \tag{2.2.2.7}$$

Combining equations 2.2.2.5 and 2.2.2.7, we have the relationship:

$$k\sqrt{g\bar{h}}O(\eta') = \frac{d}{\bar{h}}\kappa O(U') \tag{2.2.2.8}$$

and everything we need is a relation between u' and U'. From the horizontal momentum equation we find:

$$\frac{\partial U'}{\partial t} = -\frac{1}{\rho_M}\frac{\partial P'}{\partial x'} + \nu\frac{\partial^2 U'}{\partial Z'^2} \tag{2.2.2.9}$$

Since the mud layer is thin,

$$\frac{\partial P'}{\partial Z'} \simeq 0 \tag{2.2.2.10}$$

and

$$\frac{\partial P'}{\partial x'} = \frac{\partial p'}{\partial x'} = \rho_W g\frac{\partial \zeta'}{\partial x'} \tag{2.2.2.11}$$

It follows that:

$$k\sqrt{g\bar{h}}U' = O(gk\zeta') \tag{2.2.2.12}$$

which means:

$$U' = O\left(\sqrt{\frac{g}{\bar{h}}}\zeta'\right) \tag{2.2.2.13}$$

Combining this result with equation 2.2.2.2, we find:

$$O(U') = O(u') \tag{2.2.2.14}$$

We conclude by combining equations 2.2.2.2, 2.2.2.8 and 2.2.2.14 and we obtain:

$$O(\eta') = \frac{d}{\bar{h}}O(\zeta') \tag{2.2.2.15}$$

that is to say:

$$\boxed{O\left(\frac{\eta'}{\zeta'}\right) = \kappa_d = O(\kappa)} \tag{2.2.2.16}$$

2.2.3 Non-dimensional variables in mud

From the relation 2.2.2.16, we introduce the dimensionless variables in mud:

$$\begin{array}{lll} x = kx' & Z = \frac{Z'}{d} & t = k(g\bar{h})^{1/2}t' \\ P = \frac{P'}{\rho_W g A} & U = \frac{1}{\epsilon\sqrt{g\bar{h}}}U' & V = \frac{1}{\epsilon\kappa\kappa_d\sqrt{g\bar{h}}}V' \\ \eta = \frac{\eta'}{\kappa_d A} & \mathcal{U} = \frac{k}{\epsilon}\mathcal{U}' & \mathcal{V} = \frac{k}{\epsilon\kappa\kappa_d}\mathcal{V}' \\ T_{ij} = \frac{T'_{ij}}{\rho_W g A} & E_{ij,t} = \frac{d}{\epsilon\sqrt{g\bar{h}}}E'_{ij,t'} & \tau_{ij} = \frac{d}{\epsilon\mu\sqrt{g\bar{h}}}\tau'_{ij} \end{array} \tag{2.2.3.1}$$

where $\mathcal{U}'$ and $\mathcal{V}'$ are respectively the horizontal and the vertical displacements, U' and V' are respectively the horizontal and the vertical velocity and $E'_{ij,t}$ the rate of strain tensor. T'_{ij} is the total stress tensor, such as $T'_{ij} = -P'\delta_{ij} + \tau'_{ij}$. μ is the mud viscosity.

2.3 Equations in water to order $O(\kappa^2)$

In this section, we shall derive the approximate equations to high order because this may be useful for later studies. However, we will only make use of the first and the second order ($O(1)$ and $O(\kappa)$) in the rest of this thesis. These orders will be highlighted at the end of the calculations for clarity.

Let us express the velocity potential in the water as a power series:

$$\boxed{\phi(x,z,t) = \sum_{n=0}^{\infty} \frac{(z+1)^n}{n!}\phi^{(n)}(x,t)} \tag{2.3.0.2}$$

We then obtain

$$\frac{\partial^2\phi}{\partial x^2} = \sum_{n=0}^{\infty} \frac{(z+1)^n}{n!}\frac{\partial^2\phi^{(n)}}{\partial x^2}(x,t) \tag{2.3.0.3}$$

and:

$$\phi_{zz} = \sum_{n=0}^{\infty} \frac{(z+1)^n}{n!}\phi^{(n+2)}(x,t) \tag{2.3.0.4}$$

2.3.1 Laplace equation

From the Laplace equation in dimensionless variables, we know:

$$\kappa^2\frac{\partial^2\phi}{\partial x^2} + \frac{\partial^2\phi}{\partial z^2} = 0 \tag{2.3.1.1}$$

and from 2.3.0.3 and 2.3.0.4 we deduce:

$$\forall n,\quad \phi^{(n)} = -\kappa^2\frac{\partial^2\phi^{(n-2)}}{\partial x^2} \tag{2.3.1.2}$$

From the kinematic boundary conditions at the interface 2.1.1.4, we know that:

$$\phi_z = \kappa_d\kappa^2\frac{\partial\eta}{\partial t} + \epsilon\kappa_d\kappa^2\frac{\partial\eta}{\partial x}\frac{\partial\phi}{\partial x},\quad z = -1 + \epsilon\kappa_d\eta(x,t) \tag{2.3.1.3}$$

We use a Taylor series expansion of this equation to obtain:

$$\phi_z + \epsilon\kappa_d\eta\phi_{zz} + (\epsilon\kappa_d)^2\eta^2\phi_{zzz} = \epsilon\kappa_d\kappa^2\frac{\partial\eta}{\partial x}\frac{\partial\phi}{\partial x} + \kappa^2\kappa_d\frac{\partial\eta}{\partial t} + O(\kappa^5), \quad z = -1 \tag{2.3.1.4}$$

As a consequence, from the series of equation 2.3.0.2 we obtain:

$$\phi^{(1)} + \epsilon\kappa_d\eta\phi^{(2)} + (\epsilon\kappa_d)^2\eta^2\phi^{(3)} = \epsilon\kappa_d\kappa^2\frac{\partial\eta}{\partial x}\frac{\partial\phi}{\partial x} + \kappa^2\kappa_d\frac{\partial\eta}{\partial t} + O(\kappa^5) \tag{2.3.1.5}$$

From the result of equation 2.3.1.2, we can express $\phi^{(2)}$ in terms of $\phi^{(0)}$:

$$\phi^{(2)} = -\kappa^2\frac{\partial^2\phi^{(0)}}{\partial x^2} \tag{2.3.1.6}$$

and $\phi^{(3)}$ in terms of $\phi^{(1)}$:

$$\phi^{(3)} = -\kappa^2\frac{\partial^2\phi^{(1)}}{\partial x^2} \tag{2.3.1.7}$$

and $\phi^{(1)}$ from equation 2.3.1.5:

$$\phi^{(1)} = \kappa_d\kappa^2\frac{\partial\eta}{\partial t} + \epsilon\kappa_d\kappa^2\frac{\partial\eta}{\partial x}\frac{\partial\phi}{\partial x} + O(\kappa^5) \tag{2.3.1.8}$$

Then equation 2.3.1.2 allows us to deduce $\phi^{(3)}$ as:

$$\begin{aligned}\phi^{(3)} &= -\kappa^2\frac{\partial^2\phi^{(1)}}{\partial x^2} \\ &= -\kappa^2\frac{\partial^2}{\partial x^2}\left(\kappa_d\kappa^2\frac{\partial\eta}{\partial t} + \epsilon\kappa_d\kappa^2\frac{\partial\eta}{\partial x}\frac{\partial\phi}{\partial x}\right) + O(\kappa^7) \\ &= O(\kappa^5)\end{aligned} \tag{2.3.1.9}$$

and $\phi^{(4)}$:

$$\begin{aligned}\phi^{(4)} &= -\kappa^2\frac{\partial^2\phi^{(2)}}{\partial x^2} \\ &= \kappa^4\frac{\partial^4\phi^{(0)}}{\partial x^4} + O(\kappa^5)\end{aligned} \tag{2.3.1.10}$$

We also deduce:

$$\forall n > 4, \quad \phi^{(n)} = O(\kappa^5) \tag{2.3.1.11}$$

As a consequence, we can truncate the series 2.3.0.2:

$$\phi = \phi^{(0)} + (z+1)\phi^{(1)} + \frac{(z+1)^2}{2!}\phi^{(2)} + \frac{(z+1)^4}{4!}\phi^{(4)} + O(\kappa^5) \tag{2.3.1.12}$$

and combining equations 2.3.1.5, 2.3.1.6, 2.3.1.9 and 2.3.1.10 in equation 2.3.1.12, we obtain the highly useful representation of ϕ to order $O(\kappa^5)$:

$$\begin{aligned}\phi =&\phi^{(0)} + \kappa_d\kappa^2(z+1)\left[\frac{\partial\eta}{\partial t} + \epsilon\frac{\partial}{\partial x}\left(\eta\frac{\partial\phi^{(0)}}{\partial x}\right)\right] - \kappa^2\frac{(z+1)^2}{2!}\frac{\partial^2\phi^{(0)}}{\partial x^2} \\ &+ \kappa^4\frac{(z+1)^4}{4!}\frac{\partial^4\phi^{(0)}}{\partial x^4} + O(\kappa^5)\end{aligned} \tag{2.3.1.13}$$

2.3.2 Depth-averaged law of mass conservation

The kinematic boundary condition at the surface can be written as:

$$\kappa^2\left(\zeta_t + \epsilon\frac{\partial\phi}{\partial x}\frac{\partial\zeta}{\partial x}\right) = \phi_z, \quad z = \epsilon\zeta \tag{2.3.2.1}$$

Since from the equation 2.3.1.13,

$$\phi_z = \kappa_d\kappa^2\left[\frac{\partial\eta}{\partial t} + \epsilon\frac{\partial}{\partial x}\left(\eta\frac{\partial\phi^{(0)}}{\partial x}\right)\right] - \kappa^2(z+1)\frac{\partial^2\phi^{(0)}}{\partial x^2} + \kappa^4\frac{(z+1)^3}{6}\frac{\partial^4\phi^{(0)}}{\partial x^4} + O(\kappa^5) \tag{2.3.2.2}$$

we obtain:

$$\zeta_t + \epsilon\frac{\partial\phi^{(0)}}{\partial x}\frac{\partial\zeta}{\partial x} = \kappa_d\left[\frac{\partial\eta}{\partial t} + \epsilon\frac{\partial}{\partial x}\left(\eta\frac{\partial\phi^{(0)}}{\partial x}\right)\right] - (1+\epsilon\zeta)\frac{\partial^2\phi^{(0)}}{\partial x^2} + \frac{\kappa^2}{6}\frac{\partial^4\phi^{(0)}}{\partial x^4} + O(\kappa^3) \tag{2.3.2.3}$$

Let us now introduce the horizontal velocity at the bottom $u^{(0)} = \frac{\partial\phi^{(0)}}{\partial x}$, so that

$$\zeta_t + \epsilon u^{(0)}\frac{\partial\zeta}{\partial x} = \kappa_d\left[\frac{\partial\eta}{\partial t} + \epsilon\frac{\partial}{\partial x}\left(\eta u^{(0)}\right)\right] - (1+\epsilon\zeta)\frac{\partial u^{(0)}}{\partial x} + \frac{\kappa^2}{6}\frac{\partial^3 u^{(0)}}{\partial x^3} + O(\kappa^3) \tag{2.3.2.4}$$

Let the depth-averaged velocity be $\bar{u}$, which is related to u_0 by the following relation:

$$\begin{aligned}\bar{u} &= \frac{1}{H}\int_{-1+\epsilon\kappa_d\eta}^{\epsilon\zeta}\frac{\partial\phi}{\partial x}dz \\ &= \frac{1}{H}\int_{-1+\epsilon\kappa_d\eta}^{\epsilon\zeta}\left(u^{(0)} - \kappa^2\frac{(z+1)^2}{2}\frac{\partial^2 u^{(0)}}{\partial x^2} + O(\kappa^3)\right)dz \\ &= u^{(0)} - \frac{\kappa^2}{6}\frac{(1+\epsilon\zeta)^3}{1+\epsilon\zeta-\epsilon\kappa_d\eta}\frac{\partial^2\bar{u}}{\partial x^2} + O(\kappa^3) \\ &= u^{(0)} - \frac{\kappa^2}{6}\frac{\partial^2\bar{u}}{\partial x^2} + O(\kappa^3)\end{aligned} \tag{2.3.2.5}$$

Turning this last result around, we obtain the relation:

$$u^{(0)} = \bar{u} + \frac{\kappa^2}{6}\frac{\partial^2 \bar{u}}{\partial x^2} + O(\kappa^3) \tag{2.3.2.6}$$

Using this relationship, we obtain the equation 2.3.2.4 with respect to $\bar{u}$ instead of $u^{(0)}$:

$$\zeta_t + \epsilon\bar{u}\frac{\partial\zeta}{\partial x} = \kappa_d\frac{\partial\eta}{\partial t} + \kappa_d\epsilon\frac{\partial(\eta\bar{u})}{\partial x} - \frac{\partial\bar{u}}{\partial x} - \frac{\kappa^2}{6}\frac{\partial^3\bar{u}}{\partial x^3} - \epsilon\zeta\frac{\partial\bar{u}}{\partial x} + \frac{\kappa^2}{6}\frac{\partial^3\bar{u}}{\partial x^3} + O(\kappa^3) \tag{2.3.2.7}$$

and so:

$$\zeta_t - \kappa_d\frac{\partial\eta}{\partial t} + \frac{\partial\bar{u}}{\partial x} + \epsilon\bar{u}\frac{\partial\zeta}{\partial x} + \epsilon\zeta\frac{\partial\bar{u}}{\partial x} - \kappa_d\epsilon\frac{\partial(\eta\bar{u})}{\partial x} = -\frac{\kappa^2}{6}\frac{\partial^3\bar{u}}{\partial x^3} + \frac{\kappa^2}{6}\frac{\partial^3\bar{u}}{\partial x^3} + O(\kappa^3) \tag{2.3.2.8}$$

From equation 2.3.2.8, we finally obtain the simplified form of the kinematic boundary condition:

$$\zeta_t - \kappa_d\eta_t + \frac{\partial}{\partial x}[(1 + \epsilon\zeta - \kappa_d\epsilon\eta)\bar{u}] = O(\kappa^3) \tag{2.3.2.9}$$

Note the effect of the interface displacement.

Even though we carried the calculations up to order $O(\kappa^3)$, we will only use the orders $O(1)$ and $O(\kappa)$ later on in this thesis:

$$\boxed{\zeta_t - \kappa_d\eta_t + \frac{\partial}{\partial x}[(1 + \epsilon\zeta)\bar{u}] = O(\kappa^2)} \tag{2.3.2.10}$$

2.3.3 Depth-averaged horizontal momentum

From the dynamic boundary condition at the surface we know:

$$\kappa^2(\phi_t + \zeta) + \frac{1}{2}\epsilon[\kappa^2\phi_x^2 + \phi_z^2] = 0, \quad z = \epsilon\zeta(x,t) \tag{2.3.3.1}$$

From the expansion of ϕ of the equation 2.3.1.13, we deduce:

$$\phi^{(0)}{}_t - \frac{\kappa^2}{2}\frac{\partial^2\phi^{(0)}{}_t}{\partial x^2} + \zeta + \frac{1}{2}\epsilon\left(\frac{\partial\phi^{(0)}}{\partial x}\right)^2 = O(\kappa^3) \tag{2.3.3.2}$$

which can be written:

$$\frac{\partial\phi^{(0)}}{\partial t} + \zeta + \frac{1}{2}\epsilon\left(\frac{\partial\phi^{(0)}}{\partial x}\right)^2 = \frac{\kappa^2}{2}\frac{\partial^3\phi^{(0)}}{\partial x^2\partial t} + O(\kappa^3) \tag{2.3.3.3}$$

We now introduce the horizontal velocity at the bottom $u^{(0)} = \frac{\partial \phi^{(0)}}{\partial x}$:

$$\frac{\partial u^{(0)}}{\partial t} + \frac{\partial \zeta}{\partial x} + \epsilon u^{(0)} \frac{\partial u^{(0)}}{\partial x} = \frac{\kappa^2}{2} \frac{\partial^3 u^{(0)}}{\partial x^2 \partial t} + O(\kappa^3) \tag{2.3.3.4}$$

As was done for the kinematic boundary condition, we write this equation in terms of the depth-averaged velocity $\bar{u}$, using the relation between $u^{(0)}$ and $\bar{u}$ given by equation 2.3.2.6:

$$\frac{\partial \bar{u}}{\partial t} + \frac{\kappa^2}{6} \frac{\partial^3 \bar{u}}{\partial x^2 \partial t} + \frac{\partial \zeta}{\partial x} + \epsilon \bar{u} \frac{\partial \bar{u}}{\partial x} = \frac{\kappa^2}{2} \frac{\partial^3 \bar{u}}{\partial x^2 \partial t} + O(\kappa^3) \tag{2.3.3.5}$$

This last equation can be finally reduced to the simplified form of the dynamic boundary condition at the sea surface:

$$\frac{\partial \bar{u}}{\partial t} + \epsilon \bar{u} \frac{\partial \bar{u}}{\partial x} + \frac{\partial \zeta}{\partial x} = \frac{\kappa^2}{3} \frac{\partial^3 \bar{u}}{\partial x^2 \partial t} + O(\kappa^3) \tag{2.3.3.6}$$

This equation is the same as that for a rigid seabed.

Even though we carried the calculations up to order $O(\kappa^3)$, we will only use the orders $O(1)$ and $O(\kappa)$ later on in this thesis:

$$\boxed{\frac{\partial \bar{u}}{\partial t} + \epsilon \bar{u} \frac{\partial \bar{u}}{\partial x} + \frac{\partial \zeta}{\partial x} = O(\kappa^2)} \tag{2.3.3.7}$$

2.3.4 Equation of the total pressure in water

From the Bernoulli equation, we can deduce the total pressure (sum of the static and the dynamic pressure) in the water as a function of the potential:

$$\begin{aligned} p' &= p'_s + p'_d \\ &= -\rho_W \left(\frac{\partial \phi'}{\partial t'} + \frac{1}{2} (\nabla' \phi')^2 + g z' \right) \end{aligned} \tag{2.3.4.1}$$

In dimensionless form, this last equation becomes:

$$p = -\phi_t - \frac{\epsilon}{2} \left[(\phi_x)^2 + \frac{1}{\kappa^2} (\phi_z)^2 \right] - \frac{z}{\epsilon} \tag{2.3.4.2}$$

In particular, we can easily deduce the pressure at the interface between mud and water:

$$p = \frac{1}{\epsilon} - \phi_t - \frac{\epsilon}{2} \left[(\phi_x)^2 + \frac{1}{\kappa^2} (\phi_z)^2 \right] - \kappa_d \eta, \quad z = -1 + \epsilon \kappa_d \eta(x,t) \tag{2.3.4.3}$$

This equation will be needed to get the mud pressure P in the horizontal momentum equation for mud. Please remember the final objective is to get $\frac{\partial p}{\partial x}$ on the interface in terms of ζ and η.

2.4 Equations in mud to order $O(\kappa)$

2.4.1 Kinematic boundary condition at the interface in mud

In dimensional form, we know that:

$$\eta'_{t'} = V' - \eta'_{x'}U', \quad Z = 1 + \epsilon\eta \tag{2.4.1.1}$$

So in dimensionless form:

$$\boxed{\eta_t = V - \epsilon\eta_x U}, \quad Z = 1 + \epsilon\eta \tag{2.4.1.2}$$

2.4.2 Conservation of mass in the mud

In dimensional form, we know from conservation of mass:

$$\frac{\partial U'}{\partial x'} + \frac{\partial V'}{\partial Z'} = 0 \tag{2.4.2.1}$$

in the entire layer of mud.

This equation becomes in dimensionless form:

$$\boxed{U_x + V_Z = 0}, \ 0 < Z < 1 + \epsilon\eta \tag{2.4.2.2}$$

This will be used later to deduce vertical velocity from horizontal velocity in mud. Let us note that this equation is exact, contrary to most other mud equations.

2.4.3 Horizontal momentum in mud

Let us first write the Newtonian relation between the stress τ' and the strain E' in a dimensional form.

$$\tau'_{xZ} = \mu\frac{\partial E'_{xZ}}{\partial t'} \tag{2.4.3.1}$$

With the scaling we chose, we obtain that:

$$\tau_{xZ} = \frac{\partial E_{xZ}}{\partial t} \tag{2.4.3.2}$$

Introducing the horizontal velocity in mud, equation 2.4.3.2 becomes:

$$\tau_{xZ} = \frac{\partial U}{\partial Z} + O(\kappa^4) \tag{2.4.3.3}$$

The equation of momentum in mud, projected on the x-axis, gives:

$$\frac{\partial U}{\partial t} + \epsilon \left(U \frac{\partial U}{\partial x} + V \frac{\partial U}{\partial Z} \right) = -\gamma \frac{\partial P}{\partial x} + \frac{A}{Re * d} \left(\frac{\partial \tau_{xZ}}{\partial Z} + \kappa \kappa_d \frac{\partial \tau_{xx}}{\partial x} \right) \tag{2.4.3.4}$$

where γ is the ratio of densities:

$$\underline{\gamma = \rho_W / \rho_M} \tag{2.4.3.5}$$

and Re is the Reynolds number defined as:

$$\boxed{Re = \frac{\rho_M A d k \sqrt{g\bar{h}}}{\mu}} \tag{2.4.3.6}$$

From this equation we simplify:

$$\frac{\partial U}{\partial t} = \frac{1}{Re} \frac{A}{d} \frac{\partial \tau_{xZ}}{\partial Z} - \gamma \frac{\partial P}{\partial x} + \epsilon \left(U \frac{\partial U}{\partial x} + V \frac{\partial U}{\partial Z} \right) + O(\kappa^2) \tag{2.4.3.7}$$

where U is the horizontal velocity of mud, P the pressure, A the amplitude of the free surface and d the mud depth.

Let us evaluate the order of the Reynolds number. We can first rewrite it as a function of ϵ, κ, κ_d, $\bar{h}$ and the type of mud:

$$Re = \frac{\rho_M \sqrt{g} \bar{h}^{3/2} \epsilon \kappa \kappa_d}{\mu} \tag{2.4.3.8}$$

Indeed, ρ_M and μ depend on the type of mud we consider.

It will be shown in the last section of this chapter that the range of Reynolds number is no greater than $O(1)$. Because we want our study to be applicable to any type of mud, we decide to adopt the limiting case in this thesis. As a consequence, the Reynolds number will be regarded as:

$$\boxed{Re = O(1)} \tag{2.4.3.9}$$

Differentiating equation 2.4.3.3 with respect to Z, we get:

$$\frac{\partial \tau_{xZ}}{\partial Z} = \frac{\partial^2 U}{\partial Z^2} \tag{2.4.3.10}$$

Equation 2.4.3.7 can be rewritten:

$$\frac{\partial \tau_{xZ}}{\partial Z} = Re\frac{d}{A}\left[\frac{\partial U}{\partial t} + \gamma\frac{\partial P}{\partial x} + \epsilon\left(U\frac{\partial U}{\partial x} + V\frac{\partial U}{\partial Z}\right)\right] + O(\kappa^2) \tag{2.4.3.11}$$

By combining equation 2.4.3.10 and 2.4.3.11 we obtain an equation between the horizontal velocity and the pressure gradient:

$$\frac{\partial^2 U}{\partial Z^2} = Re\frac{d}{A}\left[\frac{\partial U}{\partial t} + \gamma\frac{\partial P}{\partial x} + \epsilon\left(U\frac{\partial U}{\partial x} + V\frac{\partial U}{\partial Z}\right)\right] + O(\kappa^2) \quad 0 < Z < 1 + \epsilon\eta \tag{2.4.3.12}$$

Let us now find an equation of the mud pressure P as a function of ζ and η in order to eliminate the mud pressure from equation 2.4.3.12.

2.4.4 Vertical momentum in mud

The dimensional equation of vertical momentum is:

$$\rho_M\left(\frac{\partial V'}{\partial t'} + U'\frac{\partial V'}{\partial x'} + V'\frac{\partial V'}{\partial Z'}\right) = -\frac{\partial P'}{\partial Z'} + \left(\frac{\partial \tau'_{ZZ}}{\partial Z'} + \frac{\partial \tau'_{xZ}}{\partial x'}\right) \tag{2.4.4.1}$$

and becomes, in dimensionless variables:

$$\frac{\partial V}{\partial t} + \epsilon\left(U\frac{\partial V}{\partial x} + V\frac{\partial V}{\partial Z}\right) = -\frac{\gamma}{\kappa^2\kappa_d^2}\frac{\partial P}{\partial Z} + \frac{\epsilon}{Re\kappa^2\kappa_d}\left(\frac{\partial \tau_{ZZ}}{\partial Z} + \kappa\kappa_d\frac{\partial \tau_{xZ}}{\partial x}\right) \tag{2.4.4.2}$$

So, in the end,

$$\boxed{\frac{\partial P}{\partial Z} = O(\epsilon\kappa)} \quad 0 < Z < 1 + \epsilon\eta \tag{2.4.4.3}$$

In other words, we find that the vertical pressure gradient in mud is of order $O(\kappa^2)$. This equation will be used to evaluate the pressure in the entire mud layer.

2.4.5 Dynamic boundary condition at the interface

Let us call $\underline{n} = (n_x, n_Z)$ the vector normal to the interface. In dimensional notations, we know that the components of $\underline{n}$ are:

$$\begin{aligned} n_x &= \frac{\frac{\partial \eta'}{\partial x'}}{\sqrt{1 + \left(\frac{\partial \eta'}{\partial x'}\right)^2}} \\ n_Z &= \frac{1}{\sqrt{1 + \left(\frac{\partial \eta'}{\partial x'}\right)^2}} \end{aligned} \tag{2.4.5.1}$$

In dimensionless variables, we obtain:

$$\begin{aligned} n_x &= \frac{\epsilon\kappa\kappa_d \frac{\partial \eta}{\partial x}}{\sqrt{1 + \epsilon^2\kappa^2\kappa_d^2\left(\frac{\partial \eta}{\partial x}\right)^2}} \\ n_Z &= \frac{1}{\sqrt{1 + \epsilon^2\kappa^2\kappa_d^2\left(\frac{\partial \eta}{\partial x}\right)^2}} \end{aligned} \tag{2.4.5.2}$$

Finally, n_x and n_Z can be approximated as:

$$\begin{aligned} n_x &= \epsilon\kappa\kappa_d \frac{\partial \eta}{\partial x} + O(\epsilon^2\kappa^2\kappa_d^2) \\ n_Z &= 1 + O(\epsilon^2\kappa^2\kappa_d^2) \end{aligned} \tag{2.4.5.3}$$

Continuity of total (hydrodynamic and dynamic) stress on the mud-water interface then requires:

$$\begin{aligned} T_{xx}n_x + T_{xZ}n_Z &= -pn_x, \quad Z = 1 + \epsilon\eta \\ T_{xZ}n_x + T_{ZZ}n_Z &= -pn_Z, \quad Z = 1 + \epsilon\eta \end{aligned} \tag{2.4.5.4}$$

Total stress in mud is the sum of hydrostatic and dynamic pressure:

$$T_{ij} = -P\delta_{ij} + \frac{\epsilon\kappa}{\gamma Re}\tau_{ij}, \tag{2.4.5.5}$$

Introducing this sum in equation 2.4.5.4, we obtain:

$$\begin{aligned} \left(-P + \frac{\epsilon\kappa}{\gamma Re}\tau_{xx}\right) n_x + \frac{\epsilon\kappa}{\gamma Re}\tau_{xZ}n_Z &= -pn_x, \quad Z = 1 + \epsilon\eta \\ \frac{\epsilon\kappa}{\gamma Re}\tau_{xZ}n_x + \left(-P + \frac{\epsilon\kappa}{\gamma Re}\tau_{ZZ}\right) n_Z &= -pn_Z, \quad Z = 1 + \epsilon\eta \end{aligned} \tag{2.4.5.6}$$

From the approximations of n_x and n_Z that we demonstrated in 2.4.5.3, equations 2.4.5.6 become:

$$\begin{aligned}
&\left(-P+\frac{\epsilon\kappa}{\gamma Re}\tau_{xx}\right)\epsilon\kappa\kappa_d\frac{\partial\eta}{\partial x}+\frac{\epsilon\kappa}{\gamma Re}\tau_{xZ}=-p\epsilon\kappa\kappa_d\frac{\partial\eta}{\partial x}+O(\epsilon^2\kappa^2\kappa_d^2),\quad Z=1+\epsilon\eta\\
&\frac{\epsilon\kappa}{\gamma Re}\tau_{xZ}\epsilon\kappa\kappa_d\frac{\partial\eta}{\partial x}+\left(-P+\frac{\epsilon\kappa}{\gamma Re}\tau_{ZZ}\right)=-p+O(\epsilon^2\kappa^2\kappa_d^2),\quad Z=1+\epsilon\eta
\end{aligned}\tag{2.4.5.7}$$

These last equations can easily be simplified to:

$$\begin{aligned}
&\frac{\epsilon\kappa}{\gamma Re}\tau_{xZ}=(P-p)\epsilon\kappa\kappa_d\frac{\partial\eta}{\partial x}+O(\epsilon^2\kappa^2\kappa_d),\quad Z=1+\epsilon\eta\\
&P-p=O(\epsilon\kappa),\quad Z=1+\epsilon\eta
\end{aligned}\tag{2.4.5.8}$$

Dividing the first equation of 2.4.5.8 by $\frac{\epsilon\kappa}{\gamma Re}$, these equations become:

$$\begin{aligned}
&\tau_{xZ}=\gamma Re\kappa_d(P-p)\frac{\partial\eta}{\partial x}+O(\epsilon\kappa\kappa_d),\quad Z=1+\epsilon\eta\\
&P-p=O(\epsilon\kappa),\quad Z=1+\epsilon\eta
\end{aligned}\tag{2.4.5.9}$$

Let us now make use of the second equation (corresponding to normal stress condition) to simplify the first one (corresponding to tangential stress condition). Since $P-p=O(\epsilon\kappa)$, we obtain:

$$\begin{aligned}
&\tau_{xZ}=O(\epsilon\kappa\kappa_d)=O(\kappa^3),\quad Z=1+\epsilon\eta\\
&P-p=O(\epsilon\kappa)=O(\kappa^2),\quad Z=1+\epsilon\eta
\end{aligned}\tag{2.4.5.10}$$

We now focus on the first part of equation 2.4.5.10. Through a Taylor expansion, we can approximate this equations around $Z=1$:

$$\tau_{xZ}(Z=1+\epsilon\eta)=\tau_{xZ}(Z=1)+\epsilon\eta\frac{\partial\tau_{xZ}}{\partial Z}\Big|_{Z=1}+O(\epsilon^2)\tag{2.4.5.11}$$

and as a consequence:

$$\begin{aligned}
\tau_{xZ}(Z=1)&=\tau_{xZ}(Z=1+\epsilon\eta)-\epsilon\eta\frac{\partial\tau_{xZ}}{\partial Z}\Big|_{Z=1}+O(\epsilon^2)\\
&=-\epsilon\eta\frac{\partial\tau_{xZ}}{\partial Z}\Big|_{Z=1}+O(\epsilon^2)
\end{aligned}\tag{2.4.5.12}$$

We finally obtain a boundary condition at the interface in term of the horizontal velocity U:

$$\boxed{\frac{\partial U}{\partial Z}\Big|_{Z=1} = -\epsilon\eta\frac{\partial^2 U}{\partial Z^2}\Big|_{Z=1} + O(\epsilon^2)} \tag{2.4.5.13}$$

This boundary condition will later be used to determine the drift in mud.

Let us now focus on the second part of equation 2.4.5.10. From 2.4.4.3, we know that the vertical gradient of mud pressure is of order $O(\kappa^2)$. As a consequence, we have:

$$P = p(Z = 1 + \epsilon\eta) + O(\kappa^2), \quad 0 < Z < 1 + \epsilon\eta \tag{2.4.5.14}$$

Differentiating this last equation, we know that:

$$\frac{\partial P}{\partial x} = \frac{\partial p}{\partial x}(Z = 1 + \epsilon\eta) + O(\kappa^2), \quad 0 < Z < 1 + \epsilon\eta \tag{2.4.5.15}$$

Water pressure p is known in any point of the water layer thanks to the Bernouilli equation 2.3.4.3. In particular, we know the water pressure at the interface ($z = -1 + \epsilon\kappa_d\eta$):

$$p = \frac{1}{\epsilon} - (\phi^{(0)})_t - \kappa_d\eta - \frac{\epsilon}{2}\left(\frac{\partial\phi^{(0)}}{\partial x}\right)^2 + O(\kappa^2) \tag{2.4.5.16}$$

By differentiating this equation, we obtain:

$$\frac{\partial p}{\partial x} = -\frac{\partial^2\phi^{(0)}}{\partial x\partial t} - \kappa_d\frac{\partial\eta}{\partial x} - \frac{\epsilon}{2}\frac{\partial}{\partial x}\left(\frac{\partial\phi^{(0)}}{\partial x}\right)^2 + O(\kappa^2). \quad z = -1 + \epsilon\kappa_d\eta \tag{2.4.5.17}$$

From equation 2.3.3.3, we also know:

$$\frac{\partial\phi^{(0)}}{\partial t} + \frac{\epsilon}{2}\left(\frac{\partial\phi^{(0)}}{\partial x}\right)^2 = -\zeta + O(\kappa^2) \tag{2.4.5.18}$$

which is valid for all z since $\phi^{(0)}$ and ζ do not depend on the vertical coordinate. Combining equations 2.4.5.17 and 2.4.5.18, we get the water pressure gradient at the interface:

$$\frac{\partial p}{\partial x} = \frac{\partial\zeta}{\partial x} - \kappa_d\frac{\partial\eta}{\partial x} + O(\kappa^2), \quad z = -1 + \epsilon\kappa_d\eta \tag{2.4.5.19}$$

Combining equation 2.4.5.19 with 2.4.5.15, we finally obtain the mud pressure horizontal gradient in the entire mud layer:

$$\frac{\partial P}{\partial x} = \frac{\partial\zeta}{\partial x} - \kappa_d\frac{\partial\eta}{\partial x} + O(\kappa^2), \quad 0 < Z < 1 + \epsilon\eta \tag{2.4.5.20}$$

As a consequence, we can now substitute the mud pressure P from the horizontal momentum equation 2.4.3.12, for $0 < Z < 1 + \epsilon\eta$:

$$\boxed{\frac{\partial^2 U}{\partial Z^2} = Re\frac{d}{A}\left[\frac{\partial U}{\partial t} + \gamma\left(\frac{\partial \zeta}{\partial x} - \kappa_d\frac{\partial \eta}{\partial x}\right) + \epsilon\left(U\frac{\partial U}{\partial x} + V\frac{\partial U}{\partial Z}\right)\right] + O(\kappa^2)} \quad (2.4.5.21)$$

2.4.6 Bottom kinematic boundary conditions

At the bottom, we impose the no-slip boundary condition:

$$\boxed{U = V = 0}, \quad Z = 0 \quad (2.4.6.1)$$

2.5 Asymptotic equations in water and Newtonian mud

2.5.1 Equations at dominant orders

Water equations

Let us derive the asymptotic equations of ζ and η in water. We derive here these equations up to order $O(\kappa^2)$ because this may be helpful for further studies. However, later in this thesis, we will only make use of orders $O(1)$ and order $O(\kappa)$.

By combining equations 2.3.2.9 (for mass) and 2.3.3.6 (for momentum) obtained in water, we obtain the following approximate equation between ζ, η and $\bar{u}$:

$$\frac{\partial^2 \zeta}{\partial t^2} - \frac{\partial^2 \zeta}{\partial x^2} = \kappa_d \eta_{tt} - \epsilon\frac{\partial^2(\zeta\bar{u})}{\partial x \partial t} + \epsilon\frac{\partial}{\partial x}\left(\bar{u}\frac{\partial \bar{u}}{\partial x}\right) - \frac{\kappa^2}{3}\frac{\partial^4 \bar{u}}{\partial x^3 \partial t} + \epsilon\kappa_d\frac{\partial \eta\bar{u}}{\partial x \partial t} + O(\kappa^3) \quad (2.5.1.1)$$

To simplify this equation we use the leading order approximations of 2.3.2.9 and 2.3.3.6:

$$\begin{aligned} \frac{\partial \zeta}{\partial t} &= -\frac{\partial \bar{u}}{\partial x} + \kappa_d\frac{\partial \eta}{\partial t} + O(\kappa^2) \\ \frac{\partial \zeta}{\partial x} &= -\frac{\partial \bar{u}}{\partial t} + O(\kappa^2) \end{aligned} \quad (2.5.1.2)$$

As a consequence,

$$\begin{aligned}
-\epsilon\frac{\partial^2(\zeta\bar{u})}{\partial x\partial t} &= -\epsilon\frac{\partial}{\partial t}\left(\zeta\frac{\partial\bar{u}}{\partial x}+\bar{u}\frac{\partial\zeta}{\partial x}\right)\\
&= -\epsilon\frac{\partial}{\partial t}\left(-\zeta\frac{\partial\zeta}{\partial t}+\zeta\kappa_d\frac{\partial\eta}{\partial t}-\bar{u}\frac{\partial\bar{u}}{\partial t}+O(\kappa^2)\right)\\
&= \frac{\epsilon}{2}\left(\frac{\partial^2\zeta^2}{\partial t^2}+\frac{\partial\bar{u}^2}{\partial t^2}\right)-\epsilon\kappa_d\frac{\partial\zeta\eta_t}{\partial t}+O(\kappa^3)
\end{aligned} \tag{2.5.1.3}$$

and:

$$-\frac{\kappa^2}{3}\frac{\partial^4\bar{u}}{\partial x^3\partial t}=\frac{\kappa^2}{3}\frac{\partial^4\zeta}{\partial x^4}+O(\kappa^3) \tag{2.5.1.4}$$

Thus, equation 2.5.1.1 can be written:

$$\begin{aligned}
\frac{\partial^2\zeta}{\partial t^2}-\frac{\partial^2\zeta}{\partial x^2} =&\kappa_d\frac{\partial^2\eta}{\partial t^2}+\frac{\epsilon}{2}\left(\frac{\partial^2\bar{u}^2}{\partial x^2}+\frac{\partial^2\bar{u}^2}{\partial t^2}+\frac{\partial^2\zeta^2}{\partial t^2}\right)+\frac{\kappa^2}{3}\frac{\partial^4\zeta}{\partial x^4}-\epsilon\kappa_d\frac{\partial\zeta\eta_t}{\partial t}\\
&+\epsilon\kappa_d\frac{\partial\eta\bar{u}}{\partial x\partial t}+O(\kappa^3)
\end{aligned} \tag{2.5.1.5}$$

Now let us expand the functions ζ and $\bar{u}$ as power series:

$$\begin{aligned}
\zeta &= \zeta^{(0)}+\kappa\zeta^{(1)}+\kappa^2\zeta^{(2)}+...\\
\bar{u} &= \bar{u}^{(0)}+\kappa\bar{u}^{(1)}+\kappa^2\bar{u}^{(2)}+...
\end{aligned} \tag{2.5.1.6}$$

Because we expect the typical distance of the mud induced damping to be $\kappa x = O(1)$, let us also introduce the slow coordinate X:

$$X=\kappa x \tag{2.5.1.7}$$

Applying the technique of multiple scales, we have:

$$\begin{aligned}
\frac{\partial}{\partial x} &= \frac{\partial}{\partial x}+\kappa\frac{\partial}{\partial X}\\
\frac{\partial^4}{\partial x^4} &= \frac{\partial^4}{\partial x^4}+4\kappa\frac{\partial^4}{\partial x^3\partial X}+O(\kappa^2)
\end{aligned} \tag{2.5.1.8}$$

So the equation 2.5.1.5 becomes, with the multiple scale:

$$\begin{aligned}
\frac{\partial^2\zeta}{\partial t^2}-\frac{\partial^2\zeta}{\partial x^2}-2\kappa\frac{\partial^2\zeta}{\partial x\partial X}-\kappa^2\frac{\partial^2\zeta}{\partial X^2} = \kappa_d\frac{\partial^2\eta}{\partial t^2}+\frac{\epsilon}{2}\left(\frac{\partial^2\bar{u}^2}{\partial x^2}+2\kappa\frac{\partial^2\bar{u}^2}{\partial x\partial X}+\frac{\partial^2\bar{u}^2}{\partial t^2}+\frac{\partial^2\zeta^2}{\partial t^2}\right)\\
+\frac{\kappa^2}{3}\frac{\partial^4\zeta}{\partial x^4}-\epsilon\kappa_d\frac{\partial\zeta\eta_t}{\partial t}+\epsilon\kappa_d\frac{\partial^2(\bar{u}\eta)}{\partial x\partial t}+O(\kappa^3)
\end{aligned} \tag{2.5.1.9}$$

which can be written:

$$\frac{\partial^2\zeta}{\partial t^2}-\frac{\partial^2\zeta}{\partial x^2}=2\kappa\frac{\partial^2\zeta}{\partial x\partial X}+\kappa_d\frac{\partial^2\eta}{\partial t^2}+\frac{\epsilon}{2}\left(\frac{\partial^2\bar{u}^2}{\partial x^2}+\frac{\partial^2\bar{u}^2}{\partial t^2}+\frac{\partial^2\zeta^2}{\partial t^2}\right)$$
$$+\kappa^2\frac{\partial^2\zeta}{\partial X^2}+\epsilon\kappa\frac{\partial^2\bar{u}^2}{\partial x\partial X}+\frac{\kappa^2}{3}\frac{\partial^4\zeta}{\partial x^4}-\epsilon\kappa_d\frac{\partial\zeta\eta_t}{\partial t}+\epsilon\kappa_d\frac{\partial^2(\bar{u}\eta)}{\partial x\partial t}+O(\kappa^3) \tag{2.5.1.10}$$

From this equation, we deduce for dominant orders:

- at order $O(1)$

$$\frac{\partial^2\zeta^{(0)}}{\partial t^2}-\frac{\partial^2\zeta^{(0)}}{\partial x^2}=0 \tag{2.5.1.11}$$

- at order $O(\kappa)$

$$\frac{\partial^2\zeta^{(1)}}{\partial t^2}-\frac{\partial^2\zeta^{(1)}}{\partial x^2}=2\frac{\partial^2\zeta^{(0)}}{\partial x\partial X}+\frac{\kappa_d}{\kappa}\frac{\partial^2\eta^{(0)}}{\partial t^2}+\frac{3\epsilon}{2\kappa}\frac{\partial^2(\zeta^{(0)})^2}{\partial t^2} \tag{2.5.1.12}$$

  where equation 2.5.1.12 is obtained after using the following relation valid to leading order:

$$\frac{\partial^2(\bar{u^{(0)}})^2}{\partial x^2}+\frac{\partial^2(\bar{u_0}^{(0)})^2}{\partial t^2}+\frac{\partial^2(\zeta^{(0)})^2}{\partial t^2}=3\frac{\partial^2(\zeta^{(0)})^2}{\partial t^2} \tag{2.5.1.13}$$

- at order $O(\kappa^2)$

$$\begin{aligned}\frac{\partial^2\zeta^{(2)}}{\partial t^2}-\frac{\partial^2\zeta^{(2)}}{\partial x^2}=&2\frac{\partial^2\zeta^{(1)}}{\partial X\partial x}+\frac{\kappa_d}{\kappa}\frac{\partial^2\eta^{(1)}}{\partial t^2}\\&+\frac{\epsilon}{\kappa}\left(\frac{\partial^2(\bar{u}^{(0)}\bar{u}^{(1)})}{\partial x^2}+\frac{\partial^2(\bar{u}^{(0)}\bar{u}^{(1)})}{\partial t^2}+\frac{\partial^2(\zeta^{(0)}\zeta^{(1)})}{\partial t^2}\right)\\&+\frac{\partial^2\zeta^{(0)}}{\partial X^2}+\frac{\epsilon}{\kappa}\frac{\partial^2(u^{(0)})^2}{\partial x\partial X}+\frac{1}{3}\frac{\partial^4\zeta^{(0)}}{\partial x^4}-\frac{\epsilon\kappa_d}{\kappa^2}\frac{\partial\zeta^{(0)}(\eta^{(0)})_t}{\partial t}\\&+\frac{\epsilon\kappa_d}{\kappa^2}\frac{\partial^2\bar{u}^{(0)}\eta^{(0)}}{\partial x\partial t}\end{aligned} \tag{2.5.1.14}$$

We carried the calculations up to order $O(\kappa^2)$ because it may be useful for later studies, but we won't use these equations in the rest of this thesis.

From now on, we will only carry calculations further for the orders $O(1)$ and $O(\kappa)$ (2.5.1.11 and 2.5.1.12).

Mud equations

Let us find another coupling equations between the surface and the interface, ζ and η, derived from the mud equations. The momentum equation 2.4.5.21 in mud gives:

$$\left(\alpha\frac{\partial^2}{\partial Z^2}-\frac{\partial}{\partial t}\right)U=\gamma\left(\frac{\partial\zeta}{\partial x}-\kappa_d\frac{\partial\eta}{\partial x}\right)+\epsilon\left(U\frac{\partial U}{\partial x}+V\frac{\partial U}{\partial Z}\right)+O(\kappa^2) \qquad 0<Z<1+\epsilon\eta \tag{2.5.1.15}$$

where:

$$\boxed{\alpha=\frac{\epsilon}{\kappa_d Re}} \tag{2.5.1.16}$$

which is at least of order $O(1)$.

As in water, we introduce the multiple scale coordinates x and $X=\kappa x$, so that equation 2.5.1.15 becomes:

$$\begin{aligned}\left(\alpha\frac{\partial^2}{\partial Z^2}-\frac{\partial}{\partial t}\right)U=&\gamma\left(\frac{\partial\zeta}{\partial x}+\kappa\frac{\partial\zeta}{\partial X}-\kappa_d\frac{\partial\eta}{\partial x}\right)\\&+\epsilon\left(U\frac{\partial U}{\partial x}+V\frac{\partial U}{\partial Z}\right)+O(\kappa^3)\end{aligned} \tag{2.5.1.17}$$

The continuity equation 2.4.2.2 becomes:

$$\frac{\partial(U)}{\partial x}+\kappa\frac{\partial(U)}{\partial X}+\frac{\partial(V)}{\partial Z}=0 \tag{2.5.1.18}$$

and the interface kinematic boundary condition 2.4.1.2:

$$\frac{\partial\eta}{\partial t}=V-\epsilon\frac{\partial\eta}{\partial x}U \tag{2.5.1.19}$$

By expanding U and V in ascending powers of κ, we write:

$$\begin{aligned}U&=U^{(0)}+\kappa U^{(1)}+O(\kappa^2)\\V&=V^{(0)}+\kappa V^{(1)}+O(\kappa^2)\end{aligned} \tag{2.5.1.20}$$

We can now deduce the dominant orders of equations 2.5.1.17, 2.5.1.18 and 2.5.1.19:

- at $O(\kappa^0)$:

$$\begin{aligned}\left(\frac{\partial}{\partial t}-\alpha\frac{\partial^2}{\partial Z^2}\right)U^{(0)} &= -\gamma\frac{\partial\zeta^{(0)}}{\partial x}, \quad 0<Z<1\\ \frac{\partial U^{(0)}}{\partial x}+\frac{\partial V^{(0)}}{\partial Z} &= 0, \quad 0<Z<1\\ \frac{\partial\eta_0}{\partial t} &= V^{(0)}, \quad Z=1\end{aligned} \tag{2.5.1.21}$$

- at $O(\kappa)$:

$$\begin{aligned}\left(\frac{\partial}{\partial t}-\alpha\frac{\partial^2}{\partial Z^2}\right)U^{(1)} &= -\gamma\frac{\partial\zeta^{(1)}}{\partial x}-\gamma\frac{\partial\zeta^{(0)}}{\partial X}+\gamma\frac{\kappa_d}{\kappa}\frac{\partial\eta^{(0)}}{\partial x}-\frac{\epsilon}{\kappa}\left(U^{(0)}\frac{\partial U^{(0)}}{\partial x}+V^{(0)}\frac{\partial U^{(0)}}{\partial Z}\right)\\ \frac{\partial U^{(1)}}{\partial x}+\frac{\partial U^{(0)}}{\partial X}+\frac{\partial V^{(1)}}{\partial Z} &= 0, \quad 0<Z<1\\ \frac{\partial\eta^{(1)}}{\partial t} &= V^{(1)}, \quad Z=1\end{aligned} \tag{2.5.1.22}$$

2.5.2 Equation and solution at $O(\kappa^0)$

Water equations

Because equation 2.5.1.14 clearly involves non-linear terms, we consider the evolution of a train of harmonic waves a the leading order:

$$\boxed{\zeta^{(0)}=\frac{1}{2}\sum_{m=-\infty}^{+\infty}A_m(X)e^{i\theta_m}} \qquad \boxed{\eta^{(0)}=\frac{1}{2}\sum_{m=-\infty}^{+\infty}B_m(X)e^{i\theta_m}} \tag{2.5.2.1}$$

where $\theta_m = m(x-t)$. We shall assume that $A_0 = B_0 = 0$.

Mud equations

We adopt for the horizontal and vertical velocities in mud at the zeroth order the form we used in 2.5.2.1:

$$\begin{aligned}U^{(0)} &= \frac{1}{2}\sum_{m=-\infty}^{\infty}U_m^{(0)}(Z)e^{i\theta_m}\\ V^{(0)} &= \frac{1}{2}\sum_{m=-\infty}^{\infty}V_m^{(0)}(Z)e^{i\theta_m}\end{aligned} \tag{2.5.2.2}$$

Then from the equation 2.5.1.21 we deduce an equation for $U_m^{(0)}(Z)$:

$$\frac{d^2U_m^{(0)}}{dZ^2} - {\sigma_m}^2 U_m^{(0)} = -\sigma_m^2 \gamma A_m \tag{2.5.2.3}$$

where

$$\boxed{{\sigma_m}^2 = -i\frac{m}{\alpha}} \tag{2.5.2.4}$$

We can solve exactly this second order differential equation by using the boundary conditions:

$$\begin{aligned} U_m^{(0)} &= 0, \qquad Z = 0 \\ \frac{\partial (U)_m^{(0)}}{\partial Z} &= 0, \qquad Z = 1 \end{aligned} \tag{2.5.2.5}$$

In the end we get:

$$U_m^{(0)} = \gamma A_m[1 - \cosh(\sigma_m Z) + \tanh(\sigma_m)\sinh(\sigma_m Z)] \tag{2.5.2.6}$$

From the continuity equation and the boundary conditions of 2.5.1.21 we can extract the following equations for the vertical velocity:

$$\begin{aligned} \frac{dV_m^{(0)}}{dZ} &= -imU_m^{(0)} \\ V_m^{(0)}(0) &= 0, \quad Z = 0 \end{aligned} \tag{2.5.2.7}$$

As a consequence, we can easily deduce the explicit expression of the $V_m^{(0)}$:

$$V_m^{(0)} = -i\frac{m\gamma A_m}{\sigma_m}[\sigma_m Z - \sinh(\sigma_m Z) + \tanh(\sigma_m)(\cosh(\sigma_m Z) - 1)] \tag{2.5.2.8}$$

From the kinematic boundary condition at the interface in mud, we can now deduce the interface motion:

$$\begin{aligned} B_m &= -\frac{1}{im} V_m^{(0)}(Z = 1) \\ &= \gamma A_m G(\sigma_m) \end{aligned} \tag{2.5.2.9}$$

with

$$G(\sigma_m) = 1 - \frac{\tanh(\sigma_m)}{\sigma_m} \tag{2.5.2.10}$$

As a conclusion we have:

$$\boxed{B_m = \gamma A_m \left(1 - \frac{\tanh(\sigma_m)}{\sigma_m}\right)} \tag{2.5.2.11}$$

where ${\sigma_m}^2 = -i\frac{m}{\alpha}$, $\alpha = \frac{\epsilon}{\kappa_d Re}$ and $\gamma = \frac{\rho^{(w)}}{\rho_M}$.

This term

$$G(\sigma_m) = 1 - \frac{\tanh(\sigma_m)}{\sigma_m} \tag{2.5.2.12}$$

will later be studied as a function of σ and m.

2.5.3 Equation and solution at $O(\kappa)$

Water equations

At order $O(\kappa)$, we have from 2.5.1.12:

$$\frac{\partial^2\zeta^{(1)}}{\partial t^2} - \frac{\partial^2\zeta^{(1)}}{\partial x^2} = 2\frac{\partial^2\zeta^{(0)}}{\partial x \partial X} + \frac{\kappa_d}{\kappa}\frac{\partial^2\eta^{(0)}}{\partial t^2} + \frac{3\epsilon}{2\kappa}\frac{\partial^2(\zeta^{(0)})^2}{\partial t^2} \tag{2.5.3.1}$$

By following the same procedure as in "Theory and Applications of Ocean Surface Waves" by Mei, Stiassnie and Yue, we know that:

$$\frac{3\epsilon}{2\kappa}\frac{\partial^2(\zeta^{(0)})^2}{\partial t^2} = \frac{\epsilon}{\kappa}\sum_{m=1}^{\infty} -\frac{3}{8}m^2 e^{i\theta_m}\left[\sum_{l=1}^{\infty} 2A_l^* A_{m+1l} + \sum_{l=1}^{[m/2]} \alpha_l A_l A_{m-l}\right] + c.c. \tag{2.5.3.2}$$

where $[m/2]$ is the integer part of $m/2$ and α_l is a coefficient equal to 1 for $l = [m/2]$ and equal to 2 otherwise. Use has been made of the assumption that $A_0 = B_0 = 0$.

We also have

$$\begin{aligned} 2\frac{\partial^2\zeta^{(0)}}{\partial x \partial X} &= \sum_{m=1}^{\infty} im\frac{dA_m}{dX}e^{i\theta_m} + c.c. \\ \frac{\partial^2\eta^{(0)}}{\partial t^2} &= -\frac{1}{2}\sum_{m=1}^{\infty} m^2 B_m e^{i\theta_m} + c.c. \end{aligned} \tag{2.5.3.3}$$

combining all these results, we can rewrite equation 2.5.3.1:

$$\begin{aligned} \frac{\partial^2\zeta^{(1)}}{\partial t^2} - \frac{\partial^2\zeta^{(1)}}{\partial x^2} = &\sum_{m=1}^{\infty} im\frac{dA_m}{dX}e^{i\theta_m} + \frac{\epsilon}{\kappa}\sum_{m=1}^{\infty} -\frac{3}{8}m^2 e^{i\theta_m}\left[\sum_{l=1}^{\infty} 2A_l^* A_{m+l} + \sum_{l=1}^{[m/2]} \alpha_l A_l A_{m-l}\right] \\ &- \frac{1}{2}\frac{\kappa_d}{\kappa}\sum_{m=1}^{\infty} m^2 B_m e^{i\theta_m} + c.c. \end{aligned} \tag{2.5.3.4}$$

To ensure solvability of this last equation, we must remove the secular terms propor-

tional to $e^{i\theta_m}$, yielding the differential equations:

$$\frac{dA_m}{dX} = -\frac{im}{2}\frac{\kappa_d}{\kappa}B_m - \frac{3i}{8}\frac{\epsilon}{\kappa}m\left[\sum_{l=1}^{\infty} 2A_l^* A_{m+1l} + \sum_{l=1}^{[m/2]} \alpha_l A_l A_{m-l}\right], \quad m = 1, 2, 3, ... \tag{2.5.3.5}$$

Combining this result with 2.5.2.11, we finally obtain the differential equation for the A_m, for all $m = 1, 2, 3, ...$:

$$\boxed{\frac{dA_m}{dX} = -\frac{i\gamma m}{2}\frac{\kappa_d}{\kappa}\left(1 - \frac{tanh(\sigma_m)}{\sigma_m}\right)A_m - \frac{3i}{8}\frac{\epsilon}{\kappa}m\left[\sum_{l=1}^{\infty} 2A_l^* A_{m+l} + \sum_{l=1}^{[m/2]} \alpha_l A_l A_{m-l}\right]} \tag{2.5.3.6}$$

Mud equations

We study the order $O(\kappa)$ of the mud equations because a very interesting drift phenomenon appears due to non-linearity.

We had from equation 2.5.1.22:

$$\left(\frac{\partial}{\partial t} - \alpha\frac{\partial^2}{\partial Z^2}\right)U^{(1)} = -\gamma\frac{\partial\zeta^{(1)}}{\partial x} - \gamma\frac{\partial\zeta^{(0)}}{\partial X} + \gamma\frac{\kappa_d}{\kappa}\frac{\partial\eta^{(0)}}{\partial x} - \frac{\epsilon}{\kappa}\left(U^{(0)}\frac{\partial U^{(0)}}{\partial x} + V^{(0)}\frac{\partial U^{(0)}}{\partial Z}\right) \tag{2.5.3.7}$$

In this thesis we shall not pursue the higher harmonics of ζ_1 and η_1 and focus only on the zeroth harmonic of $U^{(1)}$ which corresponds to the drift current, governed by

$$\begin{aligned}\frac{\partial^2 U_0^{(1)}}{\partial Z^2} =& \frac{Re\kappa_d}{2\kappa}\sum_{m=1}^{\infty}\Big[U_m^{(0)}(-im)U_{-m}^{(0)} + U_{-m}^{(0)}(im)U_m^{(0)} \\ &+ V_m^{(0)}\frac{\partial U_{(-m)}^{(0)}}{\partial Z} + V_{-m}^{(0)}\frac{\partial U_m^{(0)}}{\partial Z}\Big]\end{aligned} \tag{2.5.3.8}$$

The preceding equation can be simplified:

$$\frac{\partial^2 U_0^{(1)}}{\partial Z^2} = \frac{Re\kappa_d}{2\kappa}\sum_{m=1}^{\infty}\left[V_m^{(0)}\frac{\partial U_{-m}^{(0)}}{\partial Z} + V_{-m}^{(0)}\frac{\partial U_m^{(0)}}{\partial Z}\right] \tag{2.5.3.9}$$

Knowing that $V_{-m}^{(0)} = V_m^{(0)^*}$ and $U_{-m}^{(0)} = U_m^{(0)^*}$, we obtain:

$$\frac{\partial^2 U_0^{(1)}}{\partial Z^2} = \frac{Re\kappa_d}{\kappa}\sum_{m=1}^{\infty}\Re\left[V_{-m}^{(0)}\frac{\partial U_m^{(0)}}{\partial Z}\right] \tag{2.5.3.10}$$

Equation 2.5.3.10 will be integrated later to give $U_0^{(1)}$. We note that this drift only appears at the order $O(\kappa)$, and is as a consequence small.

2.6 Further details

2.6.1 Surface and the interface

We truncate the series in 2.5.3.6 , in order to obtain a differential equation for the A_m, for all m:

$$\boxed{\frac{dA_m}{dX} = -\frac{i\gamma m}{2}\frac{\kappa_d}{\kappa}\left(1 - \frac{\tanh(\sigma_m)}{\sigma_m}\right)A_m - \frac{3i}{8}\frac{\epsilon}{\kappa}m\left(\sum_{l=1}^{n-m} 2A_l^* A_{m+l} + \sum_{l=1}^{[m/2]} \alpha_l A_l A_{m-l}\right)} \tag{2.6.1.1}$$

This truncated differential system is true for $0 < m \leq n$.

2.6.2 Drift current in mud

We also truncate the series in 2.5.3.10 for the drift velocity:

$$\frac{\partial^2 U_0^{(1)}}{\partial Z^2} = \frac{Re\kappa_d}{\kappa}\sum_{m=1}^{n} \Re\left[V_{-m}^{(0)}\frac{\partial U_{(m)}^{(0)}}{\partial Z}\right] \tag{2.6.2.1}$$

On the right-hand side we get from (2.5.2.6):

$$\frac{\partial U_m^{(0)}}{\partial Z} = \gamma A_m[-\sigma_m \sinh(\sigma_m Z) + \sigma_m \tanh(\sigma_m)\cosh(\sigma_m Z)] \tag{2.6.2.2}$$

and from (2.5.2.8)

$$V_{-m}^{(0)} = i\frac{m\gamma A_m^*}{\sigma_m^*}[\sigma_m^* Z - \sinh(\sigma_m^* Z) + \tanh(\sigma_m^*)(\cosh(\sigma_m^* Z) - 1)] \tag{2.6.2.3}$$

Combining 2.6.2.2, 2.6.2.3 and 2.6.2.1, we obtain:

$$\begin{aligned}\frac{\partial^2 U_0^{(1)}}{\partial Z^2} =& \frac{Re\kappa_d}{\kappa}\sum_{m=1}^{n} \Re\Big[i\frac{m\gamma A_m^*}{\sigma_m^*}[\sigma_m^* Z - \sinh(\sigma_m^* Z) + \tanh(\sigma_m^*)(\cosh(\sigma_m^* Z) - 1)] \\ & \gamma A_m[-\sigma_m \sinh(\sigma_m Z) + \sigma_m \tanh(\sigma_m)\cosh(\sigma_m Z)]\Big]\end{aligned} \tag{2.6.2.4}$$

which can be simplified:

$$\frac{\partial^2 U_0^{(1)}}{\partial Z^2} = -\gamma^2 \frac{Re\kappa_d}{\kappa} \sum_{m=1}^{n} |A_m|^2 \Im\Big[\frac{m}{\sigma_m^*}[\sigma_m^* Z - \sinh(\sigma_m^* Z) + \tanh(\sigma_m^*)(\cosh(\sigma_m^* Z) - 1)]$$
$$[-\sigma_m \sinh(\sigma_m Z) + \sigma_m \tanh(\sigma_m)\cosh(\sigma_m Z)]\Big] \tag{2.6.2.5}$$

and expanded

$$\begin{aligned}\frac{\partial^2 U_0^{(1)}}{\partial Z^2} = &-\gamma^2 \frac{Re\kappa_d}{\kappa} \sum_{m=1}^{n} |A_m|^2 \Im\Big[\frac{m}{\sigma_m^*}\Big(-\sigma_m\sigma_m^* Z \sinh(\sigma_m Z) + \sigma\sigma_m^* Z \tanh(\sigma_m)\cosh(\sigma_m Z) \\ &+ \sigma_m \sinh(\sigma_m^* Z)\sinh(\sigma_m Z) - \sigma_m \tanh(\sigma_m)\sinh(\sigma_m^* Z)\cosh(\sigma_m Z) \\ &- (\tanh(\sigma_m))^* \sigma_m \cosh(\sigma_m^* Z)\sinh(\sigma_m Z) \\ &+ \sigma_m \tanh(\sigma_m)(\tanh(\sigma_m))^* \cosh(\sigma_m Z)\cosh(\sigma_m^* Z) + (\tanh(\sigma_m))^* \sigma_m \sinh(\sigma_m Z) \\ &- \sigma_m \tanh(\sigma_m)(\tanh(\sigma_m))^* \cosh(\sigma_m Z)\Big)\Big]\end{aligned} \tag{2.6.2.6}$$

We write $\sigma_m = \sigma_m^R + i\sigma_m^I$, σ_m^R and σ_m^I reals.

Let us first integrate once. We use the fact that $\sigma_m + \sigma_m^* = 2\sigma_m^R$ and $\sigma_m - \sigma_m^* = 2i\sigma_m^I$:

$$\begin{aligned}\frac{\partial U_0^{(1)}}{\partial Z} = &-\gamma^2 \frac{Re\kappa_d}{\kappa} \sum_{m=1}^{n} |A_m|^2 \Im\Big[\frac{m}{\sigma_m^*}\Big[-\sigma_m^*\Big(Z\cosh(\sigma_m Z) - \frac{\sinh(\sigma_m Z)}{\sigma_m}\Big) \\ &+ \sigma_m^* \tanh(\sigma_m)\Big(Z\sinh(\sigma_m Z) - \frac{\cosh(\sigma_m Z)}{\sigma_m}\Big) \\ &+ \frac{\sinh(2\sigma_m^R Z)}{4\sigma_m^R}\sigma_m(1 + \tanh(\sigma_m)(\tanh(\sigma_m))^*) \\ &+ \frac{\sinh(2i\sigma_m^I Z)}{4i\sigma_m^I}\sigma_m(\tanh(\sigma_m)(\tanh(\sigma_m))^* - 1) \\ &- \frac{\cosh(2\sigma_m^R Z)}{4\sigma_m^R}\sigma_m(\tanh(\sigma_m) + (\tanh(\sigma_m))^*) \\ &+ \frac{\cosh(2i\sigma_m^I Z)}{4i\sigma_m^I}\sigma_m(\tanh(\sigma_m) - (\tanh(\sigma_m))^*) + (\tanh(\sigma_m))^* \cosh(\sigma_m Z) \\ &- \tanh(\sigma_m)(\tanh(\sigma_m))^* \sinh(\sigma_m Z) + C_m^{(1)}\Big]\Big]\end{aligned} \tag{2.6.2.7}$$

Integrating again, we get the expression of $U_0^{(1)}$:

$$\begin{aligned}U_0^{(1)} = &-\gamma^2\frac{Re\kappa_d}{\kappa}\sum_{m=1}^{n}|A_m|^2\Im\Big[\frac{m}{\sigma_m^*}\Big[-\sigma^*\Big(\frac{Z\sinh(\sigma_m Z)}{\sigma_m}-2\frac{\cosh(\sigma_m Z)}{\sigma_m^2}\Big)\\&+\sigma_m^*\tanh(\sigma_m)\Big(\frac{Z\cosh(\sigma_m Z)}{\sigma_m}-2\frac{\sinh(\sigma_m Z)}{\sigma_m^2}\Big)\\&+\frac{\cosh(2\sigma_m^R Z)}{8(\sigma_m^R)^2}\sigma_m(1+\tanh(\sigma_m)(\tanh(\sigma_m))^*)\\&+\frac{\cosh(2i\sigma_m^I Z)}{8(\sigma_m^I)^2}\sigma_m(\tanh(\sigma_m)(\tanh(\sigma_m))^*-1)\\&-\frac{\sinh(2\sigma_m^R Z)}{8(\sigma_m^R)^2}\sigma_m(\tanh(\sigma_m)+(\tanh(\sigma_m))^*)\\&+\frac{\sinh(2i\sigma_m^I Z)}{8(\sigma_m^I)^2}\sigma_m(\tanh(\sigma_m)-(\tanh(\sigma_m))^*)+(\tanh(\sigma_m))^*\frac{\sinh(\sigma_m Z)}{\sigma_m}\\&-\tanh(\sigma_m)(\tanh(\sigma_m))^*\frac{\cosh(\sigma_m Z)}{\sigma_m}+C_m^{(1)}Z+C_m^{(2)}\Big]\Big]\end{aligned} \tag{2.6.2.8}$$

The integration constants $C_m^{(1)}$ and $C_m^{(2)}$ will now be determined from the boundary conditions.

From equation 2.4.6.1, we know that:

$$U^{(1)}(Z=0)=0 \tag{2.6.2.9}$$

As a consequence, we deduce the value of $C_m^{(2)}$:

$$\begin{aligned}C_m^{(2)} = &-\frac{2\sigma_m^*}{\sigma_m^2}-\frac{\sigma_m(1+\tanh(\sigma_m)(\tanh(\sigma_m))^*)}{8(\sigma_m^R)^2}-\frac{\sigma_m(1-\tanh(\sigma_m)(\tanh(\sigma_m))^*)}{8(\sigma_m^I)^2}\\&+\frac{\tanh(\sigma_m)(\tanh(\sigma_m))^*}{\sigma_m}\end{aligned} \tag{2.6.2.10}$$

We now make use of the interface boundary condition 2.4.5.13. From this equation, we know that:

$$\frac{\partial U^{(1)}}{\partial Z}\Big|_{Z=1}=-\frac{\epsilon}{\kappa}\eta^{(0)}\frac{\partial^2 U^{(0)}}{\partial Z^2}\Big|_{Z=1} \tag{2.6.2.11}$$

As a consequence, we know that:

$$\begin{aligned}\frac{\partial U_0^{(1)}}{\partial Z}\Big|_{Z=1} &= -\frac{\epsilon}{\kappa}\frac{1}{4}\sum_{m=1}^{\infty}\left[B_m\frac{\partial^2 U_{-m}^{(0)}}{\partial Z^2}\Big|_{Z=1} + B_{-m}\frac{\partial^2 U_m^{(0)}}{\partial Z^2}\Big|_{Z=1}\right] \\ &= -\frac{\epsilon}{\kappa}\frac{1}{4}\sum_{m=1}^{\infty}\left[B_m\Big(\frac{\partial^2 U_m^{(0)}}{\partial Z^2}\Big|_{Z=1}\Big)^* + (B_m)^*\frac{\partial^2 U_m^{(0)}}{\partial Z^2}\Big|_{Z=1}\right] \\ &= -\frac{\epsilon}{\kappa}\frac{1}{2}\sum_{m=1}^{\infty}\Re\left[B_m\Big(\frac{\partial^2 U_m^{(0)}}{\partial Z^2}\Big|_{Z=1}\Big)^*\right]\end{aligned} \tag{2.6.2.12}$$

Knowing that:

$$B_m = \gamma A_m G(\sigma_m) \tag{2.6.2.13}$$

and:

$$\frac{\partial^2 U_m^{(0)}}{\partial Z^2}\Big|_{Z=1} = -\gamma A_m \sigma_m^2 \mathrm{sech}(\sigma_m) \tag{2.6.2.14}$$

equation 2.6.2.12 becomes:

$$\begin{aligned}\frac{\partial U_0^{(1)}}{\partial Z}\Big|_{Z=1} &= \frac{\epsilon}{\kappa}\frac{1}{2}\sum_{m=1}^{\infty}\Re\left[\gamma A_m G(\sigma_m)\gamma A_m^*(\sigma_m^*)^2\mathrm{sech}(\sigma_m^*)\right] \\ &= \frac{\epsilon\gamma^2}{2\kappa}\sum_{m=1}^{\infty}|A_m|^2\Re\left[G(\sigma_m)(\sigma_m^*)^2\mathrm{sech}(\sigma_m^*)\right] \\ &= \frac{\epsilon\gamma^2}{2\kappa}\sum_{m=1}^{\infty}|A_m|^2\Im\left[iG(\sigma_m)(\sigma_m^*)^2\mathrm{sech}(\sigma_m^*)\right]\end{aligned} \tag{2.6.2.15}$$

Let us truncate this last equation:

$$\frac{\partial U_0^{(1)}}{\partial Z}\Big|_{(Z=1)} = \frac{\epsilon\gamma^2}{2\kappa}\sum_{m=1}^{n}|A_m|^2\Im\left[iG(\sigma_m)(\sigma_m^*)^2\mathrm{sech}(\sigma_m^*)\right] \tag{2.6.2.16}$$

From equation 2.6.2.7, we deduce the condition that $C_m^{(1)}$ needs to meet in order to

respect this boundary condition:

$$\begin{aligned}
&\gamma^2\frac{Re\kappa_d}{\kappa}\Im\Big[\frac{m}{\sigma_m^*}\Big(\sigma_m^*\Big(\cosh(\sigma_m)-\frac{\sinh(\sigma_m)}{\sigma_m}\Big)-\sigma_m^*\tanh(\sigma_m)\Big(\sinh(\sigma_m)-\frac{\cosh(\sigma_m)}{\sigma_m}\Big)\\
&-\frac{\sinh(2\sigma_m^R)}{4\sigma_m^R}\sigma_m(1+\tanh(\sigma_m)(\tanh(\sigma_m))^*)\\
&-\frac{\sinh(2i\sigma_m^I)}{4i\sigma_m^I}\sigma_m(\tanh(\sigma_m)(\tanh(\sigma_m))^*-1)\\
&+\frac{\cosh(2\sigma_m^R)}{4\sigma_m^R}\sigma_m(\tanh(\sigma_m)+(\tanh(\sigma_m))^*)\\
&-\frac{\cosh(2i\sigma_m^I)}{4i\sigma_m^I}\sigma_m(\tanh(\sigma_m)-(\tanh(\sigma_m))^*)\\
&-(\tanh(\sigma_m))^*\cosh(\sigma_m)+\tanh(\sigma_m)(\tanh(\sigma_m))^*\sinh(\sigma_m)-C_m^{(1)}\Big)\Big]\\
&=\frac{\epsilon\gamma^2}{2\kappa}\Im\left[iG(\sigma_m)(\sigma_m^*)^2\mathrm{sech}(\sigma_m^*)\right]
\end{aligned}\tag{2.6.2.17}$$

We finally obtain the value of $C_m^{(1)}$:

$$\begin{aligned}
C_m^{(1)}=&-\frac{\epsilon\sigma_m^*}{2Re\kappa_d m}iG(\sigma_m)(\sigma_m^*)^2\mathrm{sech}(\sigma_m^*)\\
&+\sigma_m^*\Big(\cosh(\sigma_m)-\frac{\sinh(\sigma_m)}{\sigma_m}\Big)-\sigma_m^*\tanh(\sigma_m)\Big(\sinh(\sigma_m)-\frac{\cosh(\sigma_m)}{\sigma_m}\Big)\\
&-\frac{\sinh(2\sigma_m^R)}{4\sigma_m^R}\sigma_m(1+\tanh(\sigma_m)(\tanh(\sigma_m))^*)\\
&-\frac{\sinh(2i\sigma_m^I)}{4i\sigma_m^I}\sigma_m(\tanh(\sigma_m)(\tanh(\sigma_m))^*-1)\\
&+\frac{\cosh(2\sigma_m^R)}{4\sigma_m^R}\sigma_m(\tanh(\sigma_m)+(\tanh(\sigma_m))^*)\\
&-\frac{\cosh(2i\sigma_m^I)}{4i\sigma_m^I}\sigma_m(\tanh(\sigma_m)-(\tanh(\sigma_m))^*)\\
&-(\tanh(\sigma_m))^*\cosh(\sigma_m)+\tanh(\sigma_m)(\tanh(\sigma_m))^*\sinh(\sigma_m)
\end{aligned}\tag{2.6.2.18}$$

The drift current is now found. We notice that it is a sum of the $|A_m|^2$ multiplied by coefficients depending on γ, κ, κ_d, ϵ and the σ_m, we deduce that the result of the A_m will depend on the values:

$$g, \rho_W,\ \rho_M,\ A,\ \bar{h},\ d.\ \omega',\ \mu \tag{2.6.2.19}$$

where g and ρ_W are fixed, ρ_M and the μ depend on the Newtonian mud, and A, $\bar{h}$,

ω' and d depend on the geometry and the surface wave. .

2.6.3 Energy variation in water

We recall the differential system:

$$\frac{dA_m}{dX} + \frac{3i}{8}\frac{\epsilon}{\kappa}m\left(\sum_{l=1}^{\infty} 2A_l^* A_{m+l} + \sum_{l=1}^{[m/2]} \alpha_l A_l A_{m-l}\right) + \frac{i\gamma}{2}\frac{\kappa_d}{\kappa}m\left(1 - \frac{\tanh(\sigma_m)}{\sigma_m}\right)A_m = 0 \tag{2.6.3.1}$$

which governs the free surface motion.

In [8], G. Grataloup and C.C. Mei demonstrated that if the differential equation describing the free surface is:

$$\frac{dA_m}{dX} + \beta_m A_m - \frac{im^3}{6}A_m + \frac{3i}{8}\frac{\epsilon}{\kappa}m\left(\sum_{l=1}^{\infty} 2A_l^* A_{m+l} + \sum_{l=1}^{[m/2]} \alpha_l A_l A_{m-l}\right) = 0, \tag{2.6.3.2}$$

then the general relation on the first-order wave-energy is:

$$\frac{d}{dX}\Big[\sum_{m=1}^{n} |A_m|^2\Big] = -2\sum_{m=1}^{n} \Re(\beta_m)|A_m|^2 \tag{2.6.3.3}$$

Indeed, in equation 2.6.3.2, β_m represents a dissipation source. That is why the total wave energy at the leading order decreases with relation to β_m.

In our case of a flat bottom with a thick layer of Newtonian mud, we deduce that the general relation on the first-order wave energy is:

$$\boxed{\frac{d}{dX}\Big[\sum_{m=1}^{n} |A_m|^2\Big] = -\gamma\frac{\kappa_d}{\kappa}\sum_{m=1}^{n} \Re\left[im\left(1 - \frac{\tanh(\sigma_m)}{\sigma_m}\right)\right]|A_m|^2} \tag{2.6.3.4}$$

Clearly wave energy is attenuated in X. One can define the attenuation distance for the m-th harmonic by

$$\frac{1}{L_m} = -\gamma\frac{\kappa_d}{\kappa}m\Im\Big[G(\sigma_1)\Big] \tag{2.6.3.5}$$

2.6.4 Study of $G(\sigma_m)$

Let us now study the term:

$$G(\sigma_m) = 1 - \frac{\tanh(\sigma_m)}{\sigma_m} \tag{2.6.4.1}$$

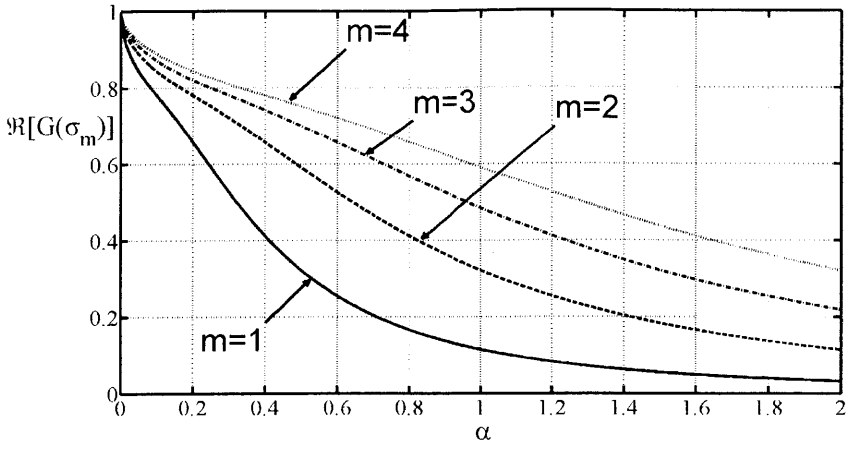

(a) Real part of $G(\sigma_m)$

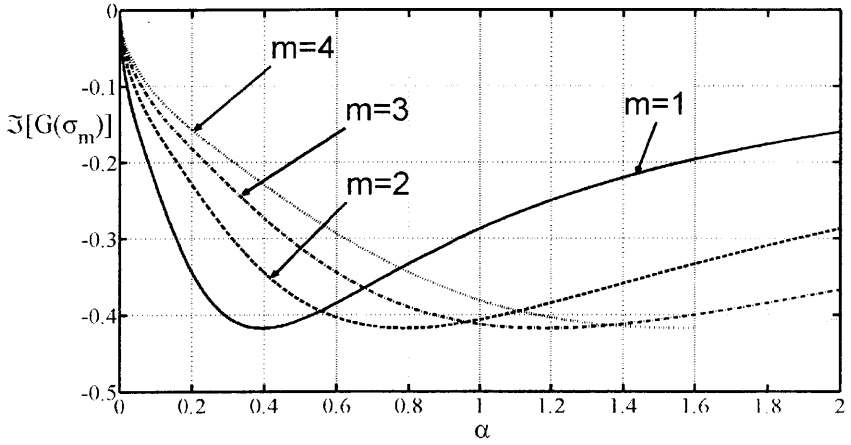

(b) Imaginary part of $G(\sigma_m)$

Figure 2-2: Variation of $G(\sigma_m)$ as a function of α and m

as a function of m.

We know that:

$$\sigma_m^2 = -\frac{im}{\alpha} \tag{2.6.4.2}$$

so G is in the end a function of m and α.

In figure 2-2, we plot G as a function of α, for different values of m. Since we previously stated that α is of order 1, we plot G for $0 < \alpha < 1$.

We can see that the real part of $G(\sigma_m)$ strictly increases with m. However, we see that the variation of $\Im(G)$ is not monotonous in m.

2.7 Numerical results by using the first ten harmonics

We now represent the numerical results in order to analyze the effect of the different parameters.

We will first study the effect of the wave amplitude A, knowing that a big wave amplitude implies high non-linearity ϵ for cases 1a, 1b and 1c listed in table 2.3.

We will then look at the effects of different wavenumbers k, and thus of different dispersion coefficient κ for cases 2a, 2b and 2c listed in Table 2.4.

Finally, we will look at the effects of different mud layer depths d, and thus different values of the parameter κ_d for cases 3a, 3b and 3c listed in Table 2.5.

For all of these representations, we arbitrarily choose the viscosity to be the modulus of the Gulf of Mexico mud complex viscosity at $\omega' = 0.5$rad/s. This value corresponds to a viscosity: $\underline{\mu = 400\text{Pa.s}}$. We also choose the density to be the density of this same mud: $\underline{\rho_M = 1140kg/m^3}$, and as a consequence $\underline{\gamma = 0.88}$

We also set the water depth $\underline{\bar{h} = 2m}$.

2.7.1 Influence of non-linearity

We set the wave period to be $T = 12s$ (which means $\omega' = 1/2rad/s$), the mud layer depth to be $d = 20$cm and the water depth $\bar{h} = 2$m. We then consider 3 possible wave amplitudes $A = 20cm$, $A = 40cm$ and $A = 60cm$, corresponding to cases 1a, 1b and 1c. From here we can deduce the value of κ and Re by:

$$\kappa = k\bar{h} = \frac{\omega'}{\sqrt{g\bar{h}}}\bar{h} = \omega'\sqrt{\frac{\bar{h}}{g}} \tag{2.7.1.1}$$

and:

$$Re = \frac{\rho_M A dk\sqrt{g\bar{h}}}{\mu} = \frac{\rho_M A d\omega'}{\mu} \tag{2.7.1.2}$$

Table 2.3 sums up the corresponding values of the parameters ϵ, κ, Re, κ_d and α. ϵ and Re both increase with A and κ does not depend on A. Case 1a corresponds to the smallest A (and thus smallest non-linearity) value and case 1c to the biggest one.

We assume the initial condition $A_1(0) = 1$

Case	ϵ	κ	Re	κ_d	$\alpha = \frac{\epsilon}{\kappa_d Re}$
1a	0.1	0.22	0.06	0.1	17
1b	0.2	0.22	0.11	0.1	18
1c	0.3	0.22	0.17	0.1	18

Table 2.3: Values of Re, κ, ϵ and α corresponding to different values of A. Case 1c corresponds to the biggest A, that is to say the biggest non-linearity.

Surface and interface

Figures 2-3 and 2-4 show the evolution of the first three harmonics of the surface and the interface. Even though we carried the resolution with 10 harmonics in order to take into account all the significant ones, we only display the three most significant harmonics for clarity.

In figure 2-3, we observe that the harmonics are smoother in the less non-linear case (1a). Variations are more significant in the most non-linear case (1c). This effect of non-linearity corresponds to what we were expecting. Even though non-linearity is very important in every case, it is even more obvious in case 1c.

Drift current in mud

Figure 2-5 represents the drift we calculated in equation 2.6.2.8.

Let us recall the equations:

$$\begin{aligned} U &= U^{(0)} + \kappa U^{(1)} + O(\kappa^2) \\ U^{(1)} &= \frac{1}{2}U_0^{(1)} + \frac{1}{2}\sum_{m=1}^{\infty}\left(U_m^{(1)} e^{i\theta_m} + cc.\right) \end{aligned} \tag{2.7.1.3}$$

This is why we plot the value $\frac{1}{2}\kappa U_0^{(1)}$, which is the value that appears in the total sum of U.

The drift is represented in the mud layer for $0 < X < 5$ for $Z = 1$. It is interesting to note how the drift naturally vanishes as X increases.

The biggest drift occurs in case 1c, in which non-linearity is the most important. This result corresponds to what we expected since the drift appears at the second order because of non-linearity.

We also note that the drift current shows strong oscillations in the most non-linear case, and moderate oscillations in the medium case (1b). As we already emphasized, the drift current is a sum of the $|A_m|^2$ multiplied by coefficients. Since these coeffi-

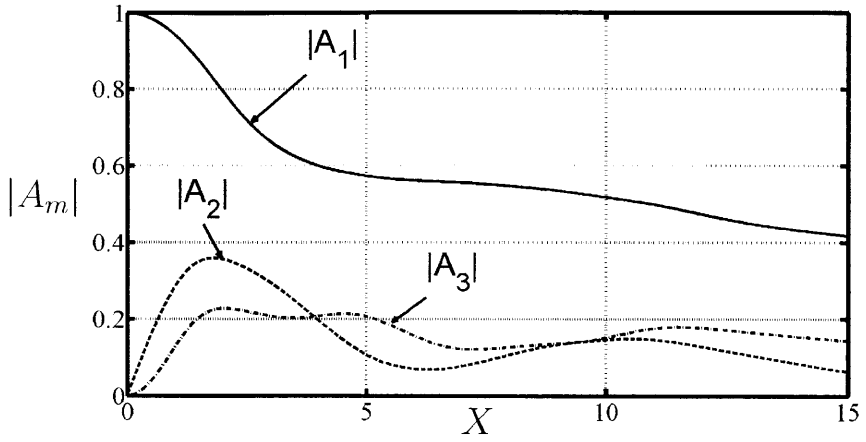

(a) Smallest non-linearity (1a)

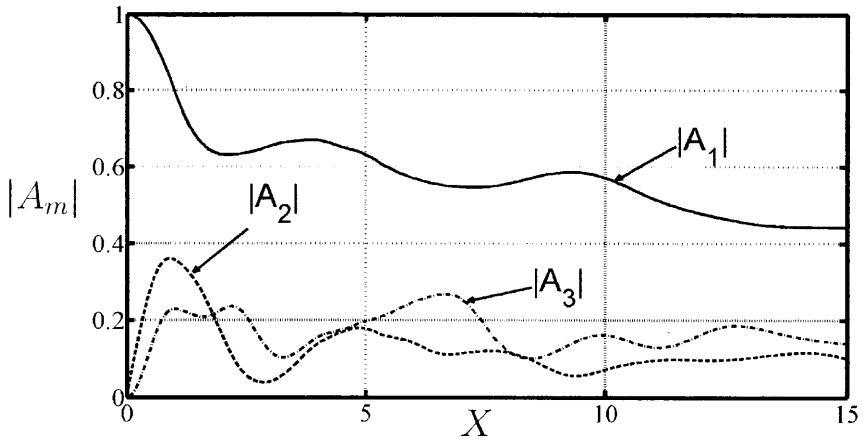

(b) Medium non-linearity (1b)

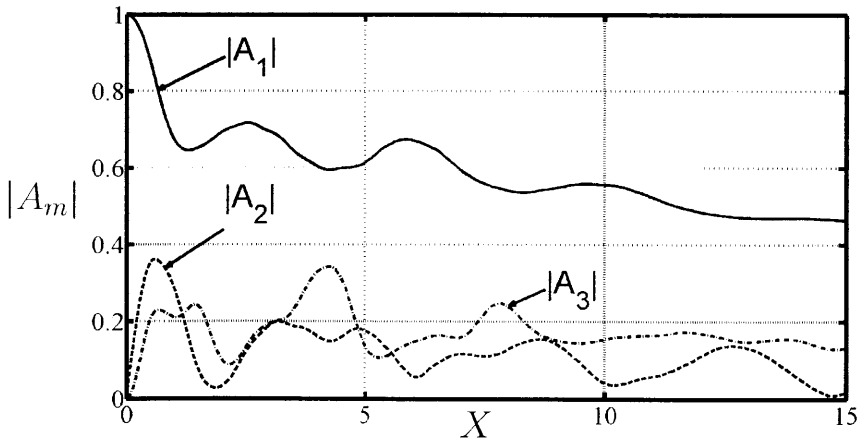

(c) Highest non-linearity (1c)

Figure 2-3: Effects of wave amplitude on the evolution of the first 3 harmonics of the free surface over a thick muddy seabed. Comparison between the cases 1a, 1b and 1c.

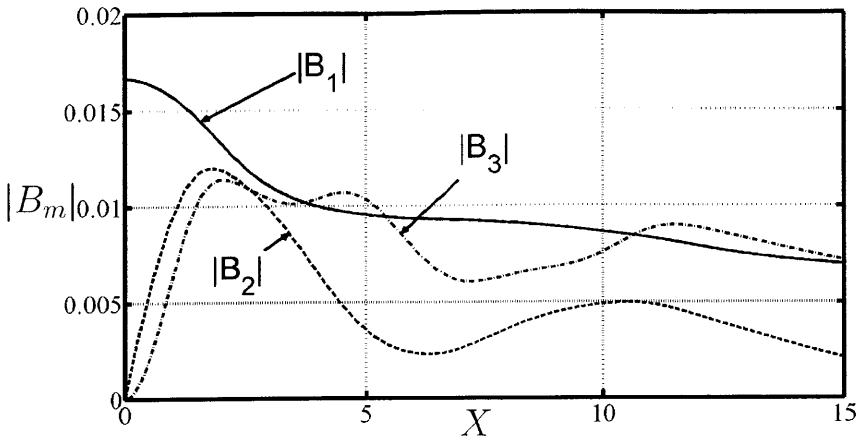

(a) Smallest non-linearity (1a)

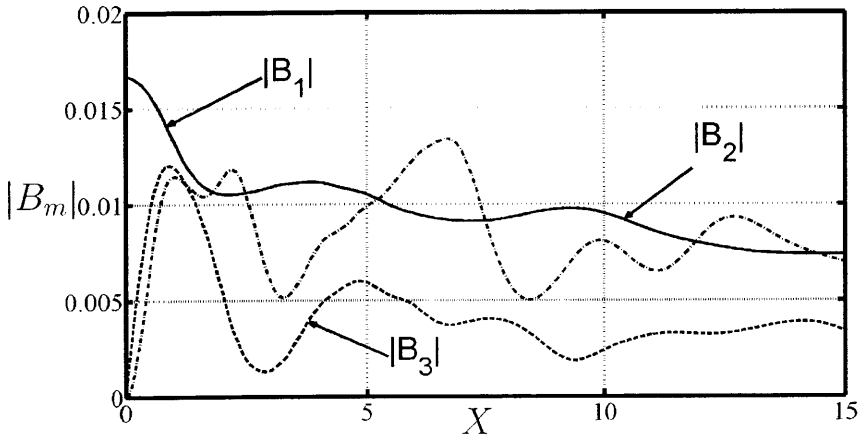

(b) Medium non-linearity (1b)

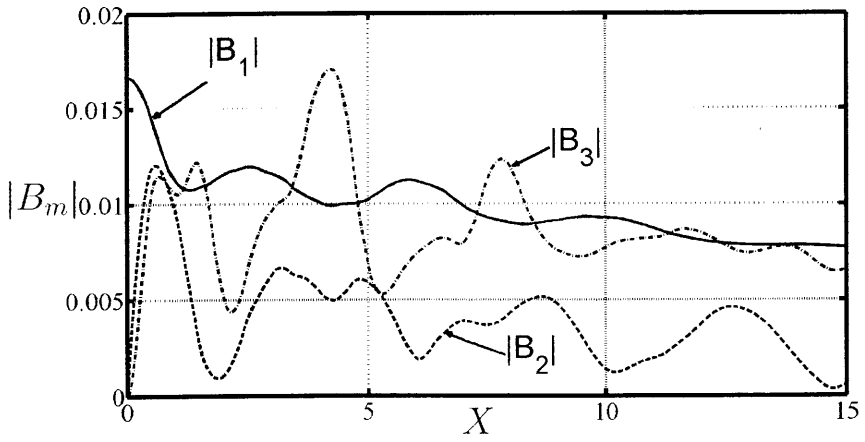

(c) Highest non-linearity (1c)

Figure 2-4: Effects of wave amplitude on the evolution of the first 3 harmonics of the interface between mud and water over a thick muddy seabed. Comparison between the cases 1a, 1b and 1c.

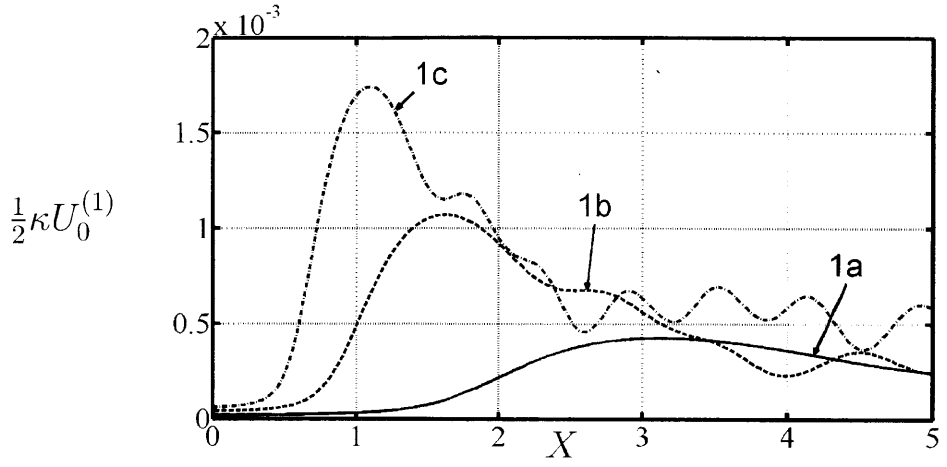

Figure 2-5: Drift velocity $\frac{1}{2}\kappa U_0^{(1)}$. Comparison between the cases 1a, 1b and 1c.

cients do not depend on X, it is logical that the oscillations in $|A_m|$ directly result in oscillations in the drift. As a consequence, based on the comments we made on the $|A_m|$ in the previous section, it is logical for the drift current to have more oscillations in the most non-linear case.

Energy variation

We display the total first-order energies for cases 1a, 1b and 1c in figures 2-6. This figure shows that the total energy logically decreases to reach a zero-value in every case, because it is dissipated in the viscous mud.

In figure 2-7, we represented the variation of total energy. The dashed line represents the right-hand side term of equation 2.6.3.4:

$$\frac{d}{dX}\left[\sum_{m=1}^{n}|A_m|^2\right] = -\gamma\frac{\kappa_d}{\kappa}\sum_{m=1}^{n}\Re\left[im\left(1-\frac{\tanh(\sigma_m)}{\sigma_m}\right)\right]|A_m|^2 \qquad (2.7.1.4)$$

It is so close to the solid line that it is very hard to distinguish. As a consequence, this figure shows that our numerical results are right.

2.7.2 Influence of dispersion κ

We now study the influence of dispersion.

We set the wave amplitude to be $A = 40cm$, the mud layer depth to be $d =$ 20cm and the water depth $\bar{h} = 2$m. We then consider 3 possible periods $T = 18s$, $T = 12s$ and $T = 6s$ (which mean $\omega' = 1/3rad/s$, $\omega' = 1/2rad/s$ and $\omega' = 1rad/s$),

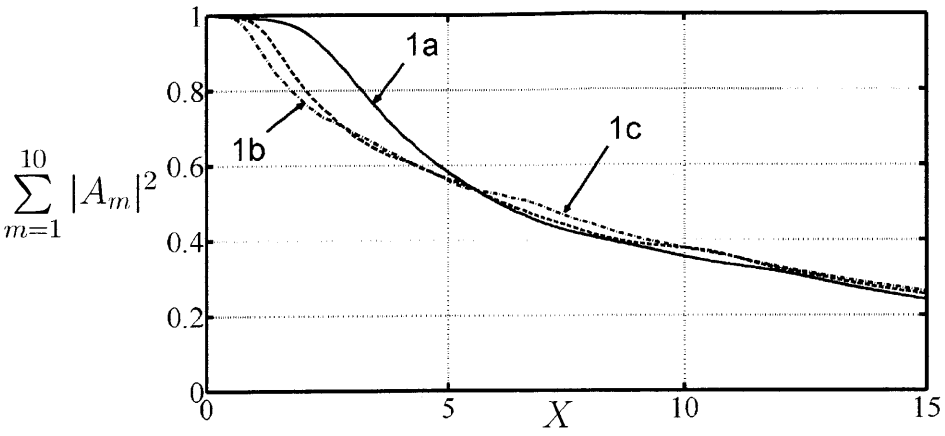

Figure 2-6: Wave energy over a flat thick muddy seabed. Comparison between the cases 1a, 1b and 1c.

Case	ϵ	κ	Re	κ_d	$\alpha = \frac{\epsilon}{\kappa_d Re}$
2a	0.2	0.15	0.08	0.1	25
2b	0.2	0.225	0.11	0.1	18
2c	0.2	0.45	0.23	0.1	8.7

Table 2.4: Values of Re, κ, ϵ, κ_d and α corresponding to different values of dispersion κ

corresponding respectively to cases 2a, 2b and 2c. We still have $\bar{h} = 2m$.

Table 2.4 sums up the corresponding values of the parameters ϵ, κ, Re, κ_d and α.

Free surface and interface

Figures 2-8 and 2-9 show the evolution of the first three harmonics of the surface and the interface for different dispersion parameters κ. Even though we carried the resolution with 10 harmonics in order to take into account all the significant ones, we chose to only display the three most significant harmonics for clarity.

In figure 2-8, we observe that the harmonics are smoother in the most dispersive case (2c). Variations are more significant in the less dispersive case (2a).

Drift

Figure 2-10 represents the drift we calculated in equation 2.6.2.8. It is interesting to note once again how the drift naturally vanishes as X increases.

As before, we choose to represent the value $\frac{1}{2}\kappa U_0^{(1)}$, because it is the value that appears in the total sum of U.

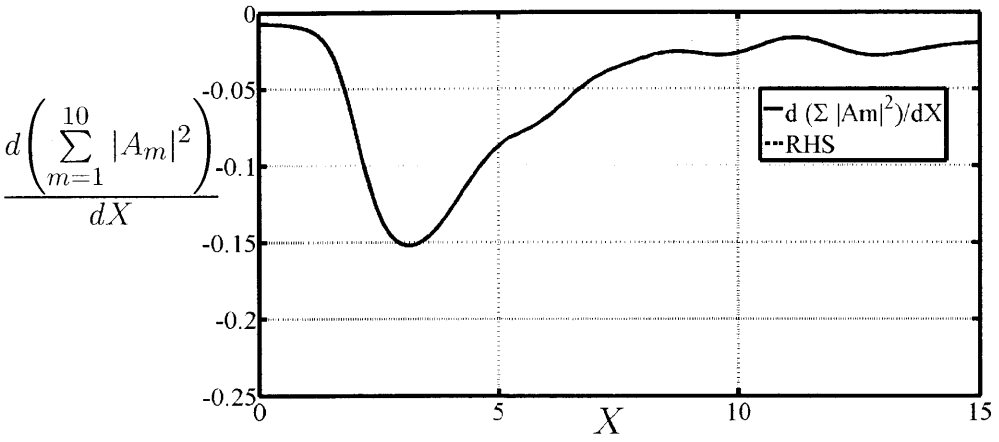

(a) Smallest non-linearity (1a)

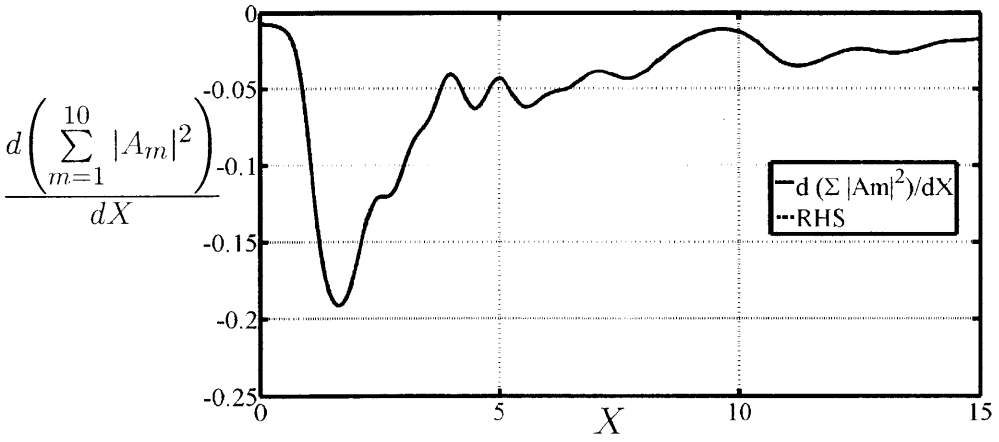

(b) Medium non-linearity (1b)

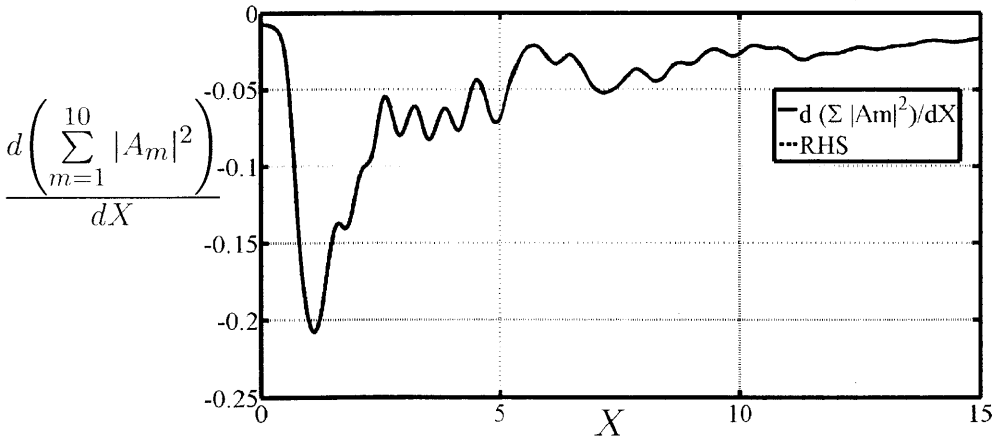

(c) Highest non-linearity (1c)

Figure 2-7: Variation of the wave energy over a flat thick muddy seabed. RHS is the value of the right-hand side term in equation 2.6.3.4. Comparison between the cases 1a, 1b and 1c.

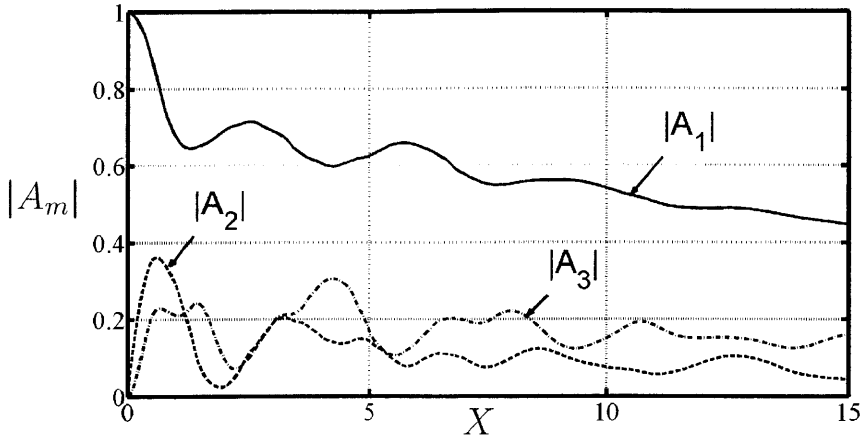

(a) Smallest dispersion (2a)

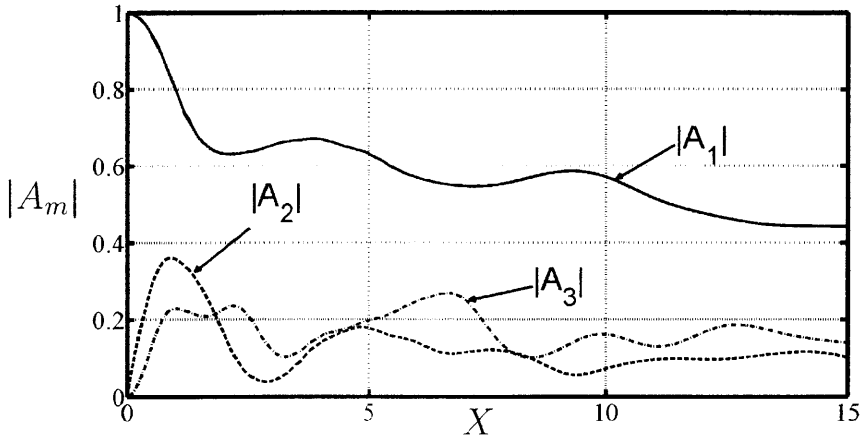

(b) Medium dispersion (2b)

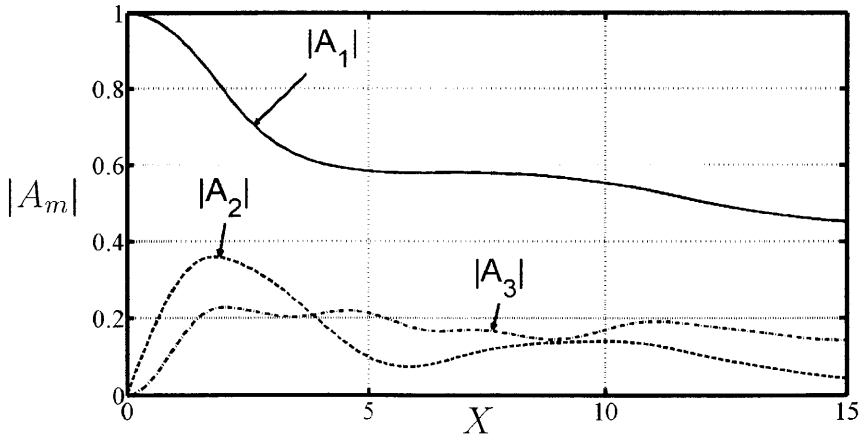

(c) Highest dispersion (2c)

Figure 2-8: Effects of dispersion on the evolution of the first 3 harmonics of the free surface over a thick muddy seabed. Comparison between the cases 2a, 2b and 2c.

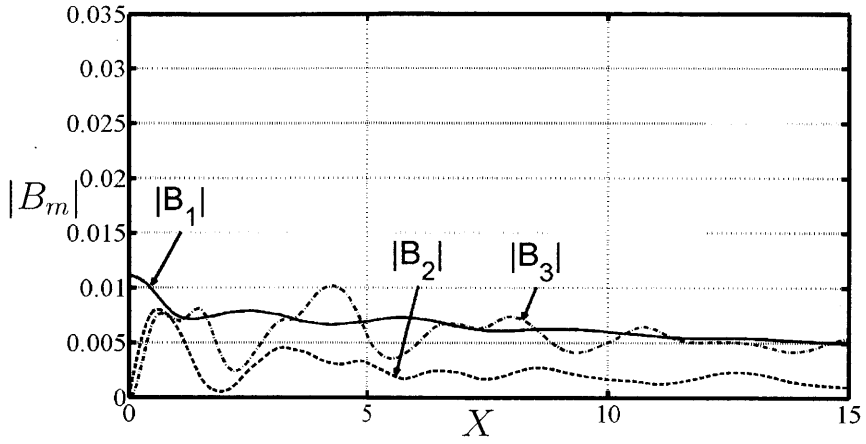

(a) Smallest dispersion (2a)

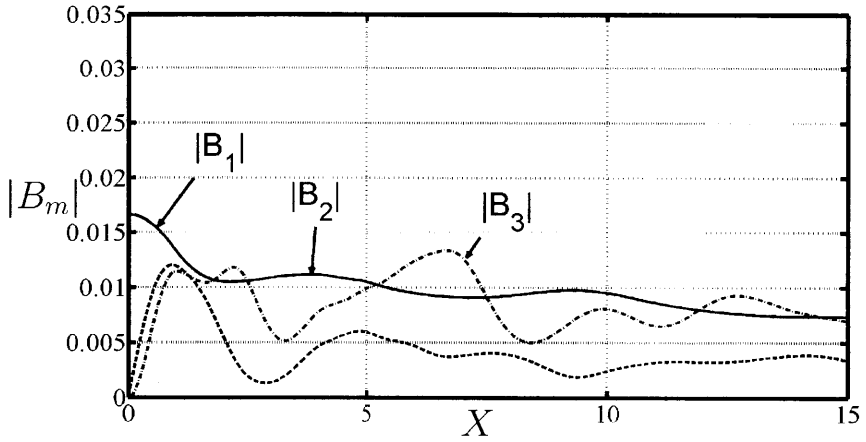

(b) Medium dispersion (2b)

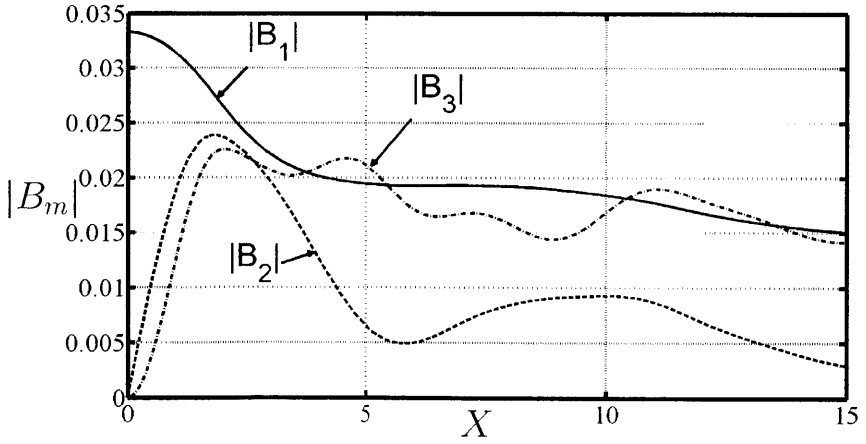

(c) Highest dispersion (2c)

Figure 2-9: Effects of dispersion on the evolution of the first 3 harmonics of the interface between mud and water over a thick muddy seabed. Comparison between the cases 2a, 2b and 2c.

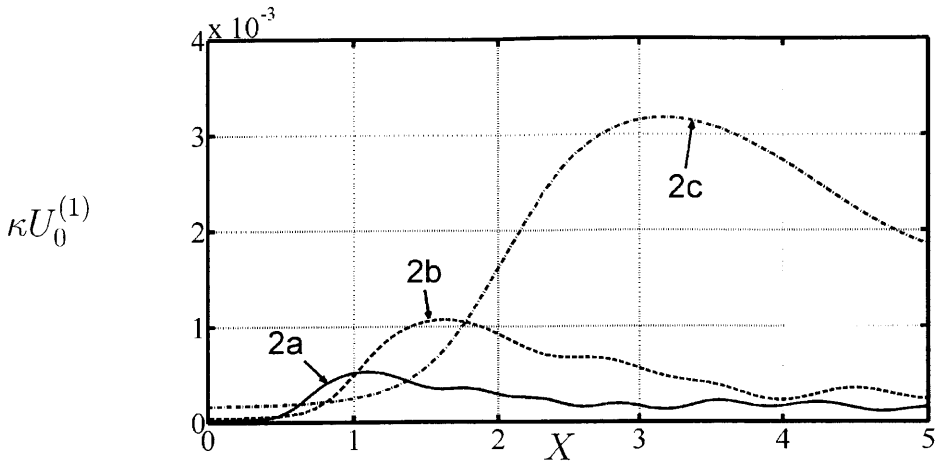

$\kappa U_0^{(1)}$

Figure 2-10: Drift velocity $\frac{1}{2}\kappa U_0^{(1)}$. Comparison between the cases 2a, 2b and 2c.

The biggest drift occurs in case 2c, in which dispersion is the most important.

Oscillations in the drift current are more significant in the small dispersion cases. As before, this is due to the fact that the $|A_m|$ themselves are less smooth in when dispersion is small (2a or 2b).

Energy variation

We show the total first-order energies for cases 2a, 2b and 2c in figure 2-11. This figure shows that the total energy expectedly decreases to reach a zero-value, because it is dissipated in the viscous mud.

In figure 2-12, we represented the variation of total energy. The dashed line represents the right-hand side term of equation 2.6.3.4, and the figure shows that our numerical results obey the law we demonstrated. Indeed, the two lines are so close that they are very hard to distinguish.

2.7.3 Influence of mud layer depth d

We now aim at studying the influence of the mud layer depth.

We set the wave period to be $T = 12s$ (which means $\omega' = 1/2rad/s$), and the wave amplitude to be $A = 40cm$. We then consider 3 possible mud layer depth $d = 10cm$, $d = 20cm$ and $d = 40cm$, corresponding respectively to cases 3a, 3b and 3c. We still have $\bar{h} = 2m$.

Table 2.5 sums up the corresponding values of the parameters ϵ, κ, Re, κ_d and α.

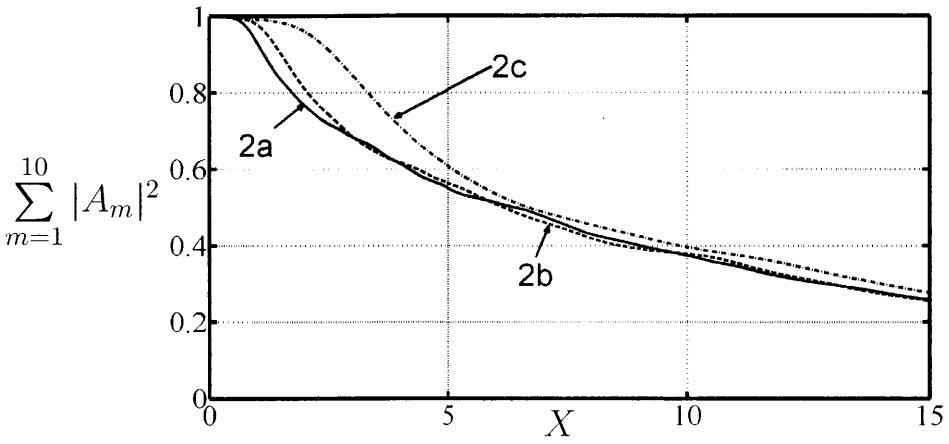

Figure 2-11: Wave energy over a flat thick muddy seabed. Comparison between the cases 2a, 2b and 2c.

Case	ϵ	κ	Re	κ_d	$\alpha = \frac{\epsilon}{\kappa_d Re}$
3a	0.2	0.22	0.06	0.05	67
3b	0.2	0.22	0.11	0.1	18
3c	0.2	0.22	0.23	0.2	4

Table 2.5: Values of Re, κ, ϵ, κ_d and α corresponding to different values of the mud depth d

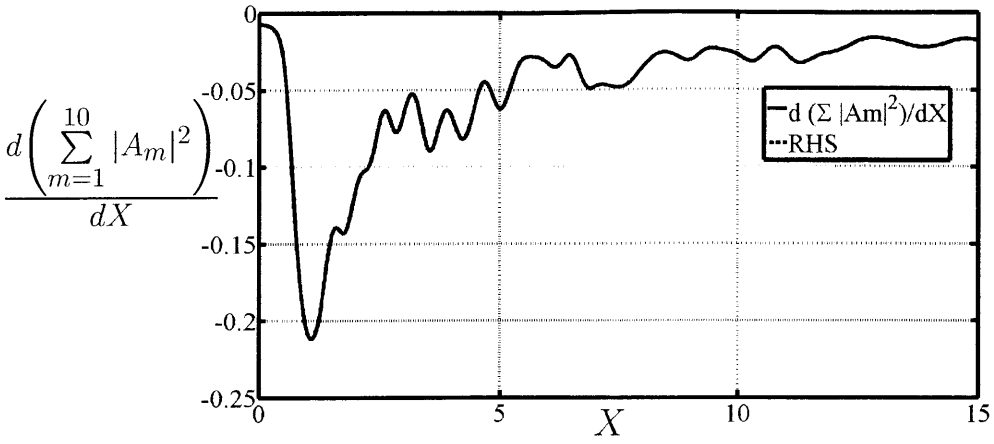

(a) Smallest dispersion (2a)

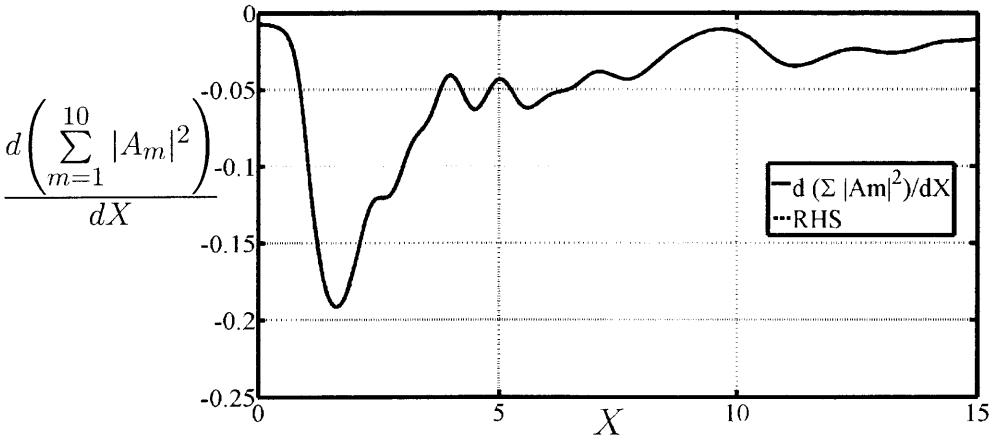

(b) Medium dispersion (2b)

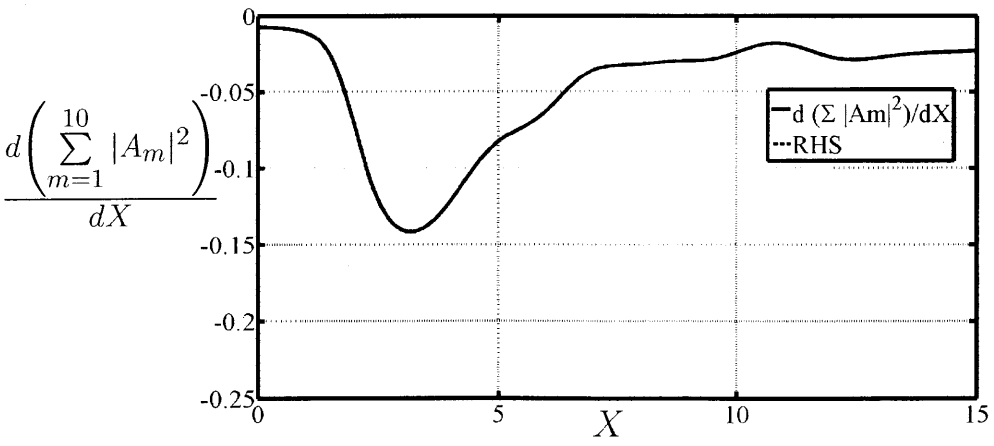

(c) Highest dispersion (2c)

Figure 2-12: Variation of the wave energy over a flat thick muddy seabed. RHS is the value of the right-hand side term in equation 2.6.3.4. Comparison between the cases 2a, 2b and 2c.

Free surface and interface

Figures 2-13 and 2-14 show the evolution of the first three harmonics of the surface and the interface for different mud layer thickness d. Even though we carried the resolution with 10 harmonics in order to take into account all the significant ones, we chose to only display the three most significant harmonics for clarity.

As expected, we observe in figure 2-13 that damping is more significant in the case of the highest mud thickness (3c) than in the case of a very thin mud layer (3a). This is due to the fact that dissipation happens in mud. As a consequence, the thicker the mud layer and the more wave damping.

We also observe in figure 2-14 that the interface variations reach a higher amplitude in the case of the thicker mud (3c).

Drift

Figure 2-15 represents the drift we calculated in equation 2.6.2.8. It is interesting to note once again how the drift naturally vanishes as X increases.

As before, we choose to represent the value $\kappa U_0^{(1)}$, because it is the value that appears in the total sum of U.

We observe in figure 2-15 that the biggest drift corresponds to the thicker mud (3c).

Energy variation

We numerically represented the total first-order energies for cases 3a, 3b and 3c in figure 2-16. This figure shows that the total energy logically decreases to reach a zero-value, because it is dissipated in the viscous mud. We can see that energy is dissipated faster in the case of the thicker mud (3c). This result seems logical since, as we said when we studied the surface amplitude, the thicker the mud and the faster the wave damping.

In figure 2-17, we represented the variation of total energy. The dashed line still represents the right-hand side term of equation 2.6.3.4, and the figure shows that our numerical results obey the law we demonstrated. Indeed, the two lines are so close that they are very hard to distinguish.

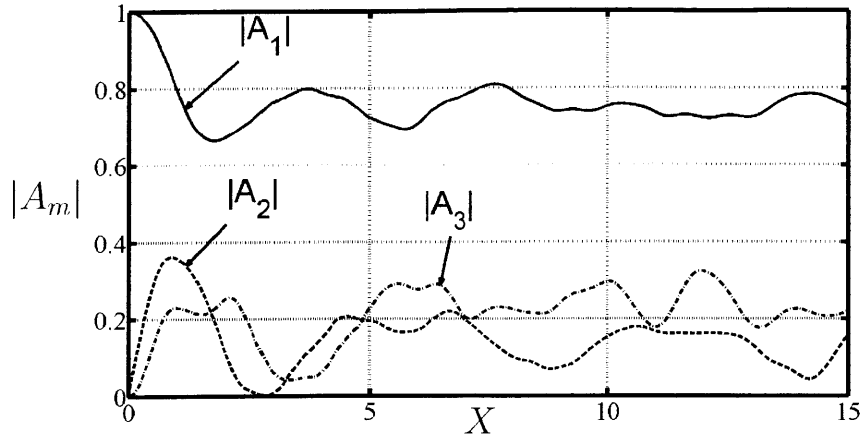

(a) Smallest mud layer thickness (3a)

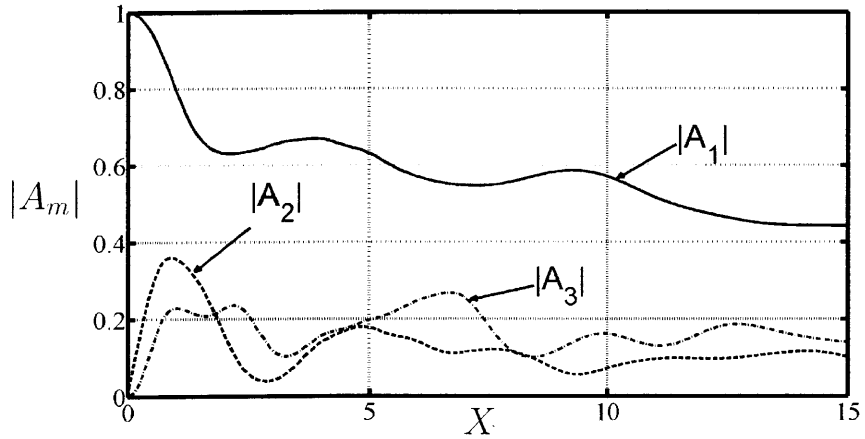

(b) Medium mud layer thickness (3b)

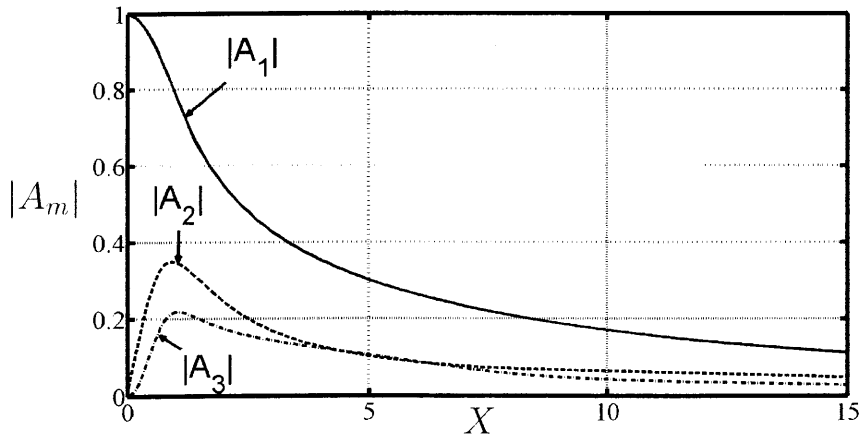

(c) Highest mud layer thickness (3c)

Figure 2-13: Effects of mud layer thickness on the evolution of the first 3 harmonics of the free surface over a thick muddy seabed. Comparison between the cases 3a, 3b and 3c.

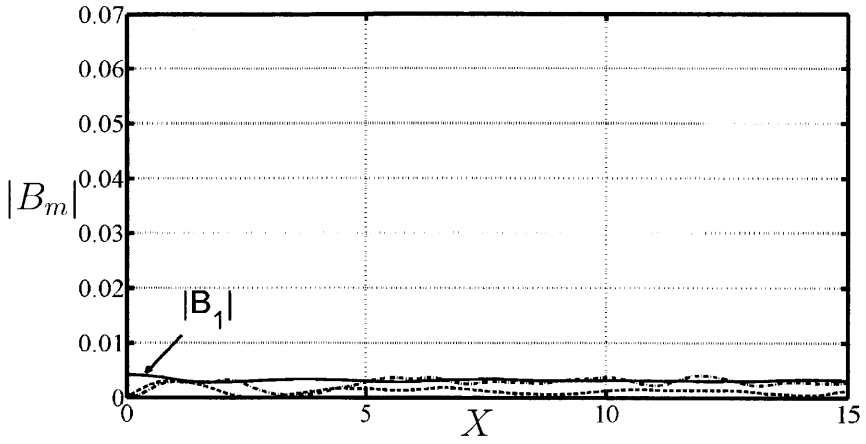

(a) Smallest mud layer thickness (3a)

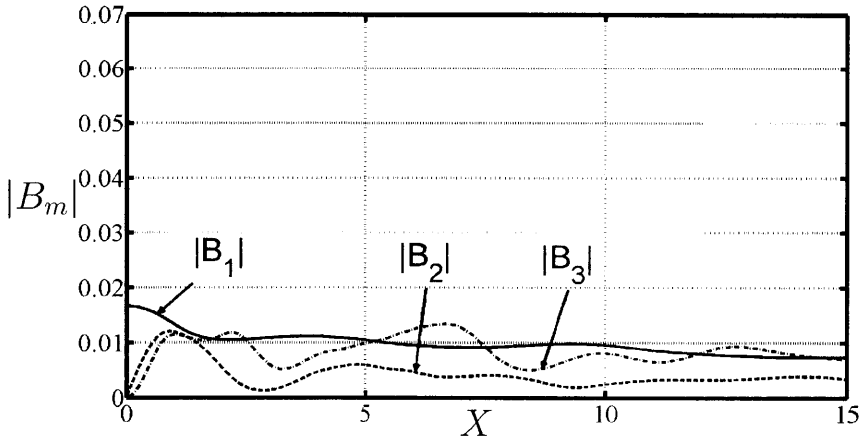

(b) Medium mud layer thickness (3b)

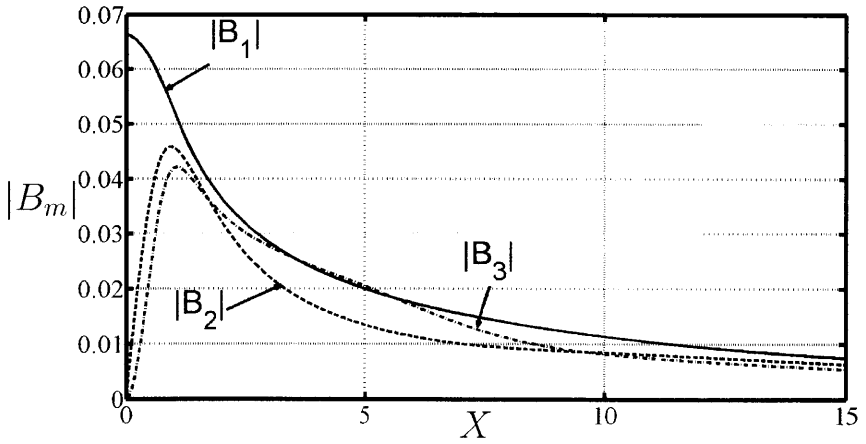

(c) Highest mud layer thickness (3c)

Figure 2-14: Effects of mud layer thickness on the evolution of the first 3 harmonics of the interface between mud and water over a thick muddy seabed. Comparison between the cases 3a, 3b and 3c.

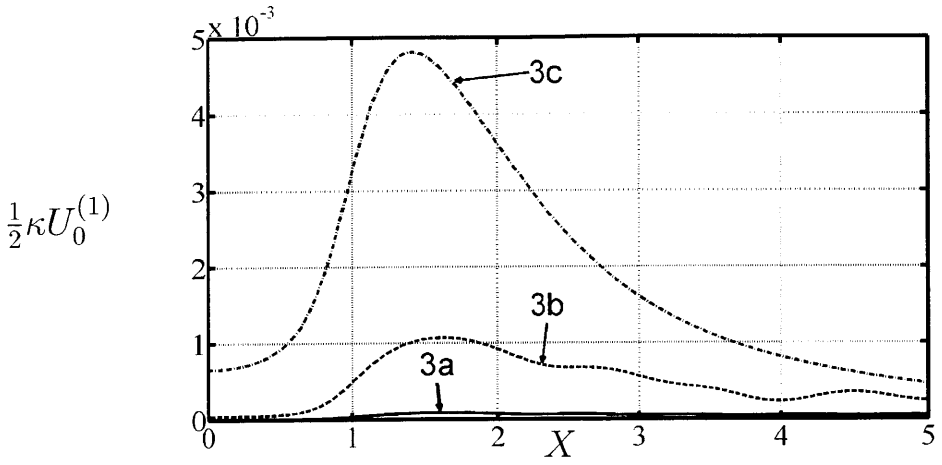

Figure 2-15: Drift velocity $\frac{1}{2}\kappa U_0^{(1)}$. Comparison between the cases 3a, 3b and 3c.

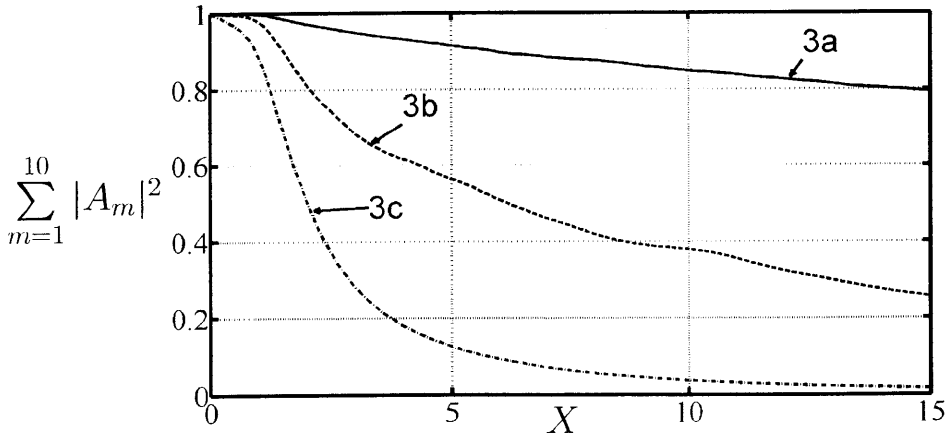

Figure 2-16: Wave energy over a flat thick muddy seabed. Comparison between the cases 3a, 3b and 3c.

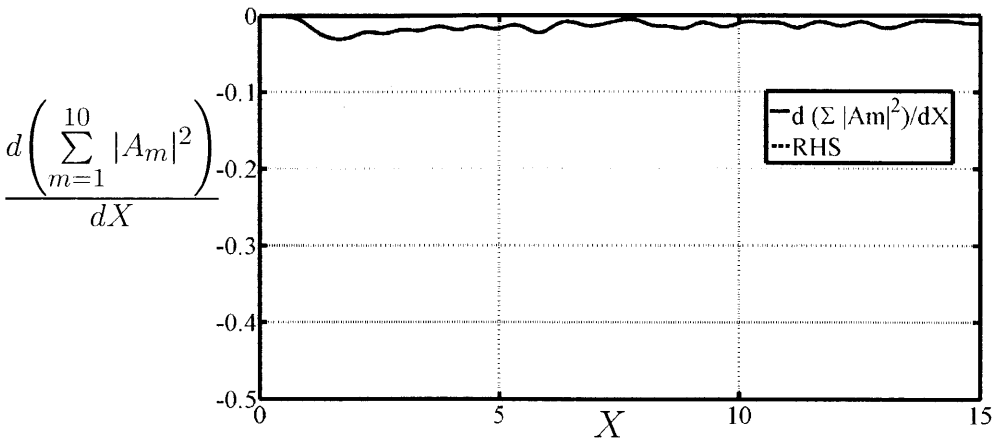

(a) Smallest mud layer thickness (3a)

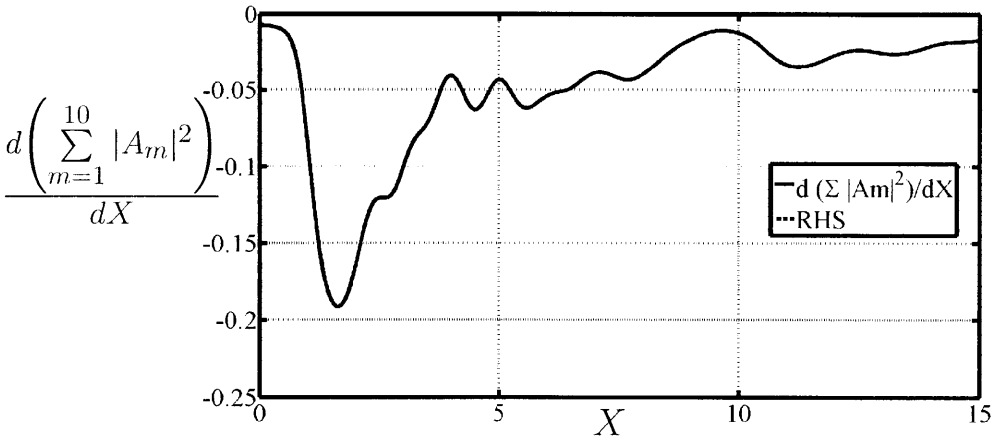

(b) Medium mud layer thickness (3b)

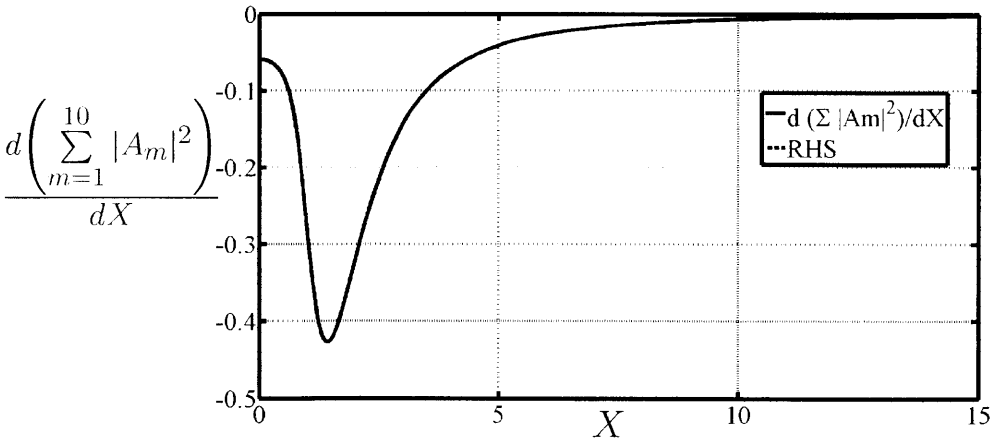

(c) Highest mud layer thickness (3c)

Figure 2-17: Variation of the wave energy over a flat thick muddy seabed. RHS is the value of the right-hand side term in equation 2.6.3.4. Comparison between the cases 3a, 3b and 3c.

2.8 Estimation of Re

We give here a range of possible Reynolds number values for different field samples of fluid-mud in tables 2.6, 2.7 and 2.8. We repeat the values of ϵ and κ in every one of these tables, even though they clearly don't depend on the mud type.

Using the rheological data for a mud sample from Gulf of Mexico, provided by Professor R. A. Dalrymple and Mr K. Melick of Johns Hopkins University, we have the following typical characteristic values: $\rho_M = 1140kg/m^3$, and $|\mu|(\omega' = 1/3) = 461$Pa.s, $|\mu|(\omega' = 1/2) = 400$Pa.s and $|\mu|(\omega' = 1) = 267$Pa.s. More information about this mud and its viscosity will be given in the following chapter, about viscoelasticity. Table 2.6 gives the calculated values of ϵ, κ and the Reynolds number Re for three sets of $\bar{h}$, A and ω'. The ratio of mud depth to water depth is fixed at $\kappa_d = 0.1$. Note that in some cases $\epsilon = O(\kappa)$. In other cases (shaded gray) in table 2.6, $\epsilon = O(\kappa^2)$. Cases with $\epsilon > 0.4$ or $\kappa > 0.4$ are outside the realm of this study. For all cases within the realm of this study, the Reynolds numbers are small.

For mud samples from Mobile Bay, Jiang & Mehta in [11]. have shown that the following properties are representative : $\rho_M = 1281kg/m^3$, and $|\mu|(\omega' = 1/3) = 16,900$ Pa.s, $|\mu|(\omega' = 1/2) = 11,600$ Pa.s and $|\mu|(\omega' = 1) = 6,270$ Pa.s. Table 2.7 gives the values of ϵ, κ and the Reynolds number Re for several sets of $\bar{h}$, A and ω' with $\kappa_d = 0.1$. Again, the Reynolds numbers are very small.

For mud samples from Lianyungang, China, studied by Mei & Krotov in [15]. the characteristic properties are : $\rho_M = 1590kg/m^3$, and $|\mu|(\omega' = 1/3) = 2,509$ Pa.s, $|\mu|(\omega' = 1/2) = 1,629$ Pa.s and $|\mu|(\omega' = 1) = 760$ Pa.s. Table 2.8 gives the values of ϵ, κ and the Reynolds number Re for several sets of : $\bar{h}$, A and ω' with $\kappa_d = 0.1$. Again, the Reynolds numbers are all small.

Finally for mud samples from Hangzhou Bay , China [10], Professor ZH. Huang of Nanyang Technological University of Singapore has provided the following properties: $\rho_M = 1561kg/m^3$, and $|\mu|(\omega' = 1/3) = 39$ Pa.s, $|\mu|(\omega' = 1/2) = 24$ Pa.s and $|\mu|(\omega' = 1) = 11$ Pa.s. Table 2.9 gives the values of ϵ, κ and the Reynolds number Re for several sets of $\bar{h}$, A and ω' with $\kappa_d = 0.1$. This mud has been studied by Huhe & Huang in [10]. Note that the Reynolds numbers are not small, $Re = O(1)$.

In all of these tables 2.6, 2.7, 2.8 and 2.9, the gray cells represent the cases where non-linearity is weak, that is to say $\epsilon = O(\kappa^2)$. This chapter is limited to $\epsilon = O(\kappa)$. We shall treat the case of $\epsilon = O(\kappa^2)$ in separate chapters.

We deduce from tables 2.6, 2.7, 2.8 and 2.9 that the Reynolds number goes from $3 * 10^{-4}$ to 10.

ϵ, κ, Re				A (cm)			
				10	20	40	60
$\bar{h}$ (m)	1	ω' (rad/s)	1/3	$\epsilon = 0.1$ $\kappa = 0.106$ $Re = 0.008$	$\epsilon = 0.2$ $\kappa = 0.106$ $Re = 0.017$	$\epsilon = 0.4$ $\kappa = 0.106$ $Re = 0.033$	$\epsilon > 0.4$
			1/2	$\epsilon = 0.1$ $\kappa = 0.159$ $Re = 0.014$	$\epsilon = 0.2$ $\kappa = 0.159$ $Re = 0.029$	$\epsilon = 0.4$ $\kappa = 0.159$ $Re = 0.06$	$\epsilon > 0.4$
			1	$\epsilon = 0.1$ $\kappa = 0.31$ $Re = 0.04$	$\epsilon = 0.2$ $\kappa = 0.31$ $Re = 0.09$	$\epsilon = 0.4$ $\kappa = 0.31$ $Re = 0.17$	$\epsilon > 0.4$
	2	ω' (rad/s)	1/3	$\epsilon = 0.05$ $\kappa = 0.15$ $Re = 0.017$	$\epsilon = 0.1$ $\kappa = 0.15$ $Re = 0.03$	$\epsilon = 0.2$ $\kappa = 0.15$ $Re = 0.07$	$\epsilon = 0.3$ $\kappa = 0.15$ $Re = 0.1$
			1/2	$\epsilon = 0.05$ $\kappa = 0.225$ $Re = 0.029$	$\epsilon = 0.1$ $\kappa = 0.225$ $Re = 0.06$	$\epsilon = 0.2$ $\kappa = 0.225$ $Re = 0.11$	$\epsilon = 0.3$ $\kappa = 0.225$ $Re = 0.17$
			1	$\kappa > 0.4$	$\kappa > 0.4$	$\kappa > 0.4$	$\kappa > 0.4$
	5	ω' (rad/s)	1/3	$\epsilon = 0.02$ $\kappa = 0.238$ $Re = 0.04$	$\epsilon = 0.04$ $\kappa = 0.238$ $Re = 0.08$	$\epsilon = 0.08$ $\kappa = 0.238$ $Re = 0.16$	$\epsilon = 0.12$ $\kappa = 0.238$ $Re = 0.24$
			1/2	$\epsilon = 0.02$ $\kappa = 0.357$ $Re = 0.07$	$\epsilon = 0.04$ $\kappa = 0.357$ $Re = 0.14$	$\epsilon = 0.08$ $\kappa = 0.357$ $Re = 0.29$	$\epsilon = 0.12$ $\kappa = 0.357$ $Re = 0.43$
			1	$\kappa > 0.4$	$\kappa > 0.4$	$\kappa > 0.4$	$\kappa > 0.4$
	10	ω' (rad/s)	1/3	$\epsilon = 0.01$ $\kappa = 0.33$ $Re = 0.08$	$\epsilon = 0.02$ $\kappa = 0.33$ $Re = 0.16$	$\epsilon = 0.04$ $\kappa = 0.33$ $Re = 0.33$	$\epsilon = 0.06$ $\kappa = 0.33$ $Re = 0.5$
			1/2	$\kappa > 0.4$	$\kappa > 0.4$	$\kappa > 0.4$	$\kappa > 0.4$
			1	$\kappa > 0.4$	$\kappa > 0.4$	$\kappa > 0.4$	$\kappa > 0.4$

Table 2.6: Values of Re for different A, frequency ω' and water depths $\bar{h}$, for the Gulf of Mexico mud. We set $\kappa_d = 0.1$.

ϵ, κ, Re				A (cm)			
				10	20	40	60
$\bar{h}$ (m)	1	ω' (rad/s)	1/3	$\epsilon = 0.1$ $\kappa = 0.106$ $Re = 0.0003$	$\epsilon = 0.2$ $\kappa = 0.106$ $Re = 0.0005$	$\epsilon = 0.4$ $\kappa = 0.106$ $Re = 0.001$	$\epsilon > 0.4$
			1/2	$\epsilon = 0.1$ $\kappa = 0.159$ $Re = 0.0006$	$\epsilon = 0.2$ $\kappa = 0.159$ $Re = 0.0011$	$\epsilon = 0.4$ $\kappa = 0.159$ $Re = 0.0022$	$\epsilon > 0.4$
			1	$\epsilon = 0.1$ $\kappa = 0.31$ $Re = 0.002$	$\epsilon = 0.2$ $\kappa = 0.31$ $Re = 0.004$	$\epsilon = 0.4$ $\kappa = 0.31$ $Re = 0.008$	$\epsilon > 0.4$
	2	ω' (rad/s)	1/3	$\epsilon = 0.05$ $\kappa = 0.15$ $Re = 0.0005$	$\epsilon = 0.1$ $\kappa = 0.15$ $Re = 0.001$	$\epsilon = 0.2$ $\kappa = 0.15$ $Re = 0.002$	$\epsilon = 0.3$ $\kappa = 0.15$ $Re = 0.003$
			1/2	$\epsilon = 0.05$ $\kappa = 0.225$ $Re = 0.0011$	$\epsilon = 0.1$ $\kappa = 0.225$ $Re = 0.0022$	$\epsilon = 0.2$ $\kappa = 0.225$ $Re = 0.0044$	$\epsilon = 0.3$ $\kappa = 0.225$ $Re = 0.007$
			1	$\kappa > 0.4$	$\kappa > 0.4$	$\kappa > 0.4$	$\kappa > 0.4$
	5	ω' (rad/s)	1/3	$\epsilon = 0.02$ $\kappa = 0.238$ $Re = 0.0013$	$\epsilon = 0.04$ $\kappa = 0.238$ $Re = 0.0025$	$\epsilon = 0.08$ $\kappa = 0.238$ $Re = 0.005$	$\epsilon = 0.12$ $\kappa = 0.238$ $Re = 0.008$
			1/2	$\epsilon = 0.02$ $\kappa = 0.357$ $Re = 0.003$	$\epsilon = 0.04$ $\kappa = 0.357$ $Re = 0.006$	$\epsilon = 0.08$ $\kappa = 0.357$ $Re = 0.011$	$\epsilon = 0.12$ $\kappa = 0.357$ $Re = 0.017$
			1	$\kappa > 0.4$	$\kappa > 0.4$	$\kappa > 0.4$	$\kappa > 0.4$
	10	ω' (rad/s)	1/3	$\epsilon = 0.01$ $\kappa = 0.33$ $Re = 0.0025$	$\epsilon = 0.02$ $\kappa = 0.33$ $Re = 0.005$	$\epsilon = 0.04$ $\kappa = 0.33$ $Re = 0.01$	$\epsilon = 0.06$ $\kappa = 0.33$ $Re = 0.02$
			1/2	$\kappa > 0.4$	$\kappa > 0.4$	$\kappa > 0.4$	$\kappa > 0.4$
			1	$\kappa > 0.4$	$\kappa > 0.4$	$\kappa > 0.4$	$\kappa > 0.4$

Table 2.7: Values of Re for different A, frequency ω' and water depths $\bar{h}$, for the Mobile Bay mud. We set$\kappa_d = 0.1$

ϵ, κ, Re				A (cm)			
				10	20	40	60
$\bar{h}$(m)		ω' (rad/s)	1/3	$\epsilon = 0.1$ $\kappa = 0.106$ $Re = 0.0021$	$\epsilon = 0.2$ $\kappa = 0.106$ $Re = 0.0042$	$\epsilon = 0.4$ $\kappa = 0.106$ $Re = 0.0084$	$\epsilon > 0.4$
			1/2	$\epsilon = 0.1$ $\kappa = 0.159$ $Re = 0.0049$	$\epsilon = 0.2$ $\kappa = 0.159$ $Re = 0.01$	$\epsilon = 0.4$ $\kappa = 0.159$ $Re = 0.02$	$\epsilon > 0.4$
			1	$\epsilon = 0.1$ $\kappa = 0.31$ $Re = 0.021$	$\epsilon = 0.2$ $\kappa = 0.31$ $Re = 0.042$	$\epsilon = 0.4$ $\kappa = 0.31$ $Re = 0.08$	$\epsilon > 0.4$
	2	ω' (rad/s)	1/3	$\epsilon = 0.05$ $\kappa = 0.15$ $Re = 0.0042$	$\epsilon = 0.1$ $\kappa = 0.15$ $Re = 0.0084$	$\epsilon = 0.2$ $\kappa = 0.15$ $Re = 0.017$	$\epsilon = 0.3$ $\kappa = 0.15$ $Re = 0.025$
			1/2	$\epsilon = 0.05$ $\kappa = 0.225$ $Re = 0.01$	$\epsilon = 0.1$ $\kappa = 0.225$ $Re = 0.02$	$\epsilon = 0.2$ $\kappa = 0.225$ $Re = 0.04$	$\epsilon = 0.3$ $\kappa = 0.225$ $Re = 0.06$
			1	$\kappa > 0.4$	$\kappa > 0.4$	$\kappa > 0.4$	$\kappa > 0.4$
	5	ω' (rad/s)	1/3	$\epsilon = 0.02$ $\kappa = 0.238$ $Re = 0.011$	$\epsilon = 0.04$ $\kappa = 0.238$ $Re = 0.021$	$\epsilon = 0.08$ $\kappa = 0.238$ $Re = 0.042$	$\epsilon = 0.12$ $\kappa = 0.238$ $Re = 0.063$
			1/2	$\epsilon = 0.02$ $\kappa = 0.357$ $Re = 0.024$	$\epsilon = 0.04$ $\kappa = 0.357$ $Re = 0.049$	$\epsilon = 0.08$ $\kappa = 0.357$ $Re = 0.1$	$\epsilon = 0.12$ $\kappa = 0.357$ $Re = 0.15$
			1	$\kappa > 0.4$	$\kappa > 0.4$	$\kappa > 0.4$	$\kappa > 0.4$
	10	ω' (rad/s)	1/3	$\epsilon = 0.01$ $\kappa = 0.33$ $Re = 0.02$	$\epsilon = 0.02$ $\kappa = 0.33$ $Re = 0.042$	$\epsilon = 0.04$ $\kappa = 0.33$ $Re = 0.085$	$\epsilon = 0.06$ $\kappa = 0.33$ $Re = 0.13$
			1/2	$\kappa > 0.4$	$\kappa > 0.4$	$\kappa > 0.4$	$\kappa > 0.4$
			1	$\kappa > 0.4$	$\kappa > 0.4$	$\kappa > 0.4$	$\kappa > 0.4$

Table 2.8: Values of Re for different A, frequency ω' and water depths $\bar{h}$, for the Lianyungang mud. We set $\kappa_d = 0.1$.

ϵ, κ, Re				A (cm)			
				10	20	40	60
$\bar{h}$(m)	1	ω' (rad/s)	1/3	$\epsilon = 0.1$ $\kappa = 0.106$ $Re = 0.13$	$\epsilon = 0.2$ $\kappa = 0.106$ $Re = 0.27$	$\epsilon = 0.4$ $\kappa = 0.106$ $Re = 0.53$	$\epsilon > 0.4$
			1/2	$\epsilon = 0.1$ $\kappa = 0.159$ $Re = 0.33$	$\epsilon = 0.2$ $\kappa = 0.159$ $Re = 0.65$	$\epsilon = 0.4$ $\kappa = 0.159$ $Re = 1.3$	$\epsilon > 0.4$
			1	$\epsilon = 0.1$ $\kappa = 0.31$ $Re = 1.4$	$\epsilon = 0.2$ $\kappa = 0.31$ $Re = 2.8$	$\epsilon = 0.4$ $\kappa = 0.31$ $Re = 5.7$	$\epsilon > 0.4$
	2	ω' (rad/s)	1/3	$\epsilon = 0.05$ $\kappa = 0.15$ $Re = 0.27$	$\epsilon = 0.1$ $\kappa = 0.15$ $Re = 0.53$	$\epsilon = 0.2$ $\kappa = 0.15$ $Re = 1$	$\epsilon = 0.3$ $\kappa = 0.15$ $Re = 1.6$
			1/2	$\epsilon = 0.05$ $\kappa = 0.225$ $Re = 0.65$	$\epsilon = 0.1$ $\kappa = 0.225$ $Re = 1.3$	$\epsilon = 0.2$ $\kappa = 0.225$ $Re = 2.6$	$\epsilon = 0.3$ $\kappa = 0.225$ $Re = 3.9$
			1	$\kappa > 0.4$	$\kappa > 0.4$	$\kappa > 0.4$	$\kappa > 0.4$
	5	ω' (rad/s)	1/3	$\epsilon = 0.02$ $\kappa = 0.238$ $Re = 0.67$	$\epsilon = 0.04$ $\kappa = 0.238$ $Re = 1.33$	$\epsilon = 0.08$ $\kappa = 0.238$ $Re = 2.67$	$\epsilon = 0.12$ $\kappa = 0.238$ $Re = 4$
			1/2	$\epsilon = 0.02$ $\kappa = 0.357$ $Re = 1.6$	$\epsilon = 0.04$ $\kappa = 0.357$ $Re = 3.2$	$\epsilon = 0.08$ $\kappa = 0.357$ $Re = 6.5$	$\epsilon = 0.12$ $\kappa = 0.357$ $Re = 9.8$
			1	$\kappa > 0.4$	$\kappa > 0.4$	$\kappa > 0.4$	$\kappa > 0.4$
	10	ω' (rad/s)	1/3	$\epsilon = 0.01$ $\kappa = 0.33$ $Re = 1.3$	$\epsilon = 0.02$ $\kappa = 0.33$ $Re = 2.7$	$\epsilon = 0.04$ $\kappa = 0.33$ $Re = 5.3$	$\epsilon = 0.06$ $\kappa = 0.33$ $Re = 8$
			1/2	$\kappa > 0.4$	$\kappa > 0.4$	$\kappa > 0.4$	$\kappa > 0.4$
			1	$\kappa > 0.4$	$\kappa > 0.4$	$\kappa > 0.4$	$\kappa > 0.4$

Table 2.9: Values of Re for different A, frequency ω' and water depths $\bar{h}$, for the Hangzhou Bay mud. We set $\kappa_d = 0.1$.

Chapter 3

Horizontal bottom, shallow viscoelastic mud

The previous chapter is limited to Newtonian mud. However, many experimental studies have demonstrated that mud behavior is non-Newtonian. Experiments carried by Jiang & Mehta, Huhe & Huang and by Dalrymple and Melick show that the viscosity of mud is a complex function of ω', implying viscoelasticity.

As shown by Mei et al ([15]), relation 2.4.3.1 will be replaced in this section by a complex relation:

$$\mathcal{L}\tau'_{xZ} = \mathcal{D}E'_{xZ} \tag{3.0.0.1}$$

where $\mathcal{L}$ and $\mathcal{D}$ are two differential operators of high degrees:

$$\begin{aligned} \mathcal{L} &= a_n \frac{\partial^n}{\partial t^n} + a_{n-1}\frac{\partial^{n-1}}{\partial t^{n-1}} + ... + a_0 \\ \mathcal{D} &= b_m \frac{\partial^m}{\partial t^m} + b_{m-1}\frac{\partial^{m-1}}{\partial t^{m-1}} + ... + b_0 \end{aligned} \tag{3.0.0.2}$$

In the special case of sinusoidal motion:

$$\begin{aligned} \tau'_{xZ} &= \bar{\tau}'_{xZ}e^{-i\omega' t} \\ E'_{xZ} &= \bar{E}'_{xZ}e^{-i\omega' t} \end{aligned} \tag{3.0.0.3}$$

and equation 3.0.0.1 reduces to:

$$\bar{\tau}'_{xZ} = G(\omega')E'_{xZ} = \mu'(\omega')\bar{u}'_{xZ} \tag{3.0.0.4}$$

We first discuss the experimental data from mud samples taken from different sites.

3.1 Complex viscosities from field mud

Let us determine μ' as a function of ω' from laboratory analysis of mud samples from different field sites. These different samples have very different rheological properties, some are rather viscous and some others are rather elastic.

3.1.1 Gulf of Mexico mud

Professor Dalrymlpe and PhD candidate Khatoon Melick from the department of civil engineering of Johns Hopkins University have carried out experiments for a mud sample of density 1.14 g/mL taken from the Gulf of Mexico.

More precisely, they imposed an oscillatory stress of a given amplitude on this mud sample. They then varied the frequency of this oscillatory stress, for ω' from 0.628 to 12.56 rad/s, and measured the resulting strain. They carried out this experiment several times, and the mean of their results are used here. From these experiments, we are able to deduce the complex viscosity as a function of the frequency ω'.

Indeed, the measured relation between strain and stress is expressed as:

$$\tau' = G^* E' \tag{3.1.1.1}$$

where $G^* = G' + iG''$ is the complex elasticity modulus, G' the storage modulus and G'' the loss modulus. From this we can easily deduce the complex viscosity μ' since:

$$G^* = i\omega'\mu' \tag{3.1.1.2}$$

and finally:

$$\begin{aligned} (\mu')^R &= \frac{G''}{\omega'} \\ (\mu')^I &= \frac{G'}{\omega'} \end{aligned} \tag{3.1.1.3}$$

Using the values G' and G'' given from Johns Hopkins, we represent the experimental values of the complex viscosity as a function of ω' (figure 3-1). We can easily interpolate these values to find the real and imaginary parts of the complex viscosity for any value of ω' shown in figures 3-2. In figure 3-3, we represent the modulus and phase of μ. In all figures dots represent the experimental data and curves the values by numerical interpolation.

The most important thing to note is that the phase of μ' is very close to $\frac{\pi}{2}$ for $\omega' > 0.6$. This means that this mud is very elastic. However, the phase gets closer

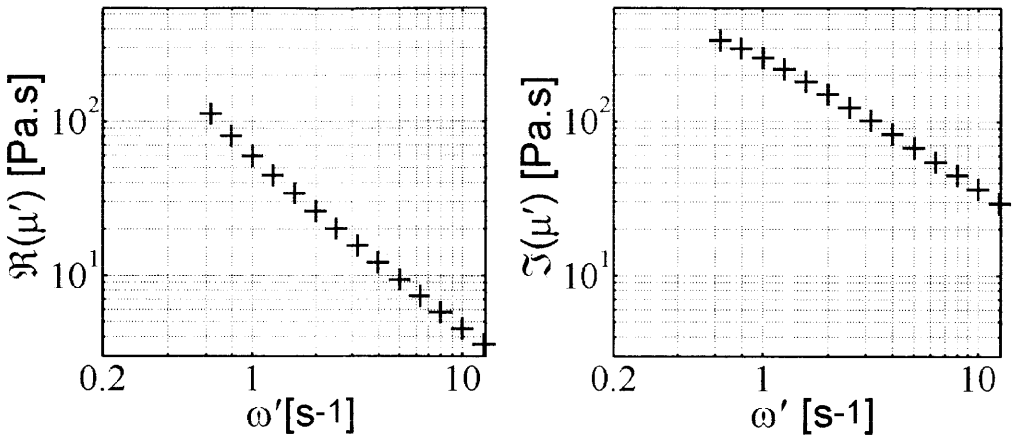

Figure 3-1: Real and Imaginary part of the dimensional complex viscosity for Gulf of Mexico mud.

to $\frac{\pi}{4}$ for $0.2 < \omega' < 0.6$. Hence the mud becomes less elastic for smaller frequencies (longer waves).

3.1.2 Mobile Bay mud

Jiang & Mehta ([11]) have tested mud sample from Mobile Bay, Kerala (India) and Lake Okeechobee. Based on experiments at eight different frequencies in the range $0.12 < \omega' < 24$ rad/s, they expressed the rheology of these muds by a three-parameter viscoelastic model:

$$\tau + \alpha_1 \tau_t = \beta_0 E + \beta_1 E_t \tag{3.1.2.1}$$

The parameters α_1, β_0 and β_1 are in turn fitted as functions of two parameters ϵ and Δ which depend on frequency, mud type and solid fraction. From the values of α_1, β_0 and β_1 at the eight frequencies we can deduce the complex viscosity μ' at these frequencies. In this way Krotov [12] found the relation between the complex viscosity and those parameters:

$$\begin{aligned} \mu'^R &= \frac{\beta_1 - \alpha_1 \beta_0}{1 + \omega'^2 \alpha_1^2} \\ \mu'^I &= \frac{\beta_0/\omega' + \alpha_1 \beta_1 \omega'}{1 + \omega'^2 \alpha_1^2} \end{aligned} \tag{3.1.2.2}$$

These equations correspond to equations 1.3.5 and 1.3.6 in Krotov's thesis ([12]), and the way to obtain them is further explained in the entire section 1.3 of [12].

Table 3.1 gives the real and imaginary parts of the complex viscosities for all the muds studied by Jiang & Mehta where KI stands for Kerala, in India, OK for Okeechobee, MB for Mobile Bay, and AK for a mud made with 50 % of attapulgite

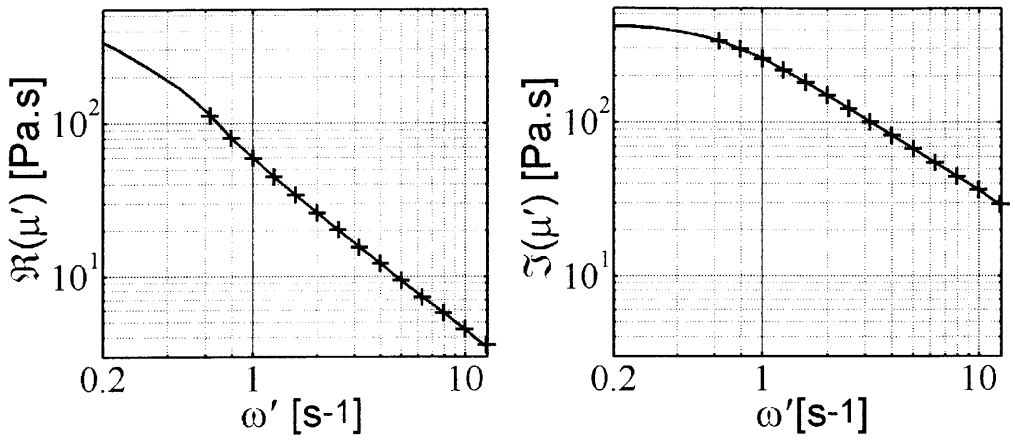

Figure 3-2: Interpolation of the real and imaginary part of the dimensional complex viscosity for Gulf of Mexico mud (line). The crosses represent the experimental values of the complex viscosity.

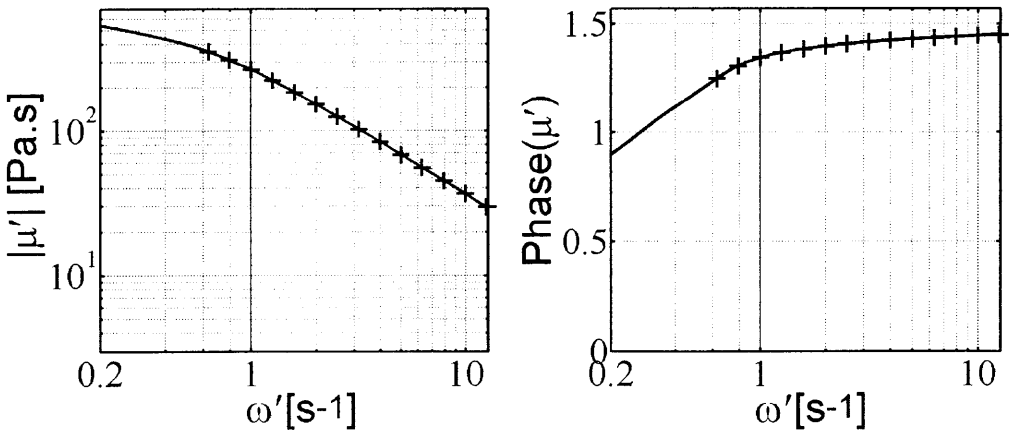

Figure 3-3: Phase and modulus of the dimensional complex viscosity interpolation for Gulf of Mexico mud (line). The crosses represent the experimental values.

ω' $[rad/s]$		0.13	0.25	0.57	1.26	2.51	5.65	12.6	25.1
KI	μ'^R	2.21	1.16	5.16	0.23	0.11	0.046	0.020	0.0094
$\phi = 0.12$	μ'^I	4.31	2.81	1.64	0.95	0.58	0.32	0.18	0.11
OK	μ'^R	0.086	0.044	0.019	0.0086	0.0042	0.0018	0.0008	0.0004
$\phi = 0.11$	μ'^I	0.21	0.12	0.06	0.031	0.017	0.0086	0.0043	0.0024
MB	μ'^R	0.019	0.0094	0.004	0.0017	0.0008	0.0003	0.0001	0.0001
$\phi = 0.07$	μ'^I	0.06	0.03	0.014	0.006	0.003	0.0013	0.0057	0.0003
MB	μ'^R	0.14	0.068	0.029	0.12	0.0056	0.0023	0.001	0.0662
$\phi = 0.11$	μ'^I	0.64	0.34	0.16	0.079	0.041	0.020	0.0095	0.005
MB	μ'^R	1.16	0.56	0.23	0.10	0.047	0.020	0.0083	0.0004
$\phi = 0.17$	μ'^I	3.73	2.05	1.02	0.50	0.27	0.13	0.07	0.036
AK	μ'^R	1.40	0.66	0.26	0.099	0.042	0.015	0.0054	0.0022
$\phi = 0.12$	μ'^I	2.27	1.40	0.75	0.39	0.22	0.11	0.053	0.029

Table 3.1: Real and imaginary part of the complex viscosity for all muds studied by Jiang & Mehta (in $N.s/cm^2$)

and 50 % of kaolinite. The mud density is $\rho_M = \phi\rho^{(s)} + (1-\phi)\rho^{(w)}$, where $\rho^{(s)}$ is the grain density and $\rho^{(w)}$ the water density and ϕ the solid fraction. In the rest of this thesis, we shall only use the data of Mobile Bay (MB), with a solid fraction $\phi = 0.17$, corresponding to a density of 1280 g/mL.

Figure 3-4 shows the real and imaginary parts of the complex viscosity. Figure 3-5 shows the phase and modulus of the complex viscosity of Mobile Bay mud The viscosity phase is around $\frac{\pi}{2}$ as well, so this mud is also rather elastic.

3.1.3 Lianyungang mud

The third mud comes from Lianyungang, China and has been experimentally analyzed by Huhe & Huang. The corresponding complex viscosity has been used by [15].

Professor Huang also provided us the data of μ_M and G_M for fourteen frequencies in the range $0.12 < \omega' < 69$rad/s, where μ_M and G_M are the parameters of a simple Kelvin-Voigt model:

$$\tau' = \left(\mu_M + \frac{iG_M}{\omega'}\right) E'_t \tag{3.1.3.1}$$

From these parameters we deduce:

$$\begin{aligned} \mu'^R &= \mu_M \\ \mu'^I &= \frac{G_M}{\omega'} \end{aligned} \tag{3.1.3.2}$$

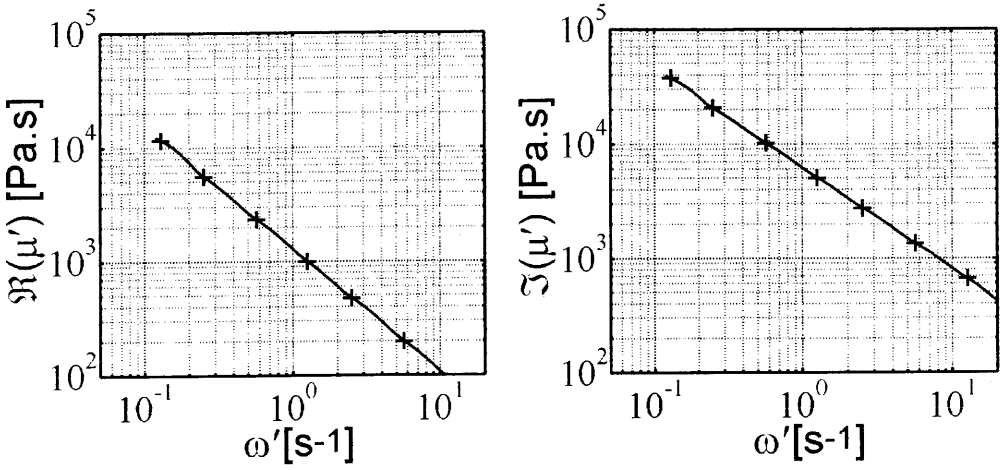

Figure 3-4: Interpolation of the real and imaginary part of the complex viscosity of Mobile Bay mud (line). The crosses represent the experimental values.

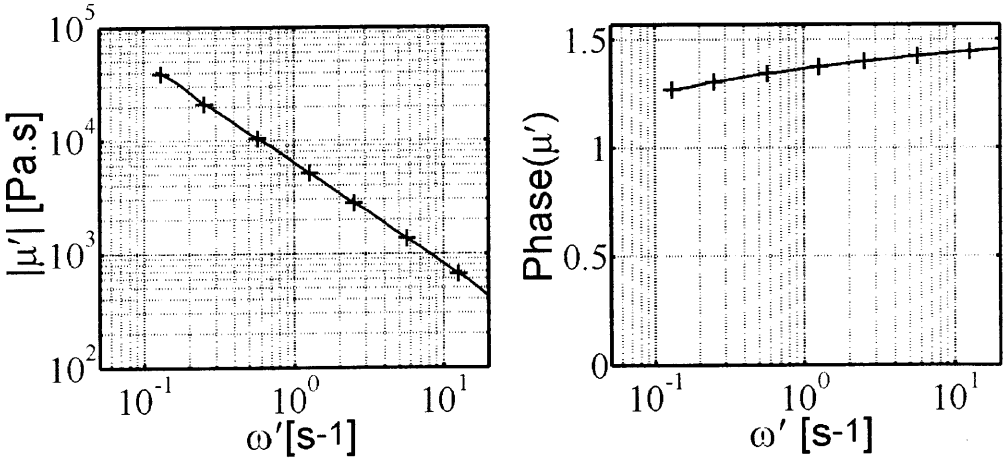

Figure 3-5: Phase and modulus of the complex viscosity interpolation of Mobile Bay mud (line). The crosses represent the experimental values.

$\phi = 0.5$			$\phi = 0.26$			$\phi = 0.17$		
ω' $[rad/s]$	μ'^R	μ'^I	ω' $[rad/s]$	μ'^R	μ'^I	ω' $[rad/s]$	μ'^R	μ'^I
0.12	6790	7578	0.12	9.57	18.46	0.12	70.7	67
0.18	3517	4328	0.19	4.38	10.31	0.18	37.4	43
0.28	1944	2435	0.30	2.61	6.13	0.26	23.8	21
0.44	1127	1497	0.48	1.23	3.24	0.56	9	6.08
0.70	666	920	0.77	0.74	1.77	0.82	6.2	4.63
1.11	397	558	1.22	0.44	1.14	1.21	4.74	3.07
1.78	234	336	2.13	0.29	0.46	1.79	3.3	1.84
2.85	140	185	3.94	0.17	0.22	2.64	2.8	1.35
4.55	86	112	7.06	0.118	0.12	3.9	2.5	1.05
7.16	54	65	12.5	0.090	0.073	5.8	2.1	0.739
11.4	38	40	22.7	0.072	0.051	8.5	1.9	0.735
18.2	27	26	39.1	0.061	0.036	12.5	1.46	0.56
29.2	19	17	69.5	0.062	0.033	18.2	1.16	0.46
45.3	15	12				26.22	0.89	0.367
71.7	11	8.1				38.98	0.654	0.29
						56.73	0.49	0.25
						83.74	0.34	0.22

Table 3.2: Real and imaginary part of the complex viscosity for all muds from Lyanyungang studied by Huhe & Huang (in $N.s/m^2$)

Table 3.2 gives the real and imaginary parts of the complex viscosities for the three different solid fractions that Huhe & Huang studied: $\phi = 0.5$, $\phi = 0.26$ and $\phi = 0.17$. For the density of the solid part of this mud is $\rho^{(s)} = 2750\text{kg}.m^{-3}$. In this thesis, we will only use the sample with the solid fraction $\phi = 0.5$, corresponding to the density $1590\ \text{kg}.m^{-3}$. In figure 3-6, we plot the complex viscosity of this particular sample. Figure 3-9 shows the phase and modulus of the complex viscosity of Lianyungang mud . The viscosity phase is around $\frac{\pi}{4}$, so this mud is as much viscous as elastic.

3.1.4 Hangzhou Bay

The last mud comes from Hanghzou Bay which has been analyzed in [10], and later used by Krotov in [12]. In table 3.3, we tabulate the complex viscosity for different solid fractions ϕ. Here, $\rho^{(s)} = 2650\text{kg}.m^{-3}$.

Once again, we shall use only one sample, corresponding to the solid fraction $\phi = 0.34$, and thus a density $1561\ \text{kg}.m^{-3}$

The complex viscosity is shown in figure 3-8. Figure 3-9 shows the phase and modulus of the complex viscosity of Hangzhou Bay mud. Note that the phase is closer

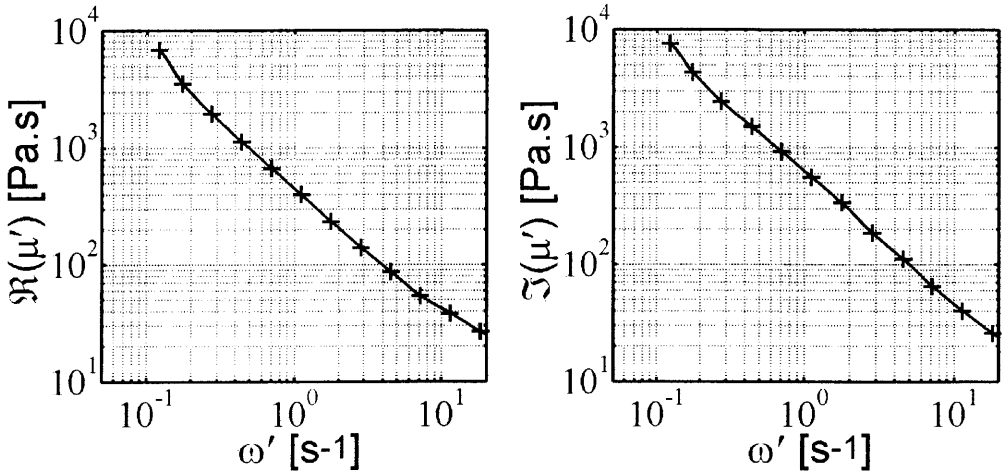

Figure 3-6: Interpolation of the real and imaginary part of the complex viscosity of Lianyungang mud (line). The crosses represent the experimental values.

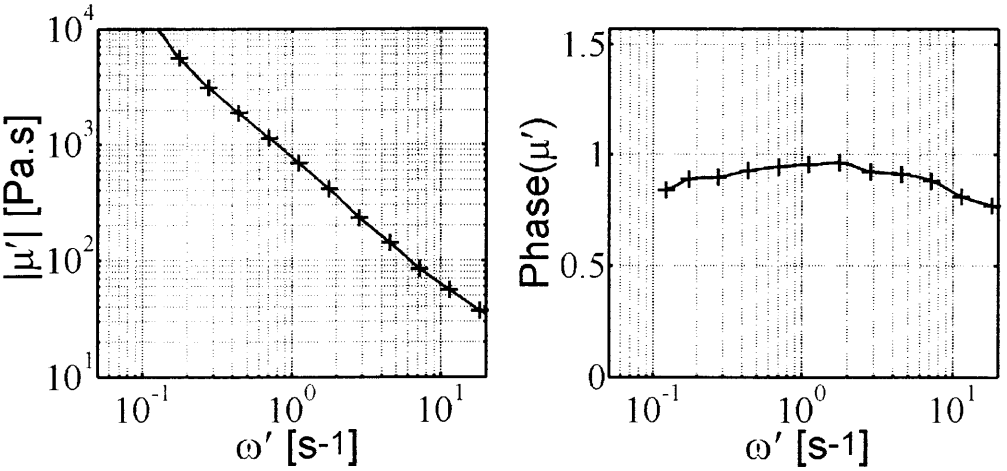

Figure 3-7: Phase and modulus of the complex viscosity interpolation of Lianyungang mud (line). The crosses represent the experimental values.

ω' $[rad/s]$		0.11	0.19	0.30	0.46	0.74	1.10	2.00	3.00	4.80	7.50	11.0	19.0
$\phi = 0.34$	μ'^R	190	75.0	40.0	21.0	12.0	9.00	6.00	4.00	3.30	3.10	2.80	2.60
	μ'^I	81.8	26.3	12.7	7.61	4.73	3.27	1.85	1.23	0.89	0.87	1.09	1.11
$\phi = 0.24$	μ'^R	17.0	7.00	4.00	2.50	2.00	1.70	1.80	1.50	1.10	0.80	0.50	0.33
	μ'^I	5.91	2.89	1.40	0.89	0.65	0.68	0.70	0.60	0.48	0.39	0.29	0.19
$\phi = 0.2$	μ'^R	7.00	2.50	1.50	0.80	0.60	0.40	0.28	0.29	0.23	0.23	0.23	0.15
	μ'^I	3.64	1.94	0.36	0.33	0.23	0.17	0.09	0.06	0.06	0.06	0.10	0.09
$\phi = 0.17$	μ'^R	5.00	2.10	1.10	0.70	0.55	0.40	0.35	0.30	0.25	0.25	0.25	0.09
	μ'^I	2.82	1.16	0.83	0.63	0.31	0.16	0.10	0.10	0.08	0.11	0.09	0.07
$\phi = 0.14$	μ'^R	5.00	2.50	1.50	0.90	0.70	0.50	0.40	0.22	0.17	0.11	0.08	0.05
	μ'^I	3.55	1.58	1.07	0.61	0.41	0.28	0.19	0.13	0.08	0.06	0.04	0.03
$\phi = 0.07$	μ'^R	0.40	0.30	0.12	0.21	0.11	0.11	0.08	0.06	0.04	0.03	0.02	0.01
	μ'^I	0.42	0.24	0.03	0.08	0.04	0.01	0.03	0.02	0.03	0.02	0.02	0.01

Table 3.3: Real and imaginary part of the complex viscosity for all muds from Hangzhou Bay studied by Huhe & Huang (in $N.s/m^2$)

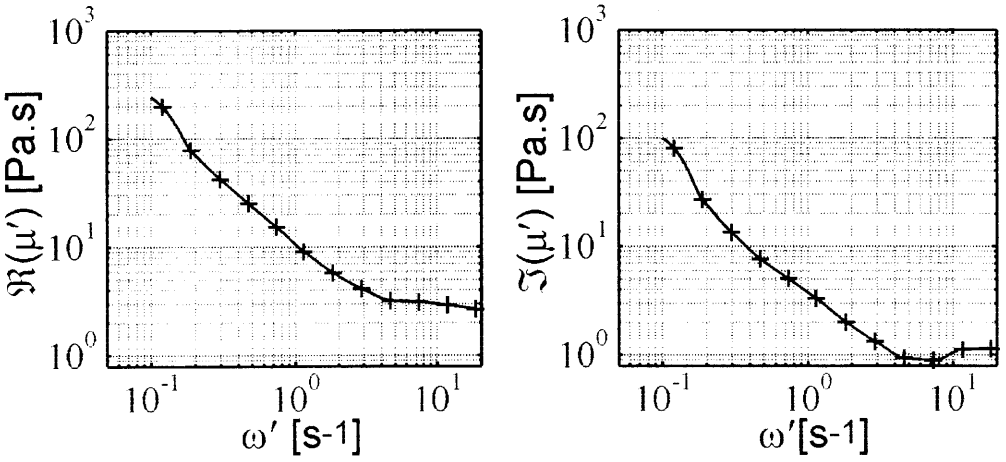

Figure 3-8: Interpolation of the real and imaginary part of the complex viscosity of Hangzhou Bay mud (line). The crosses represent the experimental values.

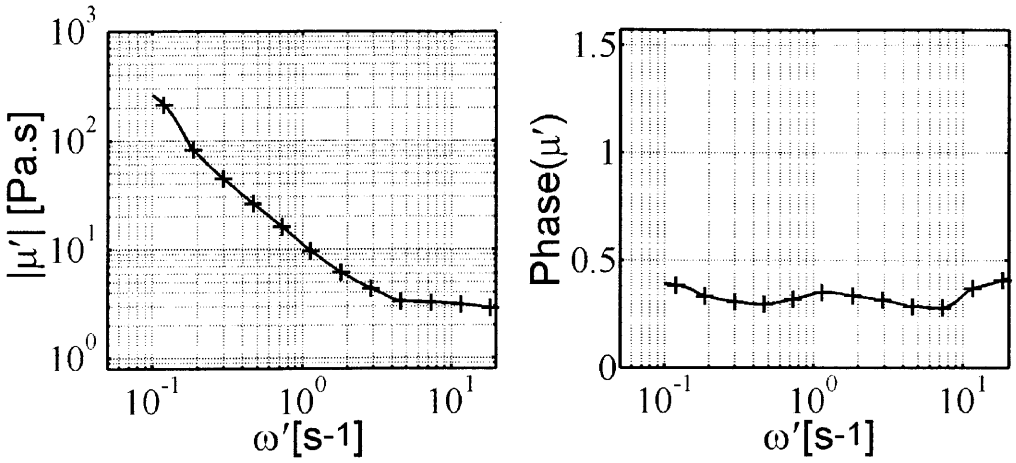

Figure 3-9: Phase and modulus of the complex viscosity interpolation of Hangzhou Bay mud (line). The crosses represent the experimental values.

Mud	Gulf of Mexico	Mobile Bay	Lianyungang	Hangzhou Bay
Density (kg.m^{-3})	1140	1281	1590	1561
$\|\mu'\|$-range (Pa.s)	$10^0 - 10^2$	$2.10^2 - 10^4$	$30 - 10^4$	$10^0 - 3.10^2$

Table 3.4: Viscosities of muds 3a,3b, 3c and 3d

to zero than to $\frac{\pi}{2}$. Hence , this mud is rather viscous. We sum up the viscosities of the different muds in table 3.4.

3.1.5 Determination of the zero-frequency viscosity μ'_0

It will be seen shortly that for calculating the drift velocity in mud we need the value of μ'_0, namely the 0-frequency viscosity of the mud (equation 3.6.2.5). This value corresponds to the viscosity at steady shear.

As the experiments are done under conditions of oscillations at finite frequencies, we have to get μ'_0 by extrapolating the measured data.

From equation 3.6.2.5, we see that the needed value is $\Re(1/\mu'_0)$. In order to find this value, we write the inverse of the complex viscosity $1/\mu'$ as a rational function of the frequency ω'. We used the method extrapolation described in the first chapter of Krotov's thesis ([12]). The principle of this method is to determine 8 coefficients a_n and b_n, based on 4 experimental values of $1/\mu'$ corresponding to 4 frequencies. These coefficients are such as:

$$\frac{1}{\mu'} = \frac{i}{\omega'} \frac{b_0 + \sum_{n=1}^{N-1} b_n (-i\omega')^n}{1 + \sum_{n=1}^{N} a_n (-i\omega')^n} \tag{3.1.5.1}$$

Mud	Reference frequencies [Hz]	$\Re(1/\mu_0') = b_1 - b_0 a_1$ [Pa.s]
Gulf of Mexico	0.2 ; 0.63 ; 1.58 ; 3.96	0.0012
Mobile Bay	0.13 ; 0.57 ; 5.65 ; 25.1	$6.39.10^{-6}$
Lianyungang	0.12 ; 0.44 ; 2.85 ; 18.2	$3.4.10^{-5}$
Hangzhou Bay	0.12 ; 0.73 ; 2.9 ; 7.3	0.0016

Table 3.5: Real value of the 0-frequency viscosity and frequencies used as references for each mud.

Once these coefficients known, $\Re(1/\mu_0')$ can easily be calculated. Indeed, when $\omega' \to 0$, $\Re(1/\mu') \to b_1 - b_0 a_1$, and thus:

$$\Re(1/\mu_0') = b_1 - b_0 a_1 \tag{3.1.5.2}$$

We have used this method for the four types of mud to be considered in this study. Table 3.5 sums up the 4 frequencies used and the values of $\Re(1/\mu_0')$ deduced for each mud.

These values will be used later in this study to represent the drift velocities in mud.

3.2 Scaling

The equations we previously obtained in water are not changed in the viscoelastic case. However, we need a new scaling for stress in mud.

We use the new scaling :

$$\tau_{ij} = \frac{d}{\epsilon \mu_s \sqrt{gh}} \tau_{ij}' \tag{3.2.0.3}$$

where μ_s is the characteristic value of the viscosity $|\mu|$.

We define the dimensionless complex viscosity:

$$\mu = \frac{\mu'}{\mu_s} \tag{3.2.0.4}$$

Because of calculation simplifications, we will see that the value μ_s is not needed to solve the last equations numerically. Indeed, we will see that neither μ_s neither any non-dimensional viscosity μ appear in the final results, but only the dimensional viscosity μ'.

To sum up, the new scaling for this section are:

$$\begin{array}{lll} x = kx' & z = \frac{z'}{h}b & t = k(g\bar{h})^{1/2}t' \\ p = \frac{p'}{\rho_W g A} & u = \frac{1}{\epsilon\sqrt{g\bar{h}}}u' & v = \frac{\kappa}{\epsilon\sqrt{g\bar{h}}}v' \\ \zeta = \frac{\zeta'}{A} & \phi = \phi' \left[\frac{A}{k\bar{h}}(g\bar{h})^{1/2}\right]^{-1} & \end{array} \tag{3.2.0.5}$$

and:

$$\begin{array}{lll} x = kx' & Z = \frac{Z'}{d} & t = k(g\bar{h})^{1/2}t' \\ P = \frac{P'}{\rho_W g A} & U = \frac{1}{\epsilon\sqrt{g\bar{h}}}U' & V = \frac{1}{\epsilon\kappa\kappa_d\sqrt{g\bar{h}}}V' \\ \eta = \frac{\eta'}{\kappa_d A} & \mathcal{U} = \frac{k}{\epsilon}\mathcal{U}' & \mathcal{V} = \frac{k}{\epsilon\kappa\kappa_d}\mathcal{V}' \\ T_{ij} = \frac{T'_{ij}}{\rho_W g A} & E_{ij,t} = \frac{d}{\epsilon\sqrt{g\bar{h}}}E'_{ij,t'} & \tau_{ij} = \frac{d}{\epsilon\mu_s\sqrt{g\bar{h}}}\tau'_{ij} \\ \mu = \frac{\mu'}{\mu_s} & & \end{array} \tag{3.2.0.6}$$

For simple harmonic waves, equation 3.0.0.4 becomes, in a non-dimensional form:

$$\tau_{xZ} = -i\omega\mu(\omega)E_{xZ} \tag{3.2.0.7}$$

3.3 Equations in water

Since only the mud behavior is modified, the equations in water are not changed. They remain exactly the same than in the Newtonian case.

The reader could thus refer to section 2.3 to follow the details of the calculations in water. In particular, the important results in water are gathered in equations 2.3.2.9, 2.3.3.6 and 2.3.4.3.

3.4 Equations in mud

Most of the equations in mud are also unchanged compared to the previous chapter. Namely equations 2.4.1.2, 2.4.2.2, 2.4.5.13, 2.4.5.20 and 2.4.6.1 remain the same:

The kinematic interface boundary condition:

$$\eta_t = V - \epsilon\eta_x U, \quad Z = 1 + \epsilon\eta \tag{3.4.0.8}$$

The conservation of mass:

$$U_x + V_Z = 0, \quad 0 < Z < 1 + \epsilon\eta \tag{3.4.0.9}$$

The tangential stress boundary condition at the interface:

$$\tau_{xZ}(Z=1) = -\epsilon\eta \frac{\partial \tau_{xZ}}{\partial Z}\Big|_{Z=1} + O(\epsilon^2) \tag{3.4.0.10}$$

The normal stress boundary condition at the interface combined with the vertical momentum equation:

$$\frac{\partial P}{\partial x} = \frac{\partial \zeta}{\partial x} - \kappa_d \frac{\partial \eta}{\partial x} + O(\kappa^2), \quad 0 < Z < 1 + \epsilon\eta \tag{3.4.0.11}$$

The bottom kinematic boundary condition:

$$U = V = 0, \quad Z = 0 \tag{3.4.0.12}$$

However, we need to find the new horizontal momentum equation, which is modified by the mud behavior.

In this case where the depth of mud d is small compared to the depth of water, we can approximate the strain as a function of the horizontal displacement $\mathcal{U}$:

$$E_{xZ} = \frac{\partial \mathcal{U}}{\partial Z} + \kappa^2 \kappa_d^2 \frac{\partial \mathcal{V}}{\partial x} = \frac{\partial \mathcal{U}}{\partial Z} + O(\kappa^4) \tag{3.4.0.13}$$

From 3.2.0.7 we deduce again for simple harmonic waves:

$$\tau_{xZ} = \mu \frac{\partial U}{\partial Z} + O(\kappa^4) \tag{3.4.0.14}$$

The equation of momentum in the mud, projected on the x-axis, gives:

$$\frac{\partial U}{\partial t} + \epsilon \left(U \frac{\partial U}{\partial x} + V \frac{\partial U}{\partial Z} \right) = -\gamma \frac{\partial P}{\partial x} + \frac{A}{Re^{(2)} * d} \left(\frac{\partial \tau_{xZ}}{\partial Z} + \kappa \kappa_d \frac{\partial \tau_{xx}}{\partial x} \right) \tag{3.4.0.15}$$

or:

$$\frac{\partial U}{\partial t} + \epsilon \left(U \frac{\partial U}{\partial x} + V \frac{\partial U}{\partial Z} \right) = -\gamma \frac{\partial P}{\partial x} + \frac{\epsilon}{Re^{(2)} * \kappa_d} \left(\frac{\partial \tau_{xZ}}{\partial Z} + \kappa \kappa_d \frac{\partial \tau_{xx}}{\partial x} \right) \tag{3.4.0.16}$$

where U is the horizontal velocity of mud, P the mud pressure, A the amplitude of the free surface, γ the ratio of densities $\gamma = \rho_W / \rho_M$, d the mud depth and $Re^{(2)}$ the new Reynolds number:

$$\boxed{Re^{(2)} = \frac{\rho_M A d k \sqrt{gh}}{\mu_s}} \tag{3.4.0.17}$$

Equation 3.4.0.16 can be rewritten:

$$\frac{\epsilon}{\kappa_d Re^{(2)}}\frac{\partial \tau_{xZ}}{\partial Z} - \frac{\partial U}{\partial t} = \gamma\frac{\partial P}{\partial x} + \epsilon\left(U\frac{\partial U}{\partial x} + V\frac{\partial U}{\partial Z}\right) + O(\kappa^2), \quad 0 < Z < 1 + \epsilon\eta \quad (3.4.0.18)$$

From equation 3.4.0.11, we know the mud pressure gradient $\frac{\partial P}{\partial x}$. As a consequence, equation 3.4.0.18 becomes:

$$\boxed{\frac{\epsilon}{\kappa_d Re^{(2)}}\frac{\partial \tau_{xZ}}{\partial Z} - \frac{\partial U}{\partial t} = \gamma\left(\frac{\partial \zeta}{\partial x} - \kappa_d\frac{\partial \eta}{\partial x}\right) + \epsilon\left(U\frac{\partial U}{\partial x} + V\frac{\partial U}{\partial Z}\right) + O(\kappa^2)} \quad (3.4.0.19)$$

which is true for $0 < Z < 1 + \epsilon\eta$.

3.5 Asymptotic equations in water and viscoelastic mud

3.5.1 Equations at dominant orders

Water equations

Since the equations in water are the same with a viscoelastic mud than with a Newtonian mud, the asymptotic equations are also exactly the same. We then simply use the results obtained in the Newtonian case (equations 2.5.1.11, 2.5.1.12, 2.5.1.14):

- at order $O(1)$

$$\frac{\partial^2 \zeta^{(0)}}{\partial t^2} - \frac{\partial^2 \zeta_0}{\partial x^2} = 0 \quad (3.5.1.1)$$

- at order $O(\kappa)$

$$\frac{\partial^2 \zeta^{(1)}}{\partial t^2} - \frac{\partial^2 \zeta_1}{\partial x^2} = 2\frac{\partial^2 \zeta^{(0)}}{\partial x \partial X} + \frac{\kappa_d}{\kappa}\frac{\partial^2 \eta^{(0)}}{\partial t^2} + \frac{3\epsilon}{2\kappa}\frac{\partial^2 (\zeta^{(0)})^2}{\partial t^2} \quad (3.5.1.2)$$

where equation 2.5.1.12 is obtained after using the following relation valid to leading order:

$$\frac{\partial^2 (\bar{u}^{(0)})^2}{\partial x^2} + \frac{\partial^2 (\bar{u}^{(0)})^2}{\partial t^2} + \frac{\partial^2 (\zeta^{(0)})^2}{\partial t^2} = 3\frac{\partial^2 (\zeta^{(0)})^2}{\partial t^2} \quad (3.5.1.3)$$

- at order $O(\kappa^2)$

$$\begin{aligned}\frac{\partial^2\zeta^{(2)}}{\partial t^2}-\frac{\partial^2\zeta^{(2)}}{\partial x^2}&=2\frac{\partial^2\zeta^{(1)}}{\partial X\partial x}+\frac{\kappa_d}{\kappa}\frac{\partial^2\eta^{(1)}}{\partial t^2}\\&+\frac{\epsilon}{\kappa}\left(\frac{\partial^2(\bar{u}^{(0)}\bar{u}^{(1)})}{\partial x^2}+\frac{\partial^2(\bar{u}^{(0)}\bar{u}^{(1)})}{\partial t^2}+\frac{\partial^2(\zeta^{(0)}\zeta^{(1)})}{\partial t^2}\right)\\&+\frac{\partial^2\zeta^{(0)}}{\partial X^2}+\frac{\epsilon}{\kappa}\frac{\partial^2(\bar{u}^{(0)})^2}{\partial x\partial X}+\frac{1}{3}\frac{\partial^4\zeta^{(0)}}{\partial x^4}-\frac{\epsilon\kappa_d}{\kappa^2}\frac{\partial\zeta^{(0)}(\eta^{(0)})_t}{\partial t}\\&+\frac{\epsilon\kappa_d}{\kappa^2}\frac{\partial^2\bar{u}^{(0)}\eta^{(0)}}{\partial x\partial t}\end{aligned}\tag{3.5.1.4}$$

Even though we carried the calculations in water up to order $O(\kappa^2)$, we will not use these results later in this thesis.

Indeed, we will only use the results at the order $O(\kappa^0)$ and $O(\kappa)$ in order to find a differential equation for the surface ζ.

Mud equations

From equation 3.4.0.19, we know:

$$\begin{aligned}\frac{\epsilon}{\kappa Re^{(2)}}\frac{\partial\tau_{xZ}}{\partial Z}-\frac{\partial U}{\partial t}&=\gamma\left(\frac{\partial\zeta}{\partial x}-\kappa_d\frac{\partial\eta}{\partial x}\right)+\epsilon\left(U\frac{\partial U}{\partial x}+V\frac{\partial U}{\partial Z}\right)+O(\kappa^2),\\0<Z<1+\epsilon\eta&\end{aligned}\tag{3.5.1.5}$$

To simplify this equation we introduce $\alpha^{(2)}$:

$$\alpha^{(2)}=\frac{\epsilon}{\kappa_d Re^{(2)}}=O(1)\tag{3.5.1.6}$$

and equation 3.5.1.5 becomes:

$$\begin{aligned}\alpha^{(2)}\frac{\partial\tau_{xZ}}{\partial Z}-\frac{\partial U}{\partial t}&=\gamma\left(\frac{\partial\zeta}{\partial x}-\kappa_d\frac{\partial\eta}{\partial x}\right)+\epsilon\left(U\frac{\partial U}{\partial x}+V\frac{\partial U}{\partial Z}\right)+O(\kappa^2),\\0<Z<1+\epsilon\eta&\end{aligned}\tag{3.5.1.7}$$

As in the preceding section we write:

$$\begin{aligned}U&=U^{(0)}+\kappa U^{(1)}+O(\kappa^2)\\V&=V^{(0)}+\kappa V^{(1)}+O(\kappa^2)\\\tau_{xZ}&=\tau_{xZ}^{(0)}+\kappa\tau_{xZ}^{(1)}+O(\kappa^2)\end{aligned}\tag{3.5.1.8}$$

and we introduce the multiple scale coordinates x and $X = \kappa x$, to finally obtain the dominant orders:

- at $O(\kappa^0)$:

$$\begin{aligned} \alpha^{(2)}\frac{\partial \tau_{xZ}^{(0)}}{\partial Z} - \frac{\partial U^{(0)}}{\partial t} &= \gamma \frac{\partial \zeta^{(0)}}{\partial x}, \quad 0 < Z < 1 \\ \frac{\partial U^{(0)}}{\partial x} + \frac{\partial V^{(0)}}{\partial Z} &= 0 \\ \frac{\partial \eta^{(0)}}{\partial t} &= V^{(0)}, \qquad Z = 1 \end{aligned} \tag{3.5.1.9}$$

- at $O(\kappa)$:

$$\begin{aligned} \alpha^{(2)}\frac{\partial \tau_{xZ}^{(1)}}{\partial Z} - \frac{\partial U^{(1)}}{\partial t} =& \gamma \frac{\partial \zeta^{(1)}}{\partial x} + \gamma \frac{\partial \zeta_0}{\partial X} - \gamma \frac{\kappa_d}{\kappa}\frac{\partial \eta^{(0)}}{\partial x} \\ &+ \frac{\epsilon}{\kappa}\left(U^{(0)}\frac{\partial U^{(0)}}{\partial x} + V^{(0)}\frac{\partial U^{(0)}}{\partial Z} \right), \\ & 0 < Z < 1 \\ \frac{\partial U^{(1)}}{\partial x} + \frac{\partial U^{(0)}}{\partial X} + \frac{\partial V^{(1)}}{\partial Z} &= 0 \\ \frac{\partial \eta^{(1)}}{\partial t} &= V^{(1)}, \quad Z = 1 \end{aligned} \tag{3.5.1.10}$$

The equations in mud at order $O(\kappa^0)$ will be used later to determine a differential equation for the surface ζ. The order $O(\kappa)$ will be used to determine the drift in mud.

3.5.2 Equation and solution at order $O(\kappa^0)$

Water equations

Like in the Newtonian mud, we consider the evolution of a train of simple harmonic waves:

$$\boxed{\zeta^{(0)} = \frac{1}{2}\sum_{m=-\infty}^{+\infty} A_m(X)e^{i\theta_m}} \qquad \boxed{\eta^{(0)} = \frac{1}{2}\sum_{m=-\infty}^{+\infty} B_m(X)e^{i\theta_m}} \tag{3.5.2.1}$$

and we deduce: $\theta_m = m(x - t)$

Mud equations

Once again, we write:

$$\begin{aligned} U^{(0)} &= \frac{1}{2}\sum_{m=-\infty}^{\infty} U^{(0)}(Z)e^{i\theta_m} \\ V^{(0)} &= \frac{1}{2}\sum_{m=-\infty}^{\infty} V_m^{(0)}(Z)e^{i\theta_m} \\ \tau_{xZ}^{(0)} &= \frac{1}{2}\sum_{m=-\infty}^{\infty} (\tau_{xZ}^{(0)})_m(Z)e^{i\theta_m} \end{aligned} \tag{3.5.2.2}$$

From equation 3.5.1.9, we deduce:

$$\alpha^{(2)}\frac{\partial(\tau_{xZ}^{(0)})_m}{\partial Z} + imU_m^{(0)} = im\gamma A_m \tag{3.5.2.3}$$

For the term $(\tau_{xZ}^{(0)})_m(Z)$ corresponding to harmonic waves, we have from equation 3.4.0.14 that:

$$(\tau_{xZ}^{(0)})_m(Z) = \mu_m\frac{dU_m^{(0)}}{dZ} + O(\kappa^4) \tag{3.5.2.4}$$

where μ_m is the dimensionless viscosity corresponding to frequency m.

As a consequence, by equations 3.5.2.3 and 3.5.2.4, we obtain:

$$\frac{d^2U_m^{(0)}}{dZ^2} - \tilde{\sigma}_m^2 U_m^{(0)} = -\tilde{\sigma}_m^2\gamma A_m \tag{3.5.2.5}$$

where:

$$\tilde{\sigma}_m^2 = -i\frac{m}{\alpha^{(2)}\mu_m} \tag{3.5.2.6}$$

meaning:

$$\boxed{\tilde{\sigma}_m^2 = -i\frac{m\kappa_d\rho_M Adk\sqrt{gh}}{\epsilon\mu'_m}} \tag{3.5.2.7}$$

Let us note that the value of $\tilde{\sigma}_m$ does not depend on μ_s, since $\mu_s\mu_m = \mu'_m$ is the dimensional viscosity. Since $\tilde{\sigma}_m$ and γ are the only parameters that appear in equation 3.5.2.5, we will not need the value of μ_s to solve this equation.

Equation 3.5.2.5 is equivalent to equation 2.5.2.3, but in the viscoelastic case.

Since these equations only differ by the value of σ and all the others mud equations are the same than in the Newtonian case, we can straightforwardly deduce that the mud relation between the $A_m(X)$ and $B_m(X)$ is the same than equation 2.5.2.11, but

with a different coefficient σ:

$$\boxed{B_m(X) = \gamma A_m(X)\left(1 - \frac{\tanh(\tilde{\sigma}_m)}{\tilde{\sigma}_m}\right)} \tag{3.5.2.8}$$

where $\tilde{\sigma}_m^2 = -i\frac{m\kappa_d\rho_M A dk\sqrt{gh}}{\epsilon\mu'_m}$ and $\gamma = \frac{\rho_W}{\rho_M}$. Note that $U_0^{(0)} = 0$.

3.5.3 Equation and solution at order $O(\kappa)$

Water equations

The water equations are the same than in the viscous case, so equation 2.5.3.5 is still true:

$$\forall m \neq 0,\ \frac{dA_m}{dX} = -\frac{im}{2}\frac{\kappa_d}{\kappa}B_m - \frac{3i}{8}\frac{\epsilon}{\kappa}m\left[\sum_{l=1}^{\infty} 2A_l^* A_{m+1l} + \sum_{l=1}^{[m/2]} \alpha_l A_l A_{m-l}\right] \tag{3.5.3.1}$$

which can be combined to equation 3.5.2.8 to give a partial differential equation on the A_m, for all m:

$$\frac{dA_m}{dX} = -\frac{i\gamma m}{2}\frac{\kappa_d}{\kappa}A_m(X)\left(1 - \frac{\tanh(\tilde{\sigma}_m)}{\tilde{\sigma}_m}\right) - \frac{3i}{8}\frac{\epsilon}{\kappa}m\left[\sum_{l=1}^{\infty} 2A_l^* A_{m+1l} + \sum_{l=1}^{[m/2]} \alpha_l A_l A_{m-l}\right] \tag{3.5.3.2}$$

Mud equations

Once again, we study the order $O(\kappa)$ of the mud equations because non-linearity creates a very interesting drift phenomenon at this order.

We had from equation 3.5.1.10:

$$\alpha^{(2)}\frac{\partial(\tau_{xZ})^{(1)}}{\partial Z} - \frac{\partial U^{(1)}}{\partial t} = \gamma\frac{\partial\zeta^{(1)}}{\partial x} + \gamma\frac{\partial\zeta^{(0)}}{\partial X} - \gamma\frac{\kappa_d}{\kappa}\frac{\partial\eta_0}{\partial x} + \frac{\epsilon}{\kappa}\left(U^{(0)}\frac{\partial U^{(0)}}{\partial x} + (V)_0\frac{\partial U^{(0)}}{\partial Z}\right), \quad 0 < Z < 1 \tag{3.5.3.3}$$

As a consequence, the zeroth harmonic of $U^{(1)}$ is not zero:

$$\alpha^{(2)}\frac{\partial(\tau_{xZ})_0^{(1)}}{\partial Z} = \frac{1}{2}\frac{\epsilon}{\kappa}\sum_{m=1}^{\infty}\left[(-im)U_m^{(0)}U_{-m}^{(0)} + (im)U_{-m}^{(0)}U_m^{(0)} + V_m^{(0)}\frac{\partial U_{-m}^{(0)}}{\partial Z} + V_{-m}^{(0)}\frac{\partial U_m^{(0)}}{\partial Z}\right] \tag{3.5.3.4}$$

and thus:

$$\alpha^{(2)}\mu_0\frac{d^2U_0^{(1)}}{dZ^2} = \frac{1}{2}\frac{\epsilon}{\kappa}\sum_{m=1}^{\infty}\left[V_m^{(0)}\frac{\partial U_{-m}^{(0)}}{\partial Z} + V_{-m}^{(0)}\frac{\partial U_m^{(0)}}{\partial Z}\right] \tag{3.5.3.5}$$

By the same token as in the previous chapter, we easily deduce the following equation for the drift velocity:

$$\frac{d^2U_0^{(1)}}{dZ^2} = \frac{Re^{(2)}\kappa_d}{\mu_0\kappa}\sum_{m=1}^{\infty}\Re\left[V_{-m}^{(0)}\frac{\partial U_m^{(0)}}{\partial Z}\right] \tag{3.5.3.6}$$

3.6 Further details

3.6.1 Surface and the interface

We truncate the series 3.5.3.2 , in order to obtain a finite system of differential equations for the A_m, for all $0 < m \leq n$:

$$\boxed{\frac{dA_m}{dX} + \frac{i\gamma m}{2}\frac{\kappa_d}{\kappa}\left(1 - \frac{\tanh(\tilde{\sigma}_m)}{\tilde{\sigma}_m}\right)A_m + \frac{3i}{8}\frac{\epsilon}{\kappa}m\left(\sum_{l=1}^{n-m}2A_l^*A_{m+l} + \sum_{l=1}^{[m/2]}\alpha_l A_l A_{m-l}\right) = 0} \tag{3.6.1.1}$$

Let us note that this equation is the same as equation 2.6.1.1 in the case of Newtonian mud, except for the parameter σ_m that became $\tilde{\sigma}_m$ because of complex viscosity.

Since this equation depends on γ, κ, κ_d, ϵ and the $\tilde{\sigma}_m$, we deduce that the result of the A_m will depend on the values:

$$g, \rho_W, \rho_M, A, \bar{h}, d, \omega', \mu'_m \tag{3.6.1.2}$$

where g and ρ_W are fixed, ρ_M and the μ'_m depend on the mud we consider, and A, $\bar{h}$, ω' and d depend on the geometry and the surface wave.

3.6.2 Drift current in mud

We also truncate the result we got in 3.5.3.6 for the drift in velocity:

$$\frac{\partial^2U_0^{(1)}}{\partial Z^2} = \frac{Re^{(2)}\kappa_d}{\mu_0\kappa}\sum_{m=1}^{n}\Re\left[V_{-m}^{(0)}\frac{\partial U_m^{(0)}}{\partial Z}\right] \tag{3.6.2.1}$$

Since equation 3.5.1.9 is the same as equation 2.5.1.21 except that α_m is replaced

by $\alpha_m^{(2)}\mu$, we can easily deduce $\frac{\partial U_m^{(0)}}{\partial Z}$ and $V_{-m}^{(0)}$ from 2.6.2.2 and 2.6.2.3:

In the end we get:

$$\frac{\partial U_m^{(0)}}{\partial Z} = \gamma A_m[-\tilde{\sigma_m}\sinh(\tilde{\sigma_m}Z) + \tilde{\sigma_m}\tanh(\tilde{\sigma}_m)\cosh(\tilde{\sigma}_m Z)] \tag{3.6.2.2}$$

$$V_{-m}^{(0)} = i\frac{m\gamma A_m^*}{\tilde{\sigma}_m^*}[\tilde{\sigma}_m^* Z - \sinh(\tilde{\sigma}_m^* Z) + \tanh(\tilde{\sigma}_m^*)(\cosh(\tilde{\sigma}_m^* Z) - 1)] \tag{3.6.2.3}$$

Integrating as done in the Newtonian case, we get the expression of $\frac{\partial U_0^{(1)}}{\partial Z}$:

$$\begin{aligned}
\frac{\partial U_0^{(1)}}{\partial Z} = &-\sum_{m=1}^{n} |A_m|^2 \Big[\gamma^2 \frac{Re^{(2)}\kappa_d}{\mu_0\kappa}\Im\Big[\frac{m}{\tilde{\sigma}_m^*}\Big[-\tilde{\sigma}_m^*\Big(Z\cosh(\tilde{\sigma}_m Z) - \frac{\sinh(\tilde{\sigma}_m Z)}{\tilde{\sigma}_m}\Big) \\
&+ \tilde{\sigma}_m^*\tanh(\tilde{\sigma}_m)\Big(Z\sinh(\tilde{\sigma}_m Z) - \frac{\cosh(\tilde{\sigma}_m Z)}{\tilde{\sigma}_m}\Big) \\
&+ \frac{\sinh(2\tilde{\sigma}_m^R Z)}{4\tilde{\sigma}_m^R}\tilde{\sigma}_m(1 + \tanh(\tilde{\sigma}_m)(\tanh(\tilde{\sigma}_m))^*) \\
&+ \frac{\sinh(2i\tilde{\sigma}_m^I Z)}{4i\tilde{\sigma}_m^I}\tilde{\sigma}_m(\tanh(\tilde{\sigma}_m)(\tanh(\tilde{\sigma}_m))^* - 1) \\
&- \frac{\cosh(2\tilde{\sigma}_m^R Z)}{4\tilde{\sigma}_m^R}\tilde{\sigma}_m(\tanh(\tilde{\sigma}_m) + (\tanh(\tilde{\sigma}_m))^*) \\
&+ \frac{\cosh(2i\tilde{\sigma}_m^I Z)}{4i\tilde{\sigma}_m^I}\tilde{\sigma}_m(\tanh(\tilde{\sigma}_m) - (\tanh(\tilde{\sigma}_m))^*) + (\tanh(\tilde{\sigma}_m))^*\cosh(\tilde{\sigma}_m Z) \\
&- \tanh(\tilde{\sigma}_m)(\tanh(\tilde{\sigma}_m))^*\sinh(\tilde{\sigma}_m Z)\Big]\Big] + C_m^{(1)}\Big]
\end{aligned} \tag{3.6.2.4}$$

and then $U_0^{(1)}$:

$$\begin{aligned}
U_0^{(1)} = &- \sum_{m=1}^{n} |A_m|^2 \Big[\gamma^2 \frac{Re^{(2)}\kappa_d}{\mu_0 \kappa} \Im \Big[\frac{m}{\tilde{\sigma}_m^*} \Big[- \tilde{\sigma}_m^* \Big(\frac{Z \sinh(\tilde{\sigma}_m Z)}{\tilde{\sigma}_m} - 2 \frac{\cosh(\tilde{\sigma}_m Z)}{\tilde{\sigma}_m^2} \Big) \\
&+ \tilde{\sigma}_m^* \tanh(\tilde{\sigma}_m) \Big(\frac{Z \cosh(\tilde{\sigma}_m Z)}{\tilde{\sigma}_m} - 2 \frac{\sinh(\tilde{\sigma}_m Z)}{\tilde{\sigma}_m^2} \Big) \\
&+ \frac{\cosh(2\tilde{\sigma}_m^R Z)}{4(\tilde{\sigma}_m^R)^2} \tilde{\sigma}_m (1 + \tanh(\tilde{\sigma}_m)(\tanh(\tilde{\sigma}_m))^*) \\
&+ \frac{\cosh(2i\tilde{\sigma}_m^I Z)}{8(\tilde{\sigma}_m^I)^2} \tilde{\sigma}_m (\tanh(\tilde{\sigma}_m)(\tanh(\tilde{\sigma}_m))^* - 1) \\
&- \frac{\sinh(2\tilde{\sigma}_m^R Z)}{8(\tilde{\sigma}_m^R)^2} \tilde{\sigma}_m (\tanh(\tilde{\sigma}_m) + (\tanh(\tilde{\sigma}_m))^*) \\
&+ \frac{\sinh(2i\tilde{\sigma}_m^I Z)}{8(\tilde{\sigma}_m^I)^2} \tilde{\sigma}_m (\tanh(\tilde{\sigma}_m) - (\tanh(\tilde{\sigma}_m))^*) + (\tanh(\tilde{\sigma}_m))^* \frac{\sinh(\tilde{\sigma}_m Z)}{\tilde{\sigma}_m} \\
&- \tanh(\tilde{\sigma}_m)(\tanh(\tilde{\sigma}_m))^* \frac{\cosh(\tilde{\sigma}_m Z)}{\tilde{\sigma}_m} \Big] \Big] + C_m^{(1)} Z + C_m^{(2)} \Big]
\end{aligned} \tag{3.6.2.5}$$

with $\tilde{\sigma}_m = \tilde{\sigma}_m^R + i\tilde{\sigma}_m^I$, $\tilde{\sigma}_m^R$ and $\tilde{\sigma}_m^I$ are reals.

We know that:

$$U_0^{(1)}(Z = 0) = 0 \tag{3.6.2.6}$$

As a consequence, we deduce the value of $C_m^{(2)}$:

$$\begin{aligned}
C_m^{(2)} = &\gamma^2 \frac{Re^{(2)}\kappa_d}{\mu_0 \kappa} \Im \Big[\frac{m}{\sigma_m^*} \Big[- \frac{2\tilde{\sigma}_m^*}{\tilde{\sigma}_m^2} - \frac{\tilde{\sigma}_m (1 + \tanh(\tilde{\sigma}_m)(\tanh(\tilde{\sigma}_m))^*)}{8(\tilde{\sigma}_m^R)^2} \\
&- \frac{\tilde{\sigma}_m (1 - \tanh(\tilde{\sigma}_m)(\tanh(\tilde{\sigma}_m))^*)}{8(\tilde{\sigma}_m^I)^2} + \frac{\tanh(\tilde{\sigma}_m)(\tanh(\tilde{\sigma}_m))^*}{\tilde{\sigma}_m} \Big] \Big]
\end{aligned} \tag{3.6.2.7}$$

We now make use of the interface boundary condition 3.4.0.10 in order to obtain the value of $C_m^{(1)}$. From this equation, we know that:

$$\tau_{xZ}^{(1)}(Z = 1) = -\epsilon \eta^{(0)} \frac{\partial \tau_{xZ}^{(0)}}{\partial Z}\Big|_{Z=1} \tag{3.6.2.8}$$

and so:

$$(\tau_{xZ})_0^{(1)}(Z = 1) = -\frac{\epsilon}{\kappa} \frac{1}{4} \sum_{m=1}^{\infty} \left[B_m \frac{\partial (\tau_{xZ})_{-m}^{(0)}}{\partial Z}\Big|_{Z=1} + B_{-m} \frac{\partial (\tau_{xZ})_m^{(0)}}{\partial Z}\Big|_{Z=1} \right] \tag{3.6.2.9}$$

From equation 6.2.0.14, which only applies to simple harmonic waves, we know:

$$\forall p, (\tau_{xZ})_m^{(p)} = \mu_m \frac{dU_m^{(p)}}{dZ} + O(\kappa^4) \tag{3.6.2.10}$$

and we can replace τ_{xZ} in the last equation:

$$\begin{aligned}
\mu_0 \frac{\partial U_0^{(1)}}{\partial Z}\Big|_{Z=1} &= -\frac{\epsilon}{\kappa}\frac{1}{4}\sum_{m=1}^{\infty}\left[B_m\mu_{-m}\frac{\partial^2 U_{-m}^{(0)}}{\partial Z^2}\Big|_{Z=1} + B_{-m}\mu_m\frac{\partial^2 U_m^{(0)}}{\partial Z^2}\Big|_{Z=1}\right] \\
&= -\frac{\epsilon}{\kappa}\frac{1}{4}\sum_{m=1}^{\infty}\left[B_m\Big(\mu_m\frac{\partial^2 U_m^{(0)}}{\partial Z^2}\Big|_{Z=1}\Big)^* + (B_m)^*\mu_m\frac{\partial^2 U_m^{(0)}}{\partial Z^2}\Big|_{Z=1}\right] \\
&= -\frac{\epsilon}{\kappa}\frac{1}{2}\sum_{m=1}^{\infty}\Re\left[B_m\Big(\mu_m\frac{\partial^2 U_m^{(0)}}{\partial Z^2}\Big|_{Z=1}\Big)^*\right]
\end{aligned} \tag{3.6.2.11}$$

Knowing that:

$$B_m = \gamma A_m G(\tilde{\sigma}_m) \tag{3.6.2.12}$$

and:

$$\frac{\partial^2 U_m^{(0)}}{\partial Z^2}\Big|_{Z=1} = -\gamma A_m \tilde{\sigma}_m^2 \mathrm{sech}(\tilde{\sigma}_m) \tag{3.6.2.13}$$

equation 3.6.2.11 becomes:

$$\begin{aligned}
\frac{\partial U_0^{(1)}}{\partial Z}\Big|_{Z=1} &= \frac{\epsilon}{\kappa\mu_0}\frac{1}{2}\sum_{m=1}^{\infty}\Re\left[\gamma A_m G(\tilde{\sigma}_m)\mu_m^*\gamma A_m^*(\tilde{\sigma}_m^*)^2\mathrm{sech}(\tilde{\sigma}_m^*)\right] \\
&= \frac{\epsilon\gamma^2}{2\kappa\mu_0}\sum_{m=1}^{\infty}|A_m|^2\Re\left[G(\tilde{\sigma}_m)\mu_m^*(\tilde{\sigma}_m^*)^2\mathrm{sech}(\tilde{\sigma}_m^*)\right] \\
&= \frac{\epsilon\gamma^2}{2\kappa\mu_0}\sum_{m=1}^{\infty}|A_m|^2\Im\left[iG(\tilde{\sigma}_m)\mu_m^*(\tilde{\sigma}_m^*)^2\mathrm{sech}(\tilde{\sigma}_m^*)\right]
\end{aligned} \tag{3.6.2.14}$$

Let us truncate this last equation:

$$\frac{\partial U_0^{(1)}}{\partial Z}\Big|_{(Z=1)} = \frac{\epsilon\gamma^2}{2\kappa\mu_0}\sum_{m=1}^{n}|A_m|^2\Im\left[iG(\tilde{\sigma}_m)\mu_m^*(\tilde{\sigma}_m^*)^2\mathrm{sech}(\tilde{\sigma}_m^*)\right] \tag{3.6.2.15}$$

From equation 3.6.2.4, we deduce the condition that $C_m^{(1)}$ needs to meet in order to

respect this boundary condition:

$$
\begin{aligned}
&-\gamma^2\frac{Re^{(2)}\kappa_d}{\mu_0\kappa}\Im\Big[\frac{m}{\tilde\sigma_m^*}\Big(\tilde\sigma_m^*\Big(\cosh(\tilde\sigma_m)-\frac{\sinh(\tilde\sigma_m)}{\tilde\sigma_m}\Big)-\sigma_m^*\tanh(\sigma_m)\Big(\sinh(\tilde\sigma_m)-\frac{\cosh(\tilde\sigma_m)}{\tilde\sigma_m}\Big)\\
&\quad-\frac{\sinh(2\tilde\sigma_m^R)}{4\tilde\sigma_m^R}\tilde\sigma_m(1+\tanh(\tilde\sigma_m)(\tanh(\tilde\sigma_m))^*)\\
&\quad-\frac{\sinh(2i\tilde\sigma_m^I)}{4i\tilde\sigma_m^I}\tilde\sigma_m(\tanh(\tilde\sigma_m)(\tanh(\tilde\sigma_m))^*-1)\\
&\quad+\frac{\cosh(2\tilde\sigma_m^R)}{4\tilde\sigma_m^R}\tilde\sigma_m(\tanh(\tilde\sigma_m)+(\tanh(\tilde\sigma_m))^*)\\
&\quad-\frac{\cosh(2i\tilde\sigma_m^I)}{4i\tilde\sigma_m^I}\tilde\sigma_m(\tanh(\tilde\sigma_m)-(\tanh(\tilde\sigma_m))^*)\\
&\quad-(\tanh(\tilde\sigma_m))^*\cosh(\tilde\sigma_m)+\tanh(\tilde\sigma_m)(\tanh(\tilde\sigma_m))^*\sinh(\tilde\sigma_m)\Big)\Big]-C_m^{(1)}\\
&\quad=\frac{\epsilon\gamma^2}{2\kappa\mu_0}\Im\left[iG(\tilde\sigma_m)\mu_m^*(\tilde\sigma_m^*)^2\mathrm{sech}(\tilde\sigma_m^*)\right]
\end{aligned}
\tag{3.6.2.16}
$$

We finally obtain the value of $C_m^{(1)}$:

$$
\begin{aligned}
C_m^{(1)}=&-\frac{\epsilon\gamma^2}{2\kappa\mu_0}\Im\left[iG(\tilde\sigma_m)\mu_m^*(\tilde\sigma_m^*)^2\mathrm{sech}(\tilde\sigma_m^*)\right]\\
&+\gamma^2\frac{Re^{(2)}\kappa_d}{\mu_0\kappa}\Im\Big[\frac{m}{\sigma_m^*}\Big[\tilde\sigma_m^*\Big(\cosh(\tilde\sigma_m)-\frac{\sinh(\tilde\sigma_m)}{\tilde\sigma_m}\Big)\\
&-\tilde\sigma_m^*\tanh(\tilde\sigma_m)\Big(\sinh(\tilde\sigma_m)-\frac{\cosh(\tilde\sigma_m)}{\tilde\sigma_m}\Big)\\
&-\frac{\sinh(2\tilde\sigma_m^R)}{4\tilde\sigma_m^R}\tilde\sigma_m(1+\tanh(\tilde\sigma_m)(\tanh(\tilde\sigma a_m))^*)\\
&-\frac{\sinh(2i\tilde\sigma_m^I)}{4i\tilde\sigma_m^I}\tilde\sigma_m(\tanh(\tilde\sigma_m)(\tanh(\tilde\sigma_m))^*-1)\\
&+\frac{\cosh(2\tilde\sigma_m^R)}{4\tilde\sigma_m^R}\tilde\sigma_m(\tanh(\tilde\sigma_m)+(\tanh(\tilde\sigma_m))^*)\\
&-\frac{\cosh(2i\tilde\sigma_m^I)}{4i\tilde\sigma_m^I}\tilde\sigma_m(\tanh(\tilde\sigma_m)-(\tanh(\tilde\sigma_m))^*)\\
&-(\tanh(\tilde\sigma_m))^*\cosh(\tilde\sigma_m)+\tanh(\tilde\sigma_m)(\tanh(\tilde\sigma_m))^*\sinh(\tilde\sigma_m)\Big]\Big]
\end{aligned}
\tag{3.6.2.17}
$$

The drift current is now found.

Let us precise again that the drift current we found does not depend on the characteristic value of viscosity μ_s. Indeed, even though $Re^{(2)}$, μ_0 and μ_m appear,

they always do as a ratio, either $Re^{(2)}/\mu_0$ or μ_m^*/μ_0.As:

$$\begin{aligned} \frac{Re^{(2)}}{\mu_0} &= \frac{\rho_M A dk\sqrt{gh}}{\mu_0'} \\ \frac{\mu_m^*}{\mu_0} &= \frac{(\mu_m')^*}{\mu_0'}, \end{aligned} \tag{3.6.2.18}$$

the value μ_s is not needed.

We find that the drift current depends on the same parameters as $|A_m|$, namely:

$$g, \rho_W,\ \rho_M,\ A,\ \bar{h},\ d,\ \omega',\ \mu_m' \tag{3.6.2.19}$$

where g and ρ_W are fixed, ρ_M and the μ_m' depend on the mud we consider, and A, $\bar{h}$, ω' and d depend on the geometry and the surface wave.

3.6.3 Energy variation in water

We obtained the differential equation:

$$\frac{dA_m}{dX} = -\frac{i\gamma m}{2}\frac{\kappa_d}{\kappa}A_m(X)\left(1 - \frac{\tanh(\tilde{\sigma}_m)}{\tilde{\sigma}_m}\right) - \frac{3i}{8}\frac{\epsilon}{\kappa}m\left[\sum_{l=1}^{\infty} 2A_l^* A_{m+1l} + \sum_{l=1}^{[m/2]} \alpha_l A_l A_{m-l}\right] \tag{3.6.3.1}$$

to describe the free surface motion.

In [8], G. Grataloup and C.C. Mei demonstrated that if the differential equation describing the free surface is:

$$\frac{dA_m}{dX} + \beta_m A_m - \frac{im^3}{6}A_m + \frac{3i}{8}\frac{\epsilon}{\kappa}m\left(\sum_{l=1}^{\infty} 2A_l^* A_{m+l} + \sum_{l=1}^{[m/2]} \alpha_l A_l A_{m-l}\right) = 0, \tag{3.6.3.2}$$

then the general relation on the first-order wave-energy is:

$$\frac{d}{dX}\left[\sum_{m=1}^{n} |A_m|^2\right] = -2\sum_{m=1}^{n} \Re(\beta_m)|A_m|^2 \tag{3.6.3.3}$$

Indeed, in equation 3.6.3.2, β_m represents a dissipation source. That is why the total wave energy at the leading order decreases with relation to β_m.

In our case of a flat bottom with a moderately thin layer of visco-elastic mud, we

deduce that the general relation on the first-order wave energy is:

$$\boxed{\frac{d}{dX}\left[\sum_{m=1}^{n}|A_m|^2\right] = -\gamma\frac{\kappa_d}{\kappa}\sum_{m=1}^{n}\Re\left[im\left(1-\frac{\tanh(\tilde{\sigma}_m)}{\tilde{\sigma}_m}\right)\right]|A_m|^2} \tag{3.6.3.4}$$

3.7 Attenuation rate

3.7.1 Attenuation rate as a function of κ

From the energy variation equation we obtained (3.6.3.4), we know that the attenuation rate fot the $m-$th harmonic is :

$$\begin{aligned}\frac{1}{L_m} &= \gamma\frac{\kappa_d}{\kappa}\Re\left[im\left(1-\frac{\tanh(\tilde{\sigma}_m)}{\tilde{\sigma}_m}\right)\right] \\ &= -\gamma\frac{\kappa_d}{\kappa}\Im\left[m\left(1-\frac{\tanh(\tilde{\sigma}_m)}{\tilde{\sigma}_m}\right)\right]\end{aligned} \tag{3.7.1.1}$$

After the distance $O(L_m)$ the $m-$th harmonic will be damped out.

Let us first study the function:

$$G(\tilde{\sigma}) = 1-\frac{\tanh(\tilde{\sigma})}{\tilde{\sigma}} \tag{3.7.1.2}$$

For that we write $\tilde{\sigma} = |\tilde{\sigma}|e^{-i\frac{\pi}{4}-i\theta_\sigma}$ and we plot G as a function of $|\tilde{\sigma}|$ for different phase angles θ_σ, where $0 < \theta_\sigma < \frac{\pi}{4}$. The results are shown in figure 3-10. The function $G(\tilde{\sigma})$ has been studied analytically by Mei et al. ([12]).

Following the same reasoning, we write

$$\tilde{\sigma} = \alpha + i\beta \tag{3.7.1.3}$$

with α and β real numbers. Then we obtain that:

$$G(\tilde{\sigma}) = 1-\frac{1}{\tilde{\sigma}}\frac{\sinh(\alpha)\cosh(\alpha)+i\sin(\beta)\cos(\beta)}{\cos^2(\beta)\cosh^2(\alpha)+\sin^2(\beta)\sinh^2(\alpha)} \tag{3.7.1.4}$$

and in particular,

$$\Im(G(\tilde{\sigma})) = -\frac{\left[\Re\left(\frac{1}{\tilde{\sigma}}\right)\sin(\beta)\cos(\beta)+\Im\left(\frac{1}{\tilde{\sigma}}\right)\sinh(\alpha)\cosh(\alpha)\right]}{\cos^2(\beta)\cosh^2(\alpha)+\sin^2(\beta)\sinh^2(\alpha)} \tag{3.7.1.5}$$

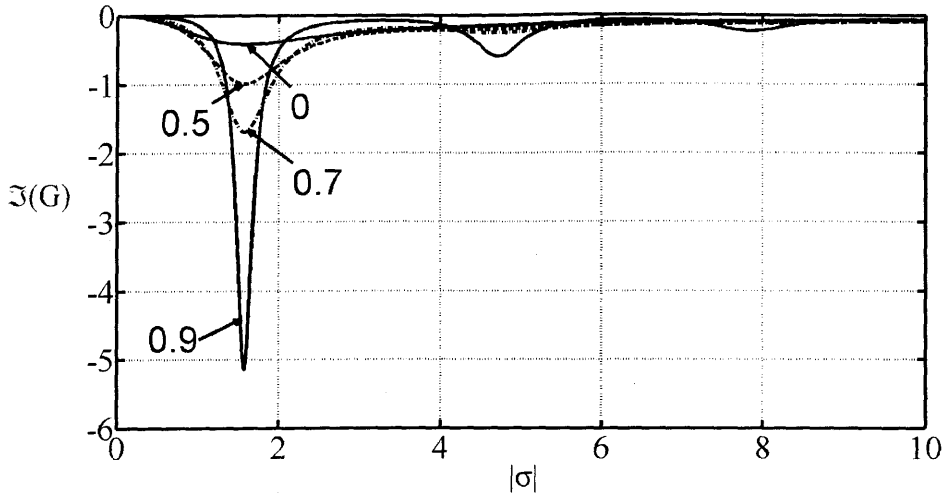

Figure 3-10: Variation of the real and imaginary parts of $G(\tilde{\sigma})$ as a function of the modulus $|\tilde{\sigma}|$, for different values of $\frac{4}{\pi}\theta_\sigma$. We see that $\Im(G)$ reaches the biggest values for $\frac{4}{\pi}\theta_\sigma = 0.9$.

As a consequence, the denominator of $\Im(G)$ vanishes if

$$\cos(\beta) = \sinh(\alpha) = 0 \tag{3.7.1.6}$$

i.e. when

$$\theta = \frac{\pi}{4}, \qquad |\tilde{\sigma}| = \left(\frac{1}{2} + n\right)\pi \tag{3.7.1.7}$$

where n is an integer.

Thus large $\Im(G)$ may occur if the mud is highly elastic $\theta \simeq \frac{\pi}{4}$ and if the modulus $|\tilde{\sigma}|$ has the special value given by 3.7.1.7. In particular the first peaks of $\Im(G)$ are at $|\tilde{\sigma}| = 1.57,\ 4.71,\ 7.85$ for $n = 0,\ 1,\ 2$.

3.7.2 Attenuation of the first harmonic

Let us first consider just the first harmonic $m = 1$.

We know the dimensional complex viscosity μ' as a function of the dimensional ω' for all the different types of muds from the previous section.

We also know that we used the scaling $\omega' = k(g\bar{h})^{1/2}$.

Let us first write $\tilde{\sigma}$ as a function of μ':

$$\begin{aligned}\tilde{\sigma}^2 &= -i\frac{\kappa_d \rho_M A d k\sqrt{g\bar{h}}}{\epsilon\mu'} \\ &= -i\frac{\kappa_d^2 \kappa \rho_M \epsilon \bar{h}\sqrt{g\bar{h}}}{\epsilon\mu'} \\ &= -i\frac{\kappa_d^2 \kappa \rho_M \bar{h}\sqrt{g\bar{h}}}{\mu'}\end{aligned} \tag{3.7.2.1}$$

The dimensional complex viscosity μ' is a function of the dimensional ω'. Since we chose the scaling of ω':

$$\begin{aligned}\omega' &= k(g\bar{h})^{1/2} \\ &= \kappa\sqrt{\frac{g}{\bar{h}}},\end{aligned} \tag{3.7.2.2}$$

ω' is a function of κ when $\bar{h}$ is given. As a consequence, μ' is a function of κ when $\bar{h}$ is given: $\mu'(\kappa)$.

We deduce that for given values of $\bar{h}$ and κ_d and for a given mud (that is to say given μ' and ρ_M), $\tilde{\sigma}$ is a function of κ:

$$\tilde{\sigma}(\kappa) = \sqrt{-i\kappa_d^2 \kappa \frac{\rho_M \bar{h}\sqrt{g\bar{h}}}{\mu'(\kappa)}} \tag{3.7.2.3}$$

As a consequence,

$$\begin{aligned}|\tilde{\sigma}| &= \sqrt{\kappa_d^2 \kappa \frac{\rho_M \bar{h}\sqrt{g\bar{h}}}{|\mu'(\kappa)|}} \\ \theta_\sigma &= \frac{arg(\mu')}{2}\end{aligned} \tag{3.7.2.4}$$

As a consequence, the peaks in $\Im(G)$ occur when $arg(\mu') \simeq \frac{\pi}{2}$, that is to say when the mud is rather elastic, and if the modulus $|\tilde{\sigma}|$ has the special value given by 3.7.1.7.

Equation 3.7.2.4 can be rewritten:

$$|\mu'(\kappa)| = \frac{\kappa_d^2 \kappa \rho_M \bar{h}^{3/2} g^{1/2}}{|\tilde{\sigma}|^2} \tag{3.7.2.5}$$

From 3.7.1.7 and 3.7.2.5, we deduce that these peaks occur for:

$$|\mu'(\kappa)| = 4\frac{\rho_M \bar{h}^{3/2} g^{1/2}}{(1+2n)^2\pi^2}\kappa_d^2 \kappa \tag{3.7.2.6}$$

From now on we will write:

$$Y_n(\kappa) = 4\frac{\rho_M \bar{h}^{3/2} g^{1/2}}{(1+2n)^2\pi^2}\kappa_d^2\kappa \tag{3.7.2.7}$$

As a consequence, our study means that elastic muds have attenuation rate peaks for $|\mu'(\kappa)| = Y_n(\kappa)$, with n an integer.

In a nutshell, we have obtained that the damping rate is proportional to $\Im(G(\sigma))$. We have demonstrated and checked in figure 3-10 that $\Im(G(\sigma))$ had peaks when $arg(\mu') \simeq \frac{\pi}{2}$, that is to say for rather elastic muds like the Gulf of Mexico or the Mobile Bay ones. And we have demonstrated that these peaks occurred for $|\mu'(\kappa)| = Y_n(\kappa)$, with n an integer.

Figure 3-11 and 3-12 represent $|\mu'|$ as a function of κ for the different mud cases, given the values $\bar{h} = 1\text{m}$ and $\kappa_d = 0.1$ and using equation 3.7.2.5.

Figure 3-11 corresponds to the elastic muds (Gulf of Mexico and Mobile Bay). These muds have $arg(\mu') \simeq \frac{\pi}{2}$ (from figures 3-3 and 3-5). We plotted the functions Y_n for $n = 1$ and $n = 2$ with dashed lines. The intersection of these dashed lines with $|\mu'|$ naturally show the values κ at which $\Im(G(\sigma))$ has a peak. That is to say, the values of κ at which the attenuation rate is the biggest. From these graphs, we expect the attenuation rate to have no peak for the Gulf of Mexico and the Mobile Bay muds when $\bar{h} = 1\text{m}$.

Figure 3-12 corresponds to the rather viscous muds (Lianyungang and Hangzhou Bay). These muds have $arg(\mu') < 0.6\frac{\pi}{4}$ (from figures 3-7 and 3-9). As a consequence, as can be seen on figure 3-10, $\Im(G(\sigma))$ only has peaks for $|\mu'| = Y_1$. The following peaks (corresponding to $n > 1$) are either extremely small either non-existent. We still plotted the functions Y_n for $n = 1$ and $n = 2$, even though Y_1 is more important.

The intersection of this dashed lines with $|\mu'|$ show the values κ at which $\Im(G(\sigma))$ has a peak. That is to say, the values of κ at which the attenuation rate is the biggest. From these graphs, we expect the attenuation rate to have no peak for the Lianyungang mud nor for the Hangzhou Bay mud.

Figure 3-13 and 3-14 also represent $|\mu'|$ as a function of κ for the different mud cases, but this time in the case $\bar{h} = 4\text{m}$.

Figure 3-13 corresponds to the elastic muds. From these graphs, we expect the attenuation rate to have no peak for the Gulf of Mexico and the Mobile Bay muds when $\bar{h} = 4\text{m}$.

Figure 3-14 corresponds to the rather viscous muds. From these graphs, we expect the attenuation rate to have no peak for the Lianyungang mud and one peak for the

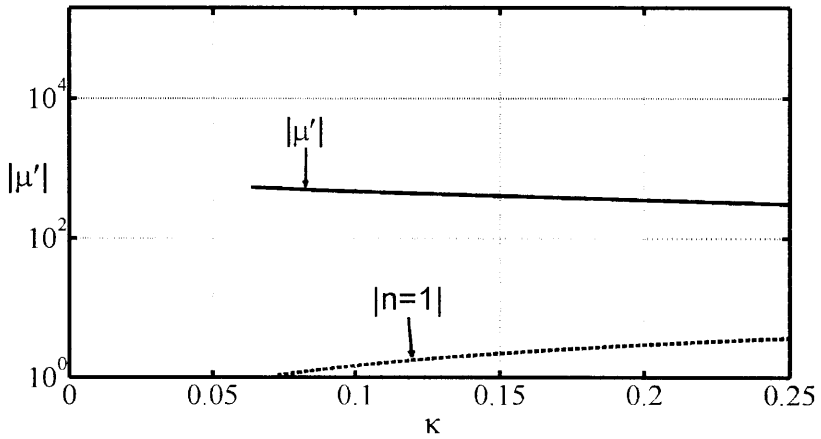

(a) Gulf of Mexico mud

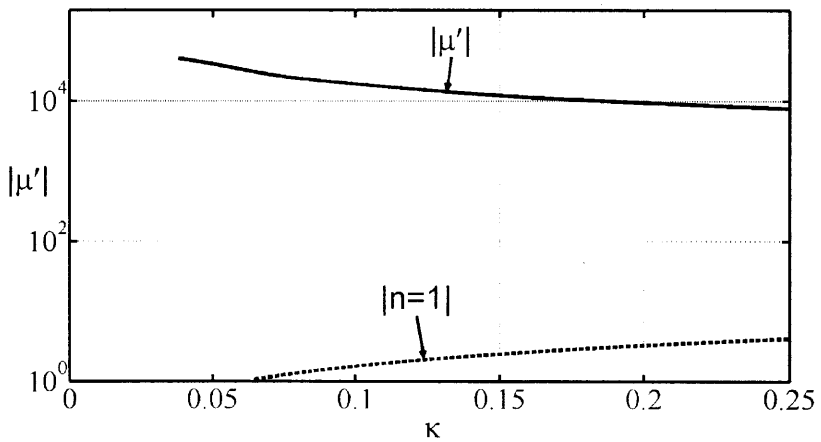

(b) Mobile Bay mud

Figure 3-11: Representation of the complex viscosity modulus as a function of κ for the elastic muds, in the case $\bar{h} = 1$ and $\kappa_d = 0.1$. The dashed lines allow us to expect the κ-values of the peaks.

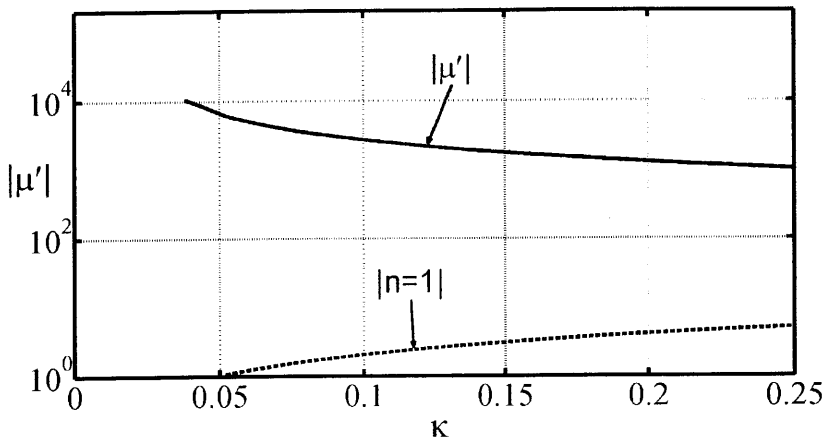

(a) Lianyungang mud

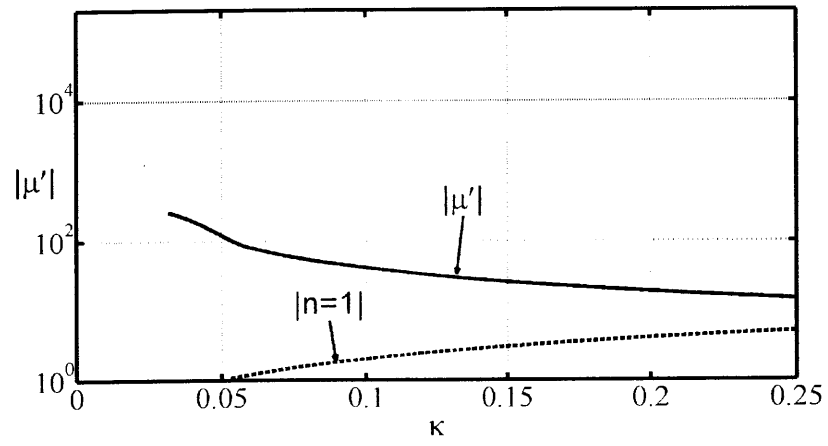

(b) Hangzhou Bay mud

Figure 3-12: Representation of the complex viscosity modulus as a function of κ for the different rather viscous muds, in the case $\bar{h} = 1$ and $\kappa_d = 0.1$. The dashed line allows us to expect the κ-value of the peak.

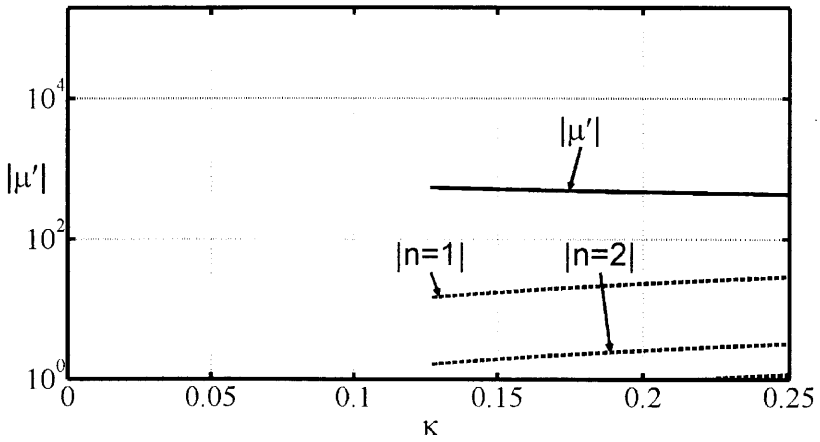

(a) Gulf of Mexico mud

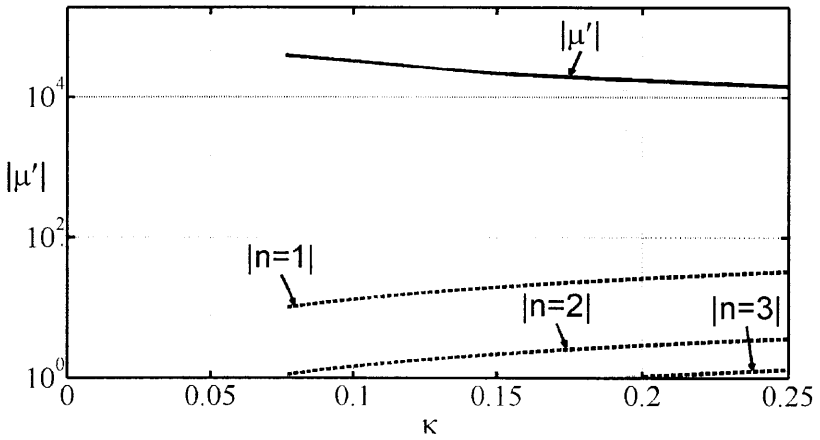

(b) Mobile Bay mud

Figure 3-13: Representation of the complex viscosity modulus as a function of κ for the elastic muds, in the case $\bar{h} = 4$ and $\kappa_d = 0.1$. The dashed lines allow us to expect the κ-values of the peaks.

Hangzhou Bay mud ($\kappa = 0.22$). As we said before, only the first peak is sensible for the viscous muds.

In figures 3-15 and 3-16, we represent the attenuation rate of the first harmonic:

$$\frac{1}{L_1} = -\gamma \frac{\kappa_d}{\kappa} \Im \left[\left(1 - \frac{\tanh(\tilde{\sigma}_1)}{\tilde{\sigma}_1} \right) \right] \tag{3.7.2.8}$$

as a function of κ for each mud, and for different values of $\bar{h}$.

Let us first look at the Gulf of Mexico mud (A). We can see on these graphs that its peaks in the attenuation rate corresponds to what we were expecting: it does not have any peak for $\bar{h} = 1$m or $\bar{h} = 4$m.

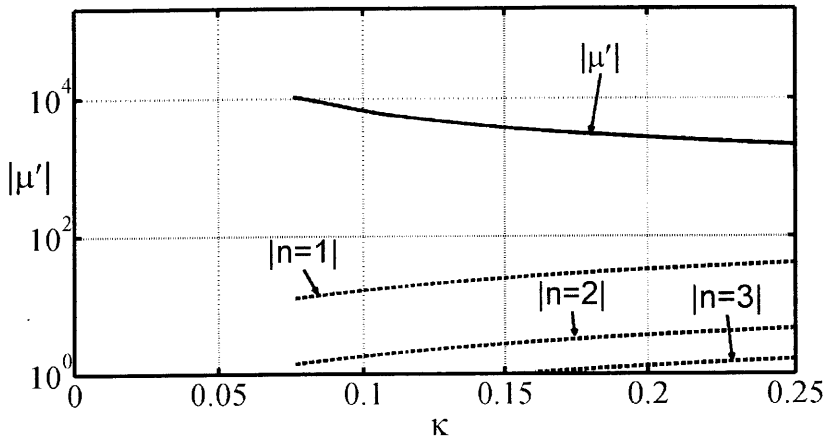

(a) Lianyungang mud

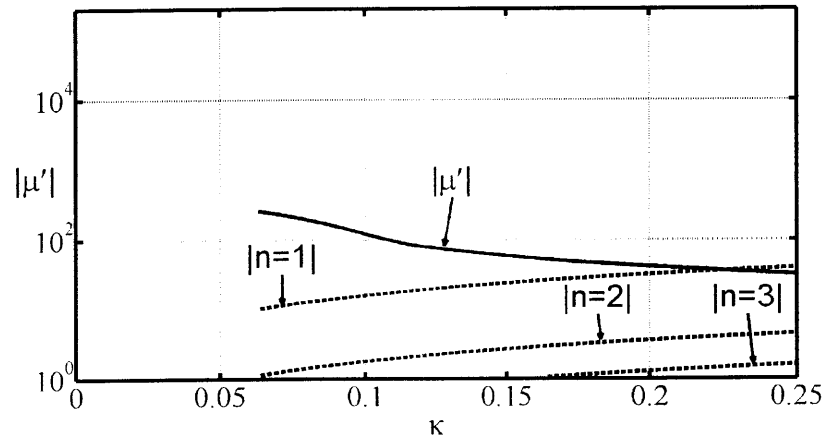

(b) Hangzhou Bay mud

Figure 3-14: Representation of the complex viscosity modulus as a function of κ for the different rather viscous muds, in the case $\bar{h} = 4$ and $\kappa_d = 0.1$. The dashed line allows us to expect the κ-value of the peak.

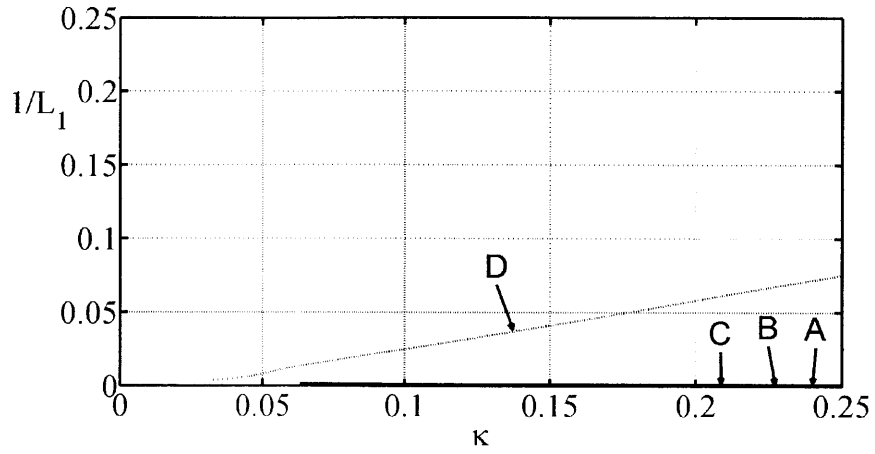

(a) $\bar{h} = 1m$

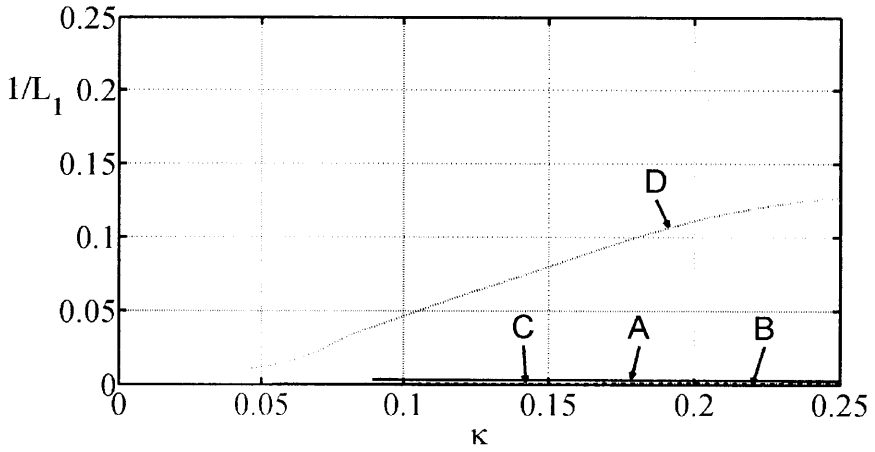

(b) $\bar{h} = 2m$

Figure 3-15: Attenuation rate of the first harmonic as a function of κ for different water depths $\bar{h}$ and $\kappa_d = 0.1$. Mud A is Gulf of Mexico mud, mud B is Mobile Bay mud, mud C is Lianyungang mud and mud D is Hangzhou Bay mud.

The attenuation rate of the Mobile Bay mud (B) does not have any attenuation rate peak for $\bar{h} = 1$m or $\bar{h} = 4$m either, as expected.

We get the same result for the Lianyungang mud (C), which were also expected.

Finally, the Hangzhou Bay mud (D) has no peak for $h = 1$m and one peak around $\kappa = 0.22$, as expected from 3-14. Thus, this result is consistent with what we predicted.

As a conclusion, the resonance peaks appear for high values of κ ($\kappa > 0.4$), corresponding to short waves, for the Gulf of Mexico, Mobile Bay and Lianyungang muds. In other words, there is no resonance for long waves, even though there is attenuation.

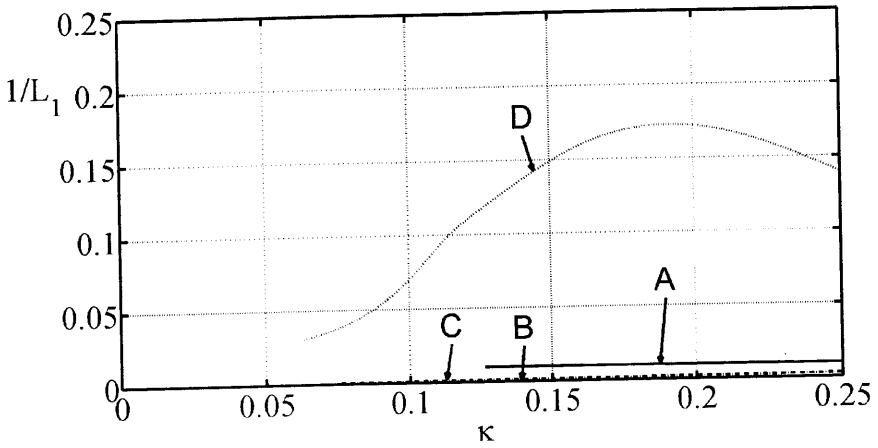

(a) $\bar{h} = 4m$

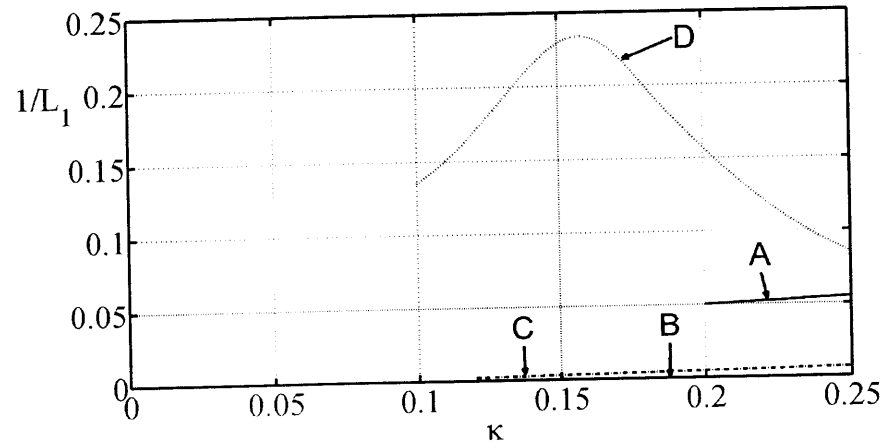

(b) $\bar{h} = 10m$

Figure 3-16: Attenuation rate of the first harmonic as a function of κ for different water depths $\bar{h}$ and $\kappa_d = 0.1$. Mud A is Gulf of Mexico mud, mud B is Mobile Bay mud, mud C is Lianyungang mud and mud D is Hangzhou Bay mud.

However, there is resonance for $\kappa = 0.2$, corresponding to long waves, for $\bar{h} = 4\text{m}$ in the case of the Hangzhou Bay mud. As a consequence, there is resonance for long waves with this mud.

3.7.3 Attenuation rate for the different harmonics

Up to now, we have only studied the variations of the attenuation rate for one harmonic. We now want to study the variation of the attenuation rate for the different harmonics, to see for instance if the attenuation rate of the first harmonic is bigger than the attenuation rate for the fourth harmonic.

Let us now study $1/L_m$ as a function of m:

$$1/L_m = -\gamma m \frac{\kappa_d}{\kappa} \Im[G(\tilde{\sigma}_m)] = -\gamma m \frac{\kappa_d}{\kappa} \Im\left[1 - \frac{\tanh(\tilde{\sigma}_m)}{\tilde{\sigma}_m}\right] \tag{3.7.3.1}$$

We know that:

$$\begin{aligned} \tilde{\sigma}_m^2 &= -i\frac{m\kappa_d \rho_M A d k\sqrt{g\bar{h}}}{\epsilon \mu'_m} \\ &= -i\frac{m\kappa_d^2 \kappa \rho_M \epsilon \bar{h}\sqrt{g\bar{h}}}{\epsilon \mu'_m} \\ &= -i\frac{m\kappa_d^2 \kappa \rho_M \bar{h}\sqrt{g\bar{h}}}{\mu'_m} \end{aligned} \tag{3.7.3.2}$$

where

$$\mu'_m = |\mu'|(\omega' = mk\sqrt{g\bar{h}}) = |\mu'|\left(\omega' = m\kappa\sqrt{\frac{g}{\bar{h}}}\right) \tag{3.7.3.3}$$

As a consequence, at given water depth $\bar{h}$ and for a given mud, μ'_m is a function of m, κ and κ_d.

That is why, for given values of the water depth $\bar{h}$ and of κ_d, we can plot the different $1/L_m$ as a function of κ for different values of m.

Figure 3-17 shows the variation of the attenuation rate $1/L_m$ as a function of κ for different values of m in the case of the Hangzhou Bay mud and for the water depths $\bar{h} = 2\text{m}$ and $\bar{h} = 4\text{m}$, with $\kappa_d = 0.1$.

We deduce from 3-17 that the attenuation rate peaks shift to small values of κ as m grows. In other words, the resonance of the high harmonics appear for smaller κ than the resonance of the first harmonics. Moreover, the peak value of the attenuation rate is bigger for the higher harmonics.

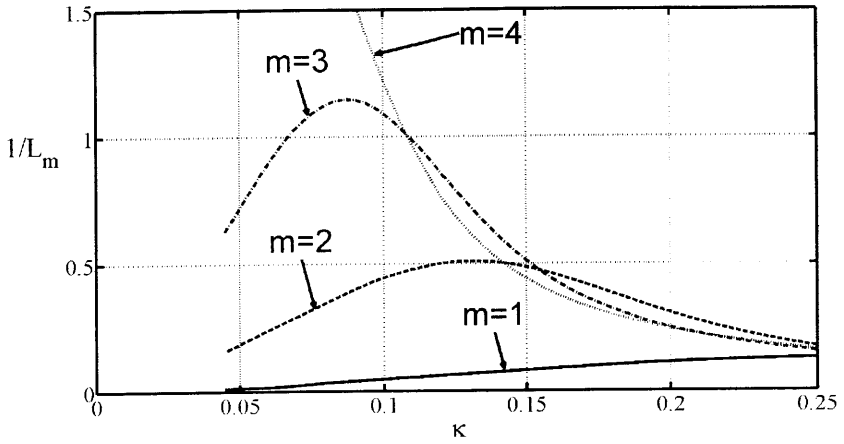

(a) $\bar{h} = 2\text{m}$

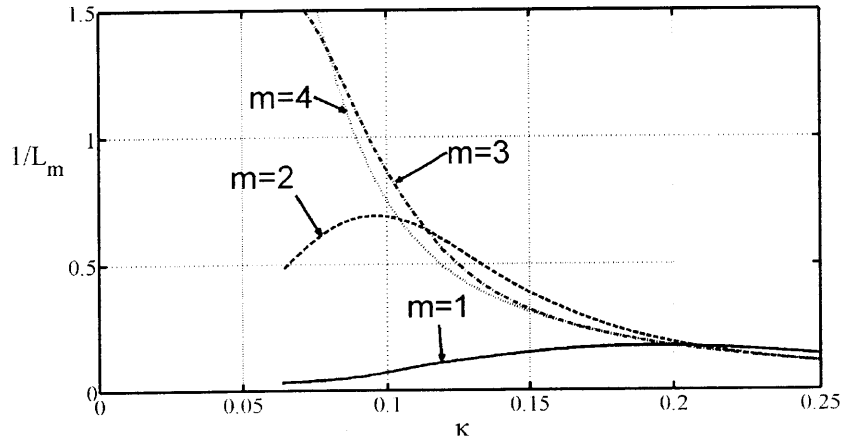

(b) $\bar{h} = 4\text{m}$

Figure 3-17: Variation of $1/L_m$ as a function of κ and m for the Hangzhou Bay mud. $\kappa_d = 0.1$.

3.7.4 Attenuation rate for high viscosities

As we saw in tables 2.6, 2.7, 2.8 and 2.9 the Reynolds number Re can become very small compared to 1 in the case of a highly viscous mud or very low frequency motion. In this case, the modulus of σ naturally becomes very small as well, since σ is proportional to $\sqrt{Re}$.

Let us study the attenuation rate $1/L = -\gamma\frac{\kappa_d}{\kappa}\Im\left(1 - \frac{\tanh(\tilde{\sigma})}{\tilde{\sigma}}\right)$ in the case of $\tilde{\sigma} \to 0$. Writing $\tilde{\sigma}$ the way we did in equation 3.7.1.3 ($\tilde{\sigma} = \alpha + i\beta$), we know that:

$$G(\tilde{\sigma}) = 1 - \frac{1}{\tilde{\sigma}}\frac{\sinh(\alpha)\cosh(\alpha) + i\sin(\beta)\cos(\beta)}{\cos^2(\beta)\cosh^2(\alpha) + \sin^2(\beta)\sinh^2(\alpha)} \tag{3.7.4.1}$$

Knowing that $|\tilde{\sigma}| \to 0$, we necessarily have $\alpha \to 0$ and $\beta \to 0$. As a consequence we can write:

$$\begin{aligned} \sinh(\beta) &= \beta + \frac{\beta^3}{3!} \\ \cosh(\beta) &= 1 + \frac{\beta^2}{2!} \\ \sin(\beta) &= \beta - \frac{\beta^3}{3!} \\ \cos(\beta) &= 1 - \frac{\beta^2}{2!} \end{aligned} \tag{3.7.4.2}$$

and the same equalities for α.

So equation 3.7.4.1 becomes:

$$\begin{aligned} G(\tilde{\sigma}) &= 1 - \frac{1}{\tilde{\sigma}}\frac{\alpha + \frac{\alpha^3}{2!} + \frac{\alpha^3}{3!} + O(\alpha^4) + i\left(\beta - \frac{\beta^3}{2!} - \frac{\beta^3}{3!} + O(\beta^4)\right)}{1 - \alpha^2 + \beta^2 + O(\alpha^4)} \\ &= 1 - \frac{1}{\tilde{\sigma}}\left[\alpha + \frac{2\alpha^3}{3} + i\left(\beta - \frac{2\beta^3}{3}\right)\right](1 + \alpha^2 - \beta^2) \\ &= 1 - \frac{1}{\alpha + i\beta}\left[\alpha + i\beta + O(\alpha^2) + O(\beta^2)\right] \\ &= 1 - 1 + \frac{O(\alpha^2) + O(\beta^2)}{\alpha + i\beta} \\ &= \frac{O(\alpha^2) + O(\beta^2)}{\alpha + i\beta} \end{aligned} \tag{3.7.4.3}$$

as a consequence, we get that $G(\tilde{\sigma}) \to 0$ when $|\tilde{\sigma}| \to 0$, and thus the attenuation rate goes to 0 when the Reynolds number is small.

We deduce that for muds that are very viscous, such as Re is small compared to 1, the attenuation is insignificant.

3.8 Numerical results by using the first ten harmonics

We are now going to plot these results for the viscoelastic muds we previously studied.

Let us sum up the different muds we are considering:

- Case A: Gulf of Mexico mud. This mud is rather elastic.
- Case B: Mobile Bay mud. This mud is rather elastic as well
- Case C: Lianyungang mud. This mud complex viscosity's phase is around $\frac{\pi}{4}$ so it is as elastic as viscous.
- Case D: Hangzhou Bay mud. This mud is rather viscous, its complex viscosity's phase being close to zero.

We choose to plot the different results for those muds in the case $\bar{h} = 2\text{m}$, $A = 0.4\text{m}$, $\omega' = 0.5\text{rad/s}$ and $d = 20\text{cm}$ (corresponding to the case 1b of the previous chapter). In this case, we know that:

$$\boxed{\kappa = 0.22,\ \epsilon = 0.2,\ \kappa_d = 0.1} \tag{3.8.0.4}$$

3.8.1 Surface and interface

In figures 3-18 and 3-19, we represent the variation of the first harmonics of the surface and the interface. Even though we carried the resolution with 10 harmonics in order to take into account all the significant ones, we chose to only display the three most significant harmonics for clarity.

In figure 3-18, we observe that the damping is more important in cases A, C and D (respectively Gulf of Mexico, Lianyungang and Hangzhou Bay mud) than for the Mobile Bay mud (B). This is what we expected from figure 3-15, that showed that the attenuation rate was insignificant for small κ for mud B (Mobile Bay mud).

In cases A, C and D, the harmonics are significantly damped for $X = 10$, that is to say $x \simeq 45$ since $\kappa = 0.22$ in the case we consider, or $x' = \frac{x}{k} = 402\text{m}$. As $\lambda = \frac{2\pi}{k}$, $\lambda \simeq 56\text{m}$, we conclude the wave is nearly damped after around 8 wavelengths.

The damping is not that significant in the case of the Mobile Bay mud (B).

We also observe that for the Hangzhou Bay mud, the $|A_m|$ have more oscillations than for the Gulf of Mexico and Lianyungang muds, even though the damping lengthscale is comparable for these three muds.

Figure 3-19 shows the variation of the interfaces. The results confirm what we previously saw: in the cases of muds A, C and D, where the damping is significant, the interface motion is strong. However, the interface motion of mud B is extremely small.

Drift current in mud

Figure 3-20 represents the drift we calculated in equation 3.6.2.5. As in chapter 2, the drift current is a sum of the $|A_m|^2$ multiplied by coefficients. As a consequence, the shape of the $|A_m|$ directly influences the drift current shape.

Let us remind the equations:

$$\begin{aligned} U &= U^{(0)} + \kappa U^{(1)} + O(\kappa^2) \\ (U)_1 &= \frac{1}{2}U_1^{(0)} + \frac{1}{2}\sum_{m=1}^{\infty}\left(U_1^{(m)}e^{i\theta_m} + cc.\right) \end{aligned} \tag{3.8.1.1}$$

This is why we represent the value $\frac{1}{2}\kappa(U)_1^{(0)}$, which is the value that appears in the total sum of U.

The drift is represented in the mud layer for $0 < X < 5$ for $Z = 1$. It is interesting to note how the drift naturally vanishes as X increases.

Once again, the results presented in this figure confirm the effect we previously described: the damping is strong for the Gulf of Mexico, Lianyungang and Hangzhou Bay muds. As a consequence, their mud's motion is stronger, and in particular the mud's drift current is stronger.

We note the presence of oscillations in the drift current for the Hangzhou Bay mud (D). We already noticed these oscillations for the same mud in the $|A_m|$ in the previous section. As we said, the drift current is a sum of the $|A_m|^2$ multiplied by coefficients. As a consequence, if the $|A_m|$ show oscillations, it is logical for the drift current to also show oscillations.

Let us recall that we already noticed oscillations in the drift current in the viscous case, and these oscillations were also correlated to oscillations in the $|A_m|$.

Finally, we note that the drift current initial value ($X = 0$) is much higher in the case of the Hangzhou Bay mud compared to all the other muds. At $X = 0$, the value

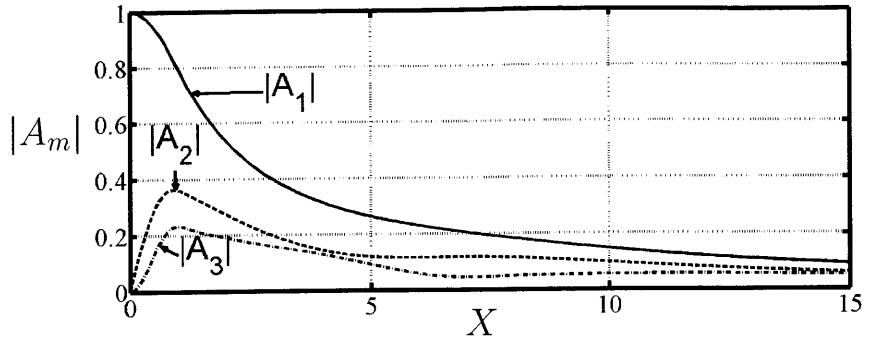

(a) Gulf of Mexico mud

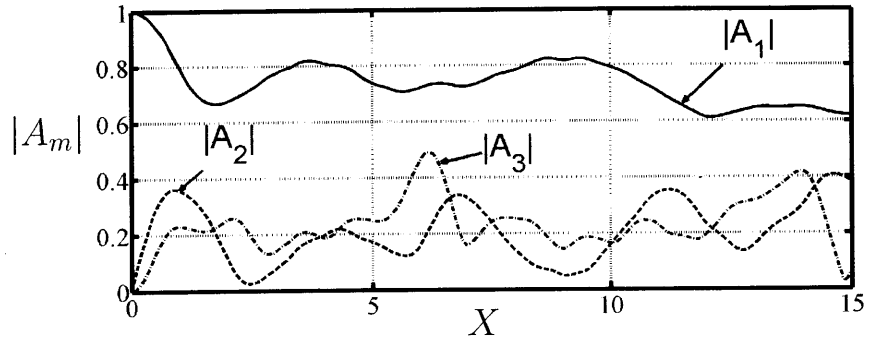

(b) Mobile Bay mud

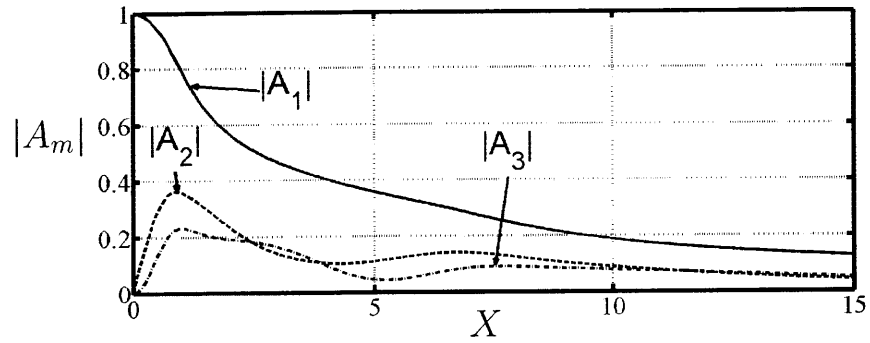

(c) Lianyungang mud

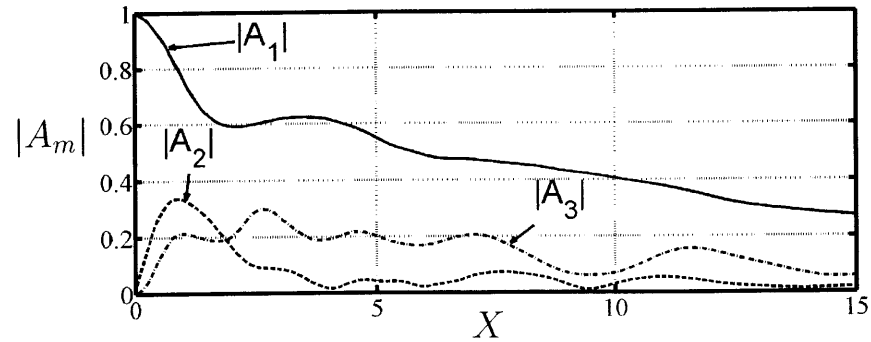

(d) Hangzhou Bay mud

Figure 3-18: Evolution of the first 3 harmonics of the free surface over different types of viscoelastic muddy seabeds.

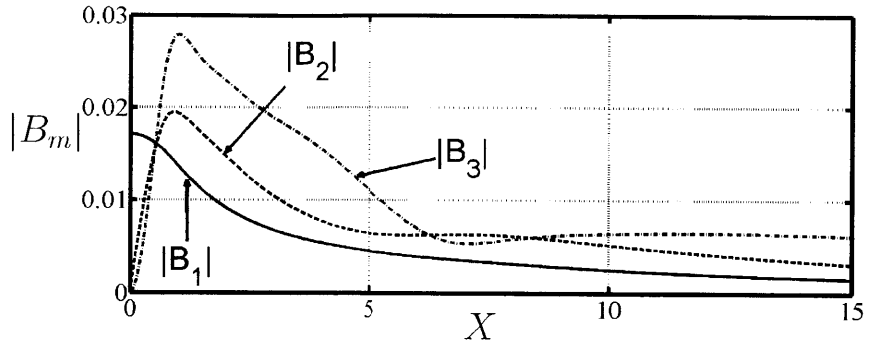

(a) Gulf of Mexico mud

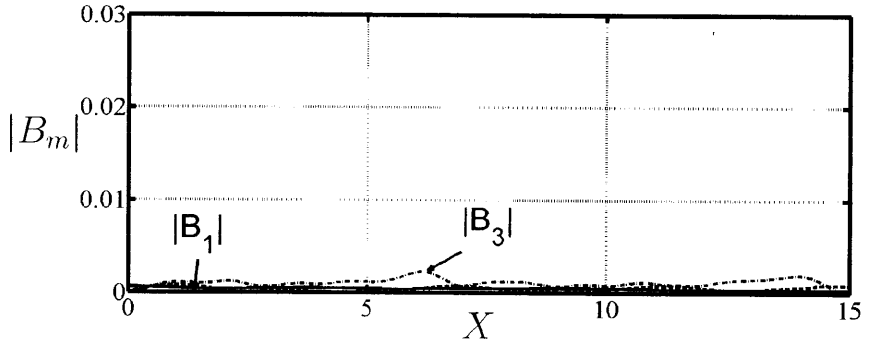

(b) Mobile Bay mud

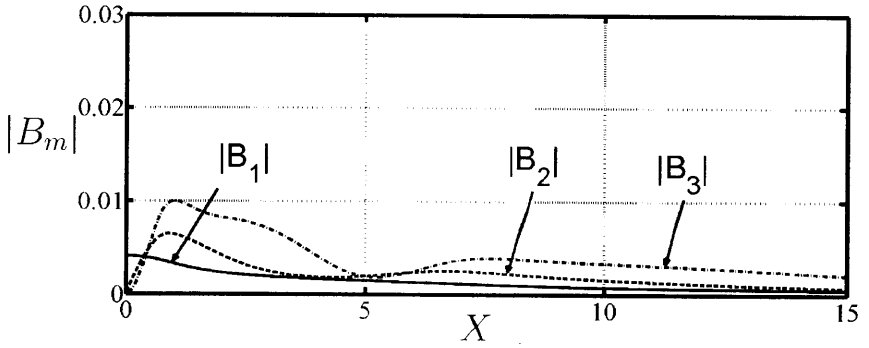

(c) Lianyungang mud

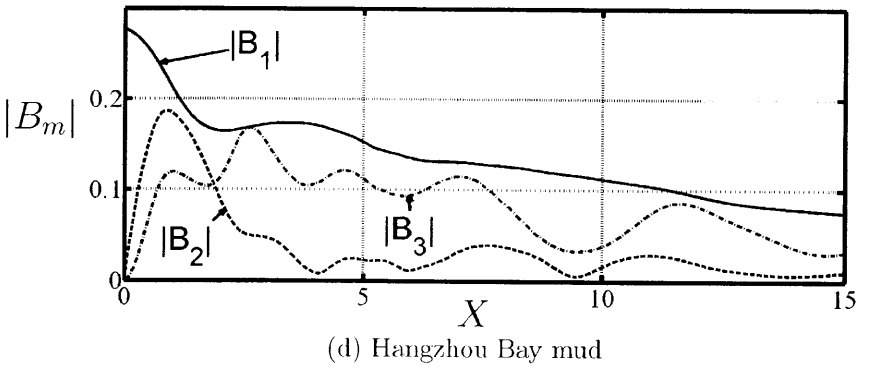

(d) Hangzhou Bay mud

Figure 3-19: Effects of wave amplitude on the evolution of the first 3 harmonics of the interface over different types of viscoelastic muddy seabeds. Warning, the scale is not the same for mud D!

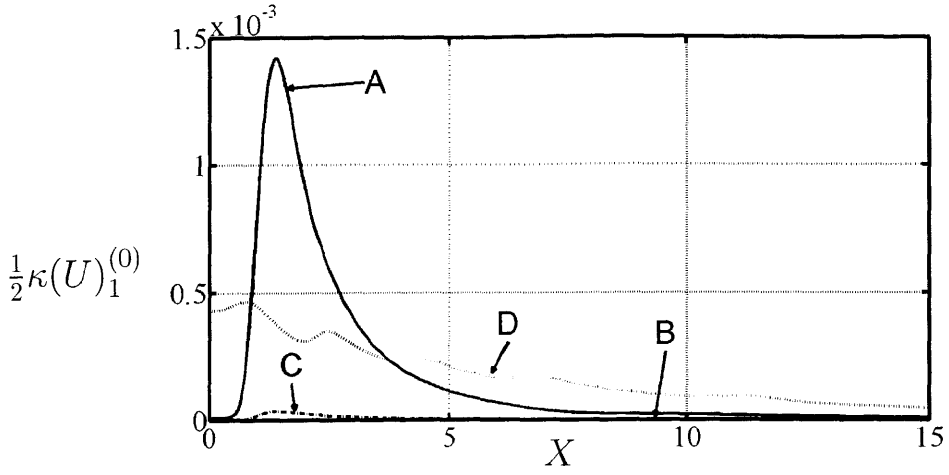

Figure 3-20: Drift velocity $\frac{1}{2}\kappa(U)_1^{(0)}$.

of the drift current is:

$$\begin{aligned}\frac{1}{2}\kappa U_0^{(1)}(X=0,Z=1) = &-\frac{1}{2}\kappa\Big[\gamma^2\frac{Re^{(2)}\kappa_d}{\mu_0\kappa}\Im\Big[\frac{1}{\tilde{\sigma}_1^*}\Big[-\tilde{\sigma}^*\Big(\frac{\sinh(\tilde{\sigma}_1)}{\tilde{\sigma}_1}-2\frac{\cosh(\tilde{\sigma}_1)}{\tilde{\sigma}_1^2}\Big)\\
&+\tilde{\sigma}_1^*\tanh(\tilde{\sigma}_1)\Big(\frac{\cosh(\tilde{\sigma}_1)}{\tilde{\sigma}_1}-2\frac{\sinh(\tilde{\sigma}_1)}{\tilde{\sigma}_1^2}\Big)\\
&+\frac{\cosh(2\tilde{\sigma}_1^R)}{4(\tilde{\sigma}_1^R)^2}\tilde{\sigma}_1(1+\tanh(\tilde{\sigma}_1)(\tanh(\tilde{\sigma}_1))^*)\\
&+\frac{\cosh(2i\tilde{\sigma}_1^I)}{8(\tilde{\sigma}_1^I)^2}\tilde{\sigma}_1(\tanh(\tilde{\sigma}_1)(\tanh(\tilde{\sigma}_1))^*-1)\\
&-\frac{\sinh(2\tilde{\sigma}_1^R)}{8(\tilde{\sigma}_1^R)^2}\tilde{\sigma}_1(\tanh(\tilde{\sigma}_1)+(\tanh(\tilde{\sigma}_1))^*)\\
&+\frac{\sinh(2i\tilde{\sigma}_1^I)}{8(\tilde{\sigma}_1^I)^2}\tilde{\sigma}_1(\tanh(\tilde{\sigma}_1)-(\tanh(\tilde{\sigma}_1))^*)\\
&+(\tanh(\tilde{\sigma}_1))^*\frac{\sinh(\tilde{\sigma}_1)}{\tilde{\sigma}_1}\\
&-\tanh(\tilde{\sigma}_1)(\tanh(\tilde{\sigma}_1))^*\frac{\cosh(\tilde{\sigma}_1)}{\tilde{\sigma}_1}\Big]\Big]+C_1^{(1)}+C_1^{(2)}\Big]\end{aligned} \tag{3.8.1.2}$$

since A_1=1 and all the other A_m are 0.

By calculating this value for the different muds, we indeed find that the initial value of the current drift is at least 50 times higher for the Hangzhou Bay mud than for any other mud. This explains why the drift current has such a high value for the Hangzhou Bay mud at $X = 0$.

Figure 3-21 allows us to check the boundary condition at the interface corresponding to equation 3.6.2.15. Indeed, in this figure, the solid line corresponds to the actual

derivative of the drift current at the interface, numerically obtained. The dashed line corresponds to the actual value of this derivative based on the boundary condition 3.6.2.15:

$$\frac{\partial U_0^{(1)}}{\partial Z}\Big|_{(Z=1)} = \frac{\epsilon\gamma^2}{2\kappa\mu_0}\sum_{m=1}^{n}|A_m|^2\Im\left[iG(\tilde{\sigma}_m)\mu_m^*(\tilde{\sigma}_m^*)^2\mathrm{sech}(\tilde{\sigma}_m^*)\right] \tag{3.8.1.3}$$

The two lines are so close that they are difficult to distinguish on the figure. This verifies the numerical resolution of the drift current.

We only plotted these figures for the Gulf of Mexico, Lianyungang and Hangzhou Bay muds because the values were extremely small for the Mobile Bay mud (B) (around 10^{-7} and thus not representative).

Energy variation

We numerically represented the total first-order energies in figure 2-6. This figure shows that the total energy logically decreases, because it is dissipated in the viscous mud.

In the case of muds A, C and D, the energy reaches a nearly zero-value for $X = 10$, meaning that the dissipation is fast. However, we observe once again that dissipation is slower to occur for the Mobile Bay mud (B). Indeed, energy only decreases by 10% between $X = 0$ and $X = 10$.

In figure 3-23, we represented the variation of total energy. The dashed line represents the right-hand side term of equation 3.6.3.4:

$$\boxed{\frac{d}{dX}\left[\sum_{m=1}^{n}|A_m|^2\right] = -\gamma\frac{\kappa_d}{\kappa}\sum_{m=1}^{n}\Re\left[im\left(1-\frac{\tanh(\tilde{\sigma}_m)}{\tilde{\sigma}_m}\right)\right]|A_m|^2} \tag{3.8.1.4}$$

As in the Newtonian case of chapter 2, the dashed line is so close to the solid line that it is very hard to distinguish, meaning that our numerical results are right.

3.9 Horizontal bottom without mud

3.9.1 Governing equations

From the study we just led in the particular case of viscoelastic mud, it is very easy to deduce the surface waves behavior in the absence of mud. Indeed, the absence of mud simply means that $B_m = 0$ in equation 3.5.3.1.

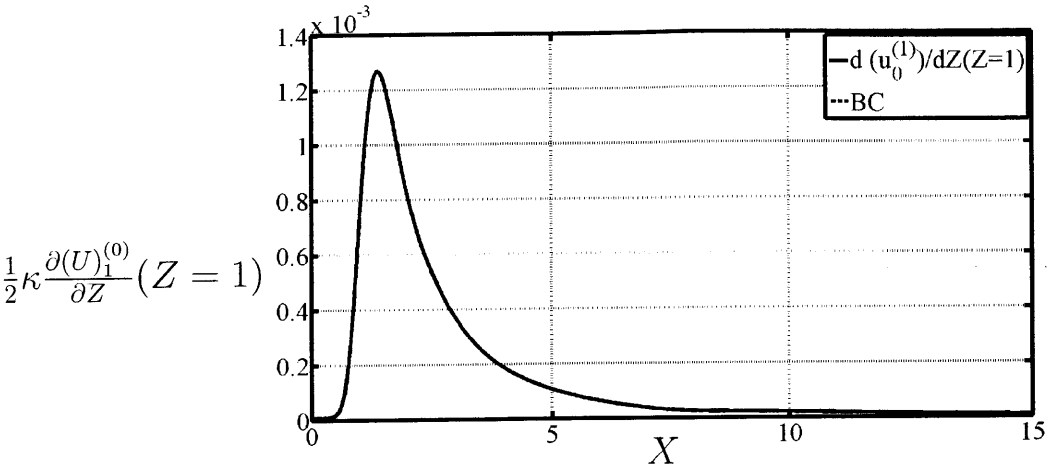

(a) Gulf of Mexico mud

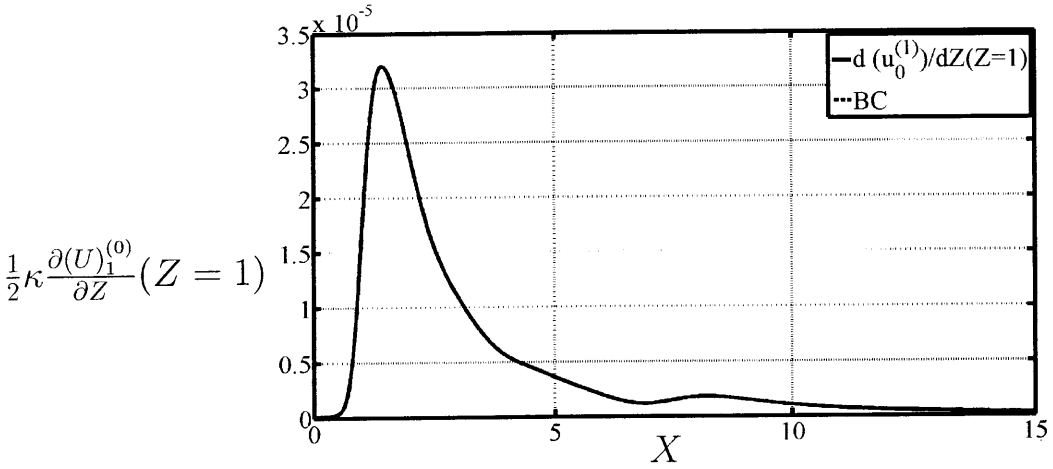

(b) Lianyungang mud

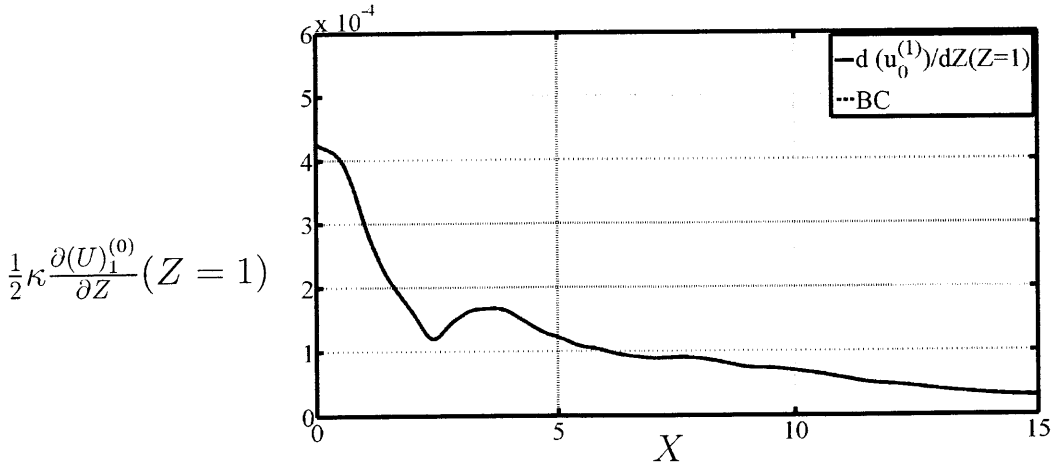

(c) Hangzhou Bay mud

Figure 3-21: Drift velocity derivative boundary condition $Z = 1$. The dashed line "BC" corresponds to the boundary condition, the right hand side term of equation 3.6.2.15

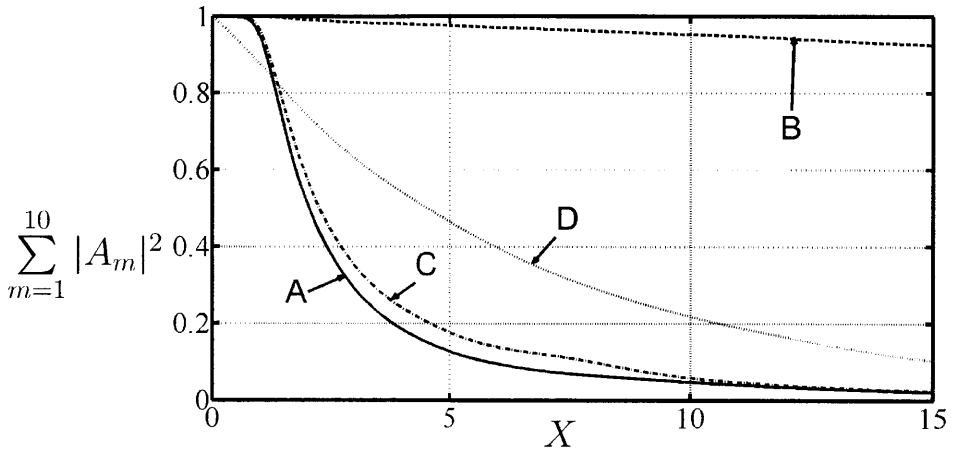

Figure 3-22: Wave energy over a flat thick muddy seabed.

As a consequence, the governing equation 3.6.1.1 for the surface waves become:

$$\forall m, \quad \boxed{\frac{dA_m}{dX} + \frac{3i}{8}\frac{\epsilon}{\kappa} m \left(\sum_{l=1}^{n-m} 2A_l^* A_{m+l} + \sum_{l=1}^{[m/2]} \alpha_l A_l A_{m-l} \right) = 0} \tag{3.9.1.1}$$

The same way, the energy variation can be deduced from equation 3.6.3.4, that becomes:

$$\frac{d}{dX}\Big[\sum_{m=1}^{n} |A_m|^2\Big] = 0 \tag{3.9.1.2}$$

This result looks very logical, since it means that in the absence of mud, there is no energy dissipation in water.

3.9.2 Numerical results by using the first ten harmonics

Since we don't consider mud anymore, there are only tree parameters remaining: $\bar{h}$, A, and ω'. These parameters are only present in equation 3.9.1.1 in the ratio ϵ/κ, which is around 1.

In figure 3-24, we compare the surface displacement for three different cases: $\epsilon/\kappa = 0.5$ (A), $\epsilon/\kappa = 1$ (B) and $\epsilon/\kappa = 1.5$(C). These cases correspond to different non-linearity/dispersion ratios. The first case $\epsilon/\kappa = 0.5$ means that non-linearity is less important than dispersion, whereas the case $\epsilon/\kappa = 1.5$ means that non-linearity is predominant. Once again, even though we carried the numerical resolution with ten harmonics, we choose to only display the first three harmonics.

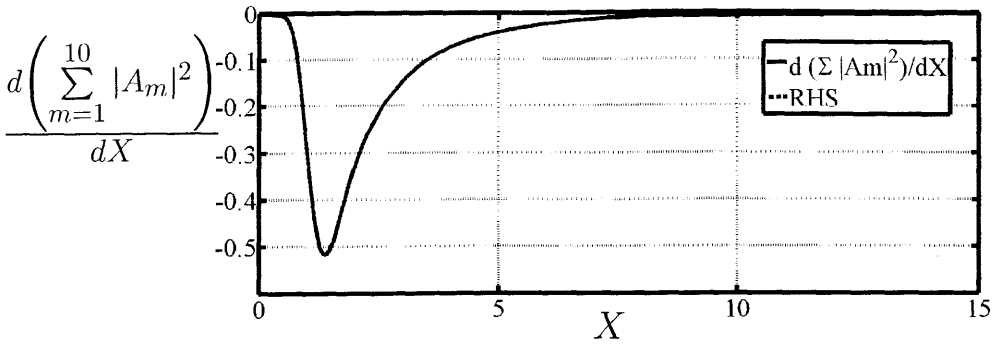

(a) Gulf of Mexico mud

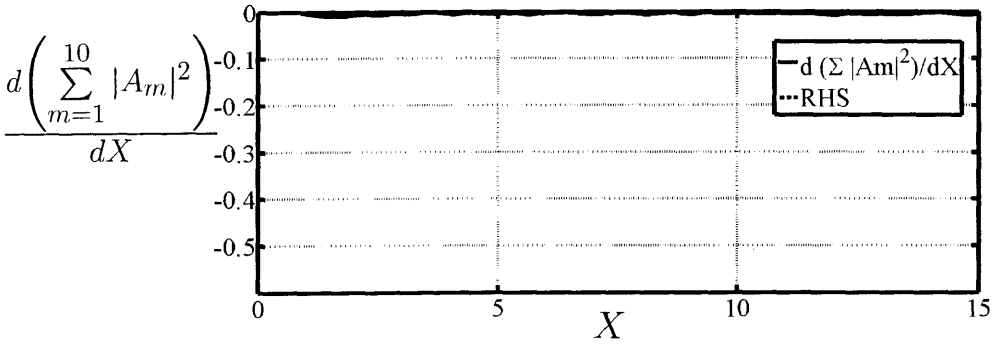

(b) Mobile Bay mud

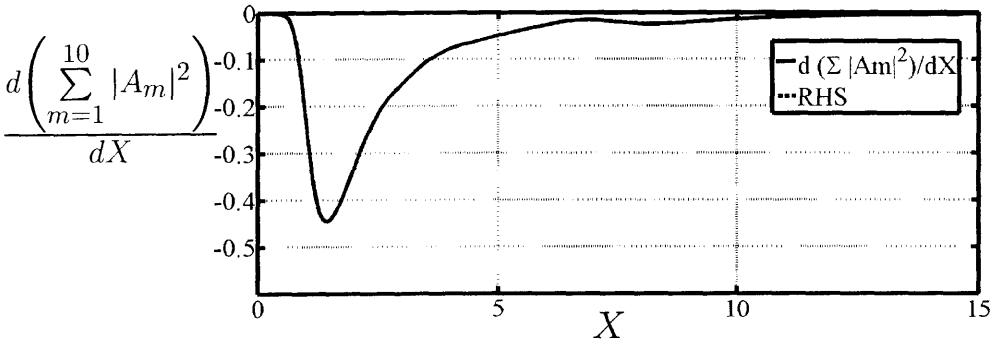

(c) Lianyungang mud

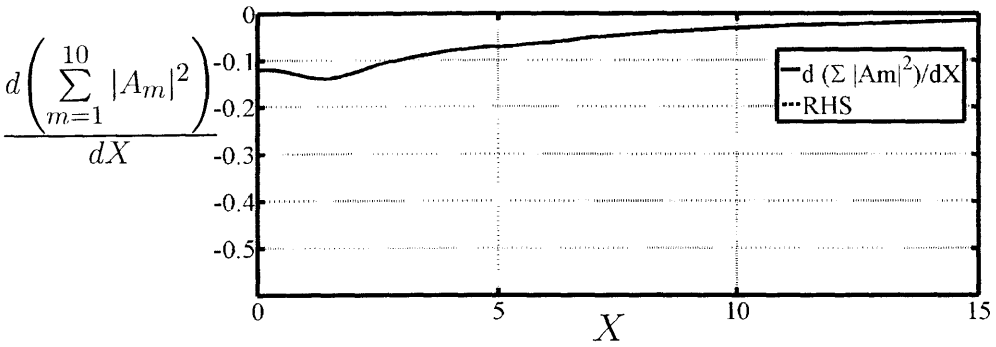

(d) Hangzhou Bay mud

Figure 3-23: Variation of the wave energy over a flat thick muddy seabed. RHS is the value of the right-hand side term in equation 3.6.3.4.

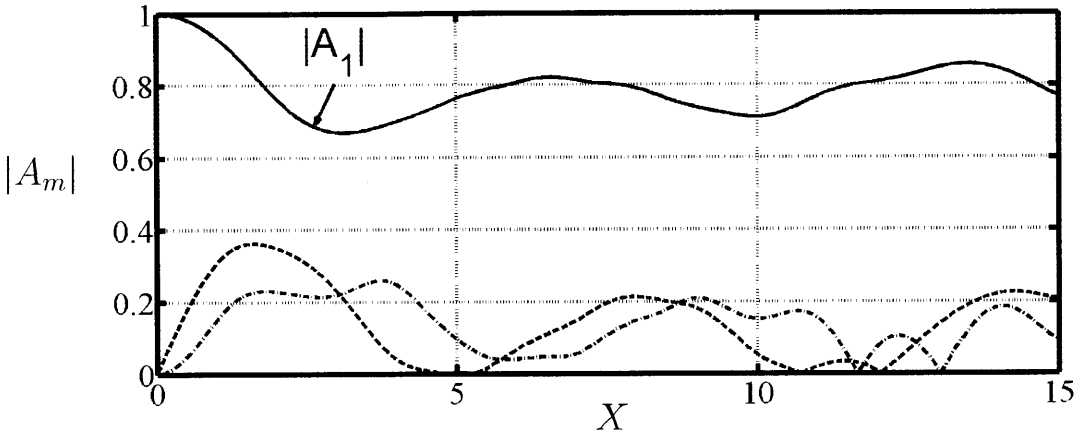

(a) Smallest ratio $\epsilon/\kappa = 0.5$

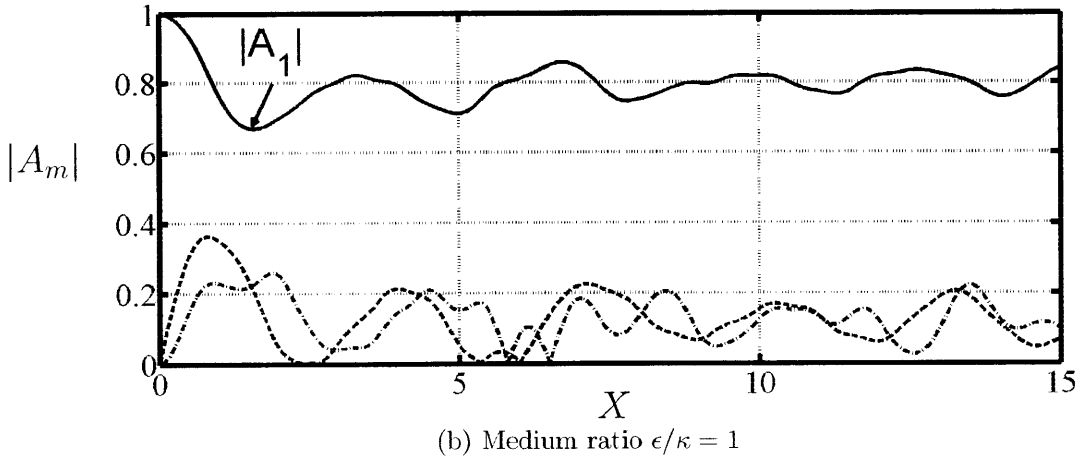

(b) Medium ratio $\epsilon/\kappa = 1$

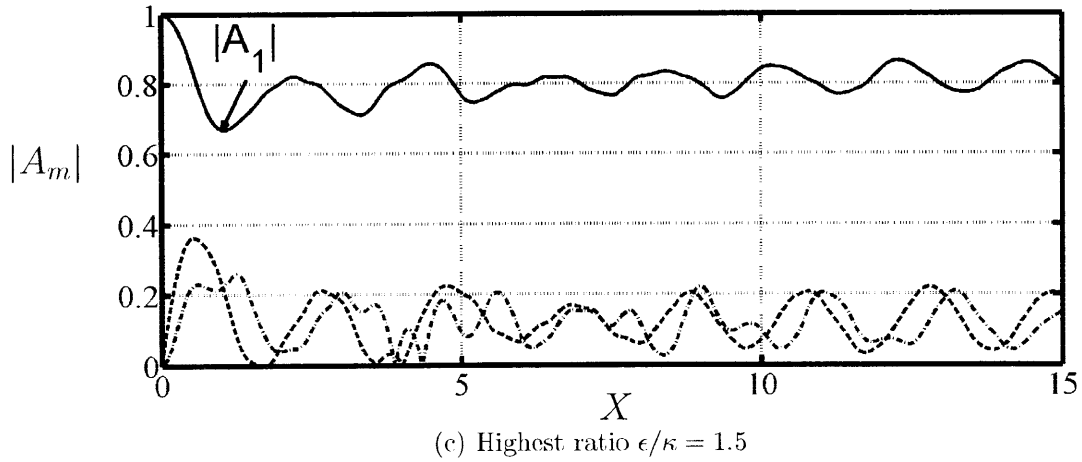

(c) Highest ratio $\epsilon/\kappa = 1.5$

Figure 3-24: Effects of wave amplitude on the evolution of the first 3 harmonics of the free surface on a solid seabed. Comparison between different values of ϵ/κ.

Chapter 4

Horizontal bottom, very shallow Newtonian mud

As we pointed in chapter 2, non-linearity ϵ is sometimes small compared to dispersion, that is to say ϵ small compared to κ, for some values of the water depth $\bar{h}$, the frequency ω' and the wave amplitude A. Some of these cases are for instance listed in the gray cells of tables 2.6, 2.7, 2.8 and 2.9.

That is why we carry in this chapter the same calculations made in chapter 2, but in the case:

$$\boxed{O(\epsilon) = O(\kappa^2)} \tag{4.0.2.1}$$

In other words, we consider weak non-linearity of Boussinesq class.

In order to see the effect of non-linearity on mud-induced damping, we now consider the mud layer to be thiner than in the previous chapters:

$$\boxed{\frac{d}{\bar{h}} = \kappa_d = O(\kappa^2)} \tag{4.0.2.2}$$

so that non-linearity and mud-induced damping act at the same order.

4.1 Scaling

The scaling in water is logically kept the same as in the previous case, that is to say:

$$\begin{array}{lll} x = kx' & z = \frac{z'}{h}b & t = k(g\bar{h})^{1/2}t' \\ p = \frac{p'}{\rho_W g A} & u = \frac{1}{\epsilon\sqrt{g\bar{h}}}u' & v = \frac{\kappa}{\epsilon\sqrt{g\bar{h}}}v' \\ \zeta = \frac{\zeta'}{A} & \phi = \phi'\left[\frac{A}{k\bar{h}}(g\bar{h})^{1/2}\right]^{-1} & \end{array} \tag{4.1.0.3}$$

The scaling in mud is also conserved:

$$\begin{array}{lll} x = kx' & Z = \frac{Z'}{d} & t = k(g\bar{h})^{1/2}t' \\ P = \frac{P'}{\rho_W g A} & U = \frac{1}{\epsilon\sqrt{g\bar{h}}}U' & V = \frac{1}{\epsilon\kappa\kappa_d\sqrt{g\bar{h}}}V' \\ \eta = \frac{\eta'}{\kappa_d A} & \mathcal{U} = \frac{k}{\epsilon}\mathcal{U}' & \mathcal{V} = \frac{k}{\epsilon\kappa\kappa_d}\mathcal{V}' \\ T_{ij} = \frac{T'_{ij}}{\rho_W g A} & E_{ij,t} = \frac{d}{\epsilon\sqrt{g\bar{h}}}E'_{ij,t'} & \tau_{ij} = \frac{d}{\epsilon\mu\sqrt{g\bar{h}}}\tau'_{ij} \end{array} \tag{4.1.0.4}$$

but we now have: $\frac{d}{\bar{h}} = \kappa_d = O(\kappa^2)$.

4.2 Equations in water

Let us first study the water layer in order to determine the equation equivalent to equation 2.5.1.5 in this new case. Because this may be useful for later studies, we carried the calculations up to order $O(\kappa^6)$. However, we will only use the results at $O(\kappa^0)$ and $O(\kappa^2)$ in the rest of this thesis.

We still consider ϕ to be the series 2.3.0.2:

$$\boxed{\phi(x,z,t) = \sum_{n=0}^{\infty} \frac{(z+1)^n}{n!}\phi^{(n)}(x,t)} \tag{4.2.0.5}$$

4.2.1 Laplace equation

The Laplace equation still gives the result given by equation 2.3.1.2:

$$\forall n, \quad \phi^{(n)} = -\kappa^2 \frac{\partial^2 \phi^{(n-2)}}{\partial x^2} \tag{4.2.1.1}$$

4.2.2 Kinematic boundary condition at the interface

Equation 2.3.1.3 becomes:

$$\phi_z = \kappa_d\kappa^2\frac{\partial \eta}{\partial t} + \epsilon\kappa_d\kappa^2\frac{\partial \eta}{\partial x}\frac{\partial \phi}{\partial x}, \quad z = -1 + \epsilon\kappa_d\eta(x,t) \tag{4.2.2.1}$$

and the Taylor series expansion gives:

$$\phi_z + \epsilon\kappa_d\eta\phi_{zz} = \epsilon\kappa_d\kappa^2\frac{\partial \eta}{\partial x}\left(\frac{\partial \phi}{\partial x} + \epsilon\kappa_d\eta\frac{\partial \phi_z}{\partial x}\right) + \kappa_d\kappa^2\frac{\partial \eta}{\partial t} + O(\kappa^7), \quad z = -1 \tag{4.2.2.2}$$

Using the same reasoning than in the previous case, we obtain that:

$$\phi^{(1)} + \epsilon\kappa_d\eta\phi^{(2)} = \epsilon\kappa_d\kappa^2\frac{\partial\eta}{\partial x}\frac{\partial\phi^{(0)}}{\partial x} + \kappa_d\kappa^2\frac{\partial\eta}{\partial t} + O(\kappa^8) \tag{4.2.2.3}$$

And finally:

$$\phi^{(1)} = \kappa_d\kappa^2\frac{\partial\eta}{\partial t} + \epsilon\kappa_d\kappa^2\frac{\partial}{\partial x}\left(\eta\frac{\partial\phi^{(0)}}{\partial x}\right) \tag{4.2.2.4}$$

This last equation is true because we know from the result of the equation 4.2.1.1 that:

$$\phi^{(2)} = -\kappa^2\frac{\partial^2\phi^{(0)}}{\partial x^2} \tag{4.2.2.5}$$

We finally deduce an explicit expression of ϕ at the order κ^8:

$$\begin{aligned}\phi =&\phi^{(0)} + \kappa_d\kappa^2(z+1)\left[\frac{\partial\eta}{\partial t} + \epsilon\frac{\partial}{\partial x}\left(\eta\frac{\partial\phi^{(0)}}{\partial x}\right)\right] - \kappa^2\frac{(z+1)^2}{2}\frac{\partial^2\phi^{(0)}}{\partial x^2} - \kappa_d\kappa^4\frac{(z+1)^3}{3!}\frac{\partial^2\eta_t}{\partial x}\\ &+ \kappa^4\frac{(z+1)^4}{4!}\frac{\partial^4\phi^{(0)}}{\partial x^4} - \kappa^6\frac{(z+1)^6}{6!}\frac{\partial^6\phi^{(0)}}{\partial x^6} + O(\kappa^8)\end{aligned} \tag{4.2.2.6}$$

4.2.3 Kinematic Boundary condition at the free surface

The expression of the kinematic boundary condition at the free surface is naturally unchanged:

$$\kappa^2\left(\zeta_t + \epsilon\frac{\partial\phi}{\partial x}\frac{\partial\zeta}{\partial x}\right) = \phi_z, \quad z = \epsilon\zeta \tag{4.2.3.1}$$

From equation 4.2.2.6, we know that:

$$\begin{aligned}\phi_z =&\kappa_d\kappa^2\left(\frac{\partial\eta}{\partial t} + \epsilon\frac{\partial}{\partial x}\left(\eta\frac{\partial\phi^{(0)}}{\partial x}\right)\right) - \kappa^2(z+1)\frac{\partial^2\phi^{(0)}}{\partial x^2} - \kappa_d\kappa^4\frac{(z+1)^2}{2!}\frac{\partial^2\eta_t}{\partial x}\\ &+ \kappa^4\frac{(z+1)^3}{6}\frac{\partial^4\phi^{(0)}}{\partial x^4} - \kappa^6\frac{(z+1)^5}{5!}\frac{\partial^6\phi^{(0)}}{\partial x^6} + O(\kappa^8)\end{aligned} \tag{4.2.3.2}$$

Plugging this result in equation 4.2.3.1, we obtain:

$$\begin{aligned}\zeta_t + \epsilon\frac{\partial\phi^{(0)}}{\partial x}\frac{\partial\zeta}{\partial x} =&\frac{\epsilon\kappa^2}{2}\frac{\partial^3\phi^{(0)}}{\partial x^3}\frac{\partial\zeta}{\partial x} + \kappa_d\left(\frac{\partial\eta}{\partial t} + \epsilon\frac{\partial}{\partial x}\left(\eta\frac{\partial\phi^{(0)}}{\partial x}\right)\right) - (1+\epsilon\zeta)\frac{\partial^2\phi^{(0)}}{\partial x^2}\\ &- \frac{\kappa_d\kappa^2}{2!}\frac{\partial^2\eta_t}{\partial x} + \frac{\kappa^2}{6}\frac{\partial^4\phi^{(0)}}{\partial x^4} + \frac{\kappa^2\epsilon\zeta}{2}\frac{\partial^4\phi^{(0)}}{\partial x^4} + O(\kappa^6)\end{aligned} \tag{4.2.3.3}$$

We introduce the horizontal velocity at the bottom $u^{(0)} = \frac{\partial \phi^{(0)}}{\partial x}$ and the depth-averaged velocity $\bar{u}$. We have the following relation between these two quantities:

$$\begin{aligned}
\bar{u} &= \frac{1}{1+\epsilon\zeta-\epsilon\kappa_d\eta}\int_{-1+\epsilon\kappa_d\eta}^{\epsilon\zeta}\frac{\partial\phi}{\partial x}dz \\
&= \frac{1}{1+\epsilon\zeta-\epsilon\kappa_d\eta}\int_{-1+\epsilon\kappa_d\eta}^{\epsilon\zeta}\Big(u^{(0)} - \kappa^2\frac{(z+1)^2}{2}\frac{\partial^2 u^{(0)}}{\partial x^2} + \kappa_d\kappa^2(z+1)\frac{\partial\eta_t}{\partial x} \\
&+ \kappa^4\frac{(z+1)^4}{4!}\frac{\partial^4 u^{(0)}}{\partial x^4} + O(\kappa^6)\Big)dz \\
&= u^{(0)} - \frac{\kappa^2}{6}\frac{(1+\epsilon\zeta)^3}{1+\epsilon\zeta-\epsilon\kappa_d\eta}\frac{\partial^2 u^{(0)}}{\partial x^2} + \frac{\kappa_d\kappa^2}{2}\frac{(1+\epsilon\zeta)^2}{1+\epsilon\zeta-\epsilon\kappa_d\eta}\frac{\partial\eta_t}{\partial x} + \frac{\kappa^4}{5!}\frac{\partial^4 u^{(0)}}{\partial x^4} + O(\kappa^6) \\
&= u^{(0)} - \frac{\kappa^2}{6}(1+2\epsilon\zeta)\frac{\partial^2 u^{(0)}}{\partial x^2} + \frac{\kappa_d\kappa^2}{2}\frac{(1+\epsilon\zeta)^2}{1+\epsilon\zeta-\epsilon\kappa_d\eta}\frac{\partial\eta_t}{\partial x} + \frac{\kappa^4}{5!}\frac{\partial^4 u^{(0)}}{\partial x^4} + O(\kappa^6) \\
&= u^{(0)} - \frac{\kappa^2}{6}\frac{\partial^2 u^{(0)}}{\partial x^2} - \frac{\epsilon\kappa^2}{3}\zeta\frac{\partial^2 u^{(0)}}{\partial x^2} + \frac{\kappa_d\kappa^2}{2}\frac{\partial\eta_t}{\partial x} + \frac{\kappa^4}{5!}\frac{\partial^4 u^{(0)}}{\partial x^4} + O(\kappa^6)
\end{aligned} \tag{4.2.3.4}$$

Turning this last result around, we obtain the relation:

$$u^{(0)} = \bar{u} + \frac{\kappa^2}{6}\frac{\partial^2\bar{u}}{\partial x^2} + \frac{\kappa^4}{36}\frac{\partial^4\bar{u}}{\partial x^4} + \frac{\epsilon\kappa^2}{3}\zeta\nabla^2\bar{u} - \frac{\kappa_d\kappa^2}{2}\frac{\partial\eta_t}{\partial x} - \frac{\kappa^4}{5!}\frac{\partial^4\bar{u}}{\partial x^4} + O(\kappa^6) \tag{4.2.3.5}$$

We first express equation 4.2.3.3 as a function of the water velocity u_0 instead of the potential:

$$\begin{aligned}
\zeta_t + \epsilon u^{(0)}\frac{\partial\zeta}{\partial x} =& \frac{\epsilon\kappa^2}{2}\frac{\partial^2 u^{(0)}}{\partial x^2}\frac{\partial\zeta}{\partial x} + \kappa_d\left(\frac{\partial\eta}{\partial t} + \epsilon\frac{\partial}{\partial x}(\eta u^{(0)})\right) - (1+\epsilon\zeta)\frac{\partial u^{(0)}}{\partial x} \\
&- \frac{\kappa_d\kappa^2}{2!}\frac{\partial^2\eta_t}{\partial x} + \frac{\kappa^2}{6}\frac{\partial^3 u^{(0)}}{\partial x^3} + \frac{\kappa^2\epsilon\zeta}{2}\frac{\partial^3 u^{(0)}}{\partial x^3} + O(\kappa^6)
\end{aligned} \tag{4.2.3.6}$$

Using 4.2.3.5, we obtain the equation 4.2.3.6 with respect to $\bar{u}$ instead of $u^{(0)}$. Many terms cancel and we finally obtain the simplified form of the kinematic boundary condition, that does not contain any additional term compared to equation 2.3.2.9:

$$\zeta_t - \kappa_d\eta_t + \frac{\partial}{\partial x}[(1+\epsilon\zeta-\epsilon\kappa_d\eta)\bar{u}] = O(\kappa^6) \tag{4.2.3.7}$$

In the rest of this thesis, we will only use this equation up to order $O(\kappa^2)$:

$$\boxed{\zeta_t - \kappa_d\eta_t + \frac{\partial}{\partial x}[(1+\epsilon\zeta)\bar{u}] = O(\kappa^4)} \tag{4.2.3.8}$$

4.2.4 Dynamic boundary condition at the free surface

The same way, the dynamic boundary condition at the free surface is unchanged compared to equation 2.3.3.1:

$$\kappa^2(\phi_t + \zeta) + \frac{1}{2}\epsilon[\kappa^2\phi_x^2 + \phi_z^2] = 0, \quad z = \epsilon\zeta(x,t) \tag{4.2.4.1}$$

From the development of ϕ given by equation 4.2.2.6, we deduce the following equalities:

$$\begin{aligned}
\phi_t &= (\phi^{(0)})_t - \kappa^2\frac{(1+2\epsilon\zeta)}{2}\frac{\partial^2(\phi^{(0)})_t}{\partial x^2} + \kappa_d\kappa^2\eta_{tt} + \frac{\kappa^4}{4!}\frac{\partial^4(\phi^{(0)})_t}{\partial x^4} + O(\kappa^6) \\
{\phi_x}^2 &= \left(\frac{\partial\phi^{(0)}}{\partial x}\right)^2 - \kappa^2\frac{\partial\phi^{(0)}}{\partial x}\frac{\partial^3\phi^{(0)}}{\partial x^3} + O(\kappa^4) \\
{\phi_z}^2 &= \kappa^4\left(\frac{\partial^2\phi^{(0)}}{\partial x^2}\right)^2 + O(\kappa^6)
\end{aligned} \tag{4.2.4.2}$$

And as a consequence:

$$\begin{aligned}
(\phi^{(0)})_t - \frac{\kappa^2}{2}\frac{\partial^2(\phi^{(0)})_t}{\partial x^2} - \epsilon\kappa^2\zeta\frac{\partial^2(\phi^{(0)})_t}{\partial x^2} + \kappa_d{\kappa^2}\frac{\partial^2\eta}{\partial t^2} + \frac{\kappa^4}{4!}\frac{\partial^4{\phi^{(0)}}_t}{\partial x^4} + \zeta \\
+ \frac{1}{2}\epsilon\left[\left(\frac{\partial\phi^{(0)}}{\partial x}\right)^2 - {\kappa^2}\frac{\partial\phi^{(0)}}{\partial x}\frac{\partial^2\phi^{(0)}}{\partial x^2} + \kappa^2\left(\frac{\partial^3\phi^{(0)}}{\partial x^3}\right)^2\right] = O(\kappa^6)
\end{aligned} \tag{4.2.4.3}$$

This equation is rewritten:

$$\begin{aligned}
(\phi^{(0)})_t + \frac{1}{2}\epsilon\left(\frac{\partial\phi^{(0)}}{\partial x}\right)^2 + \zeta =& \frac{\kappa^2}{2}\frac{\partial^2(\phi^{(0)})_t}{\partial x^2} + \epsilon\kappa^2\zeta\frac{\partial^2(\phi^{(0)})_t}{\partial x^2} - {\kappa_d\kappa^2}\frac{\partial^2\eta}{\partial t^2} - \frac{\kappa^4}{4!}\frac{\partial^4(\phi^{(0)})_t}{\partial x^4} \\
&+ \frac{1}{2}\epsilon\kappa^2\left[\frac{\partial\phi^{(0)}}{\partial x}\frac{\partial^3\phi^{(0)}}{\partial x^3} - \left(\frac{\partial^2\phi^{(0)}}{\partial x^2}\right)^2\right] + O(\kappa^6)
\end{aligned} \tag{4.2.4.4}$$

As done for the kinematic boundary condition case, we write this equation as a function of the velocity $u^{(0)}$:

$$\begin{aligned}
\frac{\partial u^{(0)}}{\partial t} + \epsilon u^{(0)}\frac{\partial u^{(0)}}{\partial x} + \frac{\partial\zeta}{\partial x} =& \frac{\kappa^2}{2}\frac{\partial^2(u^{(0)})_t}{\partial x^2} + \epsilon\kappa^2\frac{\partial\zeta}{\partial x}\frac{\partial(u^{(0)})_t}{\partial x} + \epsilon\kappa^2\zeta\frac{\partial^2(u^{(0)})_t}{\partial x^2} - \kappa_d\kappa^2\frac{\partial\eta_{tt}}{\partial x} \\
&- \frac{\kappa^4}{4!}\frac{\partial^4(u^{(0)})_t}{\partial x^4} + \frac{1}{2}\epsilon\kappa^2\frac{\partial}{\partial x}\left(u^{(0)}\frac{\partial^2u^{(0)}}{\partial x^2}\right) - \frac{1}{2}\epsilon\kappa^2\frac{\partial}{\partial x}\left(\frac{\partial u^{(0)}}{\partial x}\right)^2 + O(\kappa^6)
\end{aligned} \tag{4.2.4.5}$$

And from equation 4.2.3.5 we deduce the relation on the depth-averaged velocity $\bar{u}$:

$$\begin{aligned}
&\frac{\partial \bar{u}}{\partial t} + \frac{\kappa^2}{6}\frac{\partial^2 \bar{u}_t}{\partial x^2} + \frac{\kappa^4}{36}\frac{\partial^4 \bar{u}_t}{\partial x^4} + \frac{\epsilon\kappa^2}{3}\zeta\frac{\partial^2 \bar{u}_t}{\partial x^2} + \frac{\epsilon\kappa^2}{3}\frac{\partial \zeta}{\partial t}\frac{\partial^2 \bar{u}}{\partial x^2} - \frac{\kappa_d\kappa^2}{2}\frac{\partial \eta_{tt}}{\partial x} - \frac{\kappa^4}{5!}\frac{\partial^4 \bar{u}_t}{\partial x^4} \\
&+ \epsilon\bar{u}\frac{\partial}{\partial x}\left(\bar{u} + \frac{\kappa^2}{6}\frac{\partial^2 \bar{u}}{\partial x^2}\right) + \epsilon\frac{\kappa^2}{6}\frac{\partial^2 \bar{u}}{\partial x^2}\frac{\partial \bar{u}}{\partial x} + \frac{\partial \zeta}{\partial x} = \frac{\kappa^2}{2}\frac{\partial^2 \bar{u}_t}{\partial x^2} + \frac{\kappa^4}{12}\frac{\partial^4 \bar{u}_t}{\partial x^4} + \epsilon\kappa^2\frac{\partial \zeta}{\partial x}\frac{\partial \bar{u}_t}{\partial x} + \epsilon\kappa^2\zeta\frac{\partial^2 \bar{u}_t}{\partial x^2} \\
&- \kappa_d\kappa^2\frac{\partial^2 \eta_{tt}}{\partial x} - \frac{\kappa^4}{4!}\frac{\partial^4 \bar{u}_t}{\partial x^4} + \frac{1}{2}\epsilon\kappa^2\frac{\partial}{\partial x}\left(\bar{u}\frac{\partial^2 \bar{u}}{\partial x^2}\right) - \frac{1}{2}\epsilon\kappa^2\frac{\partial}{\partial x}\left(\frac{\partial \bar{u}}{\partial x}\right)^2 + O(\kappa^6)
\end{aligned} \tag{4.2.4.6}$$

$$\begin{aligned}
\frac{\partial \bar{u}}{\partial t} + \epsilon\bar{u}\frac{\partial \bar{u}}{\partial x} + \frac{\partial \zeta}{\partial x} = &- \frac{\kappa^2}{6}\frac{\partial^3 \bar{u}}{\partial t \partial x^2} - \frac{\kappa^4}{36}\frac{\partial^5 \bar{u}}{\partial x^4 \partial t} - \frac{\epsilon\kappa^2}{3}\zeta\frac{\partial^3 \bar{u}}{\partial x^2 \partial t} - \frac{\epsilon\kappa^2}{3}\frac{\partial \zeta}{\partial t}\frac{\partial^2 \bar{u}}{\partial x^2} \\
&+ \frac{\kappa_d\kappa^2}{2}\frac{\partial^3 \eta}{\partial x \partial t^2} + \frac{\kappa^4}{5!}\frac{\partial^5 \bar{u}}{\partial x^4 \partial t} - \frac{\epsilon\kappa^2}{6}\bar{u}\frac{\partial^3 \bar{u}}{\partial x^3} - \epsilon\frac{\kappa^2}{6}\frac{\partial^2 \bar{u}}{\partial x^2}\frac{\partial \bar{u}}{\partial x} + \frac{\kappa^2}{2}\frac{\partial^3 \bar{u}}{\partial x^2 \partial t} \\
&+ \frac{\kappa^4}{12}\frac{\partial^5 \bar{u}}{\partial x^4 \partial t} + \epsilon\kappa^2\frac{\partial \zeta}{\partial x}\frac{\partial^2 \bar{u}}{\partial x \partial t} + \epsilon\kappa^2\zeta\frac{\partial^3 \bar{u}}{\partial x^2 \partial t} - \kappa_d\kappa^2\frac{\partial^3 \eta}{\partial x \partial t^2} - \frac{\kappa^4}{4!}\frac{\partial^5 \bar{u}}{\partial x^4 \partial t} \\
&+ \frac{1}{2}\epsilon\kappa^2\frac{\partial}{\partial x}\left(\bar{u}\frac{\partial^2 \bar{u}}{\partial x^2}\right) - \frac{1}{2}\epsilon\kappa^2\frac{\partial}{\partial x}\left(\frac{\partial \bar{u}}{\partial x}\right)^2 + O(\kappa^6)
\end{aligned} \tag{4.2.4.7}$$

Combining terms on the right hand side, we obtain:

$$\begin{aligned}
\frac{\partial \bar{u}}{\partial t} + \epsilon\bar{u}\frac{\partial \bar{u}}{\partial x} + \frac{\partial \zeta}{\partial x} = &- \frac{\kappa^2}{6}\frac{\partial^3 \bar{u}}{\partial t \partial x^2} + \frac{\kappa^2}{2}\frac{\partial^3 \bar{u}}{\partial x^2 \partial t} \\
&- \frac{\kappa^4}{36}\frac{\partial^5 \bar{u}}{\partial x^4 \partial t} + \frac{\kappa^4}{5!}\frac{\partial^5 \bar{u}}{\partial x^4 \partial t} - \frac{\kappa^4}{4!}\frac{\partial^5 \bar{u}}{\partial x^4 \partial t} + \frac{\kappa^4}{12}\frac{\partial^5 \bar{u}}{\partial x^4 \partial t} \\
&- \frac{\epsilon\kappa^2}{3}\zeta\frac{\partial^3 \bar{u}}{\partial x^2 \partial t} + \epsilon\kappa^2\zeta\frac{\partial^3 \bar{u}}{\partial x^2 \partial t} \\
&- \frac{\epsilon\kappa^2}{3}\frac{\partial \zeta}{\partial t}\frac{\partial^2 \bar{u}}{\partial x^2} \\
&+ \frac{\kappa_d\kappa^2}{2}\frac{\partial^3 \eta}{\partial x \partial t^2} - \kappa_d\kappa^2\frac{\partial^3 \eta}{\partial x \partial t^2} \\
&+ \epsilon\kappa^2\frac{\partial \zeta}{\partial x}\frac{\partial^2 \bar{u}}{\partial x \partial t} \\
&- \frac{\epsilon\kappa^2}{6}\bar{u}\frac{\partial^3 \bar{u}}{\partial x^3} - \epsilon\frac{\kappa^2}{6}\frac{\partial^2 \bar{u}}{\partial x^2}\frac{\partial \bar{u}}{\partial x} \\
&+ \frac{1}{2}\epsilon\kappa^2\frac{\partial}{\partial x}\left(\bar{u}\frac{\partial^2 \bar{u}}{\partial x^2}\right) - \frac{1}{2}\epsilon\kappa^2\frac{\partial}{\partial x}\left(\frac{\partial \bar{u}}{\partial x}\right)^2 + O(\kappa^6)
\end{aligned} \tag{4.2.4.8}$$

$$\begin{aligned}
\frac{\partial \bar{u}}{\partial t} + \epsilon\bar{u}\frac{\partial \bar{u}}{\partial x} + \frac{\partial \zeta}{\partial x} = &\frac{\kappa^2}{3}\frac{\partial^3 \bar{u}}{\partial t \partial x^2} + \frac{\kappa^4}{12}\frac{\partial^5 \bar{u}}{\partial x^4 \partial t} + \frac{2\epsilon\kappa^2}{3}\zeta\frac{\partial^3 \bar{u}}{\partial x^2 \partial t} \\
&- \frac{\epsilon\kappa^2}{3}\frac{\partial \zeta}{\partial t}\frac{\partial^2 \bar{u}}{\partial x^2} + \epsilon\kappa^2\frac{\partial \zeta}{\partial x}\frac{\partial^2 \bar{u}}{\partial x \partial t} - \frac{\kappa_d\kappa^2}{2}\frac{\partial^3 \eta}{\partial x \partial t^2} \\
&+ \frac{1}{3}\epsilon\kappa^2\frac{\partial}{\partial x}\left(\bar{u}\frac{\partial^2 \bar{u}}{\partial x^2}\right) - \frac{1}{2}\epsilon\kappa^2\frac{\partial}{\partial x}\left(\frac{\partial \bar{u}}{\partial x}\right)^2 + O(\kappa^6)
\end{aligned} \tag{4.2.4.9}$$

Because of the relation:

$$-\frac{\epsilon\kappa^2}{6}\bar{u}\frac{\partial^3\bar{u}}{\partial x^3}-\epsilon\frac{\kappa^2}{6}\frac{\partial^2\bar{u}}{\partial x^2}\frac{\partial\bar{u}}{\partial x}=-\epsilon\frac{\kappa^2}{6}\frac{\partial}{\partial x}\left(\bar{u}\frac{\partial\bar{u}}{\partial x}\right) \tag{4.2.4.10}$$

we finally obtain the equation equivalent to equation 2.3.3.6:

$$\begin{aligned}\frac{\partial\bar{u}}{\partial t}+\epsilon\bar{u}\frac{\partial\bar{u}}{\partial x}+\frac{\partial\zeta}{\partial x}=&\frac{\kappa^2}{3}\frac{\partial^3\bar{u}}{\partial t\partial x^2}-\frac{\kappa_d\kappa^2}{2}\frac{\partial^3\eta}{\partial x\partial t^2}+\frac{\kappa^4}{12}\frac{\partial^5\bar{u}}{\partial x^4\partial t}+\frac{2}{3}\epsilon\kappa^2\zeta\frac{\partial^3\bar{u}}{\partial x^2\partial t}-\frac{1}{3}\epsilon\kappa^2\frac{\partial\zeta}{\partial t}\frac{\partial^2\bar{u}}{\partial x^2}\\&+\epsilon\kappa^2\frac{\partial\zeta}{\partial x}\frac{\partial^2\bar{u}}{\partial x\partial t}+\frac{1}{3}\epsilon\kappa^2\frac{\partial}{\partial x}\left(\bar{u}\frac{\partial^2\bar{u}}{\partial x^2}\right)-\frac{1}{2}\epsilon\kappa^2\frac{\partial}{\partial x}\left(\frac{\partial\bar{u}}{\partial x}\right)^2+O(\kappa^6)\end{aligned} \tag{4.2.4.11}$$

Many new terms of order $O(\kappa^4)$ appear on the right hand side.

In the rest of this thesis, we will once again only consider the terms up to order $O(\kappa^4)$:

$$\boxed{\frac{\partial\bar{u}}{\partial t}+\epsilon\bar{u}\frac{\partial\bar{u}}{\partial x}+\frac{\partial\zeta}{\partial x}=\frac{\kappa^2}{3}\frac{\partial^3\bar{u}}{\partial t\partial x^2}+O(\kappa^4)} \tag{4.2.4.12}$$

4.2.5 Equation of the total pressure in water

From the Bernoulli equation, we know the pressure in water at any depth z:

$$p=-\phi_t-\frac{\epsilon}{2}\left[(\phi_x)^2+\frac{1}{\kappa^2}(\phi_z)^2\right]-\frac{z}{\epsilon} \tag{4.2.5.1}$$

Thus, we deduce a relation between the pressure in water and the potential at $z=-1+\epsilon\kappa_d\eta$:

$$p=\frac{1}{\epsilon}-\phi_t-\kappa_d\eta-\frac{\epsilon}{2}\left(\frac{\partial\phi}{\partial x}\right)^2+O(\kappa^4),\quad z=-1+\epsilon\kappa_d\eta \tag{4.2.5.2}$$

By Taylor expansion, we know that:

$$\phi(z=-1+\epsilon\kappa_d\eta)=\phi(z=-1)+O(\kappa^4)=\phi_0+O(\kappa^4) \tag{4.2.5.3}$$

As a consequence, 4.2.5.2 becomes:

$$p=\frac{1}{\epsilon}-(\phi^{(0)})_t-\kappa_d\eta-\frac{\epsilon}{2}\left(\frac{\partial\phi^{(0)}}{\partial x}\right)^2+O(\kappa^4),\quad z=-1+\epsilon\kappa_d\eta \tag{4.2.5.4}$$

This equation will be later used to estimate the pressure in the mud layer. Since we will only carry the calculation at the first order in mud, we will only use the first

order of equation 4.2.5.4 in the rest of this thesis:

$$\boxed{p = \frac{1}{\epsilon} - \phi^{(0)}{}_t + O(\kappa^2)}, \quad z = -1 + \epsilon\eta \tag{4.2.5.5}$$

4.3 Equations in mud

Let us now find the governing equations in mud. We only go to the first order $O(\kappa^0)$ in this thesis. Indeed, the drift current induced by non-linearity of order $O(\epsilon) = O(\kappa^2)$ will not be considered.

4.3.1 Kinematic boundary condition at the interface in the mud

In dimensional form, we know that, exactly:

$$\eta'_{t'} = V' - \eta'_{x'}U', \quad Z = 1 + \epsilon\eta \tag{4.3.1.1}$$

In dimensionless form, and keeping only the first order, we obtain:

$$\boxed{\eta_t = V + O(\kappa^2)} \tag{4.3.1.2}$$

4.3.2 Conservation of mass in the mud

From the conservation of mass in mud in dimensionless form, we know:

$$\boxed{U_x + V_Z = 0} \tag{4.3.2.1}$$

This equation will be used later to deduce the vertical velocity in mud from the horizontal velocity.

4.3.3 Horizontal momentum in mud

Let us first write the Newtonian relation between the stress τ and the strain E in a dimensional form.

$$\tau'_{xZ} = \mu \frac{\partial E'_{xZ}}{\partial t'} \tag{4.3.3.1}$$

So we have:

$$\tau_{xZ} = \frac{\partial U}{\partial Z} + O(\kappa^4) \tag{4.3.3.2}$$

The equation of momentum in the mud, projected on the x-axis, gives:

$$\frac{\partial U}{\partial t} + \epsilon \left(U \frac{\partial U}{\partial x} + V \frac{\partial U}{\partial Z} \right) = -\gamma \frac{\partial P}{\partial x} + \frac{A}{Re * d} \left(\frac{\partial \tau_{xZ}}{\partial Z} + \kappa \kappa_d \frac{\partial \tau_{xx}}{\partial x} \right) \tag{4.3.3.3}$$

where γ is the ratio of densities:

$$\underline{\gamma = \rho_W / \rho_M} \tag{4.3.3.4}$$

From this equation we simplify:

$$\frac{\partial U}{\partial t} = \frac{1}{Re} \frac{A}{d} \frac{\partial \tau_{xZ}}{\partial Z} - \gamma \frac{\partial P}{\partial x} + O(\epsilon) \tag{4.3.3.5}$$

where U is the horizontal velocity of mud, P the pressure, A the amplitude of the free surface and d the mud depth. In equation 4.3.3.5, the convective inertia term has been neglected. Re is the Reynolds number defined as:

$$\boxed{Re = \frac{\rho_M A d k \sqrt{g\bar{h}}}{\mu}} \tag{4.3.3.6}$$

As a consequence, the Reynolds number in this chapter is the same as in chapter 2 (equation 2.4.3.6). The values of Re are thus functions of $\bar{h}$, ω', A and the type of mud. As a consequence, the values we tabulated in tables 2.6 to 2.9 are still valid.

Table 4.1 recalls the results presented in table 2.9. Let us remind the reader that the gray cells in this table correspond to the case $O(\kappa^2) = O(\epsilon)$ that we are currently studying. We chose to repeat the table corresponding to the Hangzhou Bay mud because it corresponds to the highest Reynolds number values that we found.

We see in this table that Re can be as big as 10. As a consequence, and because we want our study to be applicable to any type of mud, we decide to adopt the limiting case. This is why the Reynolds number will be regarded as:

$$\boxed{Re = O(1)} \tag{4.3.3.7}$$

Differentiating equation 4.3.3.2 with respect to Z, we get:

$$\frac{\partial \tau_{xZ}}{\partial Z} = \frac{\partial^2 U}{\partial Z^2} + O(\kappa^4) \tag{4.3.3.8}$$

ϵ, κ, Re				A (cm)			
				10	20	40	60
$\bar{h}$(m)	1	ω' (rad/s)	1/3	$\epsilon = 0.1$ $\kappa = 0.106$ $Re = 0.13$	$\epsilon = 0.2$ $\kappa = 0.106$ $Re = 0.27$	$\epsilon = 0.4$ $\kappa = 0.106$ $Re = 0.53$	$\epsilon > 0.4$
			1/2	$\epsilon = 0.1$ $\kappa = 0.159$ $Re = 0.33$	$\epsilon = 0.2$ $\kappa = 0.159$ $Re = 0.65$	$\epsilon = 0.4$ $\kappa = 0.159$ $Re = 1.3$	$\epsilon > 0.4$
			1	$\epsilon = 0.1$ $\kappa = 0.31$ $Re = 1.4$	$\epsilon = 0.2$ $\kappa = 0.31$ $Re = 2.8$	$\epsilon = 0.4$ $\kappa = 0.31$ $Re = 5.7$	$\epsilon > 0.4$
	2	ω' (rad/s)	1/3	$\epsilon = 0.05$ $\kappa = 0.15$ $Re = 0.27$	$\epsilon = 0.1$ $\kappa = 0.15$ $Re = 0.53$	$\epsilon = 0.2$ $\kappa = 0.15$ $Re = 1$	$\epsilon = 0.3$ $\kappa = 0.15$ $Re = 1.6$
			1/2	$\epsilon = 0.05$ $\kappa = 0.225$ $Re = 0.65$	$\epsilon = 0.1$ $\kappa = 0.225$ $Re = 1.3$	$\epsilon = 0.2$ $\kappa = 0.225$ $Re = 2.6$	$\epsilon = 0.3$ $\kappa = 0.225$ $Re = 3.9$
			1	$\kappa > 0.4$	$\kappa > 0.4$	$\kappa > 0.4$	$\kappa > 0.4$
	5	ω' (rad/s)	1/3	$\epsilon = 0.02$ $\kappa = 0.238$ $Re = 0.67$	$\epsilon = 0.04$ $\kappa = 0.238$ $Re = 1.33$	$\epsilon = 0.08$ $\kappa = 0.238$ $Re = 2.67$	$\epsilon = 0.12$ $\kappa = 0.238$ $Re = 4$
			1/2	$\epsilon = 0.02$ $\kappa = 0.357$ $Re = 1.6$	$\epsilon = 0.04$ $\kappa = 0.357$ $Re = 3.2$	$\epsilon = 0.08$ $\kappa = 0.357$ $Re = 6.5$	$\epsilon = 0.12$ $\kappa = 0.357$ $Re = 9.8$
			1	$\kappa > 0.4$	$\kappa > 0.4$	$\kappa > 0.4$	$\kappa > 0.4$
	10	ω' (rad/s)	1/3	$\epsilon = 0.01$ $\kappa = 0.33$ $Re = 1.3$	$\epsilon = 0.02$ $\kappa = 0.33$ $Re = 2.7$	$\epsilon = 0.04$ $\kappa = 0.33$ $Re = 5.3$	$\epsilon = 0.06$ $\kappa = 0.33$ $Re = 8$
			1/2	$\kappa > 0.4$	$\kappa > 0.4$	$\kappa > 0.4$	$\kappa > 0.4$
			1	$\kappa > 0.4$	$\kappa > 0.4$	$\kappa > 0.4$	$\kappa > 0.4$

Table 4.1: Values of Re for different A, frequency ω' and water depths $\bar{h}$, for the Hangzhou Bay mud. We set $\kappa_d = 0.1$.

Equation 4.3.3.5 can be rewritten:

$$\frac{\partial \tau_{xZ}}{\partial Z} = Re\frac{d}{A}\left(\frac{\partial U}{\partial t} + \gamma\frac{\partial P}{\partial x}\right) + O(\epsilon) \tag{4.3.3.9}$$

By combining equation 4.3.3.8 and 4.3.3.9 we obtain an equation between the horizontal velocity and the pressure gradient:

$$\frac{\partial^2 U}{\partial Z^2} = Re\frac{d}{A}\left(\frac{\partial U}{\partial t} + \gamma\frac{\partial P}{\partial x}\right) + O(\epsilon) \quad 0 < Z < 1 + \epsilon\eta \tag{4.3.3.10}$$

where

$$Re\frac{d}{A} = Re\frac{\kappa_d}{\epsilon} = O(1) \tag{4.3.3.11}$$

Let us now find an equation of the mud pressure P as a function of ζ and η in order to eliminate the mud pressure from equation 4.3.3.10.

4.3.4 Vertical momentum in mud

The dimensional equation of vertical momentum is:

$$\rho_M\left(\frac{\partial V'}{\partial t'} + U'\frac{\partial V'}{\partial x'} + V'\frac{\partial V'}{\partial Z'}\right) = -\frac{\partial P'}{\partial Z'} + \left(\frac{\partial \tau'_{ZZ}}{\partial Z'} + \frac{\partial \tau'_{xZ}}{\partial x'}\right) \tag{4.3.4.1}$$

and becomes, in dimensionless variables:

$$\frac{\partial V}{\partial t} + \epsilon\left(U\frac{\partial V}{\partial x} + V\frac{\partial V}{\partial Z}\right) = -\frac{\gamma}{\kappa^4}\frac{\partial P}{\partial Z} + \frac{\epsilon}{Re\kappa_d\kappa^2}\left(\frac{\partial \tau_{ZZ}}{\partial Z} + \kappa^2\frac{\partial \tau_{xZ}}{\partial x}\right) \tag{4.3.4.2}$$

So, in the end,

$$\boxed{\frac{\partial P}{\partial Z} = O(\kappa^2)} \quad 0 < Z < 1 + \epsilon\eta \tag{4.3.4.3}$$

In other words, we find that the vertical pressure gradient in mud is of order $O(\kappa^2)$. This equation will be used to evaluate the pressure in the entire mud layer.

4.3.5 Dynamic boundary condition at the interface

Let us call $\underline{n} = (n_x, n_Z)$ the vector normal to the interface. In dimensional notations, we know that the components of $\underline{n}$ are:

$$\begin{aligned} n_x &= \frac{\frac{\partial \eta'}{\partial x'}}{\sqrt{1+\left(\frac{\partial \eta'}{\partial x'}\right)^2}} \\ n_Z &= \frac{1}{\sqrt{1+\left(\frac{\partial \eta'}{\partial x'}\right)^2}} \end{aligned} \tag{4.3.5.1}$$

In dimensionless variables, we obtain:

$$\begin{aligned} n_x &= \frac{\epsilon\kappa\kappa_d \frac{\partial \eta}{\partial x}}{\sqrt{1+\epsilon^2\kappa^2\kappa_d^2\left(\frac{\partial \eta}{\partial x}\right)^2}} \\ n_Z &= \frac{1}{\sqrt{1+\epsilon^2\kappa^2\kappa_d^2\left(\frac{\partial \eta}{\partial x}\right)^2}} \end{aligned} \tag{4.3.5.2}$$

Finally, n_x and n_Z can be approximated as:

$$\begin{aligned} n_x &= O(\epsilon\kappa\kappa_d) \\ n_Z &= 1 + O(\epsilon^2\kappa^2\kappa_d^2) \end{aligned} \tag{4.3.5.3}$$

Continuity of total (hydrodynamic and dynamic) stress on the mud-water interface then requires:

$$\begin{aligned} T_{xx}n_x + T_{xZ}n_Z &= -pn_x, \quad Z = 1+\epsilon\eta \\ T_{xZ}n_x + T_{ZZ}n_Z &= -pn_Z, \quad Z = 1+\epsilon\eta \end{aligned} \tag{4.3.5.4}$$

Total stress in mud is the sum of hydrostatic and dynamic pressure:

$$T_{ij} = -P\delta_{ij} + \frac{\epsilon\kappa}{\gamma Re}\tau_{ij}, \tag{4.3.5.5}$$

Introducing this sum in equation 4.3.5.4, we obtain:

$$\begin{aligned} \left(-P + \frac{\epsilon\kappa}{\gamma Re}\tau_{xx}\right)n_x + \frac{\epsilon\kappa}{\gamma Re}\tau_{xZ}n_Z &= -pn_x, \quad Z = 1+\epsilon\eta \\ \frac{\epsilon\kappa}{\gamma Re}\tau_{xZ}n_x + \left(-P + \frac{\epsilon\kappa}{\gamma Re}\tau_{ZZ}\right)n_Z &= -pn_Z, \quad Z = 1+\epsilon\eta \end{aligned} \tag{4.3.5.6}$$

From the approximations of n_x and n_Z that we demonstrated in 4.3.5.3, equations 4.3.5.6 become:

$$\begin{aligned}
&\left(-P + \frac{\epsilon\kappa}{\gamma Re}\tau_{xx}\right) O(\epsilon\kappa\kappa_d) + \frac{\epsilon\kappa}{\gamma Re}\tau_{xZ}(1 + O(\epsilon^2\kappa^2\kappa_d^2)) = -pO(\epsilon\kappa\kappa_d), \quad Z = 1 + \epsilon\eta \\
&\frac{\epsilon\kappa}{\gamma Re}\tau_{xZ}O(\epsilon\kappa\kappa_d) + \left(-P + \frac{\epsilon\kappa}{\gamma Re}\tau_{ZZ}\right)(1 + O(\epsilon^2\kappa^2\kappa_d^2)) = -p(1 + O(\epsilon^2\kappa^2\kappa_d^2)), \quad Z = 1 + \epsilon\eta
\end{aligned} \tag{4.3.5.7}$$

These last equations can easily be simplified to:

$$\begin{aligned}
\frac{\epsilon\kappa}{\gamma Re}\tau_{xZ} &= O(\epsilon\kappa\kappa_d), \quad Z = 1 + \epsilon\eta \\
P - p &= O(\kappa^2), \quad Z = 1 + \epsilon\eta
\end{aligned} \tag{4.3.5.8}$$

Dividing the first equation of 4.3.5.8 by $\frac{\epsilon\kappa}{\gamma Re}$, these equations become:

$$\begin{aligned}
\tau_{xZ} &= O(\kappa_d), \quad Z = 1 + \epsilon\eta \\
P - p &= O(\kappa^2), \quad Z = 1 + \epsilon\eta
\end{aligned} \tag{4.3.5.9}$$

We now focus on the first part of equation 4.3.5.9. Through a Taylor expansion, we can approximate this equations around $Z = 1$:

$$\tau_{xZ} = O(\kappa^2), \quad Z = 1 \tag{4.3.5.10}$$

since $O(\kappa^2) = O(\epsilon) = O(\kappa_d)$. Making use of the relation 4.3.3.2, we finally obtain a boundary condition at the interface in term of the horizontal velocity U:

$$\boxed{\frac{\partial U}{\partial Z}\Big|_{Z=1} = O(\kappa^2)} \tag{4.3.5.11}$$

Let us now focus on the second part of equation 4.3.5.9. From 4.3.4.3, we know that the vertical gradient of mud pressure is of order $O(\kappa^2)$. As a consequence, by a Taylor expansion of the mud pressure P, we obtain:

$$P = p(Z = 1 + \epsilon\eta) + O(\kappa^2), \quad 0 < Z < 1 + \epsilon\eta \tag{4.3.5.12}$$

Differentiating this last equation, we know that:

$$\frac{\partial P}{\partial x} = \frac{\partial p}{\partial x}(Z = 1 + \epsilon\eta) + O(\kappa^2), \quad 0 < Z < 1 + \epsilon\eta \tag{4.3.5.13}$$

Water pressure p is known in any point of the water layer thanks to the Bernouilli equation. In particular, we know from equation 4.2.5.5 the water pressure at the interface ($z = -1 + \epsilon\kappa_d\eta$):

$$p = \frac{1}{\epsilon} - \phi^{(0)}{}_t + O(\kappa^2), \quad z = -1 + \epsilon\eta \tag{4.3.5.14}$$

By differentiating this equation, we obtain:

$$\frac{\partial p}{\partial x} = -\frac{\partial^2 \phi^{(0)}}{\partial x \partial t} + O(\kappa^2), \quad z = -1 + \epsilon\kappa_d\eta \tag{4.3.5.15}$$

From equation 4.2.4.4, we also know:

$$\frac{\partial \phi^{(0)}}{\partial t} = -\zeta + O(\kappa^2) \tag{4.3.5.16}$$

which is valid for all z since $\phi^{(0)}$ and ζ do not depend on the vertical coordinate.

Combining equations 4.3.5.15 and 4.3.5.16, we get the water pressure gradient at the interface:

$$\frac{\partial p}{\partial x} = \frac{\partial \zeta}{\partial x} + O(\kappa^2), \quad z = -1 + \epsilon\kappa_d\eta \tag{4.3.5.17}$$

Combining equation 4.3.5.17 with 4.3.5.13, we finally obtain the mud pressure horizontal gradient in the entire mud layer:

$$\frac{\partial P}{\partial x} = \frac{\partial \zeta}{\partial x} + O(\kappa^2), \quad 0 < Z < 1 + \epsilon\eta \tag{4.3.5.18}$$

As a consequence, we can now substitute the mud pressure P from the horizontal momentum equation 4.3.3.10, for $0 < Z < 1 + \epsilon\eta$:

$$\boxed{\frac{\partial^2 U}{\partial Z^2} = Re\frac{d}{A}\left(\frac{\partial U}{\partial t} + \gamma\frac{\partial \zeta}{\partial x}\right) + O(\kappa^2)} \quad 0 < Z < 1 + \epsilon\eta \tag{4.3.5.19}$$

4.3.6 Bottom kinematic boundary conditions

At the bottom, we impose the no-slip boundary condition:

$$\boxed{U = V = 0}, \quad Z = 0 \tag{4.3.6.1}$$

4.4 Asymptotic equations in water and Newtonian mud

4.4.1 Equations at dominant orders

Water equations

By combining equations 4.2.3.8 and 4.2.4.12 at order $O(\epsilon^2)$, we obtain:

$$\frac{\partial^2\zeta}{\partial t^2} - \frac{\partial^2\zeta}{\partial x^2} = -\epsilon\frac{\partial^2\zeta\bar{u}}{\partial t\partial x} + \kappa_d\frac{\partial^2\eta}{\partial t^2} + \epsilon\frac{\partial}{\partial x}\left(\bar{u}\frac{\partial\bar{u}}{\partial x}\right) - \frac{\kappa^2}{3}\frac{\partial^4\bar{u}}{\partial t\partial x^3} + O(\epsilon^2) \tag{4.4.1.1}$$

To simplify this equation we use the leading order approximations of 4.2.3.8 and 4.2.4.12:

$$\begin{aligned}\frac{\partial\zeta}{\partial t} &= -\frac{\partial\bar{u}}{\partial x} + O(\epsilon)\\ \frac{\partial\zeta}{\partial x} &= -\frac{\partial\bar{u}}{\partial t} + O(\epsilon)\end{aligned} \tag{4.4.1.2}$$

As a consequence,

$$\begin{aligned}-\epsilon\frac{\partial^2(\zeta\bar{u})}{\partial x\partial t} &= -\epsilon\frac{\partial}{\partial t}\left(\zeta\frac{\partial\bar{u}}{\partial x} + \bar{u}\frac{\partial\zeta}{\partial x}\right)\\ &= -\epsilon\frac{\partial}{\partial t}\left(-\zeta\frac{\partial\zeta}{\partial t} - \bar{u}\frac{\partial\bar{u}}{\partial t} + O(\epsilon)\right)\\ &= \frac{\epsilon}{2}\left(\frac{\partial^2\zeta^2}{\partial t^2} + \frac{\partial\bar{u}^2}{\partial t^2}\right) + O(\epsilon^2)\end{aligned} \tag{4.4.1.3}$$

and:

$$-\frac{\kappa^2}{3}\frac{\partial^4\bar{u}}{\partial x^3\partial t} = \frac{\kappa^2}{3}\frac{\partial^4\zeta}{\partial x^4} + O(\epsilon^2) \tag{4.4.1.4}$$

Thus, equation 4.4.1.1 can be written:

$$\frac{\partial^2\zeta}{\partial t^2} - \frac{\partial^2\zeta}{\partial x^2} = \kappa_d\eta_{tt} + \frac{\epsilon}{2}\left(\frac{\partial^2\bar{u}^2}{\partial x^2} + \frac{\partial^2\bar{u}^2}{\partial t^2} + \frac{\partial^2\zeta^2}{\partial t^2}\right) + \frac{\kappa^2}{3}\frac{\partial^4\zeta}{\partial x^4} + O(\epsilon^2) \tag{4.4.1.5}$$

In equation 4.4.1.5, the interface $\eta(x)$ appears at order $O(\kappa_d) = O(\kappa^2)$. Since we expect this term to be responsible for the attenuation in ζ, we expect the typical distance of the mud induced damping to be $\kappa^2 x$.

Now let us expand the functions ζ and $\bar{u}$ as power series:

$$\begin{aligned}\zeta &= \zeta^{(0)} + \kappa^2\zeta^{(1)} + \kappa^4\zeta^{(2)} + ...\\ \bar{u} &= \bar{u}^{(0)} + \kappa^2\bar{u}^{(1)} + \kappa^4\bar{u}^{(2)} + ...\end{aligned} \tag{4.4.1.6}$$

Let us also introduce the slow coordinate X:

$$X = \kappa^2 x \tag{4.4.1.7}$$

Applying the technique of multiple scales, we have:

$$\begin{aligned} \frac{\partial}{\partial x} &= \frac{\partial}{\partial x} + \kappa^2 \frac{\partial}{\partial X} \\ \frac{\partial^4}{\partial x^4} &= \frac{\partial^4}{\partial x^4} + 4\kappa^2 \frac{\partial^4}{\partial x^3 \partial X} + O(\kappa^2) \end{aligned} \tag{4.4.1.8}$$

So the equation 4.4.1.1 becomes, with the multiple scale:

$$\begin{aligned} \frac{\partial^2 \zeta}{\partial t^2} - \frac{\partial^2 \zeta}{\partial x^2} - 2\kappa^2 \frac{\partial^2 \zeta}{\partial x \partial X} =& \kappa_d \frac{\partial^2 \eta}{\partial t^2} + \frac{\epsilon}{2}\left(\frac{\partial^2 \bar{u}^2}{\partial x^2} + \frac{\partial^2 \bar{u}^2}{\partial t^2} + \frac{\partial^2 \zeta^2}{\partial t^2}\right) \\ &+ \frac{\kappa^2}{3}\frac{\partial^4 \zeta}{\partial x^4} + O(\epsilon^2) \end{aligned} \tag{4.4.1.9}$$

which can be written:

$$\begin{aligned} \frac{\partial^2 \zeta}{\partial t^2} - \frac{\partial^2 \zeta}{\partial x^2} =& 2\kappa^2 \frac{\partial^2 \zeta}{\partial x \partial X} + \kappa_d \frac{\partial^2 \eta}{\partial t^2} + \frac{\epsilon}{2}\left(\frac{\partial^2 \bar{u}^2}{\partial x^2} + \frac{\partial^2 \bar{u}^2}{\partial t^2} + \frac{\partial^2 \zeta^2}{\partial t^2}\right) \\ &+ \frac{\kappa^2}{3}\frac{\partial^4 \zeta}{\partial x^4} + O(\epsilon^2) \end{aligned} \tag{4.4.1.10}$$

From this equation, we deduce for dominant orders:

- at order $O(1)$

$$\frac{\partial^2 \zeta^{(0)}}{\partial t^2} - \frac{\partial^2 \zeta^{(0)}}{\partial x^2} = 0 \tag{4.4.1.11}$$

- at order $O(\kappa^2)$

$$\frac{\partial^2 \zeta^{(1)}}{\partial t^2} - \frac{\partial^2 \zeta^{(1)}}{\partial x^2} = 2\frac{\partial^2 \zeta^{(0)}}{\partial x \partial X} + \frac{\kappa_d}{\kappa^2}\frac{\partial^2 \eta^{(0)}}{\partial t^2} + \frac{3\epsilon}{2\kappa^2}\frac{\partial^2 (\zeta^{(0)})^2}{\partial t^2} + \frac{1}{3}\frac{\partial^4 \zeta^{(0)}}{\partial x^4} \tag{4.4.1.12}$$

where equation 4.4.1.12 is obtained after using the following relation valid to leading order:

$$\frac{\partial^2 (\bar{u}^{(0)})^2}{\partial x^2} + \frac{\partial^2 (\bar{u}^{(0)})^2}{\partial t^2} + \frac{\partial^2 (\zeta^{(0)})^2}{\partial t^2} = 3\frac{\partial^2 (\zeta^{(0)})^2}{\partial t^2} \tag{4.4.1.13}$$

Let us compare these results with the ones we obtained in the case where nonlinearity was more important than dispersion (chapter 2). We first note that the

equations at order $O(\kappa^0)$ are the same in both cases: equations 2.5.1.11 and 4.4.1.11 are the same.

However, the first order, that is to say equations 2.5.1.12 and 4.4.1.12 differ. A new term appears in equation 4.4.1.12, namely $\frac{1}{3}\frac{\partial^4\zeta^{(0)}}{\partial x^4}$, which is due to dispersion. This term did not appear before because dispersion was less important compared to non-linearity.

Mud equations

Let us find the descriptive equations of the mud at order $O(\kappa^0)$.

From equation 4.3.5.19, we obtain:

$$\left(\alpha\frac{\partial^2}{\partial Z^2} - \frac{\partial}{\partial t}\right)U = \gamma\frac{\partial\zeta}{\partial x} + O(\epsilon), \quad 0 < Z < 1 + \epsilon\eta \tag{4.4.1.14}$$

where:

$$\boxed{\alpha = \frac{\epsilon}{\kappa_d Re} = O(1)} \tag{4.4.1.15}$$

As in water, we introduce the multiple scale coordinates x and $X = \kappa^2 x$, so that equation 4.4.1.14 becomes:

$$\left(\alpha\frac{\partial^2}{\partial Z^2} - \frac{\partial}{\partial t}\right)U = \gamma\frac{\partial\zeta}{\partial x} + O(\epsilon) \tag{4.4.1.16}$$

The continuity equation 4.3.2.1 becomes:

$$\frac{\partial U}{\partial x} + \frac{\partial V}{\partial Z} = O(\epsilon) \tag{4.4.1.17}$$

and the interface kinematic boundary condition 4.3.1.2:

$$\frac{\partial\eta}{\partial t} = V + O(\epsilon) \tag{4.4.1.18}$$

We can now deduce the dominant order of equations 4.4.1.16, 4.4.1.17 and 4.4.1.18 at $O(\kappa^0)$:

$$\begin{aligned}\left(\frac{\partial}{\partial t} - \alpha\frac{\partial^2}{\partial Z^2}\right)U^{(0)} &= -\gamma\frac{\partial\zeta^{(0)}}{\partial x}, \quad 0 < Z < 1\\ \frac{\partial U^{(0)}}{\partial x} + \frac{\partial V^{(0)}}{\partial Z} &= 0\\ \frac{\partial\eta^{(0)}}{\partial t} &= V^{(0)}, \qquad Z = 1\end{aligned} \tag{4.4.1.19}$$

4.4.2 Equation and solution at $O(\kappa^0)$

Water equations

Because equation 4.4.1.12 clearly involves non-linear terms, we consider the evolution of a train of harmonic waves:

$$\boxed{\zeta^{(0)} = \frac{1}{2}\sum_{m=-\infty}^{+\infty} A_m(X)e^{i\theta_m}} \quad \boxed{\eta^{(0)} = \frac{1}{2}\sum_{m=-\infty}^{+\infty} B_m(X)e^{i\theta_m}} \tag{4.4.2.1}$$

where $\theta_m = m(x-t)$. We shall assume that $A_0 = B_0 = 0$.

Mud equations

We adopt for the horizontal and vertical velocities in mud at the zeroth order the form we used in 4.4.2.1:

$$\begin{aligned} U^{(0)} &= \frac{1}{2}\sum_{m=-\infty}^{\infty} U_m^{(0)}(Z)e^{i\theta_m} \\ V^{(0)} &= \frac{1}{2}\sum_{m=-\infty}^{\infty} V_m^{(0)}(Z)e^{i\theta_m} \end{aligned} \tag{4.4.2.2}$$

Then from the equation 4.4.1.19 we deduce an equation for $U_m^{(0)}(Z)$:

$$\frac{d^2U_m^{(0)}}{dZ^2} - {\sigma_m}^2 U_m^{(0)} = -{\sigma_m}^2 \gamma A_m \tag{4.4.2.3}$$

where:

$$\boxed{{\sigma_m}^2 = -i\frac{m}{\alpha}} \tag{4.4.2.4}$$

We can solve exactly this second order differential equation by using the boundary conditions:

$$\begin{aligned} U_m^{(0)} &= 0, \qquad Z = 0 \\ \frac{\partial U_m^{(0)}}{\partial Z} &= 0, \qquad Z = 1 \end{aligned} \tag{4.4.2.5}$$

In the end we get:

$$U_m^{(0)} = \gamma A_m[1 - \cosh(\sigma_m Z) + \tanh(\sigma_m)\sinh(\sigma_m Z)] \tag{4.4.2.6}$$

From the continuity equation and the boundary conditions of 4.4.1.19 we can extract the following equations for the vertical velocity:

$$\begin{aligned} \frac{dV_m^{(0)}}{dZ} &= -imU_m^{(0)} \\ V_m^{(0)} &= 0, \quad Z = 0 \end{aligned} \tag{4.4.2.7}$$

As a consequence, we can easily deduce the explicit expression of the $V_m^{(0)}$:

$$V_m^{(0)} = -i\frac{m\gamma A_m}{\sigma_m}[\sigma_m Z - \sinh(\sigma_m Z) + \tanh(\sigma_m)(\cosh(\sigma_m Z) - 1)] \tag{4.4.2.8}$$

From the kinematic boundary condition at the interface in mud, we can now deduce the interface motion:

$$\begin{aligned} B_m &= -\frac{1}{im}V_m^{(0)}(Z = 1) \\ &= \gamma A_m G(\sigma_m) \end{aligned} \tag{4.4.2.9}$$

with

$$\boxed{G(\sigma_m) = 1 - \frac{\tanh(\sigma_m)}{\sigma_m}} \tag{4.4.2.10}$$

As a conclusion we have:

$$\boxed{B_m = \gamma A_m \left(1 - \frac{\tanh(\sigma_m)}{\sigma_m}\right)} \tag{4.4.2.11}$$

where ${\sigma_m}^2 = -i\frac{m}{\alpha}$, $\alpha = \frac{\epsilon}{\kappa_d Re}$ and $\gamma = \frac{\rho_W}{\rho_M}$.

4.4.3 Equation and solution at $O(\epsilon)$

At this order, we will only study water equations.

At order $O(\epsilon)$, we have from 4.4.1.12:

$$\frac{\partial^2\zeta^{(1)}}{\partial t^2} - \frac{\partial^2\zeta^{(1)}}{\partial x^2} = 2\frac{\partial^2\zeta^{(0)}}{\partial x \partial X} + \frac{\kappa_d}{\kappa^2}\frac{\partial^2\eta^{(0)}}{\partial t^2} + \frac{3\epsilon}{2\kappa^2}\frac{\partial^2(\zeta^{(0)})^2}{\partial t^2} + \frac{1}{3}\frac{\partial^4\zeta^{(0)}}{\partial x^4} \tag{4.4.3.1}$$

By following the same procedure as in [6], we know that:

$$\frac{3\epsilon}{2\kappa^2}\frac{\partial^2(\zeta^{(0)})^2}{\partial t^2} = \frac{\epsilon}{\kappa^2}\sum_{m=1}^{\infty} -\frac{3}{8}m^2 e^{i\theta_m}\left[\sum_{l=1}^{\infty} 2A_l^* A_{m+l} + \sum_{l=1}^{[m/2]} \alpha_l A_l A_{m-l}\right] + c.c. \tag{4.4.3.2}$$

where $[m/2]$ is the integer part of $m/2$ and α_l is a coefficient equal to 1 for $l = [m/2]$

and equal to 2 otherwise. We also have

$$\begin{aligned} 2\frac{\partial^2\zeta^{(0)}}{\partial x\partial X} &= \sum_{m=1}^{\infty} im\frac{dA_m}{dX}e^{i\theta_m} + c.c. \\ \frac{\partial^2\eta^{(0)}}{\partial t^2} &= -\frac{1}{2}\sum_{m=1}^{\infty} m^2 B_m e^{i\theta_m} + c.c. \end{aligned} \tag{4.4.3.3}$$

combining all this results, we can rewrite the equation 4.4.3.1:

$$\begin{aligned} \frac{\partial^2\zeta^{(1)}}{\partial t^2} - \frac{\partial^2\zeta^{(1)}}{\partial x^2} = \sum_{m=1}^{\infty} im\frac{dA_m}{dX}e^{i\theta_m} + \frac{\epsilon}{\kappa^2}\sum_{m=1}^{\infty} -\frac{3}{8}m^2 e^{i\theta_m}\left[\sum_{l=1}^{\infty} 2A_l^* A_{m+l} + \sum_{l=1}^{[m/2]}\alpha_l A_l A_{m-l}\right] \\ -\frac{1}{2}\frac{\kappa_d}{\kappa^2}\sum_{m=1}^{\infty} m^2 B_m e^{i\theta_m} + \frac{1}{6}\sum_{m=1}^{\infty} m^4 A_m e^{i\theta_m} + c.c. \end{aligned} \tag{4.4.3.4}$$

To ensure solvability of this last equation, we know that secular terms proportional to $e^{i\theta_m}$ must be removed. This is how we get the differential equations:

$$\forall m,\ \frac{dA_m}{dX} = -\frac{im}{2}\frac{\kappa_d}{\kappa^2}B_m + \frac{im^3}{6}A_m - \frac{3i}{8}\frac{\epsilon}{\kappa}m\left[\sum_{l=1}^{\infty} 2A_l^* A_{m+1l} + \sum_{l=1}^{[m/2]}\alpha_l A_l A_{m-l}\right] \tag{4.4.3.5}$$

Combining this result with 4.4.2.11, we finally obtain the differential equation for the A_m: $\forall m$,

$$\begin{aligned} \frac{dA_m}{dX} = -\frac{i\gamma m}{2}\frac{\kappa_d}{\kappa^2}\left(1 - \frac{\tanh(\sigma_m)}{\sigma_m}\right)A_m + \frac{im^3}{6}A_m \\ -\frac{3i}{8}\frac{\epsilon}{\kappa^2}m\left[\sum_{l=1}^{\infty} 2A_l^* A_{m+l} + \sum_{l=1}^{[m/2]}\alpha_l A_l A_{m-l}\right] \end{aligned} \tag{4.4.3.6}$$

Let us compare this equation to what we found in the case where non-linearity was more important than dispersion (chapter 2). We observe that equations 2.5.3.6 and 4.4.3.6 only differ by one term, which is due to dispersion, namely $\frac{im^3}{6}A_m$.

As we already pointed out, this term did not appear before because dispersion was less important compared to non-linearity.

4.5 Further details

4.5.1 Surface and the interface

We truncate the series 4.4.3.6 , in order to obtain a differential equation for the A_m:

$$\begin{aligned}\frac{dA_m}{dX} + \frac{i\gamma}{2}\frac{\kappa_d}{\kappa^2}m\left(1-\frac{\tanh(\sigma_m)}{\sigma_m}\right)A_m - \frac{im^3}{6}A_m \\ + \frac{3i}{8}\frac{\epsilon}{\kappa^2}m\left(\sum_{l=1}^{n-m}2A_l^*A_{m+l} + \sum_{l=1}^{[m/2]}\alpha_l A_l A_{m-l}\right) = 0\end{aligned} \tag{4.5.1.1}$$

This truncated differential system is true for $0 < m \leq n$.

4.5.2 Energy variation in water

We obtained the differential equation:

$$\begin{aligned}\frac{dA_m}{dX} - \frac{im^3}{6}A_m + \frac{3i}{8}\frac{\epsilon}{\kappa^2}m\left(\sum_{l=1}^{\infty}2A_l^*A_{m+l} + \sum_{l=1}^{[m/2]}\alpha_l A_l A_{m-l}\right) \\ + \frac{i\gamma}{2}\frac{\kappa_d}{\kappa^2}m\left(1-\frac{\tanh(\sigma_m)}{\sigma_m}\right)A_m = 0\end{aligned} \tag{4.5.2.1}$$

to describe the free surface motion.

The last term of this equation represents the damping due to dissipation in the Newtonian mud.

In [8], G. Grataloup and C.C. Mei demonstrated that if the differential equation describing the free surface is:

$$\frac{dA_m}{dX} + \beta_m A_m - \frac{im^3}{6}A_m + \frac{3i}{8}\frac{\epsilon}{\kappa^2}m\left(\sum_{l=1}^{\infty}2A_l^*A_{m+l} + \sum_{l=1}^{[m/2]}\alpha_l A_l A_{m-l}\right) = 0, \tag{4.5.2.2}$$

then the general relation on the first-order wave-energy is:

$$\frac{d}{dX}\left[\sum_{m=1}^{n}|A_m|^2\right] = -2\sum_{m=1}^{n}Re(\beta_m)|A_m|^2 \tag{4.5.2.3}$$

Indeed, in equation 4.5.2.2, β_m represents a dissipation source. That is why the total wave energy at the leading order decreases with relation to β_m.

In our case of a flat bottom with a thin layer of Newtonian mud, we deduce that

the general relation on the first-order wave energy is:

$$\boxed{\frac{d}{dX}\left[\sum_{m=1}^{n}|A_m|^2\right] = -\gamma\frac{\kappa_d}{\kappa^2}\sum_{m=1}^{n} Re\left[im\left(1-\frac{\tanh(\sigma_m)}{\sigma_m}\right)\right]|A_m|^2} \qquad (4.5.2.4)$$

4.6 Numerical results by using the first ten harmonics

We now represent the numerical results in order to analyze the effect of the different parameters.

We will first study the effect of the wave amplitude A, knowing that a big wave amplitude implies high non-linearity ϵ (cases 1a, 1b and 1c).

We will then look at the effects of different wavenumbers k, and thus of different dispersion coefficient κ (cases 2a, 2b and 2c).

Finally, we will look at the effects of different mud layer depths d, and thus different values of the parameter κ_d (cases 3a, 3b and 3c).

From the experiments on mud that we already cited in the previous chapter, we know that viscosity in mud varies with the frequency. However, since we are here considering the mud as Newtonian, we need to choose one value of viscosity for all frequencies.

The waves that we study in this thesis have a frequency of around $\omega' = 0.5$rad/s, which correspond to a period $T = 12s$. This is why we choose to adopt the modulus of the Gulf of Mexico mud complex viscosity at $\omega' = 0.5$rad/s as the viscosity. This value is: $\underline{\mu = 400\text{Pa.s}}$, as can be read in figure 3-3. We naturally choose the density to be the density of this same mud: $\underline{\rho_M = 1140kg/m^3}$, and as a consequence $\underline{\gamma = 0.88}$

For all of the following computations, we set the water depth to be $\underline{\bar{h} = 5m}$.

4.6.1 Influence of non-linearity

We set the wave period to be $T = 18s$ (which means $\omega' = 1/3rad/s$), and the mud layer depth to be $d = 25$cm. We then consider 3 possible wave amplitudes $A = 20cm$, $A = 40cm$ and $A = 60cm$, corresponding to cases 1a, 1b and 1c. From here we can deduce the value of κ and Re by:

$$\kappa = k\bar{h} = \frac{\omega'}{\sqrt{g\bar{h}}}\bar{h} = \omega'\sqrt{\frac{\bar{h}}{g}} \qquad (4.6.1.1)$$

Case	ϵ	κ	Re	κ_d	$\alpha = \frac{\epsilon}{\kappa_d Re}$
1a	0.04	0.24	0.05	0.05	17
1b	0.08	0.24	0.09	0.05	17
1c	0.12	0.24	0.14	0.05	17

Table 4.2: Values of Re, κ, ϵ, κ_d and α corresponding to different values of A. Case 1c corresponds to the biggest A, that is to say the biggest non-linearity.

and:

$$Re = \frac{\rho_M A dk\sqrt{g\bar{h}}}{\mu} = \frac{\rho_M A d\omega'}{\mu} \tag{4.6.1.2}$$

Table 4.2 sums up the corresponding values of the parameters ϵ, κ, Re, κ_d and α.

ϵ and Re both increase with A and κ does not depend on A. Case 1a corresponds to the smallest A (and thus smallest non-linearity) value and case 1c to the biggest one.

We assume the initial condition:

$$t = 0, \quad A_1(0) = 1 \tag{4.6.1.3}$$

Surface and interface

Figures 4-1 and 4-2 show the evolution of the first three harmonics of the surface and the interface. Even though we carried the resolution with 10 harmonics in order to take into account all the significant ones, we chose to only display the three most significant harmonics for clarity.

In figure 4-1, we observe that the harmonics are smoother in the less non-linear case (1a). Variations are more significant in the most non-linear case. This effect is due to non-linearity, and is logical. Even though non-linearity is very important in every case, it is even more obvious in case 1c.

Figure 4-1 also shows that the first harmonic $|A_1|$ is more quickly damped out in the most non-linear case (1c). This is because non-linearity results in a transfer from the first harmonics to the second harmonics.

From figure 4-2 we observe that the interface follows the same tendency as the free surface: non-linearity results in more oscillations and a fastest damping of the first harmonic.

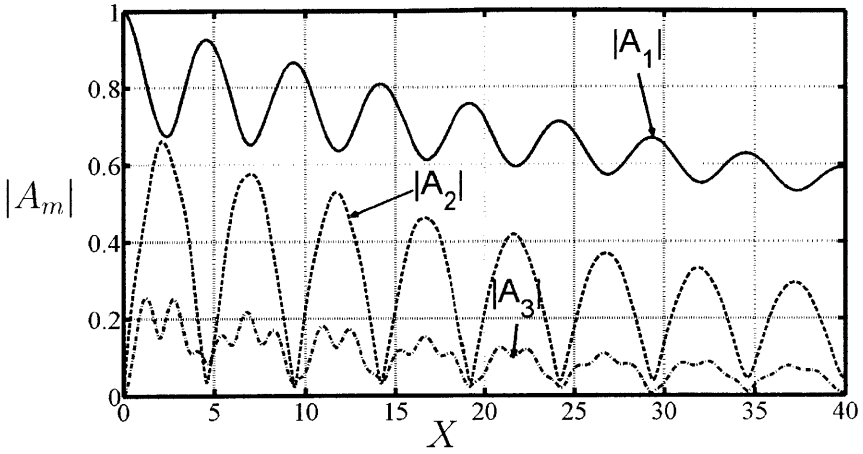

(a) Smallest non-linearity (1a)

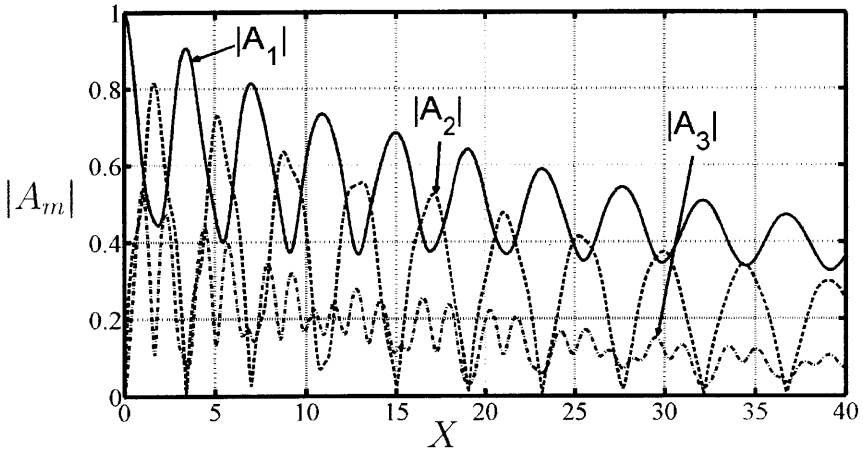

(b) Medium non-linearity (1b)

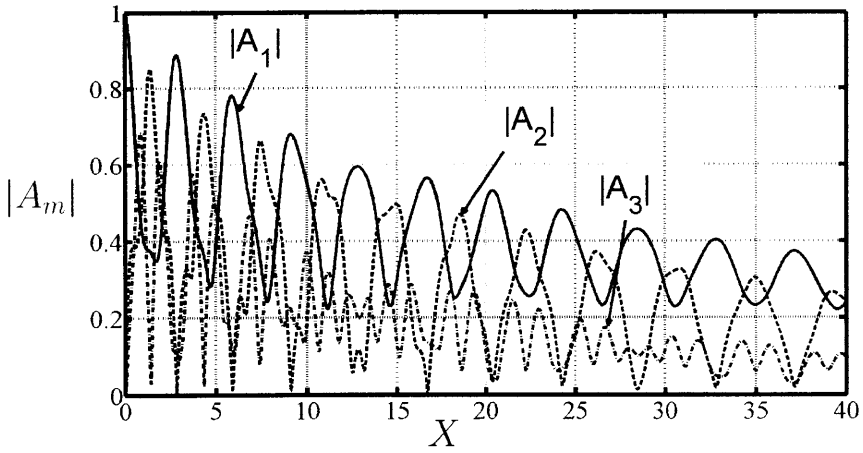

(c) Highest non-linearity (1c)

Figure 4-1: Effects of wave amplitude on the evolution of the first 3 harmonics of the free surface over a thick muddy seabed. Comparison between the cases 1a, 1b and 1c.

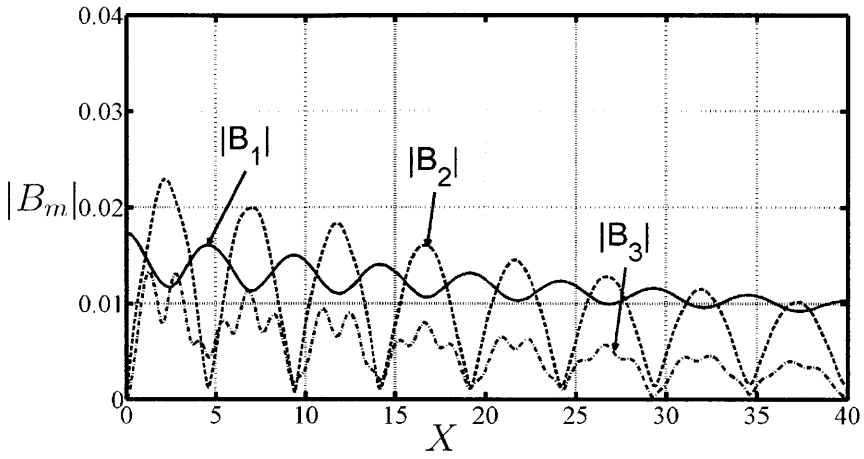

(a) Smallest non-linearity (1a)

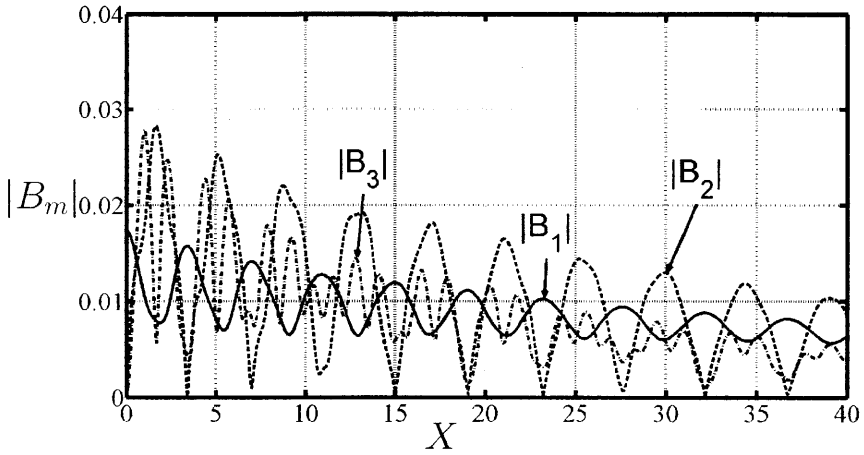

(b) Medium non-linearity (1b)

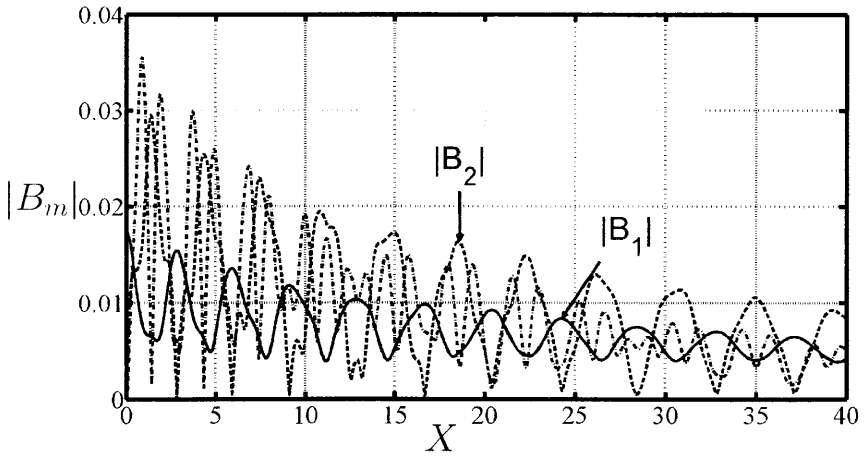

(c) Highest non-linearity (1c)

Figure 4-2: Effects of wave amplitude on the evolution of the first 3 harmonics of the interface between mud and water over a thick muddy seabed. Comparison between the cases 1a, 1b and 1c.

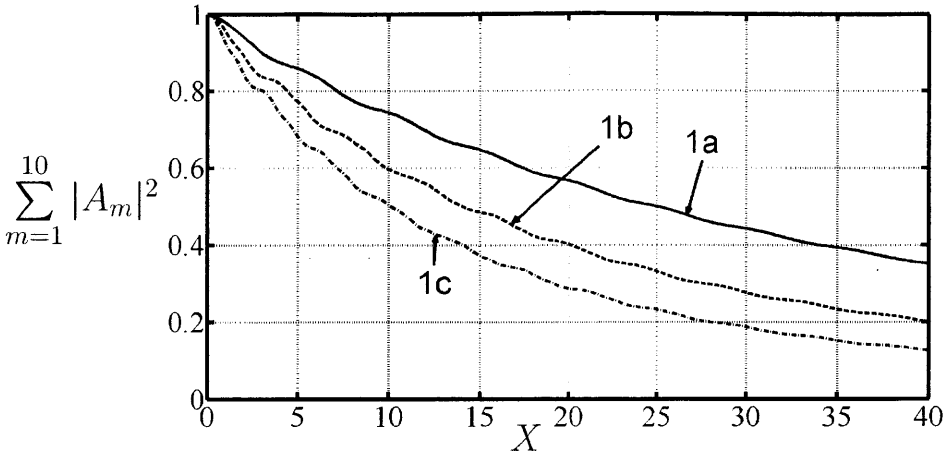

Figure 4-3: Wave energy over a flat thick muddy seabed. Comparison between the cases 1a, 1b and 1c.

Energy variation

We numerically represented the total first-order energies for cases 1a, 1b and 1c in figures 2-6. This figure shows that the total energy logically decreases, because it is dissipated in the viscous mud.

However, contrary to what we saw in chapter 2, the decrease in energy is very slow. For cases 1a, 1b and 1c, energy only decreases by around 50% between $X = 0$ and $X = 40$.This is simply due to the fact that we are considering a very thin layer of mud, since $O(\kappa_d) = O(\kappa^2)$ in this chapter. It is as a consequence logical for the mud-induced damping to be less important than in the case $O(\kappa_d) = O(\kappa)$.

In figure 4-4, we represented the variation of total energy. The dashed line represents the right-hand side term of equation 4-4. It is so close to the solid line that it is very hard to distinguish. As a consequence, this figure shows that our numerical results obey the law we demonstrated

4.6.2 Influence of dispersion κ

We now aim to study the influence of dispersion.

We set the wave amplitude to be $A = 40cm$ and the mud layer depth to be $d = 25$cm. We then consider 2 possible periods $T = 18s$ and $T = 12s$ (which mean $\omega' = 1/3rad/s$, $\omega' = 1/2rad/s$), corresponding respectively to cases 2a and 2b. We still have $\bar{h} = 5m$.

Table 4.3 sums up the corresponding values of the parameters ϵ, κ, Re, κ_d and α.

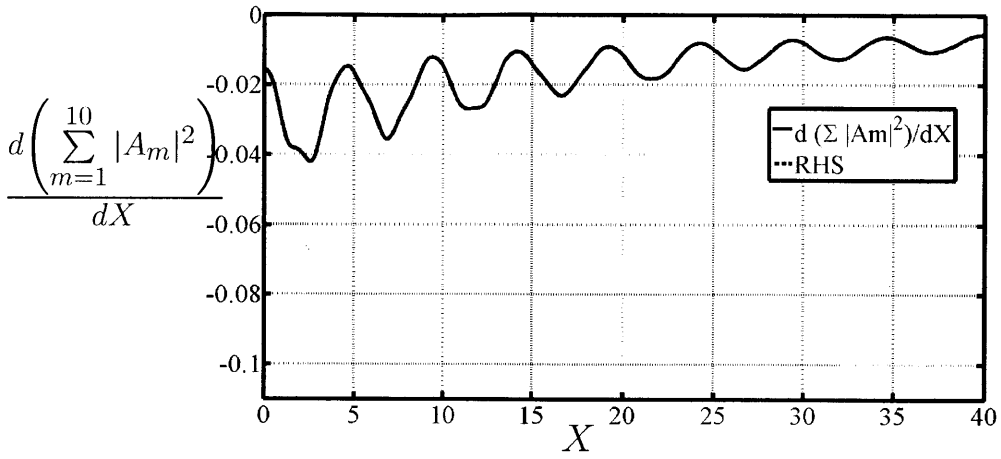

(a) Smallest non-linearity (1a)

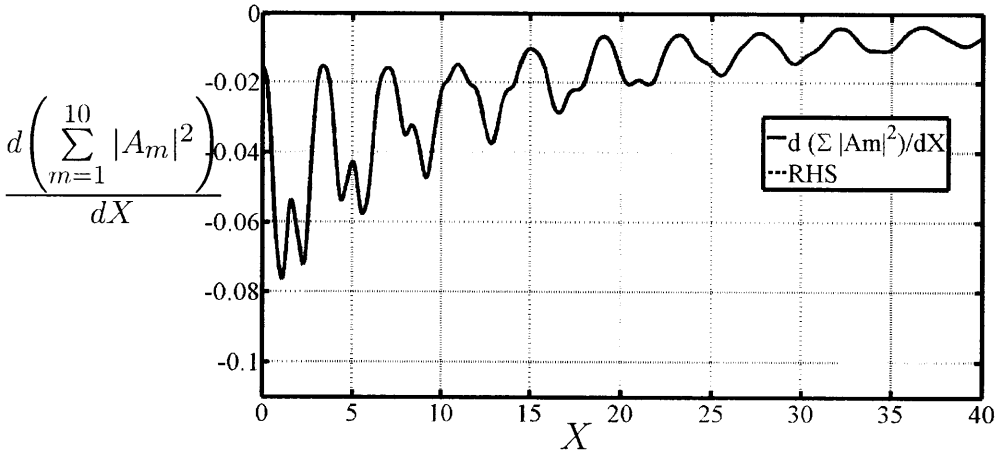

(b) Medium non-linearity (1b)

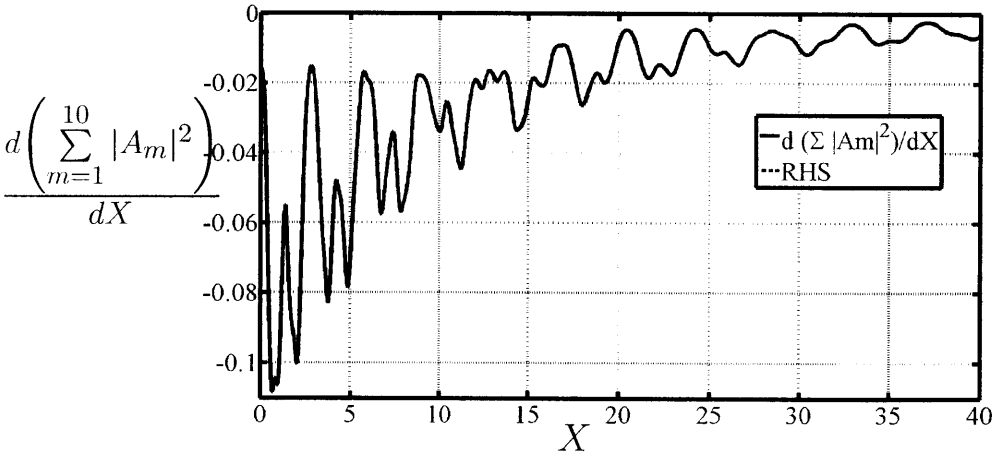

(c) Highest non-linearity (1c)

Figure 4-4: Variation of the wave energy over a flat thick muddy seabed. RHS is the value of the right-hand side term in equation . Comparison between the cases 1a, 1b and 1c.

Case	ϵ	κ	Re	κ_d	$\alpha = \frac{\epsilon}{\kappa_d Re}$
2a	0.08	0.24	0.09	0.05	17
2b	0.08	0.36	0.14	0.05	11.4

Table 4.3: Values of Re, κ, ϵ, κ_d and α corresponding to different values of dispersion κ

Free surface and interface

Figures 4-5 and 4-6 show the evolution of the first three harmonics of the surface and the interface. Even though we carried the resolution with 10 harmonics in order to take into account all the significant ones, we chose to only display the three most significant harmonics for clarity.

In figure 4-5, we observe mud-induced damping is faster in the less dispersive case (2a).

From figure 4-6 we observe one again that the interface follows the same tendency as the free surface.

Energy variation

We numerically represented the total first-order energies for cases 2a and 2b in figure 2-11. This figure shows that the total energy logically decreases, because it is dissipated in the viscous mud. As for surface harmonics, we observe that damping is very slow compared to chapter 2. Damping is even slower in the most dispersive case.

In figure 4-8, we represented the variation of total energy. The dashed line represents the right-hand side term of equation 4-4, and the figure shows that our numerical results obey the law we demonstrated. Indeed, the two lines are so close that they are very hard to distinguish.

4.6.3 Influence of mud layer depth d

We now aim at srudying the influence of the mud layer depth.

We set the wave period to be $T = 18s$ (which means $\omega' = 1/3rad/s$), and the wave amplitude to be $A = 40cm$. We then consider 3 possible mud layer depth $d = 12cm$, $d = 25cm$ and $d = 50cm$, corresponding respectively to cases 3a, 3b and 3c. We still have $\bar{h} = 5m$.

Table 4.4 sums up the corresponding values of the parameters ϵ, κ, Re, κ_d and α.

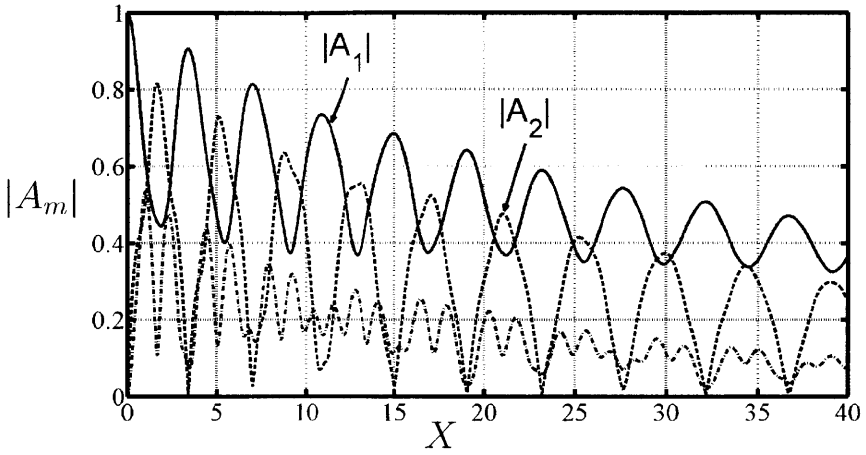

(a) Smallest dispersion (2a)

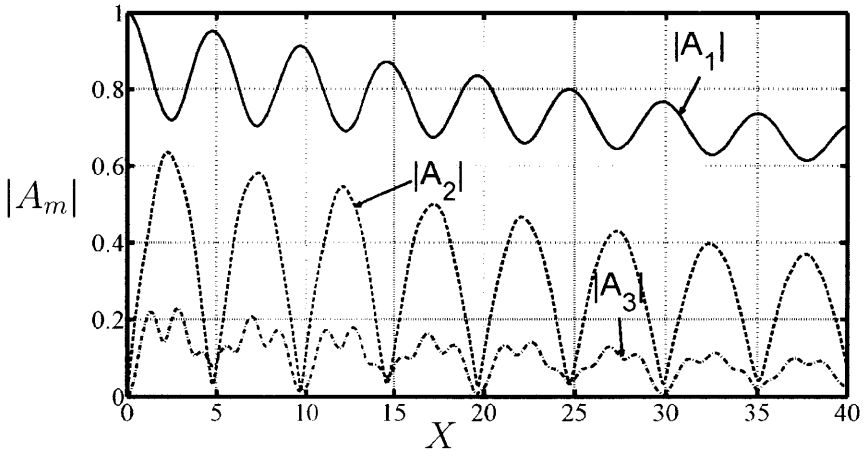

(b) Medium dispersion (2b)

Figure 4-5: Effects of wave amplitude on the evolution of the first 3 harmonics of the free surface over a thick muddy seabed. Comparison between the cases 2a and 2b.

Case	ϵ	κ	Re	κ_d	$\alpha = \frac{\epsilon}{\kappa_d Re}$
3a	0.08	0.24	0.045	0.025	71
3b	0.08	0.24	0.09	0.05	17
3c	0.08	0.24	0.19	0.1	4.2

Table 4.4: Values of Re, κ, ϵ, κ_d and α corresponding to different values of the mud depth d

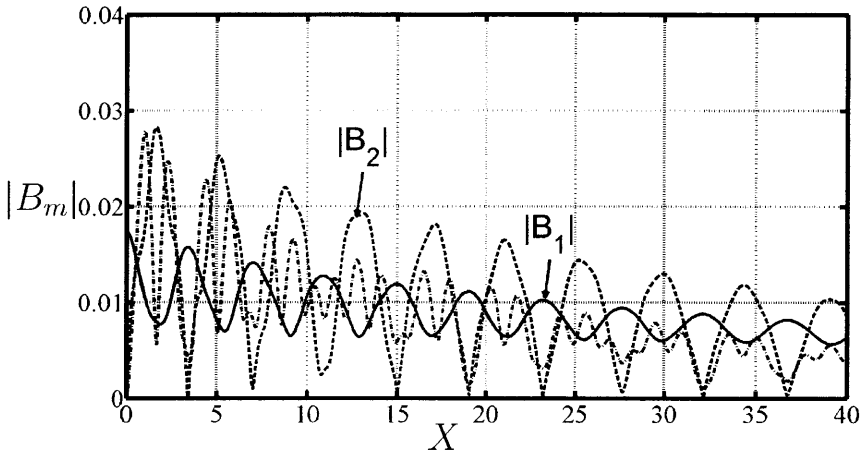

(a) Smallest dispersion (2a)

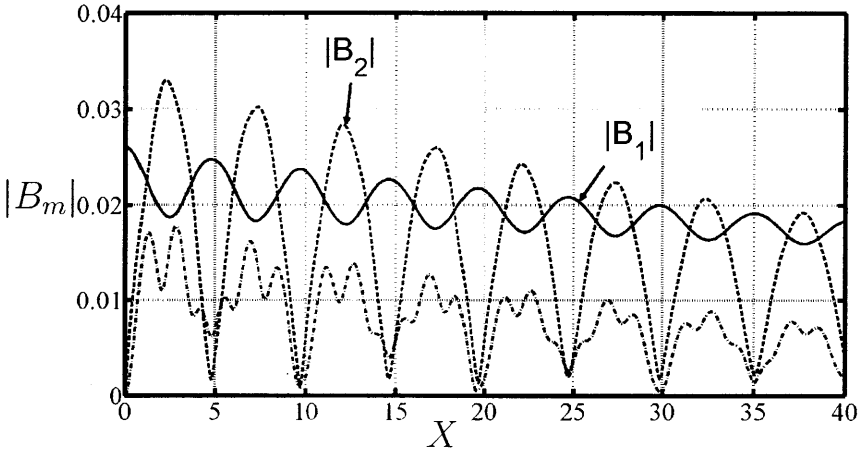

(b) Medium dispersion (2b)

Figure 4-6: Effects of wave amplitude on the evolution of the first 3 harmonics of the interface between mud and water over a thick muddy seabed. Comparison between the cases 2a and 2b.

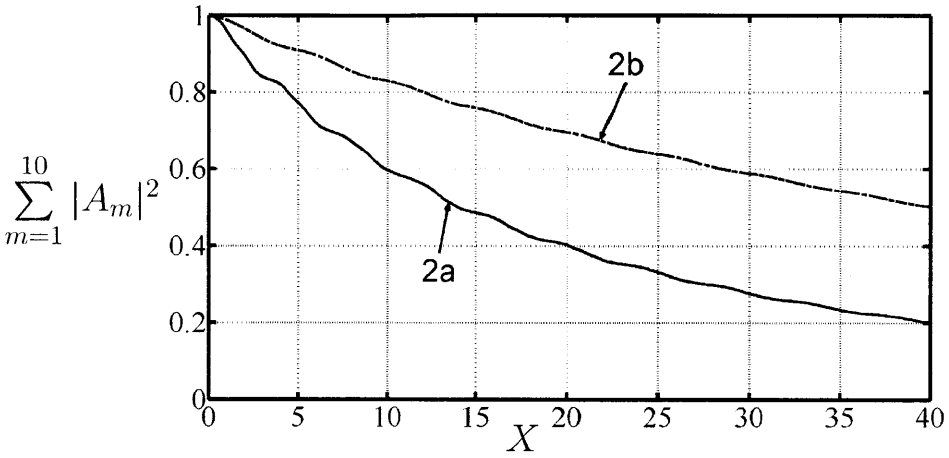

Figure 4-7: Wave energy over a flat thick muddy seabed. Comparison between the cases 2a and 2b.

Free surface and interface

Figures 4-9 and 4-10 show the evolution of the first three harmonics of the surface and the interface for different mud layer thickness d. Even though we carried the resolution with 10 harmonics in order to take into account all the significant ones, we chose to only display the three most significant harmonics for clarity.

As expected, we observe in figure 4-9 that damping is more significant in the case of the highest mud thickness (3c) than in the case of a very thin mud layer (3a). This is due to the fact that dissipation happens in mud. As a consequence, the thicker the mud layer and the more wave damping.

We also observe in figure 4-10 that the interface variations reach a higher amplitude in the case of the thicker mud (3c).

As the consequence, the influence of d on the interface and free surface is the same as in the case $O(\kappa_d) = O(\kappa)$ described in chapter 2.

Energy variation

We numerically represented the total first-order energies for cases 3a, 3b and 3c in figure 4-11. This figure shows that the total energy logically decreases, because it is dissipated in the viscous mud. We can see that energy is dissipated faster in the case of the thicker mud (3c). This result seems logical since, as we said when we studied the surface amplitude, the thicker the mud and the faster the wave damping.

In figure 4-12, we represented the variation of total energy. The dashed line still represents the right-hand side term of equation 2.6.3.4, and the figure shows that our

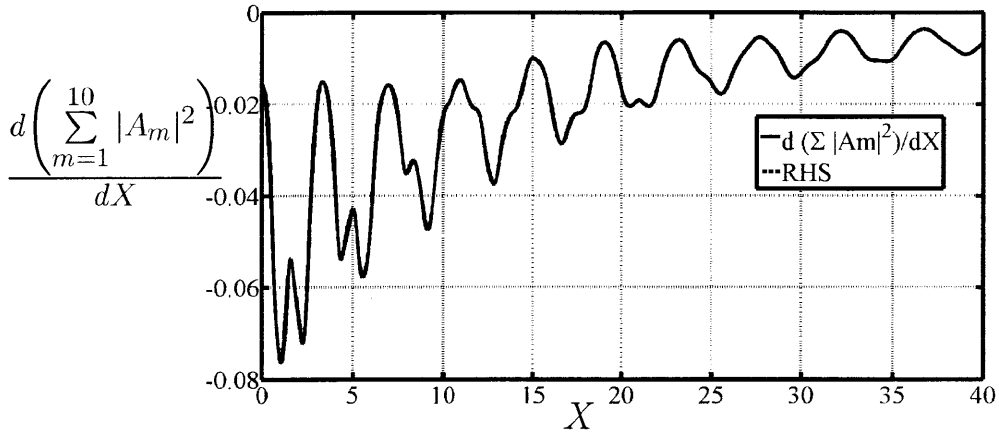

(a) Smallest dispersion (2a)

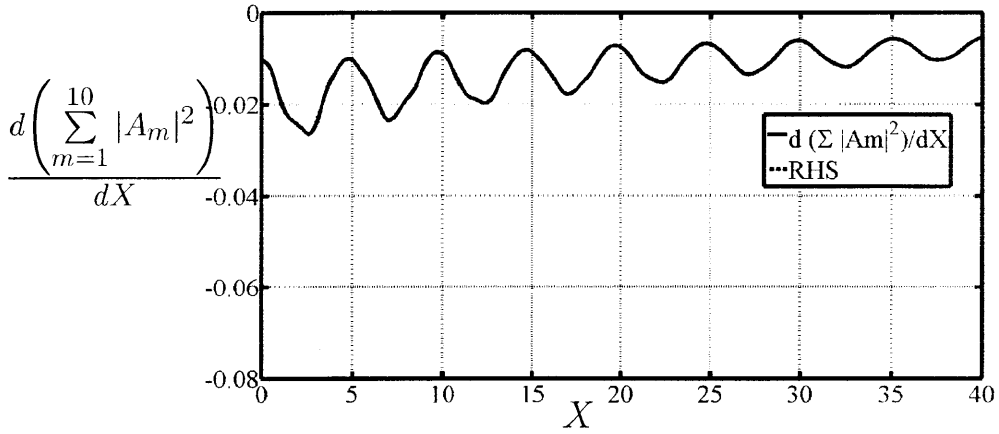

(b) Medium dispersion (2b)

Figure 4-8: Variation of the wave energy over a flat thick muddy seabed. RHS is the value of the right-hand side term in equation . Comparison between the cases 2a and 2b.

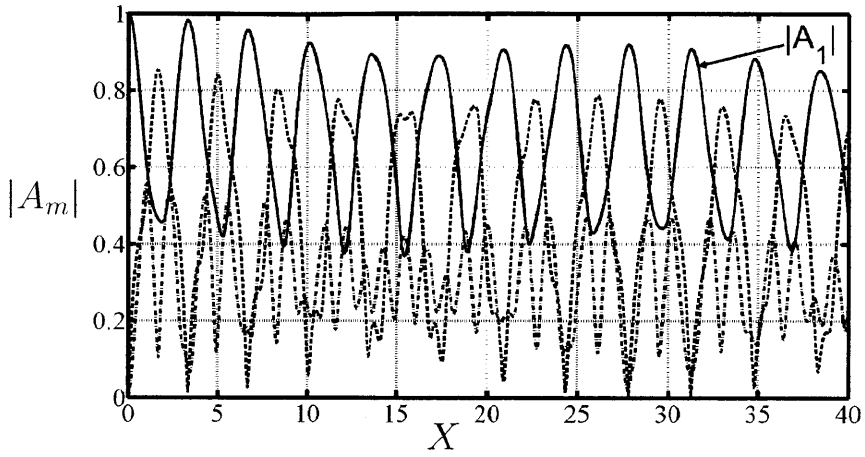

(a) Smallest mud layer thickness (3a)

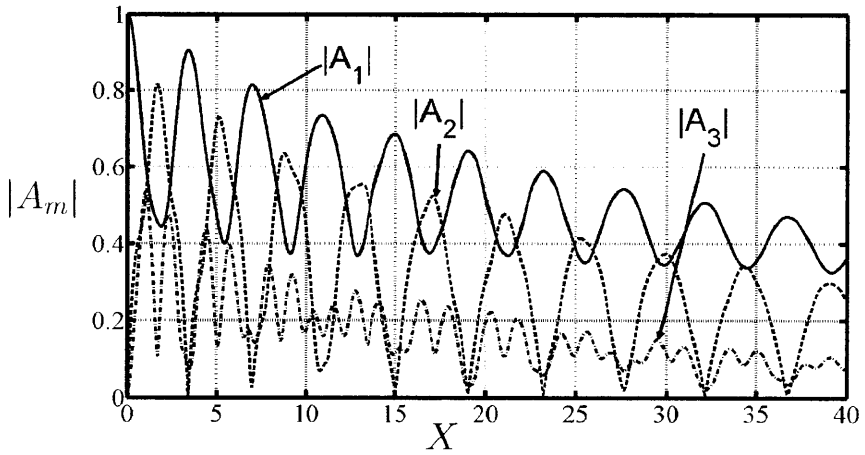

(b) Medium mud layer thickness (3b)

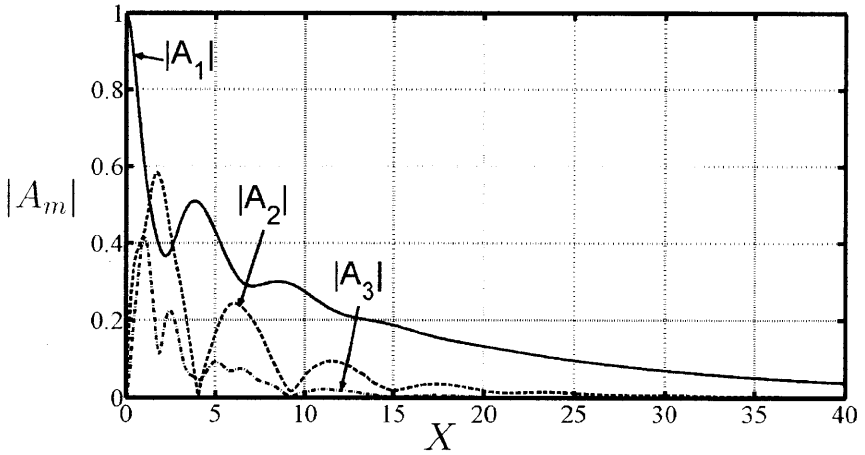

(c) Highest mud layer thickness (3c)

Figure 4-9: Effects of mud layer thickness on the evolution of the first 3 harmonics of the free surface over a thick muddy seabed. Comparison between the cases 3a, 3b and 3c.

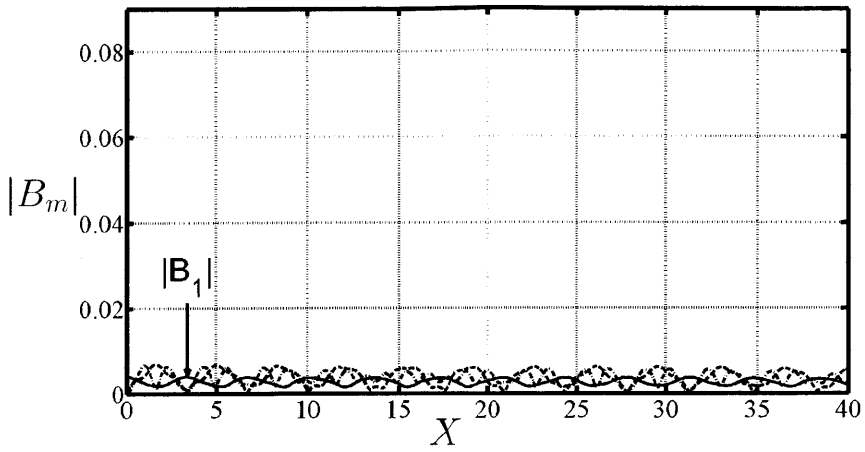

(a) Smallest mud layer thickness (3a)

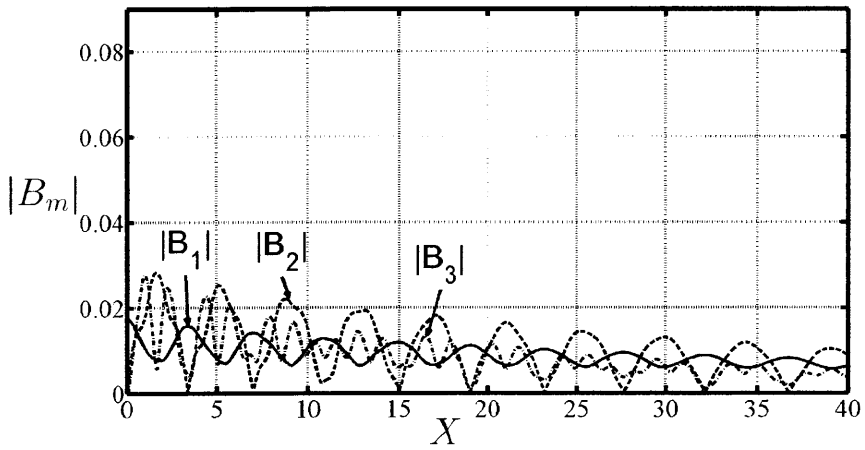

(b) Medium mud layer thickness (3b)

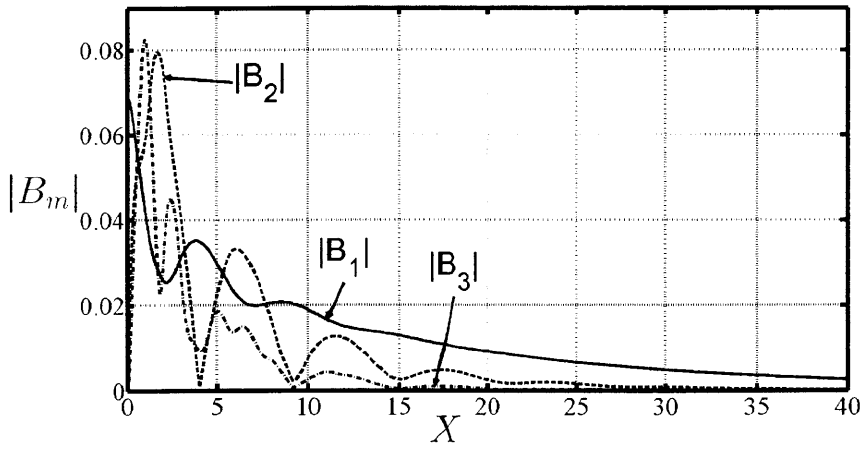

(c) Highest mud layer thickness (3c)

Figure 4-10: Effects of mud layer thickness on the evolution of the first 3 harmonics of the interface between mud and water over a thick muddy seabed. Comparison between the cases 3a, 3b and 3c.

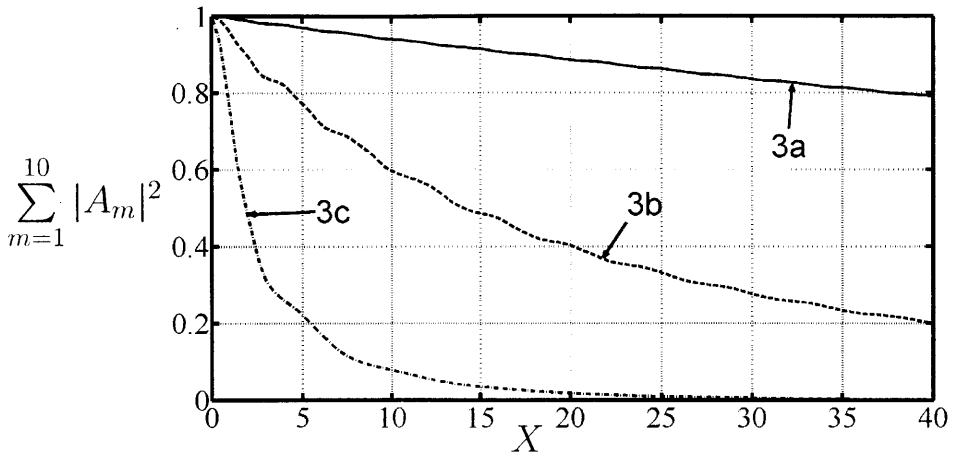

Figure 4-11: Wave energy over a flat thick muddy seabed. Comparison between the cases 3a, 3b and 3c.

numerical results obey the law we demonstrated. Indeed, and as always before, the two lines are so close that they are very hard to distinguish.

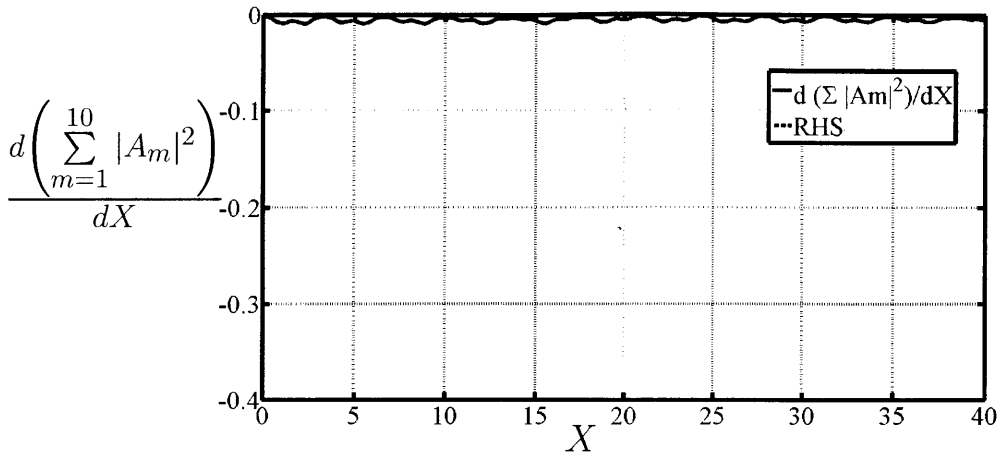

(a) Smallest mud layer thickness (3a)

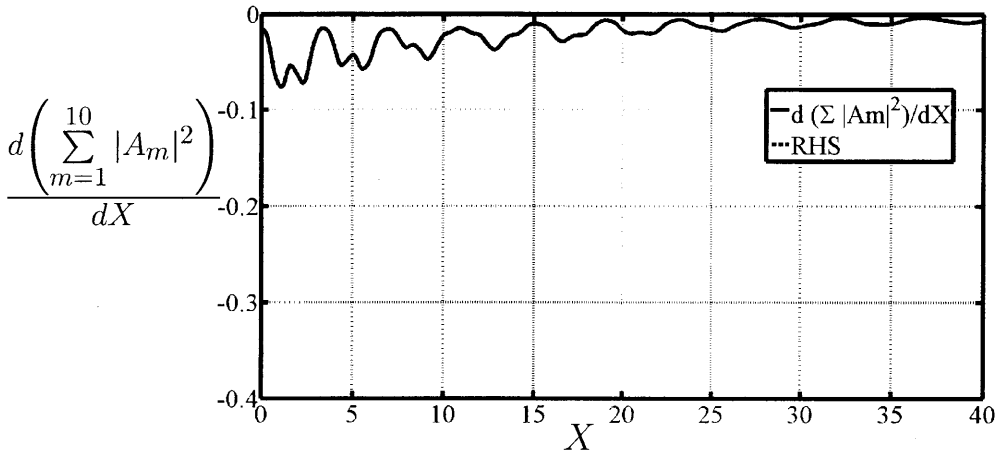

(b) Medium mud layer thickness (3b)

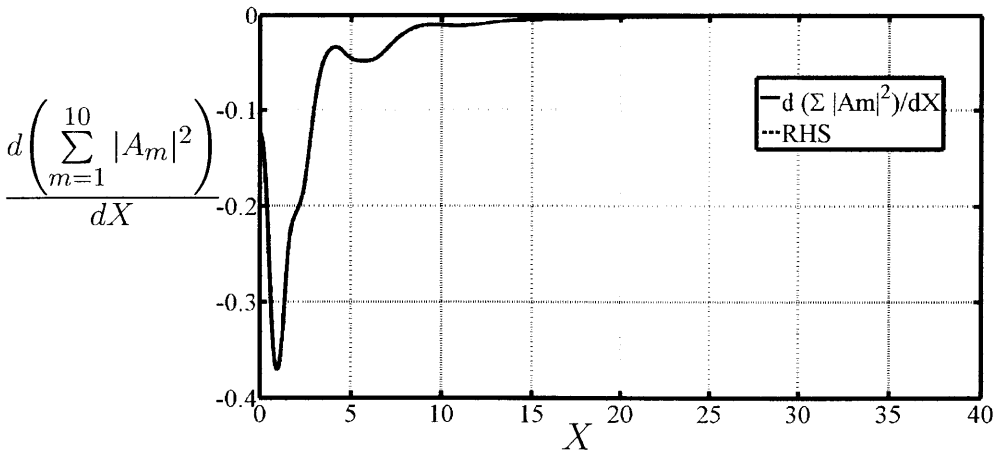

(c) Highest mud layer thickness (3c)

Figure 4-12: Variation of the wave energy over a flat thick muddy seabed. RHS is the value of the right-hand side term in equation 2.6.3.4. Comparison between the cases 3a, 3b and 3c.

Chapter 5

Horizontal bottom, very shallow viscoelastic mud

As in the previous chapter, we assume that non-linearity effects are less important than dispersion ($O(\epsilon) = O(\kappa^2)$). However, mud is not modeled as a Newtonian fluid anymore, but as viscoelastic.

As we did in chapter 3, we need to change the horizontal momentum equation in mud. We will demonstrate again that this modification only affects the σ coefficient in the equations.

5.1 Scaling

The equations we previously obtained in water are clearly not changed in the viscoelastic case, that is why we keep the scaling in water:

$$\begin{array}{lll} x = kx' & z = \frac{z'}{h}b & t = k(g\bar{h})^{1/2}t' \\ p = \frac{p'}{\rho_W g A} & u = \frac{1}{\epsilon\sqrt{g\bar{h}}}u' & v = \frac{\kappa}{\epsilon\sqrt{g\bar{h}}}v' \\ \zeta = \frac{\zeta'}{A} & \phi = \phi' \left[\frac{A}{k\bar{h}}(g\bar{h})^{1/2}\right]^{-1} & \end{array} \tag{5.1.0.1}$$

However, we need to modify the scaling for stress in mud. As in chapter 3, we choose :

$$\tau_{ij} = \frac{d}{\epsilon\mu_s\sqrt{g\bar{h}}}\tau'_{ij} \tag{5.1.0.2}$$

with μ defined as:

$$\mu = \frac{\mu'}{\mu_s} \tag{5.1.0.3}$$

Because of calculation simplifications, we will see that the value μ_s is not needed

to solve the last equations numerically. Indeed, we will see that neither μ_s neither non-dimensional viscosity μ will be needed to carry the final calculations, but only the dimensional viscosity μ'.

As a consequence, the scaling in mud for this chapter is:

$$\begin{array}{lll} x = kx' & Z = \frac{Z'}{d} & t = k(g\bar{h})^{1/2}t' \\ P = \frac{P'}{\rho_W g A} & U = \frac{1}{\epsilon\sqrt{g\bar{h}}}U' & V = \frac{1}{\epsilon\kappa\kappa_d\sqrt{g\bar{h}}}V' \\ \eta = \frac{\eta'}{\kappa_d A} & \mathcal{U} = \frac{k}{\epsilon}\mathcal{U}' & \mathcal{V} = \frac{k}{\epsilon\kappa\kappa_d}\mathcal{V}' \\ T_{ij} = \frac{T'_{ij}}{\rho_W g A} & E_{ij,t} = \frac{d}{\epsilon\sqrt{g\bar{h}}}E'_{ij,t'} & \tau_{ij} = \frac{d}{\epsilon\mu_s\sqrt{g\bar{h}}}\tau'_{ij} \end{array} \tag{5.1.0.4}$$

5.2 Equations in water

Since only the mud behavior is modified, the equations in water are the same as with a Newtonian type of mud: they remain exactly the same as in the previous chapter.

5.3 Equations in mud

Most of the equations in mud are also unchanged compared to the previous chapter. Namely equations 4.3.1.2, 4.3.2.1, 4.3.5.11, 4.3.5.18 and 4.3.6.1 remain the same:

The kinematic interface boundary condition:

$$\eta_t = V + O(\kappa^2), \quad Z = 1 + \epsilon\eta \tag{5.3.0.5}$$

The conservation of mass:

$$U_x + V_Z = 0, \quad 0 < Z < 1 + \epsilon\eta \tag{5.3.0.6}$$

The tangential stress boundary condition at the interface:

$$\frac{\partial U}{\partial Z}\Big|_{Z=1} = O(\kappa^2) \tag{5.3.0.7}$$

The normal stress boundary condition at the interface combined with the vertical momentum equation:

$$\frac{\partial P}{\partial x} = \frac{\partial \zeta}{\partial x} + O(\kappa^2), \quad 0 < Z < 1 + \epsilon\eta \tag{5.3.0.8}$$

The bottom kinematic boundary condition:

$$U = V = 0, \quad Z = 0 \tag{5.3.0.9}$$

However, we need to find the new horizontal momentum equation, which is modified by the mud behavior.

In this case where the depth of mud d is small compared to the depth of water, we can approximate the strain as a function of the horizontal displacement $\mathcal{U}$:

$$E_{xZ} = \frac{\partial \mathcal{U}}{\partial Z} + \kappa^2 \kappa_d^2 \frac{\partial \mathcal{V}}{\partial x} = \frac{\partial \mathcal{U}}{\partial Z} + O(\kappa^4) \tag{5.3.0.10}$$

We know for simple harmonic waves:

$$\tau_{xZ} = \mu \frac{\partial U}{\partial Z} + O(\kappa^4) \tag{5.3.0.11}$$

The equation of momentum in the mud, projected on the x-axis, gives:

$$\frac{\partial U}{\partial t} + \epsilon \left(U \frac{\partial U}{\partial x} + V \frac{\partial U}{\partial Z} \right) = -\gamma \frac{\partial P}{\partial x} + \frac{A}{Re^{(2)} * d} \left(\frac{\partial \tau_{xZ}}{\partial Z} + \kappa \kappa_d \frac{\partial \tau_{xx}}{\partial x} \right) \tag{5.3.0.12}$$

or:

$$\frac{\partial U}{\partial t} + \epsilon \left(U \frac{\partial U}{\partial x} + V \frac{\partial U}{\partial Z} \right) = -\gamma \frac{\partial P}{\partial x} + \frac{\epsilon}{Re^{(2)} * \kappa_d} \left(\frac{\partial \tau_{xZ}}{\partial Z} + \kappa \kappa_d \frac{\partial \tau_{xx}}{\partial x} \right) \tag{5.3.0.13}$$

where U is the horizontal velocity of mud, P the pressure, A the amplitude of the free surface, γ the ratio of densities $\gamma = \rho_W / \rho_M$ and d the mud depth, and $Re^{(2)}$ the new Reynolds number:

$$\boxed{Re^{(2)} = \frac{\rho_M A d k \sqrt{g\bar{h}}}{\mu_s}} \tag{5.3.0.14}$$

Equation 5.3.0.13 can be rewrittento $O(\kappa^0)$ accuracy only:

$$Re^{(2)} \frac{\kappa_d}{\epsilon} \left(\frac{\partial U}{\partial t} + \gamma \frac{\partial P}{\partial x} \right) = \frac{\partial^2 U}{\partial Z^2} + O(\epsilon) \quad 0 < Z < 1 + \epsilon\eta \tag{5.3.0.15}$$

From equation 5.3.0.8, we know the mud pressure gradient $\frac{\partial P}{\partial x}$. As a consequence, equation 3.4.0.18 becomes:

$$Re^{(2)} \frac{\kappa_d}{\epsilon} \left(\frac{\partial U}{\partial t} + \gamma \frac{\partial \zeta}{\partial x} \right) = \frac{\partial^2 U}{\partial Z^2} + O(\epsilon) \quad 0 < Z < 1 + \epsilon\eta \tag{5.3.0.16}$$

which is true for $0 < Z < 1 + \epsilon\eta$.

5.4 Asymptotic equations in water and viscoelastic mud

5.4.1 Water equations

Since mud-induced damping should appear at the same order as with Newtonian mud, we define the same slow coordinate X as in the previous chapter:

$$X = \kappa^2 x \tag{5.4.1.1}$$

and we expand the functions ζ and $\bar{u}$ as power series:

$$\begin{aligned} \zeta &= \zeta^{(0)} + \kappa^2\zeta^{(1)} + \kappa^4\zeta^{(2)} + ... \\ \bar{u} &= \bar{u}^{(0)} + \kappa^2\bar{u}^{(1)} + \kappa^4\bar{u}^{(2)} + ... \end{aligned} \tag{5.4.1.2}$$

We then consider the evolution of a train of harmonic waves:

$$\zeta^{(0)} = \frac{1}{2}\sum_{m=-\infty}^{+\infty} A_m(X)e^{i\theta_m} \quad \eta^{(0)} = \frac{1}{2}\sum_{m=-\infty}^{+\infty} B_m(X)e^{i\theta_m} \tag{5.4.1.3}$$

where $\theta_m = m(x - t)$

As a consequence, and since we got the same water equations as in the Newtonian case, the asymptotic equation in water is the same as equation 4.4.3.6:

$$\forall m, \quad \boxed{\frac{dA_m}{dX} = -\frac{im\gamma}{2}\frac{\kappa_d}{\kappa^2}B_m + \frac{im^3}{6}A_m - \frac{3i}{8}\frac{\epsilon}{\kappa^2}m\left[\sum_{l=1}^{\infty} 2A_l^* A_{m+l} + \sum_{l=1}^{[m/2]} \alpha_l A_l A_{m-l}\right]} \tag{5.4.1.4}$$

5.4.2 Mud equations

We adopt for the horizontal and vertical velocities in mud at the zeroth order the form we used in 4.4.2.2:

$$\begin{aligned} U^{(0)} &= \frac{1}{2}\sum_{m=-\infty}^{\infty} U_m^{(0)}(Z)e^{i\theta_m} \\ V^{(0)} &= \frac{1}{2}\sum_{m=-\infty}^{\infty} V_m^{(0)}(Z)e^{i\theta_m} \end{aligned} \tag{5.4.2.1}$$

Since only the horizontal momentum has changed compared to the Newtonian case, we obtain the same results as before except for σ that becomes $\tilde{\sigma}$:

$$\tilde{\sigma}_m^2 = -\frac{im}{\alpha^{(2)}\mu_m} \tag{5.4.2.2}$$

which means:

$$\boxed{\tilde{\sigma}_m^2 = -i\frac{m\kappa_d\rho_M A dk\sqrt{gh}}{\epsilon\mu'_m}} \tag{5.4.2.3}$$

Let us note that the value of $\tilde{\sigma}_m$ does not depend on μ_s, since $\mu_s\mu_m = \mu'_m$ is the dimensional viscosity.

In the end, the asymptotic equation in mud at the first order is derived from equation 4.4.2.11 with $\tilde{\sigma}_m$ instead of σ_m:

$$\boxed{B_m = \gamma A_m\left(1 - \frac{\tanh(\tilde{\sigma}_m)}{\tilde{\sigma}_m}\right)} \tag{5.4.2.4}$$

5.5 Further details

5.5.1 Surface and the interface

We now combine equation 5.4.1.4 and 5.4.2.4 and truncate the series to obtain the differential equation:

$$\begin{aligned} &\frac{dA_m}{dX} + \frac{i\gamma}{2}\frac{\kappa_d}{\kappa^2}m\left(1 - \frac{\tanh(\tilde{\sigma}_m)}{\tilde{\sigma}_m}\right)A_m - \frac{im^3}{6}A_m \\ &\quad + \frac{3i}{8}\frac{\epsilon}{\kappa^2}m\left(\sum_{l=1}^{n-m} 2A_l^* A_{m+l} + \sum_{l=1}^{[m/2]}\alpha_l A_l A_{m-l}\right) = 0 \end{aligned} \tag{5.5.1.1}$$

This truncated differential system is true for $0 < m \leq n$.

We observe that equation 5.5.1.1 is the same as equation 4.5.1.1 except for σ_m

that became $\tilde{\sigma}_m$.

Since this equation depends on γ, κ, κ_d, ϵ and the $\tilde{\sigma}_m$, we deduce that the result of the A_m will depend on the values:

$$g,\ \rho_W,\ \rho_M,\ A,\ \bar{h},\ d,\ \omega',\ \mu'_m \tag{5.5.1.2}$$

where g and ρ_W are fixed, ρ_M and the μ'_m depend on the mud we consider, and A, $\bar{h}$, ω' and d depend on the geometry and the surface wave.

5.5.2 Energy variation in water

Following the same demonstration as in the Newtonian mud case, we naturally come to the energy variation law:

$$\boxed{\frac{d}{dX}\left[\sum_{m=1}^{n}|A_m|^2\right] = -\gamma\frac{\kappa_d}{\kappa^2}\sum_{m=1}^{n} Re\left[im\left(1-\frac{\tanh(\tilde{\sigma}_m)}{\tilde{\sigma}_m}\right)\right]|A_m|^2} \tag{5.5.2.1}$$

Equation 5.5.2.1 is actually the same equation as 4.5.2.4, except for σ_m which has again been replaced by $\tilde{\sigma}_m$.

5.6 Numerical results by using the first ten harmonics

As we did in chapter 3, we are now going to plot these results for the viscoelastic muds we previously studied.

Let us sum up the different muds we are considering:

- Case A: Gulf of Mexico mud. This mud is rather elastic.
- Case B: Mobile Bay mud. This mud is rather elastic as well
- Case C: Lianyungang mud. This mud complex viscosity's phase is around $\frac{\pi}{4}$ so it is as elastic as viscous.
- Case D: Hangzhou Bay mud. This mud is rather viscous, its complex viscosity's phase being close to zero.

We choose to plot the different results for those muds in the case $\bar{h} = 5$m, $A = 0.4$m, $\omega' = 0.33$rad/s and $d = 25$cm (corresponding to the case 1b of the previous

chapter). In this case, we know:

$$\boxed{\kappa = 0.24,\ \epsilon = 0.08,\ \kappa_d = 0.05} \tag{5.6.0.2}$$

Surface and interface

In figures 5-1 and 5-2, we represent the variation of the first harmonics of the surface and the interface. As usual, and even though we carried the resolution with 10 harmonics in order to take into account all the significant ones, we only display the three most significant harmonics for clarity.

In figure 5-1, we observe that the damping is more important in cases A, C and D than in case B. This is what we expected from chapter 3, that showed that the attenuation rate was insignificant for mud B (Mobile Bay mud). We also observe that the Hangzhou Bay mud has a faster damping than the Gulf of Mexico and Lianyungang muds.

Damping is way slower to occur than in chapter 3. This is due to the fact that we are considering a very thin layer of mud (since $O(\kappa_d) = O(\kappa^2)$).

Figure 5-2 show the variation of the interfaces. The results confirm what we previously stated: the interface motion is strongest for the muds with the highest damping. As a consequence, the Hangzhou Bay mud, which is the one with the fastest damping, has the strongest interface motion. The Mobile Bay mud has the smallest interface motion.

Energy variation

We numerically represented the total first-order energies in figure 4-3. This figure shows that the total energy logically decreases, because it is dissipated in the viscous mud.

In the case of the Hangzhou Bay mud (D), the energy reaches a nearly 0-value for $X = 20$ that is to say $x \simeq 83$ since $\kappa = 0.24$ in the case we consider, or $x' = \frac{x}{k} =$ 1670m. As $\lambda = \frac{2\pi}{k}$, $\lambda \simeq$ 126m, we conclude that the wave is nearly damped after around 13 wavelengths.

However, damping is slower for the Gulf of Mexico and the Lianyungang muds. Their total energy only decreases by around 50% after around 25 wavelengths.

Damping is even slower for the Mobile Bay mud, where it nearly becomes insignificant. Indeed, energy has not even decreased by 5% after 25 wavelengths.

In figure 5-4, we represented the variation of total energy. The dashed line repre-

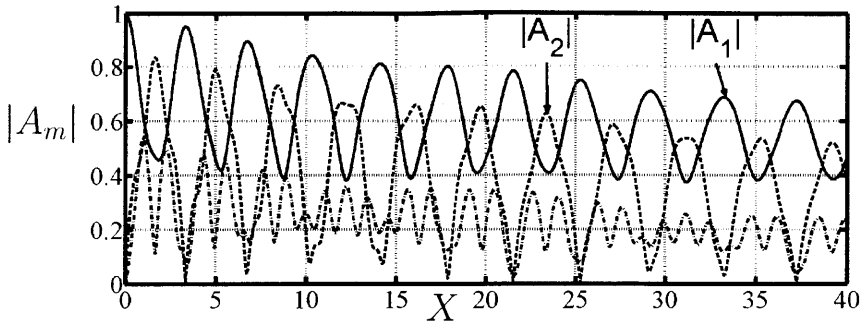

(a) Gulf of Mexico mud

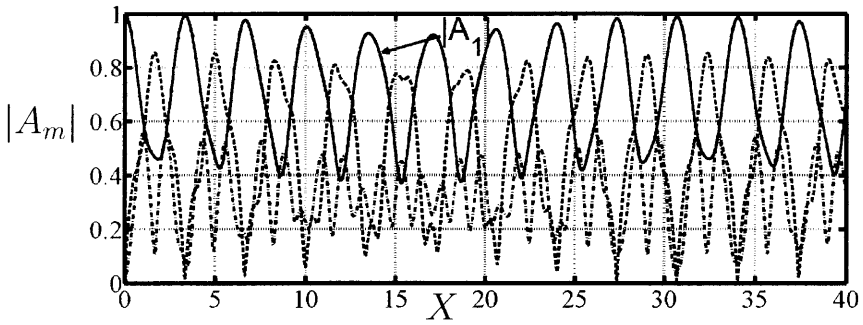

(b) Mobile Bay mud

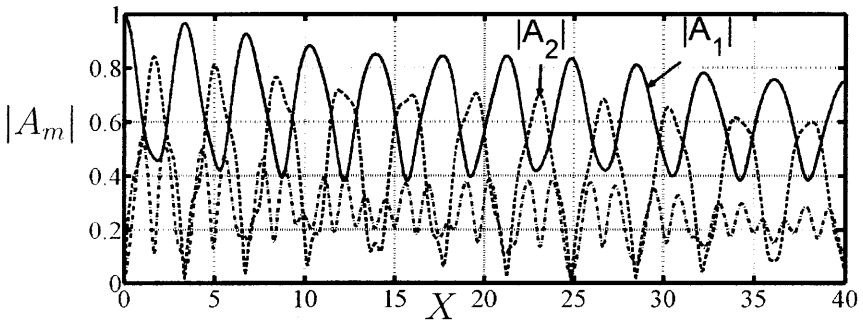

(c) Lianyungang mud

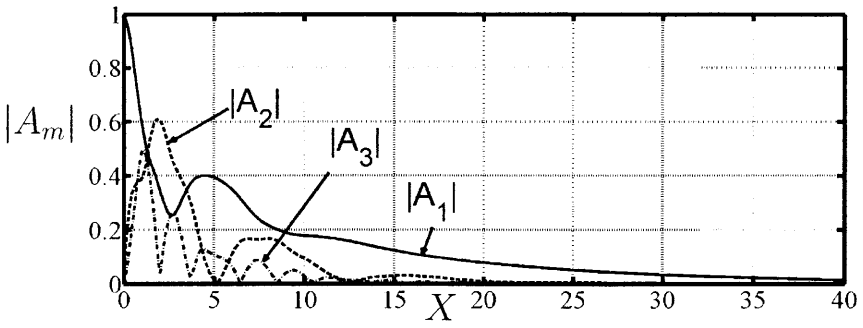

(d) Hangzhou Bay mud

Figure 5-1: Evolution of the first 3 harmonics of the free surface over different types of viscoelastic muddy seabeds.

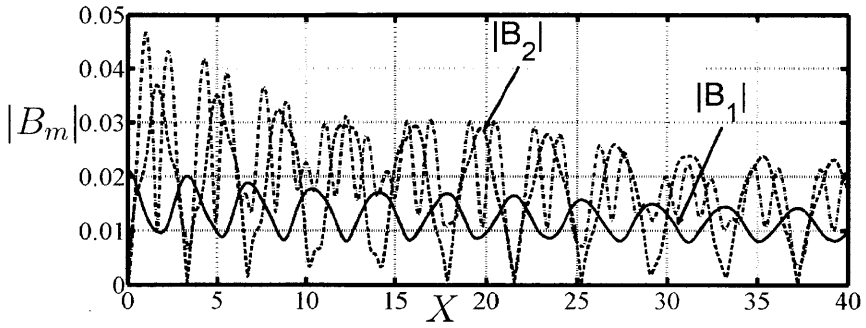

(a) Gulf of Mexico mud

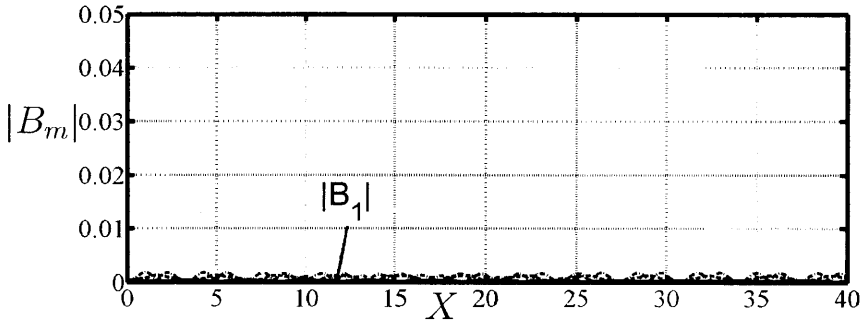

(b) Mobile Bay mud

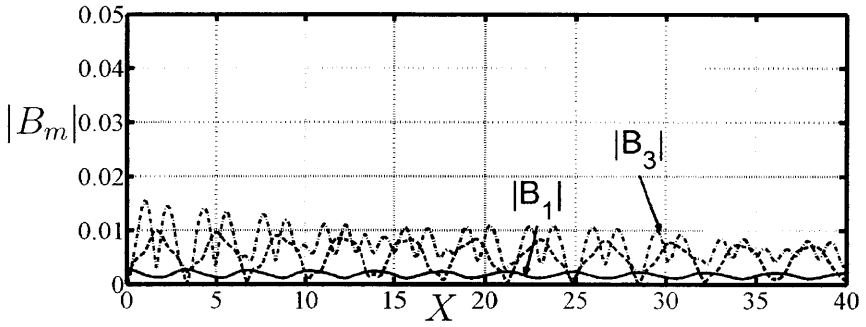

(c) Lianyungang mud

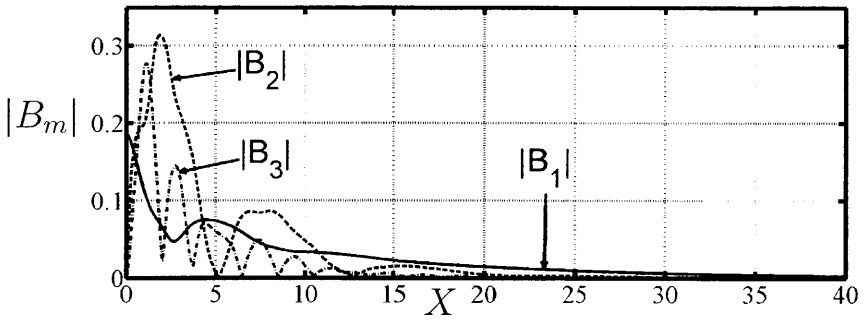

(d) Hangzhou Bay mud

Figure 5-2: Effects of wave amplitude on the evolution of the first 3 harmonics of the interface over different types of viscoelastic muddy seabeds. Warning, the scale is not the same for mud D!

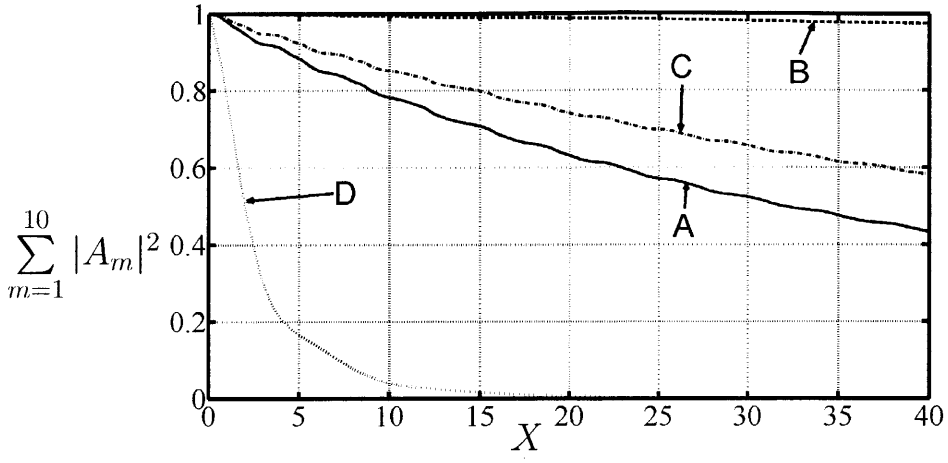

Figure 5-3: Wave energy over a flat thick muddy seabed.

sents the right-hand side term of the following equation:

$$\boxed{\frac{d}{dX}\left[\sum_{m=1}^{n}|A_m|^2\right] = -\gamma\frac{\kappa_d}{\kappa^2}\sum_{m=1}^{n}\Re\left[im\left(1-\frac{\tanh(\sigma_m)}{\sigma_m}\right)\right]|A_m|^2} \qquad (5.6.0.3)$$

As in the Newtonian case, the dashed line is so close to the solid line that it is very hard to distinguish, meaning that our numerical results are right.

5.7 Flat bottom without mud, Boussinesq class

5.7.1 Governing equations

From the governing equation we found in the case of a thin layer of mud at the bottom, it is easy to deduce the governing equation in the absence of mud. Indeed, the absence of mud corresponds to $B = 0$ in equation 4.4.3.6, which leads to:

$$\forall m,\ \frac{dA_m}{dX} = \frac{im^3}{6}A_m - \frac{3i}{8}\frac{\epsilon}{\kappa^2}m\left[\sum_{l=1}^{\infty}2A_l^*A_{m+1l} + \sum_{l=1}^{[m/2]}\alpha_l A_l A_{m-l}\right] \qquad (5.7.1.1)$$

A a consequence, we obtain the following differential equation:

$$\boxed{\frac{dA_m}{dX} - \frac{im^3}{6}A_m + \frac{3i}{8}\frac{\epsilon}{\kappa^2}m\left(\sum_{l=1}^{\infty}2A_l^*A_{m+l} + \sum_{l=1}^{[m/2]}\alpha_l A_l A_{m-l}\right) = 0} \qquad (5.7.1.2)$$

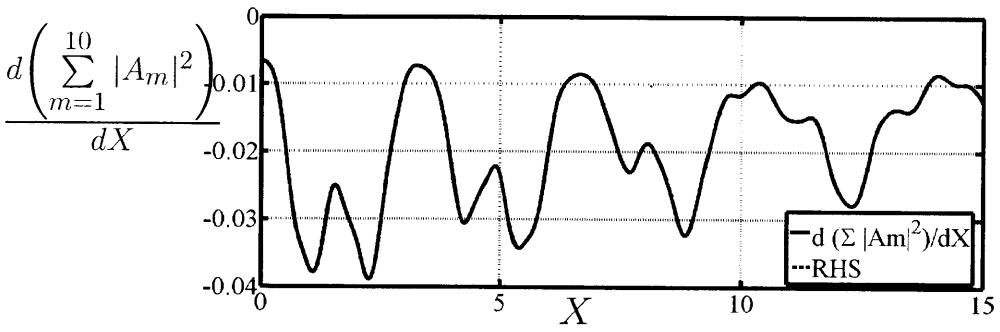

(a) Gulf of Mexico mud

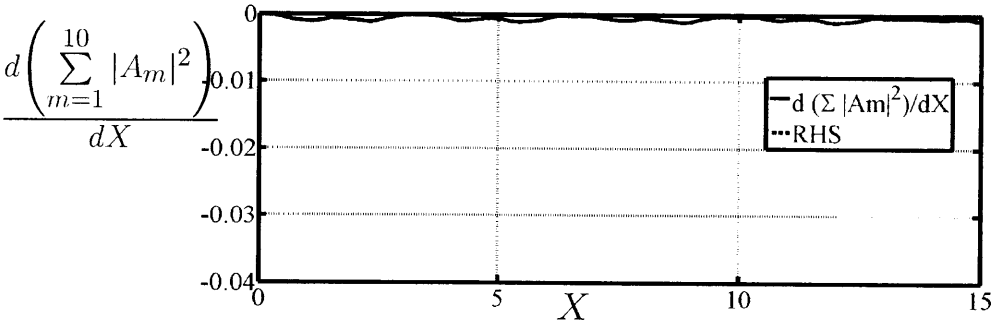

(b) Mobile Bay mud

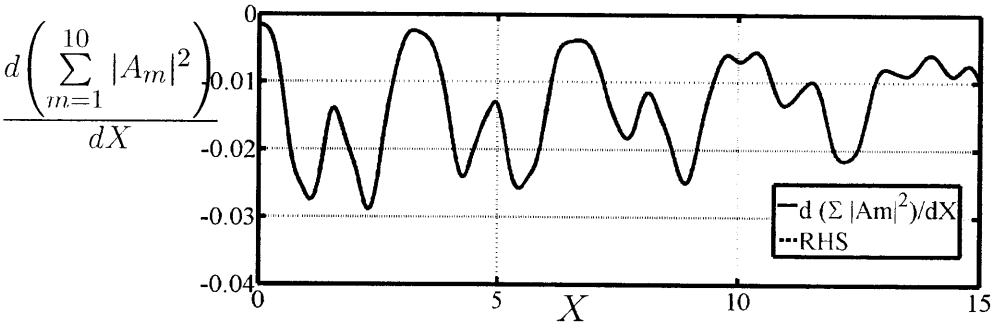

(c) Lianyungang mud

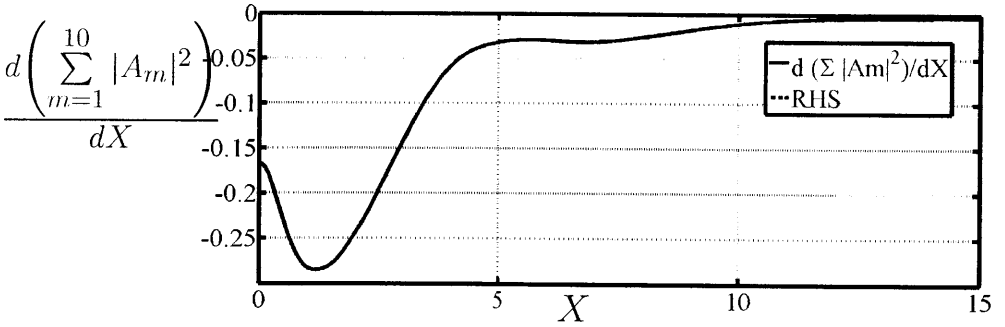

(d) Hangzhou Bay mud

Figure 5-4: Variation of the wave energy over a flat thick muddy seabed. RHS is the value of the right-hand side term in equation 5.5.2.1. Warning, the scale is not the same for mud D!

The same way, the energy variation becomes:

$$\boxed{\frac{d}{dX}\left[\sum_{m=1}^{n}|A_m|^2\right]=0} \tag{5.7.1.3}$$

This result looks very logical, since it means that in the absence of mud, there is no energy dissipation in water.

5.7.2 Numerical results by using the first ten harmonics

Since we don't consider mud anymore, there are only tree parameters remaining: $\bar{h}$, A, and ω. These parameters are only present in equation 5.7.1.2 in the ratio ϵ/κ^2, which is around 1.

In figure 5-5, we compare the surface displacement for three different cases: $\epsilon/\kappa^2 = 0.5$ (A), $\epsilon/\kappa^2 = 1$ (B) and $\epsilon/\kappa^2 = 1.5$ (C). These cases correspond to different non-linearity/dispersion ratios. The first case $\epsilon/\kappa^2 = 0.5$ means that non-linearity is less important than dispersion, whereas the case $\epsilon/\kappa^2 = 1.5$ means that non-linearity is predominant. Once again, even though we carried the numerical resolution with ten harmonics, we choose to only display the first three harmonics.

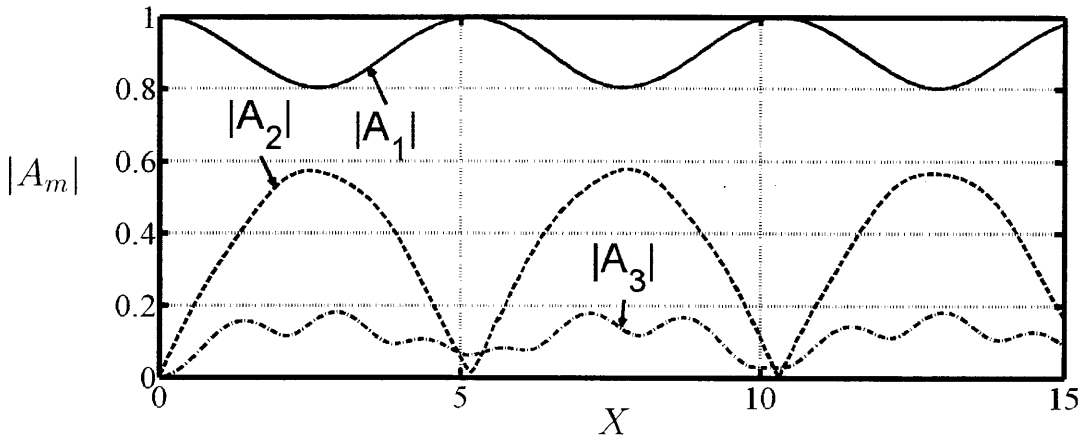

(a) Smallest ratio $\epsilon/\kappa^2 = 0.5$

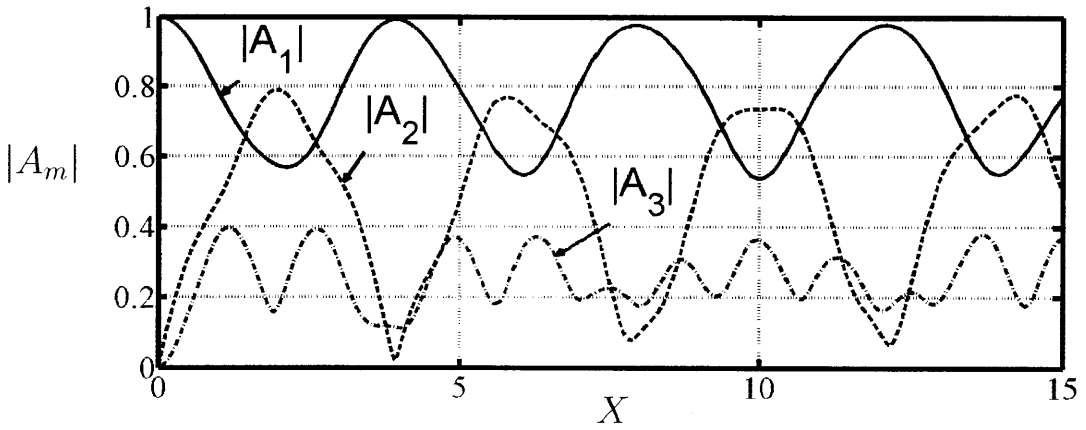

(b) Medium ratio $\epsilon/\kappa^2 = 1$

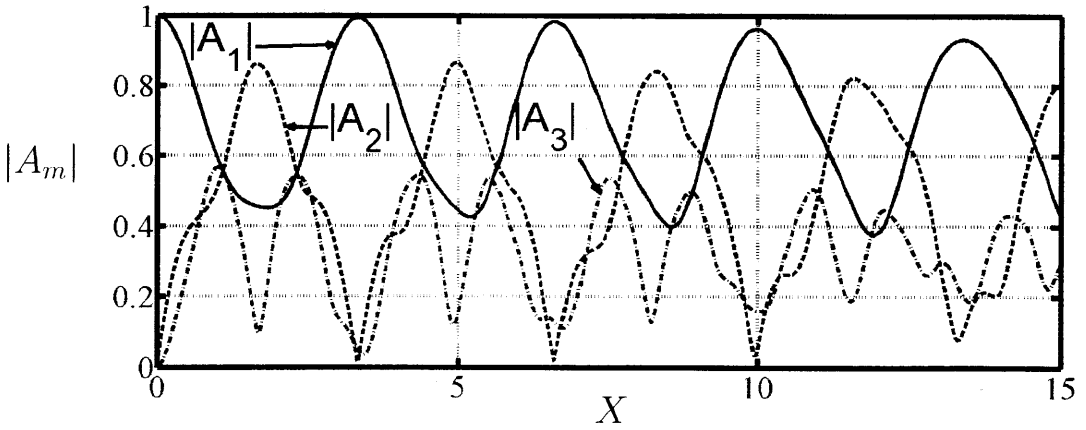

(c) Highest ratio $\epsilon/\kappa^2 = 1.5$

Figure 5-5: Effects of wave amplitude on the evolution of the first 3 harmonics of the free surface over a thick muddy seabed. Comparison between different values of ϵ/κ^2.

Chapter 6

Sloping bottom, with shallow viscoelastic mud

We now consider the bottom of the ocean to have a gentle slope, as shown on figure 6-1. We decide this slope to be of order $O(\kappa)$, so that it is comparable to the rate of damping previously found in the flat bottom case. This means that in this chapter, we will consider:

$$\frac{dh'}{dx'} = O(\kappa), \quad \frac{d^2h'}{dx'^2} = O(\kappa^2) \tag{6.0.2.1}$$

If the mud was Newtonian, it would naturally flow down the slope, even in a static case (without any wave at the surface). This mud flow would disqualify the assumptions we made up to now in this thesis, and this is why we decide not to study the case of Newtonian mud.

As a consequence, we consider in this chapter that the mud is a viscoelastic fluid, as done in chapters 3 and 5. We will show that viscoelastic mud does not flow down the slope, but is only subject to a displacement in a static case. Thus, viscoelastic mud does not disqualify the assumptions we made up to now.

6.1 Static case of viscoelastic mud on a sloping bottom

In this section, we want to determine what happens in the mud layer in the static case, ie in the absence of surface waves. For that, we won't use any scaling and dimensionless coordinates in this section. All the terms in this section are dimensional. This is why in this section, and this section only, dimensional quantities are written without primes.

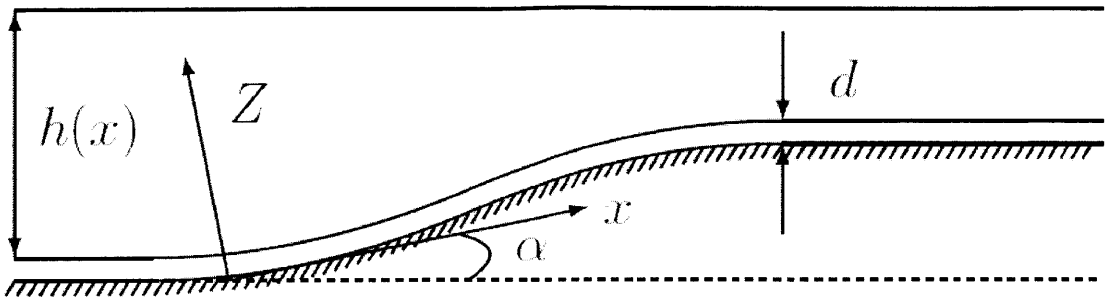

Figure 6-1: Sketch of the axis used in the static case.

Also, we will not use in this section the fact that the slope is gentle. We only use the approximation that the mud layer is thin.

6.1.1 Coordinates

In order to study the static behavior of a mud layer on a sloping bottom, we choose to use the axis x and Z, respectively parallel and normal to the slope, as shown in figure 6-1.

As shown on the figure, $h(x)$ is the water depth and α is the angle between the bottom slope and a horizontal line. $Z = 0$ corresponds to the bottom of the mud layer.

Since the problem we are considering is uniform by translation along x, we naturally have:

$$\frac{\partial}{\partial x} = 0 \tag{6.1.1.1}$$

Because we are considering a static problem, we also naturally have:

$$\frac{\partial}{\partial t} = 0 \tag{6.1.1.2}$$

As a consequence, all quantities only depend on one variable: Z, which is normal to the slope.

6.1.2 Mud equations in the static case

In the static case, all the forces acting in the mud are the gravity g and the shear stress τ_{xZ}. Since we are considering the static case, the sum of these forces is zero.

Let us project this equality on the x-axis, tangent to the slope. We obtain:

$$-\rho_W g h(x) \sin(\alpha) + \frac{\partial \tau_{xZ}}{\partial Z} = 0 \tag{6.1.2.1}$$

Viscoelasticity can be represented with a Kelvin-Voigt model, where stress τ_{ij} is a function of the strain E_{ij} and the strain rate $\frac{\partial E_{ij}}{\partial t}$:

$$\tau_{ij} = G E_{ij} + \mu \frac{\partial E_{ij}}{\partial t} \tag{6.1.2.2}$$

where E is the elastic modulus and μ the viscosity of the material. Since we already stated that all differentiation with respect to time was zero, equation 6.1.2.2 becomes:

$$\tau_{ij} = G E_{ij} \tag{6.1.2.3}$$

In other words, viscosity does not appear in the static case, only elasticity does.

From equation 6.1.2.3, we know in particular:

$$\tau_{xZ} = G E_{xZ} \tag{6.1.2.4}$$

Introducing the displacement $\mathcal{U}$ tangent to the slope, equation 6.1.2.4 becomes:

$$\tau_{xZ} = G \frac{\partial \mathcal{U}}{\partial Z} \tag{6.1.2.5}$$

Combining equation 6.1.2.1 and 6.1.2.5, we obtain a differential equation for the displacement $\mathcal{U}$:

$$-\rho_W g h(x) \sin(\alpha) + G \frac{d^2 \mathcal{U}}{dZ^2} = 0 \tag{6.1.2.6}$$

By integrating this equation twice, we obtain $\mathcal{U}^{(0)}$:

$$\mathcal{U}(Z) = \frac{\rho_W g h(x) \sin(\alpha)}{2G} Z^2 + C^{(1)} Z + C^{(2)} \tag{6.1.2.7}$$

with $C^{(1)}$ and $C^{(2)}$ two real numbers. From the boundary condition at the bottom, we deduce:

$$\mathcal{U}(Z = 0) = 0 \tag{6.1.2.8}$$

and thus $C^{(2)} = 0$. The same way, we deduce from the shear stress at the interface:

$$\tau_{xZ} = \frac{d\mathcal{U}}{dZ} = 0, \quad Z = d \tag{6.1.2.9}$$

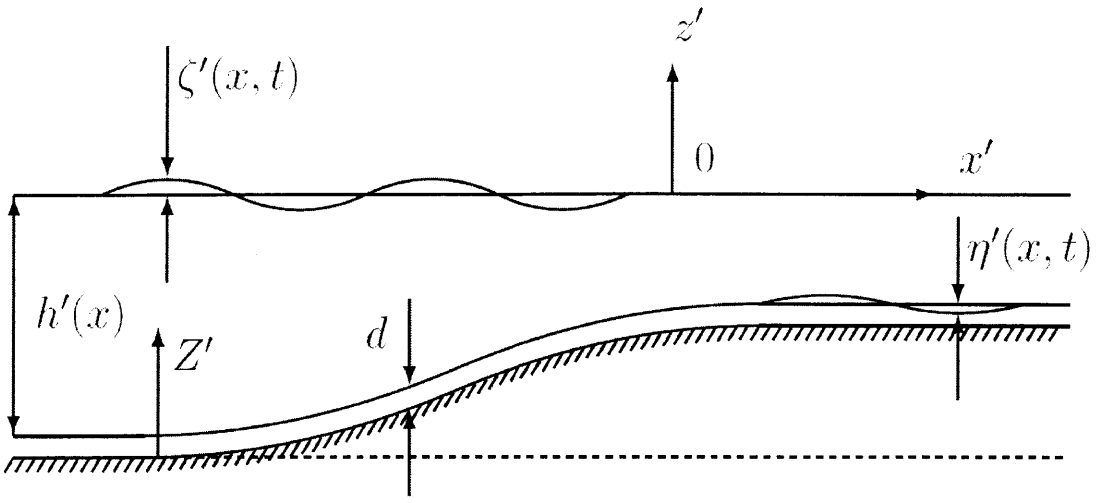

Figure 6-2: Sketch of the studied case. d is the mud layer depth measured vertically.

and thus:

$$C^{(1)} = -\frac{\rho_W g h(x) \sin(\alpha)}{G} \tag{6.1.2.10}$$

In the end, equation 6.1.2.7 becomes:

$$\boxed{\mathcal{U}(Z) = \frac{\rho_W g h(x) \sin(\alpha)}{2G} Z(Z - 2d)} \tag{6.1.2.11}$$

We obtain that the displacement in mud is a parabola, with a 0-value at the bottom of the layer and its highest absolute value at the interface with water ($Z = d$). Let us note that if $\sin(\alpha) > 0$ - meaning that the water depth decreases with x - $\mathcal{U} < 0$ for all $0 < Z < d$. This is what we expected since the displacement should be down the slope.

This closes the study of the static case. We obtain that, with a viscoelastic mud, there is only a displacement of the mud down the slope. We do not have a steady flow as we would have with a viscous mud. As a consequence, we can definitely study the influence of water waves at the surface without the static case having any influence on the motion.

6.2 Scaling

Now that we already studied the static case, we focus on the effect of ocean waves at the water surface, as done in the previous chapters.

As before, we define a dimensionless complex viscosity:

$$\mu = \frac{\mu'}{\mu_s} \tag{6.2.0.12}$$

We will use the same scaling in water as in the flat bottom case (chapter 3) :

$$\tau_{ij} = \frac{d}{\epsilon\mu_s\sqrt{g\bar{h}}}\tau'_{ij} \tag{6.2.0.13}$$

where μ_s is the characteristic viscosity deduced from the different sets of experiments. Because of calculation simplifications, we will see that we still do not need to assign a particular value to μ_s for the different muds. Indeed, we will see that neither μ_s neither any non-dimensional viscosity μ will be appear in the final results, but only the dimensional viscosity μ'.

For simple harmonic waves:

$$\tau_{xZ} = -i\omega\mu(\omega)E_{xZ} \tag{6.2.0.14}$$

To sum up, the new scaling for this section are:

$$\begin{array}{lll} x = kx' & z = \frac{z'}{\bar{h}}b & t = k(g\bar{h})^{1/2}t' \\ p = \frac{p'}{\rho_W gA} & u = \frac{1}{\epsilon\sqrt{g\bar{h}}}u' & v = \frac{\kappa}{\epsilon\sqrt{g\bar{h}}}v' \\ \zeta = \frac{\zeta'}{A} & \phi = \phi'\left[\frac{A}{k\bar{h}}(g\bar{h})^{1/2}\right]^{-1} & \end{array} \tag{6.2.0.15}$$

We decide to use a new axis Z' in mud:

$$Z' = z' - h'(x') - d \tag{6.2.0.16}$$

as shown in figure 6-2. This way, $Z' = 0$ is the bottom of the mud layer.

$$\begin{array}{lll} x = kx' & Z = \frac{Z'}{d} & t = k(g\bar{h})^{1/2}t' \\ P = \frac{P'}{\rho_W gA} & U = \frac{1}{\epsilon\sqrt{g\bar{h}}}U' & V = \frac{1}{\epsilon\kappa\kappa_d\sqrt{g\bar{h}}}V' \\ \eta = \frac{\eta'}{\kappa_d A} & \mathcal{U} = \frac{k}{\epsilon}\mathcal{U}' & \mathcal{V} = \frac{k}{\epsilon\kappa\kappa_d}\mathcal{V}' \\ T_{ij} = \frac{T'_{ij}}{\rho_W gA} & E_{ij,t} = \frac{d}{\epsilon\sqrt{g\bar{h}}}E'_{ij,t'} & \tau_{ij} = \frac{d}{\epsilon\mu_s\sqrt{g\bar{h}}}\tau'_{ij} \\ \mu = \frac{\mu'}{\mu_s} & & \end{array} \tag{6.2.0.17}$$

Let us compare our new coordinates in mud with the ones we had in the flat bottom case. Now, the axes follow the slope. This fact brings a correction in the differentia-

tions, that become:

$$\begin{aligned} \frac{\partial}{\partial z} &\to \frac{\partial}{\partial Z} \\ \frac{\partial}{\partial x} &\to \frac{\partial}{\partial x} - \frac{1}{\kappa_d}\frac{dh}{dx}\frac{\partial}{\partial Z} \end{aligned} \tag{6.2.0.18}$$

In order to emphasize the fact that $\frac{dh}{dx}$ is small, let us introduce the slow coordinate:

$$X = \kappa x. \tag{6.2.0.19}$$

Thus:

$$\begin{aligned} \frac{dh}{dx} &\to \kappa \frac{dh}{dX} \\ \frac{d^2h}{dx^2} &\to \kappa^2 \frac{d^2h}{dX^2} \end{aligned} \tag{6.2.0.20}$$

We can now rewrite relation 6.2.0.18:

$$\begin{aligned} \frac{\partial}{\partial z} &\to \frac{\partial}{\partial Z} \\ \frac{\partial}{\partial x} &\to \frac{\partial}{\partial x} - \frac{\kappa}{\kappa_d}\frac{dh}{dX}\frac{\partial}{\partial Z} \end{aligned} \tag{6.2.0.21}$$

6.3 Equations in water to order $O(\kappa^2)$

Let us express the velocity potential in water as a power series:

$$\boxed{\phi(x,z,t) = \sum_{n=0}^{\infty} \frac{(z+h(x))^n}{n!}\phi^{(n)}(x,t)} \tag{6.3.0.22}$$

where $z = -h(x) + \epsilon\kappa_d\eta$ corresponds to the mud-water interface. We then obtain

$$\frac{\partial\phi}{\partial x} = \sum_{n=0}^{\infty} \frac{(z+h(x))^n}{n!}\left[\frac{\partial\phi^{(n)}}{\partial x} + \frac{dh}{dx}\phi^{(n+1)}\right] \tag{6.3.0.23}$$

And thus:

$$\frac{\partial^2\phi}{\partial x^2} = \sum_{n=0}^{\infty} \frac{(z+h)^n}{n!}\left[\frac{\partial^2\phi^{(n)}}{\partial x^2}(x,t) + 2\frac{dh}{dx}\frac{\partial\phi^{(n+1)}}{\partial x} + \left(\frac{dh}{dx}\right)^2\phi^{(n+2)} + \frac{d^2h}{dx^2}\phi^{(n+1)}\right] \tag{6.3.0.24}$$

and

$$\phi_{zz} = \sum_{n=0}^{\infty} \frac{(z+h)^n}{n!}\phi^{(n+2)}(x,t) \tag{6.3.0.25}$$

6.3.1 Laplace equation

From the Laplace equation in dimensionless variables, we know:

$$\kappa^2 \frac{\partial^2 \phi}{\partial x^2} + \frac{\partial^2 \phi}{\partial z^2} = 0 \tag{6.3.1.1}$$

and from 6.3.0.24 and 6.3.0.25 we deduce:

$$\forall n, \quad \phi^{(n)} = -\kappa^2 \left(\frac{\partial^2 \phi^{(n-2)}}{\partial x^2} + 2\kappa \frac{dh}{dX} \frac{\partial \phi^{(n-1)}}{\partial x} + \kappa^2 \frac{d^2 h}{dX^2} \phi^{(n-1)} + \kappa^2 \left(\frac{dh}{dX} \right)^2 \phi^{(n)} \right) \tag{6.3.1.2}$$

6.3.2 Kinematic Boundary condition at the interface

In dimensional form, the interface kinematic boundary condition is:

$$\frac{\partial \phi'}{\partial z'} = -\frac{\partial [h'(x') - \eta'(x,t)]}{\partial t'} - \frac{\partial [h'(x') - \eta'(x,t)]}{\partial x'} \frac{\partial \phi'}{\partial x'}, \quad z = -h(x) + \epsilon \kappa_d \eta(x,t) \tag{6.3.2.1}$$

In dimensionless form we obtain:

$$\frac{\partial \phi}{\partial z} = \kappa_d \kappa^2 \frac{\partial \eta}{\partial t} - \kappa_d \kappa^2 \frac{\partial \phi}{\partial x} \frac{dh}{dX} + \epsilon \kappa_d \kappa^2 \frac{\partial \phi}{\partial x} \frac{\partial \eta}{\partial x}, \quad z = -h(x) + \epsilon \kappa_d \eta(x,t) \tag{6.3.2.2}$$

We use a Taylor series expansion of this equation to obtain:

$$\frac{\partial \phi}{\partial z} + \epsilon \kappa_d \eta \frac{\partial^2 \phi}{\partial z^2} = \kappa^2 \kappa_d \frac{\partial \eta}{\partial t} + \kappa^2 \left(-\kappa \frac{dh}{dX} + \epsilon \kappa_d \frac{\partial \eta}{\partial x} \right) \frac{\partial \phi}{\partial x} + O(\kappa^4), \quad z = -h \tag{6.3.2.3}$$

As a consequence, from the series of equation 6.3.0.22 we obtain:

$$\phi^{(1)} + \epsilon \kappa_d \eta \phi^{(2)} = \kappa_d \kappa^2 \frac{\partial \eta}{\partial t} - \kappa^3 \frac{dh}{dX} \frac{\partial \phi^{(0)}}{\partial x} + O(\kappa^4), \quad z = -h \tag{6.3.2.4}$$

From the relationship 6.3.1.2 and knowing that $\phi(z = -h) = \phi^{(0)}$, $\frac{\partial^n \phi}{\partial z^n}(z = -h) = \phi^{(n)}$, we deduce:

$$\phi^{(1)} = \kappa_d \kappa^2 \frac{\partial \eta}{\partial t} - \kappa^3 \frac{dh}{dX} \frac{\partial \phi^{(0)}}{\partial x} + O(\kappa^4) \tag{6.3.2.5}$$

and as a consequence:

$$\phi^{(1)} = \kappa_d \kappa^2 \frac{\partial \eta}{\partial t} - \kappa^3 \frac{dh}{dX} \frac{\partial \phi^{(0)}}{\partial x} + O(\kappa^4) \tag{6.3.2.6}$$

As a consequence, from equation 6.3.2.6, we can deduce an explicit expression of all the $\phi^{(n)}$:

$$\begin{aligned}\phi^{(2)} &= -\kappa^2\left(\frac{\partial^2\phi^{(0)}}{\partial x^2} + 2\kappa\frac{dh}{dX}\frac{\partial\phi^{(1)}}{\partial x} + \kappa^2\frac{d^2h}{dX^2}\phi^{(1)} + \kappa^2\left(\frac{dh}{dX}\right)^2\phi^{(2)}\right) \\ &= -\kappa^2\frac{\partial^2\phi^{(0)}}{\partial x^2} + O(\kappa^4)\end{aligned} \tag{6.3.2.7}$$

$$\begin{aligned}\phi^{(3)} &= -\kappa^2\left(\frac{\partial^2\phi^{(1)}}{\partial x^2} + 2\kappa\frac{dh}{dX}\frac{\partial\phi^{(2)}}{\partial x} + \kappa^2\frac{d^2h}{dX^2}\phi^{(2)} + \kappa^2\left(\frac{dh}{dX}\right)^2\phi^{(3)}\right) \\ &= -\kappa^2\left(\kappa_d\kappa^3\frac{\partial\eta}{\partial t} - \kappa^4\frac{dh}{dX}\frac{\partial\phi^{(0)}}{\partial x}\right) + O(\kappa^4) \\ &= O(\kappa^4)\end{aligned} \tag{6.3.2.8}$$

Combining all these equations together, the final expression of ϕ becomes:

$$\phi = \phi^{(0)} + \kappa^2(z+h)\left[\kappa_d\frac{\partial\eta}{\partial t} - \kappa\frac{dh}{dX}\frac{\partial\phi^{(0)}}{\partial x}\right] - \kappa^2\frac{(z+h)^2}{2}\frac{\partial^2\phi^{(0)}}{\partial x^2} + O(\kappa^4) \tag{6.3.2.9}$$

6.3.3 Kinematic Boundary condition at the free surface

The kinematic boundary condition at the surface can be written as:

$$\kappa^2\left(\zeta_t + \epsilon\frac{\partial\phi}{\partial x}\frac{\partial\zeta}{\partial x}\right) = \phi_z, \quad z = \epsilon\zeta \tag{6.3.3.1}$$

Knowing from equation 6.3.2.9 that:

$$\phi_z = \kappa^2\left[\kappa_d\frac{\partial\eta}{\partial t} - \kappa\frac{dh}{dX}\frac{\partial\phi^{(0)}}{\partial x}\right] - \kappa^2(z+h)\frac{\partial^2\phi^{(0)}}{\partial x^2} + O(\kappa^4) \tag{6.3.3.2}$$

we obtain:

$$\zeta_t + \epsilon\frac{\partial\zeta}{\partial x}\frac{\partial\phi^{(0)}}{\partial x} = \kappa_d\frac{\partial\eta}{\partial t} - \kappa\frac{dh}{dX}\frac{\partial\phi^{(0)}}{\partial x} - (h+\epsilon\zeta)\frac{\partial^2\phi^{(0)}}{\partial x^2} + O(\kappa^2) \tag{6.3.3.3}$$

Let us now introduce the horizontal velocity at the bottom:

$$u^{(0)} = \frac{\partial\phi^{(0)}}{\partial x}, \quad z + h(x) = 0 \tag{6.3.3.4}$$

$$\zeta_t + \frac{\partial}{\partial x}\left[(h+\epsilon\zeta)u^{(0)}\right] = \kappa_d\eta_t + O(\kappa^2) \tag{6.3.3.5}$$

Let us now introduce the depth-averaged velocity $\bar{u}$. It is related to $u^{(0)}$ by the following relation:

$$\begin{aligned}\bar{u} &= \frac{1}{h+\epsilon\zeta-\epsilon\kappa_d\eta}\int_{-h+\epsilon\kappa_d\eta}^{\epsilon\zeta}\frac{\partial\phi}{\partial x}dz \\ &= \frac{1}{h+\epsilon\zeta-\epsilon\kappa_d\eta}\int_{-h+\epsilon\kappa_d\eta}^{\epsilon\zeta}[u^{(0)}+O(\kappa^2)]dz \\ &= u^{(0)}+O(\kappa^2)\end{aligned} \tag{6.3.3.6}$$

Turning this last result around, we obtain the relation:

$$u^{(0)} = \bar{u} + O(\kappa^2) \tag{6.3.3.7}$$

Using this relationship, we obtain equation 6.3.3.5 in terms of $\bar{u}$ instead of u_0:

$$\zeta_t + \frac{\partial}{\partial x}\left[(h+\epsilon\zeta)\bar{u}\right] = \kappa_d\eta_t + O(\kappa^2) \tag{6.3.3.8}$$

We can rewrite this equation:

$$\boxed{\zeta_t - \kappa_d\eta_t + \frac{\partial}{\partial x}\left[(h+\epsilon\zeta)\bar{u}\right] = O(\kappa^2)} \tag{6.3.3.9}$$

This result agrees with the equation we obtained in the flat bottom case (chapters 2 or 3 since the mud model does not change the calculations in water). Indeed, equation 6.3.3.9 reduces to equation 2.3.2.9 in the case $h(x,t)=1$, and this allows us to check the calculations.

6.3.4 Dynamic boundary condition at the free surface

From the dynamic boundary condition at the surface we know:

$$\kappa^2(\phi_t+\zeta)+\frac{1}{2}\epsilon[\kappa^2\phi_x^2+\phi_z^2]=0,\quad z=\epsilon\zeta(x,t) \tag{6.3.4.1}$$

From the development of ϕ of the equation 6.3.2.9, we know that:

$$\frac{\partial\phi}{\partial t} = \frac{\partial\phi^{(0)}}{\partial t} + \kappa^2 h\left[\kappa_d\frac{\partial^2\eta}{\partial t^2} - \kappa\frac{dh}{dX}\frac{\partial^2\phi^{(0)}}{\partial t\partial x}\right] - \frac{\kappa^2}{2}(h^2+2\epsilon\zeta h)\frac{\partial^3\phi^{(0)}}{\partial x^2\partial t} + O(\kappa^4) \tag{6.3.4.2}$$

$$\left(\frac{\partial\phi}{\partial x}\right)^2 = \left(\frac{\partial\phi^{(0)}}{\partial x}\right)^2 - \kappa^2h^2\frac{\partial\phi^{(0)}}{\partial x}\frac{\partial^3\phi^{(0)}}{\partial x^3} + O(\kappa^4) \tag{6.3.4.3}$$

and:

$$\left(\frac{\partial\phi}{\partial z}\right)^2 = O(\kappa^4) \tag{6.3.4.4}$$

So we can deduce:

$$\frac{\partial\phi^{(0)}}{\partial t} + \zeta + \frac{1}{2}\epsilon\left(\frac{\partial\phi^{(0)}}{\partial x}\right)^2 = O(\kappa^2) \tag{6.3.4.5}$$

Let us differentiate this expression with respect to x:

$$\frac{\partial^2\phi^{(0)}}{\partial t\partial x} + \frac{\partial\zeta}{\partial x} + \frac{1}{2}\epsilon\frac{\partial}{\partial x}\left(\frac{\partial\phi^{(0)}}{\partial x}\right)^2 = O(\kappa^2) \tag{6.3.4.6}$$

and we can now introduce the horizontal velocity at the bottom $u^{(0)} = \frac{\partial\phi^{(0)}}{\partial x}$

$$\frac{\partial u^{(0)}}{\partial t} + \frac{\partial\zeta}{\partial x} + \frac{1}{2}\epsilon\frac{\partial}{\partial x}(u^{(0)})^2 = O(\kappa^2) \tag{6.3.4.7}$$

As done for the kinematic boundary condition, we write this equation as a function of the depth-averaged velocity $\bar{u}$, using the relation between $u^{(0)}$ and $\bar{u}$ of the equation 6.3.3.7:

$$\boxed{\frac{\partial\bar{u}}{\partial t} + \epsilon\bar{u}\frac{\partial\bar{u}}{\partial x} + \frac{\partial\zeta}{\partial x} = O(\kappa^2)} \tag{6.3.4.8}$$

This result agrees with the equation we obtained in the flat bottom case (equation 2.3.3.6). This equality confirms the calculations.

6.3.5 Equation of the total pressure in water

From the Bernoulli equation, we can deduce the total pressure (sum of the static and the dynamic pressure) in the water as a function of the potential:

$$\begin{aligned} p' &= p'_s + p'_d \\ &= -\rho_W\left(\frac{\partial\phi'}{\partial t'} + \frac{1}{2}(\nabla'\phi')^2 + gz'\right) \end{aligned} \tag{6.3.5.1}$$

In dimensionless form, this last equation becomes:

$$p = -\phi_t - \frac{\epsilon}{2}\left[(\phi_x)^2 + \frac{1}{\kappa^2}(\phi_z)^2\right] - \frac{z}{\epsilon}, \quad -h(x) + \epsilon\kappa_d\eta < z < \zeta \tag{6.3.5.2}$$

And since we know from 6.3.4.4 that:

$$(\phi_z)^2 = O(\kappa^4) \tag{6.3.5.3}$$

equation 6.3.5.2 can be reduced to:

$$p = -\phi_t - \frac{\epsilon}{2}(\phi_x)^2 - \frac{z}{\epsilon} + O(\kappa^2), \quad -h(x) + \epsilon\kappa_d\eta < z < \zeta \tag{6.3.5.4}$$

In particular, we obtain the pressure in water at the interface $z = -h + \epsilon\kappa_d\eta$:

$$p = \frac{h(x)}{\epsilon} - \phi_t - \kappa_d\eta - \frac{\epsilon}{2}(\phi_x)^2 + O(\kappa^2) \tag{6.3.5.5}$$

By Taylor expansion, we know that:

$$\phi(z = -h + \epsilon\kappa_d\eta) = \phi(z = -h) + O(\kappa^2) = \phi_0 + O(\kappa^2) \tag{6.3.5.6}$$

As a consequence, 6.3.5.5 becomes:

$$\boxed{p = \frac{h(x)}{\epsilon} - (\phi_0)_t - \kappa_d\eta - \frac{\epsilon}{2}((\phi_0)_x)^2 + O(\kappa^2)}, \quad z = -h + \epsilon\kappa_d\eta \tag{6.3.5.7}$$

6.4 Equations in mud to order $O(\kappa^2)$

We now want to study the mud layer in the dynamic case. Since the static case has already been studied, we only focus on the wave-induced phenomenon. In other words, we only consider the effects of the dynamic pressure, since the static pressure has already been taken into account. The way we did in the flat bottom case (chapter 3), we go to order $O(\kappa^2)$ in order to study the drift current which appears because of non-linearity at order $O(\epsilon) = O(\kappa^2)$.

6.4.1 Interface kinematic boundary condition in mud

Let us write this boundary condition at the first order. We don't need to go to second order since this boundary condition will not be needed to calculate the drift.

The instantaneous equation of the interface is:

$$F'(x', Z', t') = Z' - (d + \eta') = 0 \tag{6.4.1.1}$$

The assumption of tangential motion then requires that:

$$\frac{\partial F'}{\partial t'} + U'\left(\frac{\partial}{\partial x'} - \frac{dh'}{dx'}\frac{\partial}{\partial Z'}\right)F' + V'\frac{\partial F'}{\partial Z'} = 0, \quad Z' = d + \eta' \tag{6.4.1.2}$$

which means, using equation 6.4.1.1:

$$-\frac{\partial \eta'}{\partial t'} - U'\frac{\partial \eta'}{\partial x'} - U'\frac{dh'}{dx'} + V' = 0, \quad Z' = d + \eta' \tag{6.4.1.3}$$

or in dimensionless form:

$$-\frac{\partial \eta}{\partial t} - \epsilon U\frac{\partial \eta}{\partial x} - \frac{\kappa}{\kappa_d}U\frac{dh}{dX} + V = 0, \quad Z = 1 + \epsilon\eta \tag{6.4.1.4}$$

As a consequence we obtain the following equation:

$$\frac{\partial \eta}{\partial t} = V - \frac{\kappa}{\kappa_d}U\frac{dh}{dX} + O(\kappa), \quad Z = 1 + \epsilon\eta \tag{6.4.1.5}$$

By Taylor expansion around $Z = 1$, we obtain:

$$\boxed{\frac{\partial \eta}{\partial t} = V - \frac{\kappa}{\kappa_d}U\frac{dh}{dX} + O(\kappa)}, \quad Z = 1 \tag{6.4.1.6}$$

6.4.2 Conservation of mass in mud

$$\left(\frac{\partial}{\partial x} - \frac{\kappa}{\kappa_d}\frac{dh}{dX}\frac{\partial}{\partial Z}\right)U + \frac{\partial V}{\partial Z} = 0, \quad 0 < Z < 1 + \epsilon\eta \tag{6.4.2.1}$$

By keeping only the first order, this means:

$$\boxed{\frac{\partial U}{\partial x} - \frac{\kappa}{\kappa_d}\frac{dh}{dX}\frac{\partial U}{\partial Z} + \frac{\partial V}{\partial Z} = 0}, \quad 0 < Z < 1 + \epsilon\eta \tag{6.4.2.2}$$

This equation will be used later to deduce vertical velocity from horizontal velocity in mud. Let us note that this equation is exact, contrary to most other mud equations.

6.4.3 Horizontal momentum in mud

The equation of momentum in mud, projected on the x-axis, gives:

$$\begin{aligned}\frac{\partial U}{\partial t} + \epsilon\left[U\left(\frac{\partial}{\partial x} - \frac{\kappa}{\kappa_d}\frac{dh}{dX}\frac{\partial}{\partial Z}\right)U + V\frac{\partial U}{\partial Z}\right] &= -\gamma\left(\frac{\partial}{\partial x} - \frac{\kappa}{\kappa_d}\frac{dh}{dX}\frac{\partial}{\partial Z}\right)P_d \\ + \frac{A}{Re^{(2)} * d}\left[\frac{\partial \tau_{xZ}}{\partial Z} + \kappa\kappa_d\left(\frac{\partial}{\partial x} - \frac{\kappa}{\kappa_d}\frac{dh}{dX}\frac{\partial}{\partial Z}\right)\tau_{xx}\right]\end{aligned} \tag{6.4.3.1}$$

where the coordonates (x,Z) are defined in 6.2.0.18. From this equation we simplify:

$$\frac{\partial U}{\partial t}-\frac{1}{Re^{(2)}}\frac{A}{d}\frac{\partial \tau_{xZ}}{\partial Z}=-\gamma\frac{\partial P_d}{\partial x}+\frac{\kappa}{\kappa_d}\gamma\frac{dh}{dX}\frac{\partial P_d}{\partial Z}-\epsilon\left(U\frac{\partial U}{\partial x}-\frac{\kappa}{\kappa_d}\frac{dh}{dX}U\frac{\partial U}{\partial Z}+V\frac{\partial U}{\partial Z}\right)+O(\epsilon^2) \tag{6.4.3.2}$$

where U is the horizontal velocity of mud, P_d the hydrodynamic pressure, A the amplitude of the free surface, γ the ratio of densities $\gamma = \rho_W/\rho_M$ and d the mud depth, and $Re^{(2)}$ the Reynolds number for this chapter:

$$\boxed{Re^{(2)}=\frac{\rho_M A d k\sqrt{gh}}{\mu_s}} \tag{6.4.3.3}$$

6.4.4 Vertical momentum in mud

The dimensional equation of vertical momentum is:

$$\rho_M\left[\frac{\partial V'}{\partial t'}+U'\left(\frac{\partial}{\partial x'}-\frac{dh'}{dx'}\frac{\partial}{\partial Z'}\right)V'+V'\frac{\partial V'}{\partial Z'}\right]=-\frac{\partial P'_d}{\partial Z'}+\left[\frac{\partial \tau'_{ZZ}}{\partial Z'}+\left(\frac{\partial}{\partial x'}-\frac{dh'}{dx'}\frac{\partial}{\partial Z'}\right)\tau'_{xZ}\right] \tag{6.4.4.1}$$

and becomes, in dimensionless variables:

$$\begin{aligned}\frac{\partial V}{\partial t}+\epsilon\left[U\left(\frac{\partial}{\partial x}-\frac{\kappa}{\kappa_d}\frac{dh}{dX}\frac{\partial}{\partial Z}\right)V+V\frac{\partial V}{\partial Z}\right]&=-\frac{\gamma}{\kappa^2\kappa_d^2}\frac{\partial P_d}{\partial Z}\\&+\frac{\epsilon}{Re\kappa^2\kappa_d}\left[\frac{\partial \tau_{ZZ}}{\partial Z}+\kappa\kappa_d\left(\frac{\partial}{\partial x}-\frac{\kappa}{\kappa_d}\frac{dh}{dX}\frac{\partial}{\partial Z}\right)\tau_{xZ}\right]\end{aligned} \tag{6.4.4.2}$$

So, in the end,

$$\boxed{\frac{\partial P_d}{\partial Z}=O(\epsilon\kappa_d)}\quad 0<Z<1+\epsilon\eta \tag{6.4.4.3}$$

In other words, we find that the vertical pressure gradient in mud is of order $O(\kappa^2)$. This equation will be used to evaluate the pressure in the entire mud layer.

We can then simplify the horizontal momentum equation 6.4.3.2:

$$\frac{\partial U}{\partial t}-\frac{1}{Re^{(2)}}\frac{A}{d}\frac{\partial \tau_{xZ}}{\partial Z}=-\gamma\frac{\partial P_d}{\partial x}-\epsilon\left(U\frac{\partial U}{\partial x}-\frac{\kappa}{\kappa_d}\frac{dh}{dX}U\frac{\partial U}{\partial Z}+V\frac{\partial U}{\partial Z}\right)+O(\epsilon^2) \tag{6.4.4.4}$$

6.4.5 Interface dynamic boundary condition

Let us call $\underline{n} = (n_x, n_Z)$ the vector normal to the interface. In dimensional notations, we know that the components of $\underline{n}$ are:

$$\begin{aligned} n_x &= \frac{\frac{d(-h'+\eta')}{dx'}}{\sqrt{1+\left(\frac{d(-h'+\eta')}{dx'}\right)^2}} \\ n_z &= \frac{1}{\sqrt{1+\left(\frac{d(-h'+\eta')}{dx'}\right)^2}} \end{aligned} \tag{6.4.5.1}$$

since $h'(x')$ and η' do not depend on Z. In dimensionless variables, we obtain:

$$\begin{aligned} n_x &= \frac{-\kappa^2\frac{dh}{dX} + \epsilon\kappa\kappa_d\frac{\partial\eta}{\partial x}}{\sqrt{1+\kappa^2\left(-\kappa\frac{dh}{dX}+\epsilon\kappa_d\frac{\partial\eta}{\partial x}\right)^2}} \\ &= -\kappa^2\frac{dh}{dX} + O(\kappa^3) \\ n_z &= \frac{1}{\sqrt{1+\kappa^2\left(-\kappa\frac{dh}{dX}+\epsilon\kappa_d\frac{\partial\eta}{\partial x}\right)^2}} \\ &= 1 + O(\kappa^4) \end{aligned} \tag{6.4.5.2}$$

Continuity of total (hydrodynamic and dynamic) stress on the mud-water interface then requires:

$$\begin{aligned} T_{xx}n_x + T_{xZ}n_Z &= -pn_x, \quad Z = 1+\epsilon\eta \\ T_{xZ}n_x + T_{ZZ}n_Z &= -pn_Z, \quad Z = 1+\epsilon\eta \end{aligned} \tag{6.4.5.3}$$

Total stress in mud is the sum of hydrostatic and dynamic pressure:

$$T_{ij} = -P\delta_{ij} + \frac{\epsilon\kappa}{\gamma Re^{(2)}}\tau_{ij}, \tag{6.4.5.4}$$

Introducing this sum in equation 6.4.5.3, we obtain:

$$\begin{aligned} \left(-P + \frac{\epsilon\kappa}{\gamma Re^{(2)}}\tau_{xx}\right)n_x + \frac{\epsilon\kappa}{\gamma Re^{(2)}}\tau_{xZ}n_Z &= -pn_x, \quad Z = 1+\epsilon\eta \\ \frac{\epsilon\kappa}{\gamma Re^{(2)}}\tau_{xZ}n_x + \left(-P + \frac{\epsilon\kappa}{\gamma Re^{(2)}}\tau_{ZZ}\right)n_Z &= -pn_Z, \quad Z = 1+\epsilon\eta \end{aligned} \tag{6.4.5.5}$$

From the approximations of n_x and n_Z that we demonstrated in 6.4.5.1, equations

6.4.5.5 become:

$$\begin{aligned}
&-\left(-P+\frac{\epsilon\kappa}{\gamma Re^{(2)}}\tau_{xx}\right)\kappa^2\frac{dh}{dX}+\frac{\epsilon\kappa}{\gamma Re^{(2)}}\tau_{xZ}=p\kappa^2\frac{dh}{dX}+O(\kappa^4),\quad Z=1+\epsilon\eta\\
&-\frac{\epsilon\kappa}{\gamma Re^{(2)}}\tau_{xZ}\kappa^2\frac{dh}{dX}+\left(-P+\frac{\epsilon\kappa}{\gamma Re^{(2)}}\tau_{ZZ}\right)=-p+O(\kappa^4),\quad Z=1+\epsilon\eta
\end{aligned}\tag{6.4.5.6}$$

These last equations can easily be simplified to:

$$\begin{aligned}
\tau_{xZ}&=-\gamma Re^{(2)}(P-p)\frac{\kappa}{\epsilon}\frac{dh}{dX}+O(\kappa^4),\quad Z=1+\epsilon\eta\\
P-p&=O(\kappa^2),\quad Z=1+\epsilon\eta
\end{aligned}\tag{6.4.5.7}$$

Let us now make use of the second equation (corresponding to normal stress condition) to simplify the first one (corresponding to tangential stress condition). Since $P-p=O(\kappa^2)$, we obtain:

$$\begin{aligned}
\tau_{xZ}&=O(\kappa^2),\quad Z=1+\epsilon\eta\\
P-p&=O(\kappa^2),\quad Z=1+\epsilon\eta
\end{aligned}\tag{6.4.5.8}$$

We now focus on the first part of equation 6.4.5.8. Through a Taylor expansion, we can approximate this equations around $Z=1$:

$$\tau_{xZ}(Z=1+\epsilon\eta)=\tau_{xZ}(Z=1)+\epsilon\eta\frac{\partial\tau_{xZ}}{\partial Z}\Big|_{Z=1}+O(\epsilon^2)\tag{6.4.5.9}$$

and as a consequence:

$$\begin{aligned}
\tau_{xZ}(Z=1)&=\tau_{xZ}(Z=1+\epsilon\eta)-\epsilon\eta\frac{\partial\tau_{xZ}}{\partial Z}\Big|_{Z=1}+O(\epsilon^2)\\
&=-\epsilon\eta\frac{\partial\tau_{xZ}}{\partial Z}\Big|_{Z=1}+O(\epsilon^2)
\end{aligned}\tag{6.4.5.10}$$

Hence, we obtained an interface boundary condition that we will use later to find the drift in mud:

$$\boxed{\tau_{xZ}(Z=1)=-\epsilon\eta\frac{\partial\tau_{xZ}}{\partial Z}\Big|_{Z=1}+O(\epsilon^2)}\tag{6.4.5.11}$$

Let us now focus on the second part of equation 6.4.5.8. From this equation we know that:

$$P=p+O(\kappa^2),\quad Z=1+\epsilon\eta\tag{6.4.5.12}$$

From 6.4.4.3, we know that the vertical gradient of mud dynamic pressure is of order

$O(\kappa^2)$. As a consequence, we have:

$$P = p(Z = 1 + \epsilon\eta) + O(\kappa^2), \quad 0 < Z < 1 + \epsilon\eta \tag{6.4.5.13}$$

Water pressure p is known in any point of the water layer thanks to the Bernouilli equation. In particular, we know from 6.3.5.7 the water pressure at the interface ($z = -h + \epsilon\kappa_d\eta$):

$$p = \frac{h(x)}{\epsilon} - (\phi_0)_t - \kappa_d\eta - \frac{\epsilon}{2}((\phi_0)_x)^2 + O(\kappa^2) \tag{6.4.5.14}$$

So we conclude from 6.4.5.13:

$$P = \frac{h(x)}{\epsilon} - (\phi_0)_t - \kappa_d\eta - \frac{\epsilon}{2}((\phi_0)_x)^2 + O(\kappa^2), \quad 0 < Z < 1 + \epsilon\eta \tag{6.4.5.15}$$

and we obtain in particular the dynamic pressure in mud:

$$P_d = -(\phi_0)_t - \kappa_d\eta - \frac{\epsilon}{2}((\phi_0)_x)^2 + O(\kappa^2), \quad 0 < Z < 1 + \epsilon\eta \tag{6.4.5.16}$$

From equation 6.3.4.5, we also know:

$$\frac{\partial\phi^{(0)}}{\partial t} + \frac{\epsilon}{2}\left(\frac{\partial\phi^{(0)}}{\partial x}\right)^2 = -\zeta + O(\kappa^2) \tag{6.4.5.17}$$

which is valid for all z since $\phi^{(0)}$ and ζ do not depend on the vertical coordinate. Combining equations 6.4.5.16 and 6.4.5.17, we get the dynamic pressure in mud:

$$P_d = \zeta - \kappa_d\eta + O(\kappa^2), \quad 0 < Z < 1 + \epsilon\eta \tag{6.4.5.18}$$

and the dynamic pressure gradient in mud:

$$\frac{\partial P_d}{\partial x} = \frac{\partial\zeta}{\partial x} - \kappa_d\frac{\partial\eta}{\partial x} + O(\kappa^2), \quad 0 < Z < 1 + \epsilon\eta \tag{6.4.5.19}$$

As a consequence, we can now substitute the dynamic mud pressure P_d from the horizontal momentum equation 6.4.4.4, for $0 < Z < 1 + \epsilon\eta$:

$$\boxed{\frac{\partial U}{\partial t} - \frac{1}{Re^{(2)}}\frac{A}{d}\frac{\partial\tau_{xZ}}{\partial Z} = -\gamma\left(\frac{\partial\zeta}{\partial x} - \kappa_d\frac{\partial\eta}{\partial x}\right) - \epsilon\left(U\frac{\partial U}{\partial x} - \frac{\kappa}{\kappa_d}\frac{dh}{dX}U\frac{\partial U}{\partial Z} + V\frac{\partial U}{\partial Z}\right) + O(\kappa^2)} \tag{6.4.5.20}$$

6.4.6 Bottom kinematic boundary conditions

At the bottom, we impose the no-slip boundary condition:

$$\boxed{U = V = 0}, \quad Z = 0 \tag{6.4.6.1}$$

6.5 Asymptotic equations in water and viscoelastic mud

6.5.1 Surface and interface

Water equations

We consider that the dependence of the wavenumber on x, because of the bottom slope. As a consequence, we introduce new variables:

$$X = \kappa x, \quad \xi = \frac{1}{\kappa}\int^X h^{-1/2} dX - t \tag{6.5.1.1}$$

so that the derivatives become:

$$\begin{aligned} \frac{\partial}{\partial t} &\to -\frac{\partial}{\partial \xi} \\ \frac{\partial}{\partial x} &\to \kappa \frac{\partial}{\partial X} + \frac{1}{\sqrt{h}}\frac{\partial}{\partial \xi} \end{aligned} \tag{6.5.1.2}$$

With the new variables defined in 6.5.1.1, equations 6.3.3.9 and 6.3.4.8 become:

$$-\zeta_\xi + \kappa_d \eta_\xi + \kappa h_X \bar{u} + \kappa h \bar{u}_X + \epsilon \zeta_\xi h^{-1/2}\bar{u} + \epsilon \zeta h^{-1/2}\bar{u}_\xi + h^{1/2}\bar{u}_\xi = O(\kappa^2) \tag{6.5.1.3}$$

$$-\bar{u}_\xi + \epsilon h^{-1/2}\bar{u}\bar{u}_\xi + \kappa \zeta_X + h^{-1/2}\zeta_\xi = O(\kappa^2) \tag{6.5.1.4}$$

From equation 6.5.1.3 at the first order, we deduce:

$$\begin{aligned} \bar{u}_\xi &= h^{-1/2}\zeta_\xi + O(\kappa^2) \\ \bar{u} &= h^{-1/2}\zeta + O(\kappa^2) \\ \bar{u}_X &= h^{-1/2}\zeta_X - \frac{h_X}{2h^{3/2}}\zeta + O(\kappa^2) \end{aligned} \tag{6.5.1.5}$$

We now consider (equation 6.5.1.3 $+h^{1/2}*$ equation 6.5.1.4) at the second order and we obtain:

$$\begin{aligned}\kappa_d\eta_\xi+\kappa h_X\bar{u}+\kappa h\bar{u}_X+\epsilon\zeta_\xi h^{-1/2}\bar{u}+\epsilon\zeta h^{-1/2}\bar{u}_\xi\\ +h^{1/2}\left(\epsilon h^{-1/2}\bar{u}\bar{u}_\xi+\kappa\zeta_X\right)=O(\kappa^2)\end{aligned} \tag{6.5.1.6}$$

Using the relations 6.5.1.5, equation 6.5.1.6 becomes:

$$\begin{aligned}\frac{\kappa_d}{\kappa}\eta_\xi+h_X h^{-1/2}\zeta+h\left(h^{-1/2}\zeta_X-\frac{h_X}{2h^{3/2}}\zeta\right)+\frac{\epsilon}{\kappa}\zeta_\xi h^{-1}\zeta+\frac{\epsilon}{\kappa}\zeta h^{-1}\zeta_\xi\\ +h^{1/2}\left(\frac{\epsilon}{\kappa}h^{-1/2}h^{-1/2}\zeta h^{-1/2}\zeta_\xi+\zeta_X\right)=O(\kappa)\end{aligned} \tag{6.5.1.7}$$

and finally:

$$\boxed{2h^{1/2}\zeta_X+\frac{h_X}{2h^{1/2}}\zeta+\frac{3}{2h}\frac{\epsilon}{\kappa}(\zeta^2)_\xi=-\frac{\kappa_d}{\kappa}\eta_\xi+O(\kappa)} \tag{6.5.1.8}$$

Now let us expand the functions ζ and η as power series:

$$\begin{aligned}\zeta&=\zeta^{(0)}+\kappa\zeta^{(1)}+\kappa^2\zeta^{(2)}+...\\ \eta&=\eta^{(0)}+\kappa\eta^{(1)}+\kappa^2\eta^{(2)}+...\end{aligned} \tag{6.5.1.9}$$

Because equation 6.5.1.8 is non-linear, we decide to adopt the following form for $\zeta^{(0)}$ and $\eta^{(0)}$:

$$\zeta^{(0)}=\frac{1}{2}\sum_{m=-\infty}^{+\infty}A_m(X)e^{im\xi}\quad\eta^{(0)}=\frac{1}{2}\sum_{m=-\infty}^{+\infty}B_m(X)e^{im\xi} \tag{6.5.1.10}$$

where we set A_0 to be $A_0=0$. Then we know that:

$$\begin{aligned}\frac{\partial\zeta^{(0)}}{\partial X}&=\frac{1}{2}\sum_{m=1}^{\infty}\frac{dA_m}{dX}e^{im\xi}+cc.\\ \frac{3}{2h}\frac{\partial(\zeta^{(0)})^2}{\partial\xi}&=\sum_{m=1}^{\infty}\frac{3}{8h}ime^{im\xi}\left[\sum_{l=1}^{\infty}2A_l^*A_{m+l}+\sum_{l=1}^{[m/2]}\alpha_l A_l A_{m-l}\right]+cc.\end{aligned} \tag{6.5.1.11}$$

Then, following the procedure in section 2.5.3, we deduce from equation 6.5.1.8:

$$\forall m,\quad\sqrt{h}\frac{dA_m}{dX}+\frac{h_X}{4\sqrt{h}}A_m+\frac{\epsilon}{\kappa}\frac{3i}{8h}m\left[\sum_{l=1}^{\infty}2A_l^*A_{m+l}+\sum_{l=1}^{[m/2]}\alpha_l A_l A_{m-l}\right]+\frac{\kappa_d}{\kappa}\frac{im}{2}B_m=0 \tag{6.5.1.12}$$

where $[m/2]$ is the integer part of $m/2$ and α_l is a coefficient equal to 1 for $l=[m/2]$ and equal to 2 otherwise.

Let us observe that equation 6.5.1.12 becomes equation 2.5.3.5 in the particular case $h(X) = 1$. This result confirms our calculations.

Mud equations

Let us find other coupling equations between the surface and the interface, ζ and η, derived from the mud equations.

Equation 6.4.5.20 gives at the first order:

$$\frac{\partial U}{\partial t} - \alpha^{(2)} \frac{\partial \tau_{xZ}}{\partial Z} = -\gamma \frac{\partial \zeta}{\partial x} + O(\kappa) \tag{6.5.1.13}$$

with:

$$\boxed{\alpha^{(2)} = \frac{\epsilon}{\kappa_d Re^{(2)}}} = O(1) \tag{6.5.1.14}$$

From the change of variables 6.5.1.1, we convert equations 6.5.1.13, 6.4.2.2 and 6.4.1.6 at the first order in:

$$\begin{aligned}
\alpha^{(2)} \frac{\partial \tau_{xZ}^{(0)}}{\partial Z} + \frac{\partial U^{(0)}}{\partial \xi} &= \gamma h^{-1/2} \frac{\partial \zeta^{(0)}}{\partial \xi} + O(\epsilon), \quad 0 < Z < 1 + \epsilon\eta(x) \\
h^{-1/2} \frac{\partial U^{(0)}}{\partial \xi} - \frac{\kappa}{\kappa_d} \frac{dh}{dX} \frac{\partial U^{(0)}}{\partial Z} + \frac{\partial V^{(0)}}{\partial Z} &= O(\epsilon), \quad 0 < Z < 1 + \epsilon\eta(x) \\
-\frac{\partial \eta^{(0)}}{\partial \xi} &= V - \frac{\kappa}{\kappa_d} \frac{dh}{dX} \frac{\partial U^{(0)}}{\partial Z} + O(\epsilon), \quad Z = 1
\end{aligned} \tag{6.5.1.15}$$

Since the water equations are not linear, we consider all harmonics and write:

$$\begin{aligned}
U^{(0)} = \frac{1}{2} \sum_{m=-\infty}^{\infty} U_m^{(0)}(Z) e^{im\xi} \quad V^{(0)} = \frac{1}{2} \sum_{m=-\infty}^{\infty} V_m^{(0)}(Z) e^{im\xi} \\
(\tau_{xZ})^{(0)} = \frac{1}{2} \sum_{m=-\infty}^{\infty} (\tau_{xZ})_m^{(0)}(Z) e^{im\xi}
\end{aligned} \tag{6.5.1.16}$$

Let us find an equation between A_m and B_m from the mud equations. From the first equation of 6.5.1.15, we know:

$$\alpha^{(2)} \frac{d(\tau_{xZ})_m^{(0)}}{dZ} + imU_m^{(0)} = h^{-1/2} im\gamma A_m \tag{6.5.1.17}$$

From equation 6.2.0.14, which only applies to simple harmonic waves, we deduce:

$$(\tau_{xZ})_m^{(0)} = \mu_m \frac{dU_m^{(0)}}{dZ} + O(\kappa^4) \tag{6.5.1.18}$$

As a consequence, equation 6.5.1.17 becomes:

$$\frac{d^2U_m^{(0)}}{dZ^2} + \frac{im}{\alpha^{(2)}\mu_m}U_m^{(0)} = h^{-1/2}\frac{im}{\alpha^{(2)}\mu_m}\gamma A_m \tag{6.5.1.19}$$

which can be simplified as:

$$\frac{d^2U_m^{(0)}}{dZ^2} - \tilde{\sigma}_m^2 U_m^{(0)} = -h^{-1/2}\tilde{\sigma}_m^2\gamma A_m \tag{6.5.1.20}$$

where $\tilde{\sigma}_m^2$ is as in the flat bottom case (chapter 3):

$$\tilde{\sigma}_m^2 = -i\frac{m}{\alpha^{(2)}\mu_m} \tag{6.5.1.21}$$

Knowing the value of $\alpha^{(2)}$, we deduce:

$$\boxed{\tilde{\sigma}_m^2 = -i\frac{m\kappa_d\rho_M A dk\sqrt{g\bar{h}}}{\epsilon\mu'_m}} \tag{6.5.1.22}$$

Let us note that the value of $\tilde{\sigma}_m$ does not depend on μ_s, since $\mu_s\mu_m = \mu'_m$ is the dimensional viscosity. As $\alpha^{(2)}$ and $Re^{(2)}$ do not appear in equation 6.5.1.19, we deduce that we will not need the value of μ_s to solve it.

We also know the boundary conditions:

$$\begin{aligned} U^{(0)} &= 0, \quad Z = 0 \\ \frac{dU^{(0)}}{dZ} &= O(\epsilon), \quad Z = 1 \end{aligned} \tag{6.5.1.23}$$

and thus, $\forall m$:

$$\begin{aligned} U_m^{(0)} &= 0, \quad Z = 0 \\ \frac{dU_m^{(0)}}{dZ} &= 0, \quad Z = 1 \end{aligned} \tag{6.5.1.24}$$

We obtain the value of the horizontal velocity:

$$\begin{aligned} U_m^{(0)} = &\frac{\gamma A_m}{\sqrt{h}}\Big[1 - [1 + \tanh(\tilde{\sigma}_m)]\cosh(\tilde{\sigma}_m Z) \\ &+ [\tanh(\tilde{\sigma}_m)]\sinh(\tilde{\sigma}_m Z)\Big] \end{aligned} \tag{6.5.1.25}$$

From 6.5.1.15, we also know:

$$\forall m,\quad \frac{dV_m^{(0)}}{dZ} = -\frac{im}{\sqrt{h}}U_m^{(0)} + \frac{\kappa}{\kappa_d}\frac{dh}{dX}\frac{\partial U_m^{(0)}}{\partial Z} \tag{6.5.1.26}$$

Using the boundary condition:

$$V_m^{(0)}(Z=0) = 0 \tag{6.5.1.27}$$

we obtain:

$$\begin{aligned} V_m^{(0)} = &- im\frac{\gamma A_m}{\tilde{\sigma}_m h}\Big[\tilde{\sigma}_m Z - [1+\tanh(\tilde{\sigma}_m)]\sinh(\tilde{\sigma}_m Z) \\ &+ [\tanh(\tilde{\sigma}_m)]\cosh(\tilde{\sigma}_m Z) - \tanh(\tilde{\sigma}_m)\Big] \\ &+ \frac{\kappa}{\kappa_d}\frac{dh}{dX}U_m^{(0)} \end{aligned} \tag{6.5.1.28}$$

It is interesting to note that there is a new term in the expression of $V_m^{(0)}$ compared to the flat bottom case (chapter 3). This is due to the fact that we are not considering the same axes anymore. As a consequence, the vertical velocity must be corrected with a term proportional to the horizontal velocity and the slope $\frac{dh}{dX}$. Now, still from equation 6.5.1.15, we have:

$$\forall m, B_m(X) = -\frac{1}{im}\left(V_m^{(0)}(Z=1) - \frac{\kappa}{\kappa_d}\frac{dh}{dX}U_m^{(0)}(Z=1)\right) \tag{6.5.1.29}$$

After using equations 6.5.1.25 and 6.5.1.28, we obtain:

$$\forall m,\quad \boxed{B_m(X) = \frac{\gamma A_m}{h}\left[1 - \frac{\tanh\tilde{\sigma}_m}{\tilde{\sigma}_m}\right]} \tag{6.5.1.30}$$

Combining equations 6.5.1.12 and 6.5.1.30, we naturally obtain:

$$\begin{aligned} \forall m,\quad \sqrt{h}\frac{dA_m}{dX} + \frac{h_X}{4\sqrt{h}}A_m + \frac{\epsilon}{\kappa}\frac{3i}{8h}m\left[\sum_{l=1}^{\infty} 2A_l^* A_{m+l} + \sum_{l=1}^{[m/2]} \alpha_l A_l A_{m-l}\right] \\ + \frac{im}{2}\frac{\kappa_d}{\kappa}\frac{\gamma A_m}{h}\left[1 - \frac{\tanh\tilde{\sigma}_m}{\tilde{\sigma}_m}\right] = 0 \end{aligned} \tag{6.5.1.31}$$

where $[m/2]$ is the integer part of $m/2$ and α_l is a coefficient equal to 1 for $l = [m/2]$ and equal to 2 otherwise.

This equation will be solved numerically for A_m.

6.5.2 Drift current

Let us study the drift current in mud by going to order $O(\kappa)$.

At this order, we had for $0 < Z < 1 + \epsilon\eta$ from equation 6.4.5.20:

$$\frac{\partial U}{\partial t} - \alpha^{(2)}\frac{\partial(\tau_{xZ})}{\partial Z} = \gamma\frac{\partial}{\partial x}(\zeta - \kappa_d\eta) - \epsilon\left(U\frac{\partial U}{\partial x} - \frac{\kappa}{\kappa_d}\frac{dh}{dX}U\frac{\partial U}{\partial Z} + V\frac{\partial U}{\partial Z}\right) + O(\epsilon^2) \tag{6.5.2.1}$$

With the variables defined in 6.5.1.1, this equation becomes:

$$\begin{aligned} -\frac{\partial U}{\partial \xi} - \alpha^{(2)}\frac{\partial(\tau_{xZ})}{\partial Z} =& \frac{\gamma}{\sqrt{h}}\frac{\partial}{\partial x}(\zeta - \kappa_d\eta) - \gamma\kappa\frac{\partial \zeta}{\partial X} \\ & - \epsilon\left(\frac{1}{\sqrt{h}}U\frac{\partial U}{\partial \xi} - \frac{\kappa}{\kappa_d}\frac{dh}{dX}U\frac{\partial U}{\partial Z} + V\frac{\partial U}{\partial Z}\right) + O(\epsilon^2) \end{aligned} \tag{6.5.2.2}$$

At order $O(\kappa)$, this equation is:

$$\begin{aligned} -\frac{\partial U^{(1)}}{\partial \xi} - \alpha^{(2)}\frac{\partial(\tau_{xZ})^{(1)}}{\partial Z} =& \frac{\gamma}{\sqrt{h}}\frac{\partial}{\partial x}\left(\zeta^{(1)} - \frac{\kappa_d}{\kappa}\eta^{(0)}\right) - \gamma\frac{\partial \zeta^{(1)}}{\partial X} \\ & - \frac{\epsilon}{\kappa}\left[\frac{1}{\sqrt{h}}U^{(0)}\frac{\partial U^{(0)}}{\partial \xi} + \left(V^{(0)} - \frac{\kappa}{\kappa_d}\frac{dh}{dX}U^{(0)}\right)\frac{\partial U^{(0)}}{\partial Z}\right] \end{aligned} \tag{6.5.2.3}$$

We won't study in this thesis the harmonics of $\zeta^{(1)}$ and $\eta^{(1)}$ the way we did for $\zeta^{(0)}$ and $\eta^{(0)}$. The most interesting part of this equation is that a drifting term appears. Indeed, the zeroth harmonic of $U^{(1)}$ is not zero:

$$\begin{aligned} \frac{\partial(\tau_{xZ})_0^{(1)}}{\partial Z} =& \frac{\kappa_d Re^{(2)}}{2\kappa}\sum_{m=1}^{\infty}\left[\frac{1}{\sqrt{h}}\left(U_m^{(0)}(-im)(U_{-m}^{(0)} + U_{-m}^{(0)}(im)U_m^{(0)}\right)\right. \\ & \left. + \left(V_m^{(0)} - \frac{\kappa}{\kappa_d}\frac{dh}{dX}U_m^{(0)}\right)\frac{\partial U_{-m}^{(0)}}{\partial Z} + \left(V_{-m}^{(0)} - \frac{\kappa}{\kappa_d}\frac{dh}{dX}U_{-m}^{(0)}\right)\frac{\partial U_m^{(0)}}{\partial Z}\right] \end{aligned} \tag{6.5.2.4}$$

We can once again use the relation 6.2.0.14 applying for simple harmonic waves, and we obtain:

$$(\tau_{xZ})_m^{(1)} = \mu_m\frac{dU_m^{(1)}}{dZ} + O(\kappa^4) \tag{6.5.2.5}$$

as a consequence, equation 6.5.2.4 becomes:

$$\mu_0 \frac{\partial^2 U_0^{(1)}}{\partial Z^2} = \frac{\kappa_d Re^{(2)}}{2\kappa} \sum_{m=1}^{\infty} \left[\frac{1}{\sqrt{h}} \left(U_m^{(0)}(-im) U_{-m}^{(0)} + U_{-m}^{(0)}(im) U_m^{(0)} \right) \right.$$
$$\left. + + \left(V_m^{(0)} - \frac{\kappa}{\kappa_d} \frac{dh}{dX} U_m^{(0)} \right) \frac{\partial U_{-m}^{(0)}}{\partial Z} + \left(V_{-m}^{(0)} - \frac{\kappa}{\kappa_d} \frac{dh}{dX} U_{-m}^{(0)} \right) \frac{\partial U_m^{(0)}}{\partial Z} \right] \tag{6.5.2.6}$$

which can be simplified:

$$\frac{\partial^2 U_0^{(1)}}{\partial Z^2} = \frac{\kappa_d Re^{(2)}}{2\mu_0 \kappa} \sum_{m=1}^{\infty} \left[\left(V_m^{(0)} - \frac{\kappa}{\kappa_d} \frac{dh}{dX} U_m^{(0)} \right) \frac{\partial U_{-m}^{(0)}}{\partial Z} + \left(V_{-m}^{(0)} - \frac{\kappa}{\kappa_d} \frac{dh}{dX} U_{-m}^{(0)} \right) \frac{\partial U_m^{(0)}}{\partial Z} \right] \tag{6.5.2.7}$$

Knowing that $U_{-m}^{(0)} = (U_m^{(0)})^*$ and:

$$\left(V_{-m}^{(0)} - \frac{\kappa}{\kappa_d} \frac{dh}{dX} U_{-m}^{(0)} \right) = \left(V_m^{(0)} - \frac{\kappa}{\kappa_d} \frac{dh}{dX} U_m^{(0)} \right)^* \tag{6.5.2.8}$$

we obtain:

$$\frac{\partial^2 U_0^{(1)}}{\partial Z^2} = \frac{\kappa_d Re^{(2)}}{\mu_0 \kappa} \sum_{m=1}^{\infty} \Re \left[\left(V_{-m}^{(0)} - \frac{\kappa}{\kappa_d} \frac{dh}{dX} U_{-m}^{(0)} \right) \frac{\partial U_m^{(0)}}{\partial Z} \right] \tag{6.5.2.9}$$

Equation 6.5.2.9 will be integrated later to give $U_0^{(1)}$. We notice that this drift only appears at the order $O(\kappa)$, and is as a consequence small.

This equation is the same as the one we obtained in the flat case (equation 3.5.3.6), except that the vertical velocity $V_m^{(0)}$ is corrected by a term that accounts for the sloping bed.

6.6 Further details

6.6.1 Surface and the interface

Let us recall equation 6.5.1.31:

$$h^{1/4} \frac{dA_m}{dX} + \frac{h_X}{4h^{3/4}} A_m + \frac{\epsilon}{\kappa} \frac{3i}{8h^{5/4}} m \left[\sum_{l=1}^{\infty} 2A_l^* A_{m+l} + \sum_{l=1}^{[m/2]} \alpha_l A_l A_{m-l} \right]$$
$$+ \frac{\kappa_d}{\kappa} \frac{i\gamma}{2h^{5/4}} m \left[1 - \frac{\tanh(\tilde{\sigma}_m)}{\tilde{\sigma}_m} \right] A_m = 0 \tag{6.6.1.1}$$

Knowing that:

$$\sqrt{h}\frac{dA_m}{dX}+\frac{h_X}{4\sqrt{h}}A_m=\frac{d(h^{1/4}A_m)}{dX} \tag{6.6.1.2}$$

equation 6.6.1.1 becomes:

$$\begin{aligned}\frac{d(h^{1/4}A_m)}{dX}+\frac{\epsilon}{\kappa}\frac{3i}{8h^{5/4}}m\left[\sum_{l=1}^{\infty}2A_l^*A_{m+l}+\sum_{l=1}^{[m/2]}\alpha_l A_l A_{m-l}\right]\\ +\frac{\kappa_d}{\kappa}\frac{i\gamma}{2h^{5/4}}m\left[1-\frac{\tanh(\tilde{\sigma}_m)}{\tilde{\sigma}_m}\right]A_m=0\end{aligned} \tag{6.6.1.3}$$

By truncating the infinite series we get:

$$\begin{aligned}\frac{d(h^{1/4}A_m)}{dX}+\frac{\epsilon}{\kappa}\frac{3i}{8h^{5/4}}m\left[\sum_{l=1}^{n-m}2A_l^*A_{m+l}+\sum_{l=1}^{[m/2]}\alpha_l A_l A_{m-l}\right]\\ +\frac{\kappa_d}{\kappa}\frac{i\gamma}{2h^{5/4}}m\left[1-\frac{\tanh(\tilde{\sigma}_m)}{\tilde{\sigma}_m}\right]A_m=0\end{aligned} \tag{6.6.1.4}$$

The truncated differential system is true for $0<m\leq n$.

Once again, we note that equation 6.6.1.4 becomes equation 3.6.1.1 in the flat bottom particular case $h=1$.

6.6.2 Drift current in mud

We also truncate the result we got in 6.5.2.9 for the drifting in velocity:

$$\frac{\partial^2 U_0^{(1)}}{\partial Z^2}=\frac{\kappa_d Re^{(2)}}{\mu_0\kappa}\sum_{m=1}^{n}\Re\left[\left(V_{-m}^{(0)}-\frac{\kappa}{\kappa_d}\frac{dh}{dX}U_{-m}^{(0)}\right)\frac{\partial U_m^{(0)}}{\partial Z}\right] \tag{6.6.2.1}$$

In the end we get:

$$\frac{\partial U_m^{(0)}}{\partial Z}=\frac{\gamma A_m}{\sqrt{h}}[-\sigma_m\sinh(\sigma_m Z)+\sigma_m\tanh(\sigma_m)\cosh(\sigma_m Z)] \tag{6.6.2.2}$$

$$\left(V_{-m}^{(0)}-\frac{\kappa}{\kappa_d}\frac{dh}{dX}U_{-m}^{(0)}\right)=i\frac{m\gamma A_m^*}{\sigma_m^* h}[\sigma_m^* Z-\sinh(\sigma_m^* Z)+\tanh(\sigma_m^*)(\cosh(\sigma_m^* Z)-1)] \tag{6.6.2.3}$$

Combining 6.6.2.2, 6.6.2.3 and 6.6.2.1, we obtain:

$$\frac{\partial^2 U_0^{(1)}}{\partial Z^2} = \frac{\kappa_d Re^{(2)}}{\mu_0 \kappa h^{3/2}} \sum_{m=1}^{n} \Re\Big[i \frac{m\gamma A_m^*}{\tilde{\sigma}_m^*} [\tilde{\sigma}_m^* Z - \sinh(\tilde{\sigma}_m^* Z) + \tanh(\tilde{\sigma}_m^*)(\cosh(\tilde{\sigma}_m^* Z) - 1)] \\ \gamma A_m [-\tilde{\sigma}_m \sinh(\tilde{\sigma}_m Z) + \tilde{\sigma}_m \tanh(\tilde{\sigma}_m) \cosh(\tilde{\sigma}_m Z)] \Big] \tag{6.6.2.4}$$

which can be simplified to:

$$\frac{\partial^2 U_0^{(1)}}{\partial Z^2} = -\gamma^2 \frac{\kappa_d Re^{(2)}}{\mu_0 \kappa h^{3/2}} \sum_{m=1}^{n} |A_m|^2 \Im\Big[\frac{m}{\tilde{\sigma}_m^*} [\tilde{\sigma}_m^* Z - \sinh(\tilde{\sigma}_m^* Z) + \tanh(\tilde{\sigma}_m^*)(\cosh(\tilde{\sigma}_m^* Z) - 1)] \\ [-\tilde{\sigma}_m \sinh(\tilde{\sigma}_m Z) + \tilde{\sigma}_m \tanh(\tilde{\sigma}_m) \cosh(\tilde{\sigma}_m Z)] \Big] \tag{6.6.2.5}$$

Let us solve this equation to get the drift velocity.

$$\frac{\partial^2 U_0^{(1)}}{\partial Z^2} = -\sum_{m=1}^{n} |A_m|^2 \Big[\gamma^2 \frac{\kappa_d Re^{(2)}}{\mu_0 \kappa h^{3/2}} \Im\Big[\frac{m}{\tilde{\sigma}_m^*} \Big(-\tilde{\sigma}_m \tilde{\sigma}_m^* Z \sinh(\tilde{\sigma}_m Z) + \tilde{\sigma}_m \tilde{\sigma}_m^* Z \tanh(\tilde{\sigma}_m) \cosh(\tilde{\sigma}_m Z) \\ + \tilde{\sigma}_m \sinh(\tilde{\sigma}_m^* Z) \sinh(\tilde{\sigma}_m Z) - \tilde{\sigma}_m \tanh(\tilde{\sigma}_m) \sinh(\tilde{\sigma}_m^* Z) \cosh(\tilde{\sigma}_m Z) \\ - (\tanh(\tilde{\sigma}_m))^* \tilde{\sigma}_m \cosh(\tilde{\sigma}_m^* Z) \sinh(\tilde{\sigma}_m Z) \\ + \tilde{\sigma}_m \tanh(\tilde{\sigma}_m)(\tanh(\tilde{\sigma}_m))^* \cosh(\tilde{\sigma}_m Z) \cosh(\tilde{\sigma}_m^* Z) + (\tanh(\tilde{\sigma}_m))^* \tilde{\sigma}_m \sinh(\tilde{\sigma}_m Z) \\ - \tilde{\sigma}_m \tanh(\tilde{\sigma}_m)(\tanh(\tilde{\sigma}_m))^* \cosh(\tilde{\sigma}_m Z) \Big) \Big] \Big] \tag{6.6.2.6}$$

We write $\tilde{\sigma}_m = \tilde{\sigma}_m^R + i\tilde{\sigma}_m^I$, where $\tilde{\sigma}_m^R$ and $\tilde{\sigma}_m^I$ are real. Let us first integrate once. We use the fact that $\tilde{\sigma}_m + \tilde{\sigma}_m^* = 2\tilde{\sigma}_m^R$ and $\tilde{\sigma}_m - \tilde{\sigma}_m^* = 2i\tilde{\sigma}_m^I$:

$$\begin{aligned}
\frac{\partial U_0^{(1)}}{\partial Z} = &-\sum_{m=1}^{n} |A_m|^2 \Big[\gamma^2 \frac{\kappa_d Re^{(2)}}{\mu_0 \kappa h^{3/2}} \Im\Big[\frac{m}{\tilde{\sigma}_m^*}\Big[-\tilde{\sigma}_m^*\Big(Z\cosh(\tilde{\sigma}_m Z) - \frac{\sinh(\tilde{\sigma}_m Z)}{\tilde{\sigma}_m}\Big) \\
&+ \tilde{\sigma}_m^* \tanh(\tilde{\sigma}_m)\Big(Z\sinh(\tilde{\sigma}_m Z) - \frac{\cosh(\tilde{\sigma}_m Z)}{\tilde{\sigma}_m}\Big) \\
&+ \frac{\sinh(2\tilde{\sigma}_m^R Z)}{4\tilde{\sigma}_m^R}\tilde{\sigma}_m(1 + \tanh(\tilde{\sigma}_m)(\tanh(\tilde{\sigma}_m))^*) \\
&+ \frac{\sinh(2i\tilde{\sigma}_m^I Z)}{4i\tilde{\sigma}_m^I}\sigma_m(\tanh(\tilde{\sigma}_m)(\tanh(\tilde{\sigma}_m))^* - 1) \\
&- \frac{\cosh(2\tilde{\sigma}_m^R Z)}{4\tilde{\sigma}_m^R}\tilde{\sigma}_m(\tanh(\tilde{\sigma}_m) + (\tanh(\tilde{\sigma}_m))^*) \\
&+ \frac{\cosh(2i\tilde{\sigma}_m^I Z)}{4i\tilde{\sigma}_m^I}\tilde{\sigma}_m(\tanh(\tilde{\sigma}_m) - (\tanh(\tilde{\sigma}_m))^*) + (\tanh(\tilde{\sigma}_m))^*\cosh(\tilde{\sigma}_m Z) \\
&- \tanh(\tilde{\sigma}_m)(\tanh(\tilde{\sigma}_m))^*\sinh(\tilde{\sigma}_m Z)\Big]\Big] + C_m^{(1)}\Big]
\end{aligned} \tag{6.6.2.7}$$

with $C_m^{(1)}$ to be determined from to the boundary conditions. Integrating again, we get the expression of $U_0^{(1)}$:

$$\begin{aligned}
U_0^{(1)} = &-\sum_{m=1}^{n} |A_m|^2 \Big[\gamma^2 \frac{\kappa_d Re^{(2)}}{\mu_0 \kappa h^{3/2}} \Im\Big[\frac{m}{\tilde{\sigma}_m^*}\Big[-\tilde{\sigma}_m^*\Big(\frac{Z\sinh(\tilde{\sigma}_m Z)}{\tilde{\sigma}_m} - 2\frac{\cosh(\tilde{\sigma}_m Z)}{\tilde{\sigma}_m^2}\Big) \\
&+ \tilde{\sigma}_m^* \tanh(\tilde{\sigma}_m)\Big(\frac{Z\cosh(\tilde{\sigma}_m Z)}{\tilde{\sigma}_m} - 2\frac{\sinh(\tilde{\sigma}_m Z)}{\tilde{\sigma}_m^2}\Big) \\
&+ \frac{\cosh(2\tilde{\sigma}_m^R Z)}{4(\tilde{\sigma}_m^R)^2}\tilde{\sigma}_m(1 + \tanh(\tilde{\sigma}_m)(\tanh(\tilde{\sigma}_m))^*) \\
&+ \frac{\cosh(2i\tilde{\sigma}_m^I Z)}{8(\tilde{\sigma}_m^I)^2}\tilde{\sigma}_m(\tanh(\tilde{\sigma}_m)(\tanh(\tilde{\sigma}_m))^* - 1) \\
&- \frac{\sinh(2\tilde{\sigma}_m^R Z)}{8(\tilde{\sigma}_m^R)^2}\tilde{\sigma}_m(\tanh(\tilde{\sigma}_m) + (\tanh(\tilde{\sigma}_m))^*) \\
&+ \frac{\sinh(2i\tilde{\sigma}_m^I Z)}{8(\tilde{\sigma}_m^I)^2}\tilde{\sigma}_m(\tanh(\tilde{\sigma}_m) - (\tanh(\tilde{\sigma}_m))^*) + (\tanh(\tilde{\sigma}_m))^*\frac{\sinh(\tilde{\sigma}_m Z)}{\tilde{\sigma}_m} \\
&- \tanh(\tilde{\sigma}_m)(\tanh(\tilde{\sigma}_m))^*\frac{\cosh(\tilde{\sigma}_m Z)}{\tilde{\sigma}_m}\Big]\Big] + C_m^{(1)} Z + C_m^{(2)}\Big]
\end{aligned} \tag{6.6.2.8}$$

From equation 6.4.6.1, we know that:

$$U^{(1)}(Z = 0) = 0 \tag{6.6.2.9}$$

As a consequence, we deduce the value of $C_m^{(2)}$:

$$\begin{aligned} h^{3/2}C_m^{(2)} =&\gamma^2\frac{\kappa_d Re^{(2)}}{\mu_0\kappa}\Im\Big[\frac{m}{\tilde{\sigma}_m^*}\Big[-\frac{2\tilde{\sigma}_m^*}{\tilde{\sigma}_m^2}-\frac{\tilde{\sigma}_m(1+\tanh(\tilde{\sigma}_m)(\tanh(\tilde{\sigma}_m))^*)}{8(\tilde{\sigma}_m^R)^2} \\ &-\frac{\tilde{\sigma}_m(1-\tanh(\tilde{\sigma}_m)(\tanh(\tilde{\sigma}_m))^*)}{8(\tilde{\sigma}_m^I)^2}+\frac{\tanh(\tilde{\sigma}_m)(\tanh(\tilde{\sigma}_m))^*}{\tilde{\sigma}_m}\Big]\Big] \end{aligned} \tag{6.6.2.10}$$

We now make use of the interface boundary condition 6.4.5.11. From this equation, we know that:

$$(\tau_{xZ})^{(1)}(Z=1) = -\frac{\epsilon}{\kappa}\eta^{(0)}\frac{\partial(\tau_{xZ})^{(0)}}{\partial Z}\Big|_{Z=1} \tag{6.6.2.11}$$

and so:

$$(\tau_{xZ})_0^{(1)}(Z=1) = -\frac{\epsilon}{\kappa}\frac{1}{4}\sum_{m=1}^{\infty}\left[B_m\frac{\partial(\tau_{xZ})_{-m}^{(0)}}{\partial Z}\Big|_{Z=1}+B_{-m}\frac{\partial(\tau_{xZ})_m^{(0)}}{\partial Z}\Big|_{Z=1}\right] \tag{6.6.2.12}$$

From equation 6.2.0.14, which only applies to simple harmonic waves, we know:

$$\forall p, (\tau_{xZ})_m^{(p)} = \mu_m\frac{dU_m^{(p)}}{dZ}+O(\kappa^4) \tag{6.6.2.13}$$

can replace τ_{xZ} in this last equation:

$$\begin{aligned} \mu_0\frac{\partial U_0^{(1)}}{\partial Z}\Big|_{Z=1} &= -\frac{\epsilon}{\kappa}\frac{1}{4}\sum_{m=1}^{\infty}\left[B_m\mu_{-m}\frac{\partial^2 U_{-m}^{(0)}}{\partial Z^2}\Big|_{Z=1}+B_{-m}\mu_m\frac{\partial^2 U_m^{(0)}}{\partial Z^2}\Big|_{Z=1}\right] \\ &= -\frac{\epsilon}{\kappa}\frac{1}{4}\sum_{m=1}^{\infty}\left[B_m\Big(\mu_m\frac{\partial^2 U_m^{(0)}}{\partial Z^2}\Big|_{Z=1}\Big)^*+(B_m)^*\mu_m\frac{\partial^2 U_m^{(0)}}{\partial Z^2}\Big|_{Z=1}\right] \\ &= -\frac{\epsilon}{\kappa}\frac{1}{2}\sum_{m=1}^{\infty}\Re\left[B_m\Big(\mu_m\frac{\partial^2 U_m^{(0)}}{\partial Z^2}\Big|_{Z=1}\Big)^*\right] \end{aligned} \tag{6.6.2.14}$$

Knowing that:

$$B_m = \frac{\gamma A_m}{h}G(\tilde{\sigma}_m) \tag{6.6.2.15}$$

and:

$$\frac{\partial^2 U_m^{(0)}}{\partial Z^2}\Big|_{Z=1} = -\frac{\gamma A_m}{\sqrt{h}}\tilde{\sigma}_m^2\mathrm{sech}(\tilde{\sigma}_m) \tag{6.6.2.16}$$

equation 2.6.2.12 becomes:

$$\begin{aligned}\frac{\partial U_0^{(1)}}{\partial Z}|_{Z=1} &= \frac{\epsilon}{\kappa\mu_0}\frac{1}{h^{3/2}}\frac{1}{2}\sum_{m=1}^{\infty}\Re\left[\gamma A_m G(\tilde{\sigma}_m)\mu_m^*\gamma A_m^*(\tilde{\sigma}_m^*)^2\mathrm{sech}(\tilde{\sigma}_m^*)\right] \\ &= \frac{\epsilon\gamma^2}{2\kappa\mu_0}\frac{1}{h^{3/2}}\sum_{m=1}^{\infty}|A_m|^2\Re\left[G(\tilde{\sigma}_m)\mu_m^*(\tilde{\sigma}_m^*)^2\mathrm{sech}(\tilde{\sigma}_m^*)\right] \qquad (6.6.2.17) \\ &= \frac{\epsilon\gamma^2}{2\kappa\mu_0}\frac{1}{h^{3/2}}\sum_{m=1}^{\infty}|A_m|^2\Im\left[iG(\tilde{\sigma}_m)\mu_m^*(\tilde{\sigma}_m^*)^2\mathrm{sech}(\tilde{\sigma}_m^*)\right]\end{aligned}$$

Let us truncate this last equation:

$$\frac{\partial U_0^{(1)}}{\partial Z}|_{(Z=1)} = \frac{\epsilon\gamma^2}{2\kappa\mu_0}\frac{1}{h^{3/2}}\sum_{m=1}^{n}|A_m|^2\Im\left[iG(\tilde{\sigma}_m)\mu_m^*(\tilde{\sigma}_m^*)^2\mathrm{sech}(\tilde{\sigma}_m^*)\right] \qquad (6.6.2.18)$$

From equation 6.6.2.7, we deduce the condition that $C_m^{(1)}$ needs to meet in order to respect this boundary condition:

$$\begin{aligned}&-\gamma^2\frac{Re^{(2)}\kappa_d}{\mu_0\kappa h^{3/2}}\Im\Big[\frac{m}{\tilde{\sigma}_m^*}\Big(\tilde{\sigma}_m^*\Big(\cosh(\tilde{\sigma}_m)-\frac{\sinh(\tilde{\sigma}_m)}{\tilde{\sigma}_m}\Big)-\sigma_m^*\tanh(\sigma_m)\Big(\sinh(\tilde{\sigma}_m)-\frac{\cosh(\tilde{\sigma}_m)}{\tilde{\sigma}_m}\Big) \\ &\quad-\frac{\sinh(2\tilde{\sigma}_m^R)}{4\tilde{\sigma}_m^R}\tilde{\sigma}_m(1+\tanh(\tilde{\sigma}_m)(\tanh(\tilde{\sigma}_m))^*) \\ &\quad-\frac{\sinh(2i\tilde{\sigma}_m^I)}{4i\tilde{\sigma}_m^I}\tilde{\sigma}_m(\tanh(\tilde{\sigma}_m)(\tanh(\tilde{\sigma}_m))^*-1) \\ &\quad+\frac{\cosh(2\tilde{\sigma}_m^R)}{4\tilde{\sigma}_m^R}\tilde{\sigma}_m(\tanh(\tilde{\sigma}_m)+(\tanh(\tilde{\sigma}_m))^*) \\ &\quad-\frac{\cosh(2i\tilde{\sigma}_m^I)}{4i\tilde{\sigma}_m^I}\tilde{\sigma}_m(\tanh(\tilde{\sigma}_m)-(\tanh(\tilde{\sigma}_m))^*) \\ &\quad-(\tanh(\tilde{\sigma}_m))^*\cosh(\tilde{\sigma}_m)+\tanh(\tilde{\sigma}_m)(\tanh(\tilde{\sigma}_m))^*\sinh(\tilde{\sigma}_m)\Big)\Big]-C_m^{(1)} \\ &=\frac{\epsilon\gamma^2}{2\kappa\mu_0}\frac{1}{h^{3/2}}\Im\left[iG(\tilde{\sigma}_m)\mu_m^*(\tilde{\sigma}_m^*)^2\mathrm{sech}(\tilde{\sigma}_m^*)\right]\end{aligned} \qquad (6.6.2.19)$$

We finally obtain the value of $C_m^{(1)}$:

$$\begin{aligned}
h^{3/2}C_m^{(1)} = &-\frac{\epsilon\gamma^2}{2\kappa\mu_0}\Im\left[iG(\tilde{\sigma}_m)\mu_m^*(\tilde{\sigma}_m^*)^2\mathrm{sech}(\tilde{\sigma}_m^*)\right] \\
&+\gamma^2\frac{Re^{(2)}\kappa_d}{\mu_0\kappa}\Im\Big[\frac{m}{\tilde{\sigma}_m^*}\Big[\tilde{\sigma}_m^*\Big(\cosh(\tilde{\sigma}_m)-\frac{\sinh(\tilde{\sigma}_m)}{\tilde{\sigma}_m}\Big) \\
&-\tilde{\sigma}_m^*\tanh(\tilde{\sigma}_m)\Big(\sinh(\tilde{\sigma}_m)-\frac{\cosh(\tilde{\sigma}_m)}{\tilde{\sigma}_m}\Big) \\
&-\frac{\sinh(2\tilde{\sigma}_m^R)}{4\tilde{\sigma}_m^R}\tilde{\sigma}_m(1+\tanh(\tilde{\sigma}_m)(\tanh(\tilde{\sigma}a_m))^*) \\
&-\frac{\sinh(2i\tilde{\sigma}_m^I)}{4i\tilde{\sigma}_m^I}\tilde{\sigma}_m(\tanh(\tilde{\sigma}_m)(\tanh(\tilde{\sigma}_m))^*-1) \\
&+\frac{\cosh(2\tilde{\sigma}_m^R)}{4\tilde{\sigma}_m^R}\tilde{\sigma}_m(\tanh(\tilde{\sigma}_m)+(\tanh(\tilde{\sigma}_m))^*) \\
&-\frac{\cosh(2i\tilde{\sigma}_m^I)}{4i\tilde{\sigma}_m^I}\tilde{\sigma}_m(\tanh(\tilde{\sigma}_m)-(\tanh(\tilde{\sigma}_m))^*) \\
&-(\tanh(\tilde{\sigma}_m))^*\cosh(\tilde{\sigma}_m)+\tanh(\tilde{\sigma}_m)(\tanh(\tilde{\sigma}_m))^*\sinh(\tilde{\sigma}_m)\Big]\Big]
\end{aligned} \tag{6.6.2.20}$$

The drift current is now found.

We observe once again that $U_0^{(1)}$ reduces to what we found in the flat bottom case (equation 3.6.2.5) in the special case $h(x)=1$. Actually, the drift is the same as the one we found in the flat bottom case, except for the $h^{-3/2}$ coefficient.

6.6.3 Energy variation

We found the differential equation 6.6.1.4:

$$\begin{aligned}
&\frac{d(h^{1/4}A_m)}{dX}+\frac{3i}{8}\beta m\frac{1}{h^{5/4}}\left(\sum_{l=1}^{\infty}2A_l^*A_{m+l}+\sum_{l=1}^{[m/2]}\alpha_l A_l A_{m-l}\right) \\
&\qquad+h^{-5/4}\frac{\kappa_d}{\kappa}\frac{i\gamma}{2}m\left(1-\frac{\tanh(\tilde{\sigma}_m)}{\tilde{\sigma}_m}\right)A_m=0
\end{aligned} \tag{6.6.3.1}$$

We introduce $\tilde{A}_m=h^{1/4}A_m$, and modify equation 6.6.3.1 as:

$$\begin{aligned}
&\frac{d\tilde{A}_m}{dX}+\frac{3i}{8}\beta m\frac{1}{h^{7/4}}\left(\sum_{l=1}^{\infty}2\tilde{A}_l^*\tilde{A}_{m+l}+\sum_{l=1}^{[m/2]}\alpha_l\tilde{A}_l\tilde{A}_{m-l}\right) \\
&\qquad+h^{-3/2}\frac{\kappa_d}{\kappa}\frac{i\gamma}{2}m\left(1-\frac{\tanh(\tilde{\sigma}_m)}{\tilde{\sigma}_m}\right)\tilde{A}_m=0
\end{aligned} \tag{6.6.3.2}$$

Using the same demonstration as in the flat case, we easily deduce the variation law:

$$\frac{d}{dX}\left[\sum_{m=1}^{n}|\tilde{A}_m|^2\right] = -2h^{-3/2}\frac{\kappa_d}{\kappa}\sum_{m=1}^{n} Re\left[\frac{i\gamma}{2}m\left(1-\frac{\tanh(\tilde{\sigma}_m)}{\tilde{\sigma}_m}\right)\right]|\tilde{A}_m|^2 \qquad (6.6.3.3)$$

and we then obtain the energy variation relation:

$$\boxed{\frac{d}{dX}\left[\sqrt{h}\sum_{m=1}^{n}|A_m|^2\right] = -\frac{\gamma}{h}\frac{\kappa_d}{\kappa}\sum_{m=1}^{n} Re\left[im\left(1-\frac{\tanh(\tilde{\sigma}_m)}{\tilde{\sigma}_m}\right)\right]|A_m|^2} \qquad (6.6.3.4)$$

6.6.4 Behavior at the shore

Let us study the evolution of $|A_m|$ towards the shore, that is to say towards $h = 0$. In this study, we will consider that the water depth decreases as X increases. In other words $h_X < 0$.

Let us first study the attenuation rate of the different harmonics $|A_m|$. We already showed in chapter 3 that the attenuation rate for each harmonic is:

$$\frac{1}{L_m} = -\gamma\frac{\kappa_d}{\kappa}\Im\left[m\left(1-\frac{\tanh(\tilde{\sigma}_m)}{\tilde{\sigma}_m}\right)\right] \qquad (6.6.4.1)$$

and we plotted some examples. Let us recall our results and give more details. Figures 6-3 and 6-4 show the attenuation rates of the eight first harmonics $|A_m|$ for the 4 types of muds and for 2 different values of $\bar{h}$. We deduce from these figures that, in the κ and $\bar{h}$-ranges in which we are interested, the attenuation rate of the first harmonic is most of the time the smallest. The only case in which $1/L_1$ is not the smallest, then $1/L_5$ is the smallest.

As a consequence, one harmonic always decays last. Let us prove that this harmonic decays to zero, and we will have proven that all harmonics decay to zero at the shore. Let us call A_{dom} this harmonic.

Let us consider X_0 such as $\forall X > X_0$, all the A_m are negligible compared to A_{dom}. Such an X_0 exists because the attenuation rate of A_{dom} is the smallest.

Ignoring all modes $m \neq dom$, let us rewrite equation 6.6.3.4 for $|A_{dom}|^2$ only:

$$\frac{d}{dX}\left[\sqrt{h}|A_{dom}|^2\right] = -\frac{1}{h}\frac{|A_{dom}|^2}{L_{dom}} \qquad (6.6.4.2)$$

Let us write $\tilde{A}_{dom}$ such as:

$$\tilde{A}_{dom} = h^{1/4}A_{dom} \qquad (6.6.4.3)$$

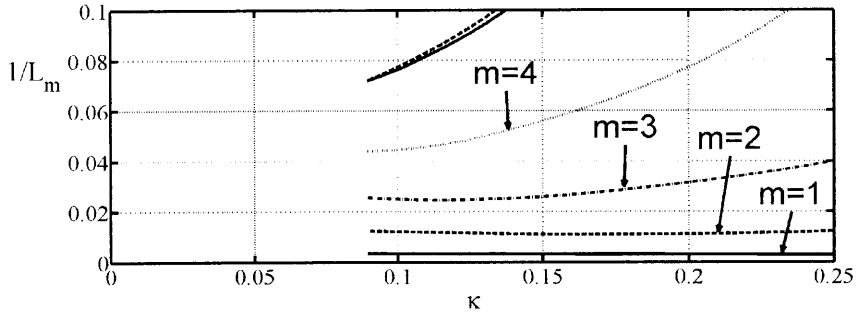

(a) Gulf of Mexico mud

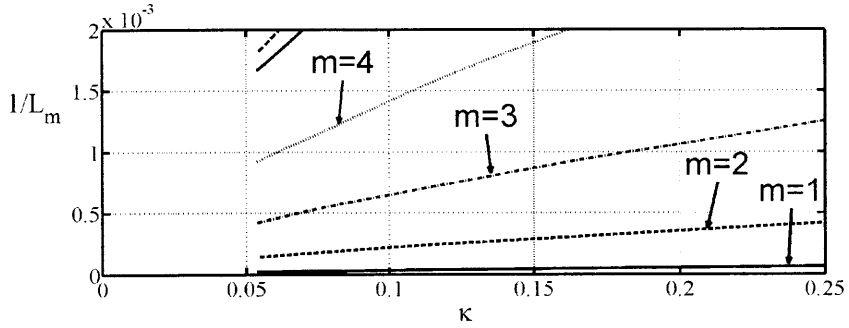

(b) Mobile Bay mud

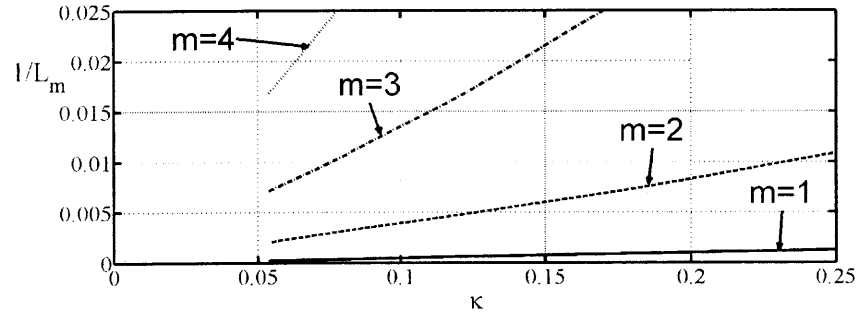

(c) Lianyungang mud

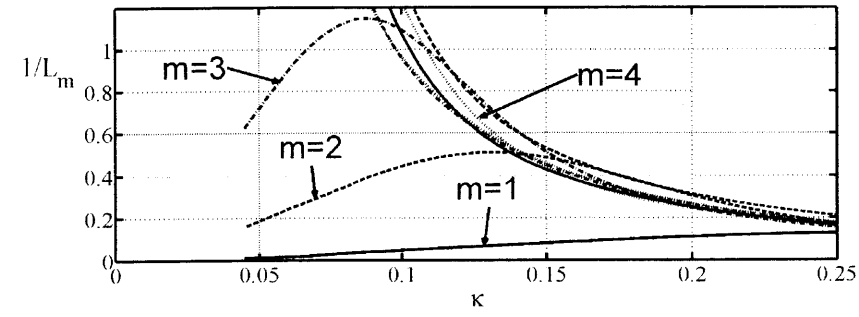

(d) Hangzhou Bay mud

Figure 6-3: Attenuation rates of the first ten harmonics, $\bar{h} = 2\text{m}$, $\kappa_d = 0.1$.

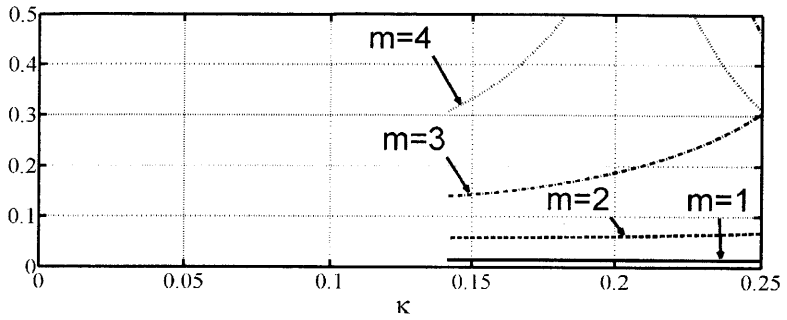

(a) Gulf of Mexico mud

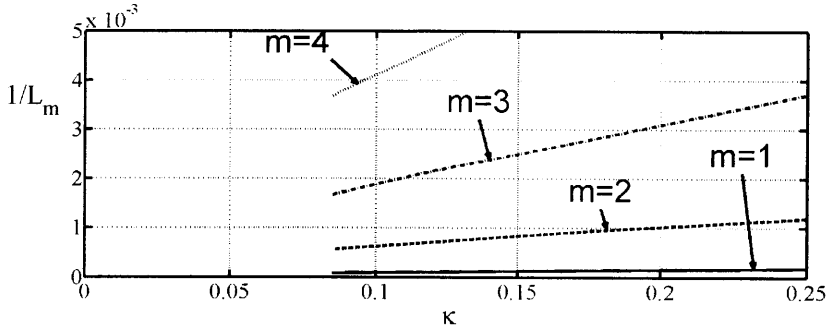

(b) Mobile Bay mud

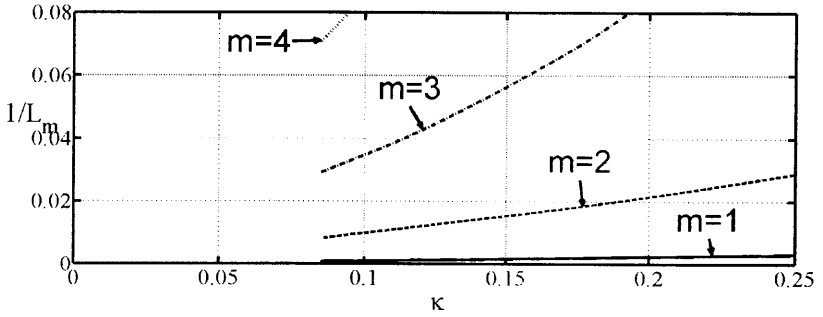

(c) Lianyungang mud

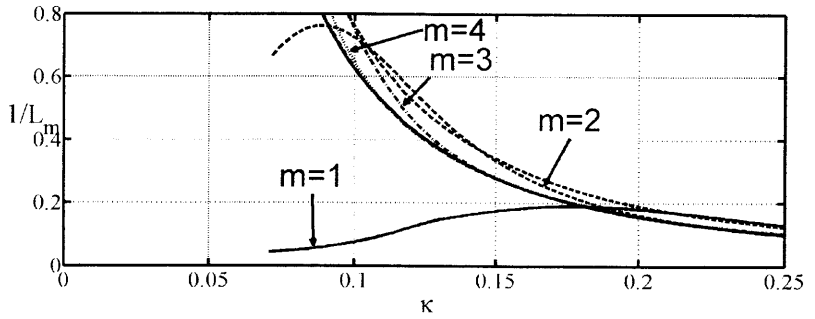

(d) Hangzhou Bay mud

Figure 6-4: Attenuation rates of the first ten harmonics, $\bar{h} = 5\text{m}$, $\kappa_d = 0.1$.

Then equation 6.6.4.2 becomes:

$$\frac{d|\tilde{A}_{dom}|^2}{dX} = -\frac{1}{h^{3/2}}\frac{|\tilde{A}_{dom}|^2}{L_{dom}} \tag{6.6.4.4}$$

Since the aim of this study is to consider the behavior very close to the shore, the beach can be approximated as a plane beach. We choose s such as $h(X) = 1 - sX$, and thus $h_X = -s$. The solution of this equation is:

$$|\tilde{A}_{dom}|^2 = \alpha_{dom} \exp\Big[-\frac{2}{L_{dom}}\frac{h^{-1/2}}{s}\Big] \tag{6.6.4.5}$$

With α_{dom} a real constant. And thus:

$$|A_{dom}|^2 = \frac{\alpha_{dom}}{h^{1/2}} \exp\Big[-\frac{2}{L_{dom}}\frac{h^{-1/2}}{s}\Big] \tag{6.6.4.6}$$

Since $L_{dom} > 0$ and $h^{-1/2}$ is a growing function of X, we deduce that $|A_{dom}|^2 \to 0$ exponentially as $h \to 0$.

Since A_{dom} is the dominant harmonic, and all the others are negligible, we deduce that: $\boxed{\text{all harmonics } |A_m|^2 \to 0 \text{ exponentially as } h \to 0}$.

Let us now study the interface harmonics B_m. From equation 6.5.1.30, we know that:

$$\forall m, \quad \boxed{B_m(X) = \frac{\gamma A_m}{h}\Big[1 - \frac{\tanh(\tilde{\sigma}_m)}{\tilde{\sigma}_m}\Big]} \tag{6.6.4.7}$$

As a consequence, by multiplying 6.6.4.7 to its complex conjugate:

$$\forall m, \quad |B_m|^2 = \frac{\gamma|A_m|^2}{h^2}\Big|1 - \frac{\tanh(\tilde{\sigma}_m)}{\tilde{\sigma}_m}\Big|^2 \tag{6.6.4.8}$$

And we deduce from the previous result on the $|A_m|^2$ that $|B_m|^2 \to 0$ exponentially as $h \to 0$.

Let us now study the drift current $U_0^{(1)}$. From equation 6.6.2.8, we can write $U_0^{(1)}$ as:

$$U_0^{(1)}(X,Z) = \frac{1}{h(X)^{3/2}}\sum_{m=1}^{n}|A_m|^2(X)f_m(Z) \tag{6.6.4.9}$$

where $f_m(Z)$ is a complex function of Z with finite values. Knowing that $|A_m|^2 \to 0$ exponentially when $h \to 0$, we deduce that $|A_m|^2/h^{3/2}$ also goes to zero exponentially as $h \to 0$. In the end, we deduce that $U_0^{(1)} \to 0$ exponentially when $h \to 0$.

6.7 Numerical results by using the first ten harmonics

We now solve this equation in the particular case:

$$\begin{aligned} h(X) &= 1, \quad 0 < X \\ h(X) &= 1 - sX, \quad 0 < X < 1/s \\ h(X) &= 0, \quad X > 1/s \end{aligned} \tag{6.7.0.10}$$

corresponding to:

$$\begin{aligned} h_X &= 0, \quad 0 < X \\ h_X &= -s, \quad 0 < X < 1/s \\ h_X &= 0, \quad X > 1/s \end{aligned} \tag{6.7.0.11}$$

We are going to plot these results for the viscoelastic muds we previously studied.

Let us sum up the different muds we have:

- Case A: Gulf of Mexico mud. This mud is rather elastic.
- Case B: Mobile Bay mud. This mud is rather elastic as well
- Case C: Lianyungang mud. This mud complex viscosity's phase is around $\frac{\pi}{4}$ so it is as elastic as viscous.
- Case D: Hangzhou Bay mud. This mud is rather viscous, its complex viscosity's phase being close to zero.

6.7.1 Comparison of the different types of mud

We first look at the results for four types of mud in the case $\bar{h} = 2\text{m}$, $A = 0.4\text{m}$, $d = 0.2\text{m}$ and $\omega' = 0.5\text{rad/s}$. (corresponding to the case 1b of the previous chapter). These values correspond to $\epsilon = 0.2$, $\kappa = 0.22$ and $\kappa_d = 0.1$. The slope is $s' = 0.01$, corresponding to $s = s'/\kappa^2 = 1/5$. So for all this section:

$$\boxed{\epsilon = 0.2,\ \kappa = 0.22,\ \kappa_d = 0.1,\ s = 0.2} \tag{6.7.1.1}$$

Surface and interface

Computations have been carried out for 10 harmonics. In figures 6-5 and 6-7, we present the variation of the first three harmonics of the surface and the interface.

Warning: the scales are not the same for every mud.

In figure 6-5, it can be observed that damping is stronger for the Gulf of Mexico, Lianyungang and Hangzhou Bay (A, C, D) than for the Mobile Bay mud (B). This result is consistent with the previous chapter for horizontal sea bed.

We also observe that for the Hangzhou Bay mud, the $|A_m|$ have more oscillations than for the Gulf of Mexico and Lianyungang muds, even though the damping lengthscale is comparable for these three muds.

We only plot the surface motion up to $X = 4.6$ for the Mobile Bay mud, because numerical accuracy does not allow us to go to higher values of X without strong oscillations appearing. However, we show in figure 6-6 a zoom-in of the interface variation for this mud at the shore. This figure allows us to see that the surface motion eventually reaches a zero-value at the shore.

Figure 6-7 shows the variation of the interfaces. The results confirm what we previously saw. In the cases of muds A, C and D, where the damping is significant, the interface motion is stronger than for the Mobile Bay mud (B). The variation of the interface is the most pronounced for the Hangzhou Bay mud. This is due to the fact that, as seen in chapter 3, the value of κ corresponds to resonance.

Figure 6-8 gives a zoom of the interface motion for the Gulf of Mexico, Mobile Bay and the Lianyungang muds. These zoomed figures allow us to see that the $|B_m|$ always go to zero at the shore, which is what we demonstrated in the previous section.

Drift

Figure 6-9 represents the drift we calculated in equation 6.6.2.8. As in chapters 2 and 3, the drift current is a sum of the $|A_m|^2$ multiplied by coefficients. As a consequence, the shape of the $|A_m|$ directly influences the drift current shape.

Let us remind the equations:

$$\begin{aligned} U &= U^{(0)} + \kappa U^{(1)} + O(\kappa^2) \\ U^{(1)} &= \frac{1}{2}U_0^{(1)} + \frac{1}{2}\sum_{m=1}^{\infty}\left(U_m^{(1)}e^{i\theta_m} + cc.\right) \end{aligned} \tag{6.7.1.2}$$

This is why we represent the value $\frac{1}{2}\kappa U_0^{(1)}$, because it is the value that appears in the total sum of U.

Once again, the results presented in this figure confirm the effect we previously described: the damping is strong for muds A and D. As a consequence, there mud motion is stronger, and in particular the drift current is stronger. The drift current

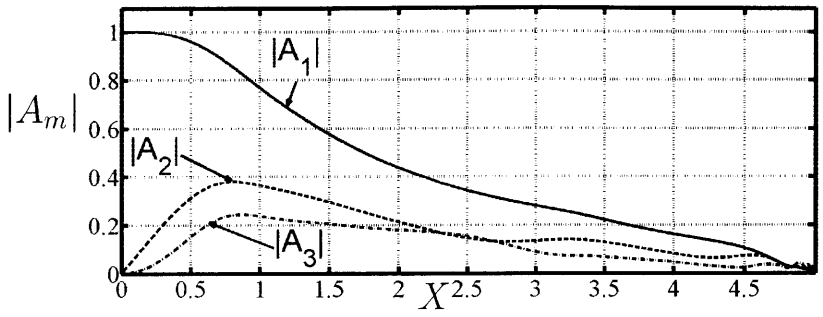

(a) Gulf of Mexico mud

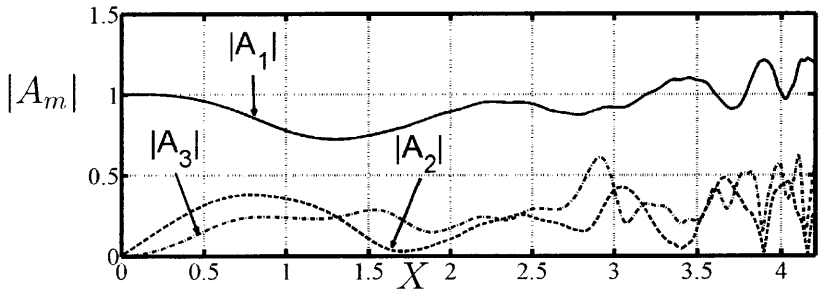

(b) Mobile Bay mud

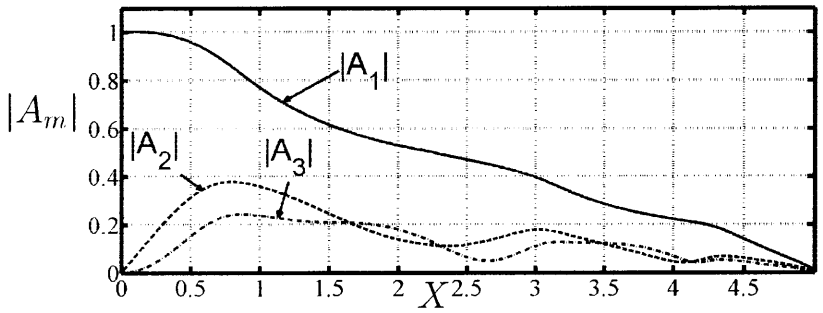

(c) Lianyungang mud

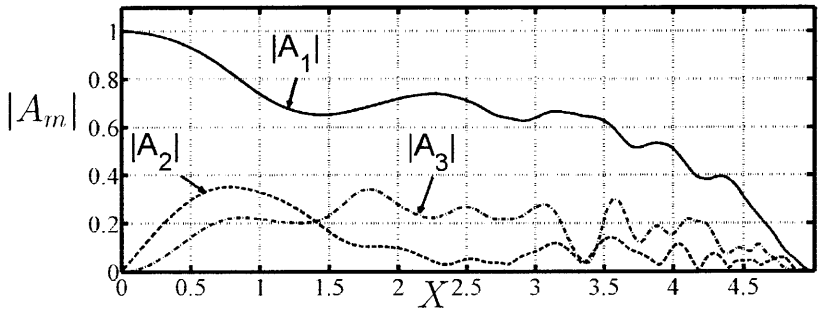

(d) Hangzhou Bay mud

Figure 6-5: Evolution of the first 3 harmonics of the free surface over different types of viscoelastic muddy seabeds. Warning: the horizontal and vertical scales are different for mud B.

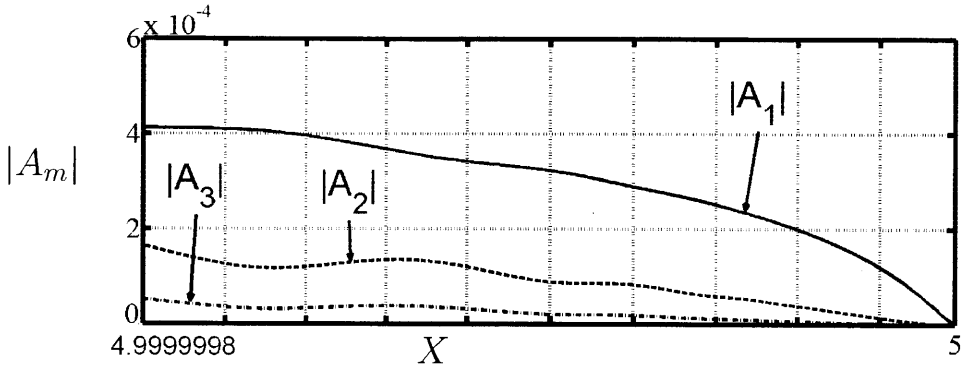

Figure 6-6: Zoom-in of the surface motion for the Mobile Bay mud.

is smaller for the Lianyungang mud, and very small for the Mobile Bay mud.

We note the presence of oscillations in the drift current for the Hangzhou Bay mud (D). We already noticed these oscillations for the same mud in the $|A_m|$ in the previous section. As we said, the drift current is a sum of the $|A_m|^2$ multiplied by coefficients. As a consequence, if the $|A_m|$ show oscillations, it is logical for the drift current to also show oscillations.

Let us compare this figure 6-9 to what we obtained in the flat case with the same values of ϵ, κ and κ_d, that is to say figure 3-20. The initial values of the drift current at $X = 0$ are the same for all muds in the flat and sloping seabed cases. Indeed, the initial values of the harmonics are the same: $|A_1(X = 0)| = 1$ and $\forall m > 1, |A_m(X = 0)| = 0$, and $h(X = 0) = 1$, so the drift values should be the same.

We also observe that the drift current for the Gulf of Mexico mud (A) has the same pattern. However, its peak value is twice bigger in the sloping bottom case. This is due to the fact that the drift in the sloping case is the drift in the flat case divided by $h(X)^{3/2}$, and $h(X) < 1$.

The Mobile Bay mud (B) has a very small drift in both flat and sloping seabed cases.

The Lianyungang mud (C) also has the same pattern in the flat and the sloping bottom cases. It has a peak occurring at the same rough value of X: $X = 1.5$, but this peak value is around 50 times smaller than the Gulf of Mexico mud peak. This confirms the fact that damping is stronger for the Gulf of Mexico mud, and hence the drift current also stronger.

Finally, the Hangzhou Bay mud (D) has small oscillations in both cases, because the $|A_m|$ have small oscillations as well. In the flat case, the drift current for D is the one that is damped the most slowly. In the sloping case, because the drift includes this $h(X)^{-3/2}$ term, the drift current reaches higher values than in the flat case. It

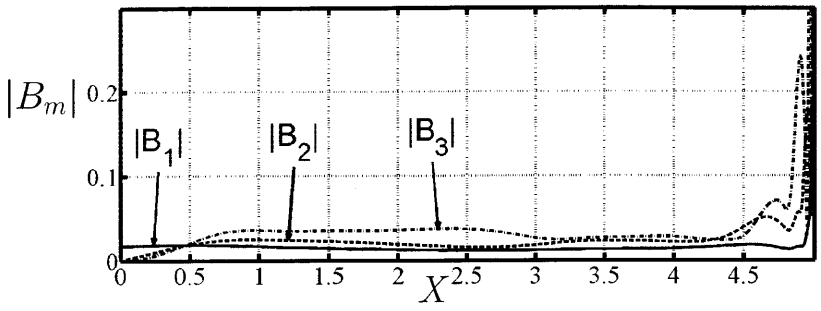

(a) Gulf of Mexico mud

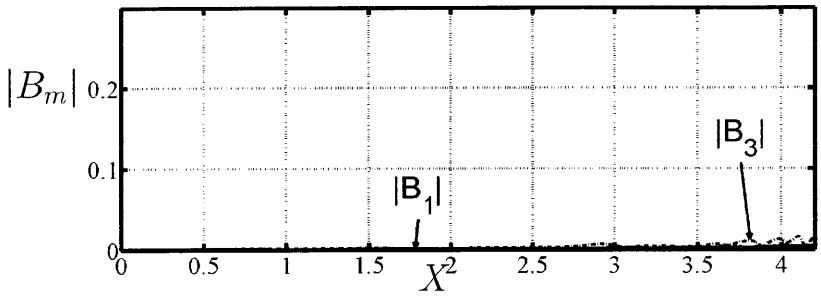

(b) Mobile Bay mud

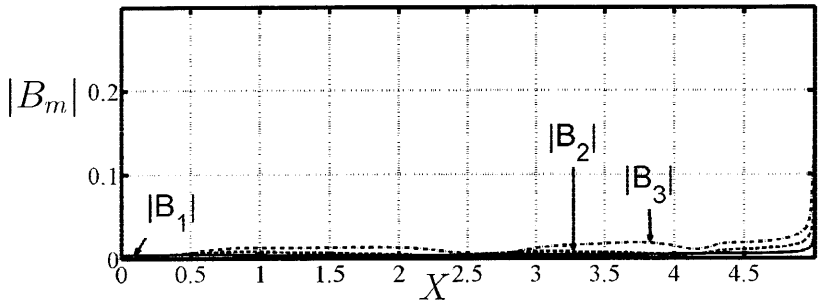

(c) Lianyungang mud

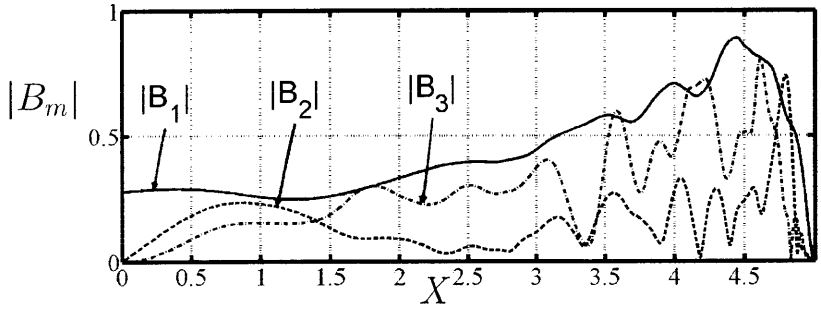

(d) Hangzhou Bay mud

Figure 6-7: Evolution of the first 3 harmonics of the interface over different types of viscoelastic muddy seabeds. Warning: the vertical scale is different for mud D and the horizontal scale is different for mud B.

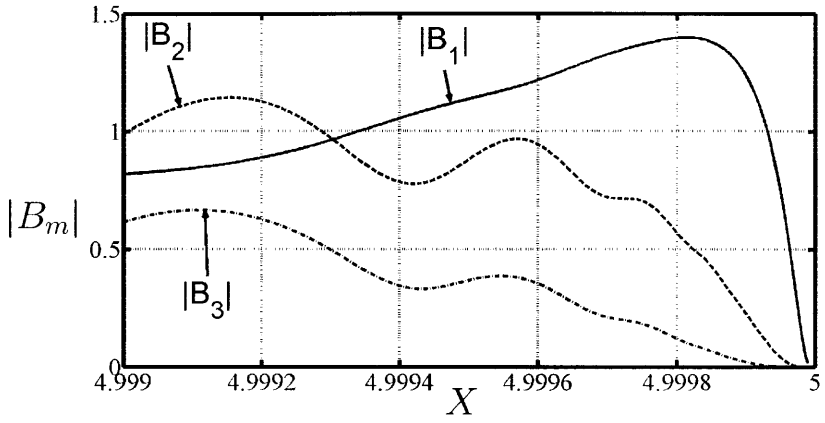

(a) Gulf of Mexico mud

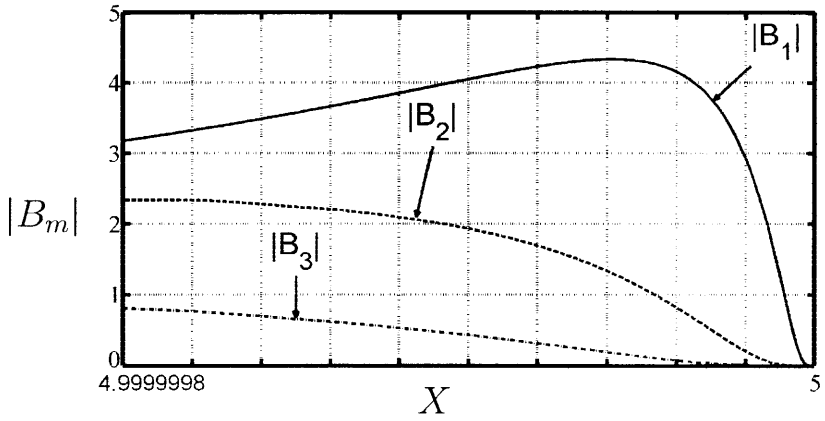

(b) Mobile Bay mud

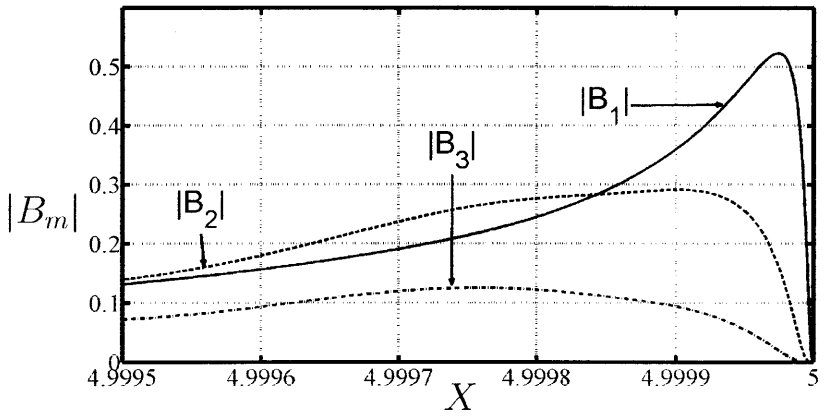

(c) Lianyungang mud

Figure 6-8: Evolution of the first 3 harmonics of the interface near the shore for the Gulf of Mexico, Mobile Bay and the Lianyungang muds.

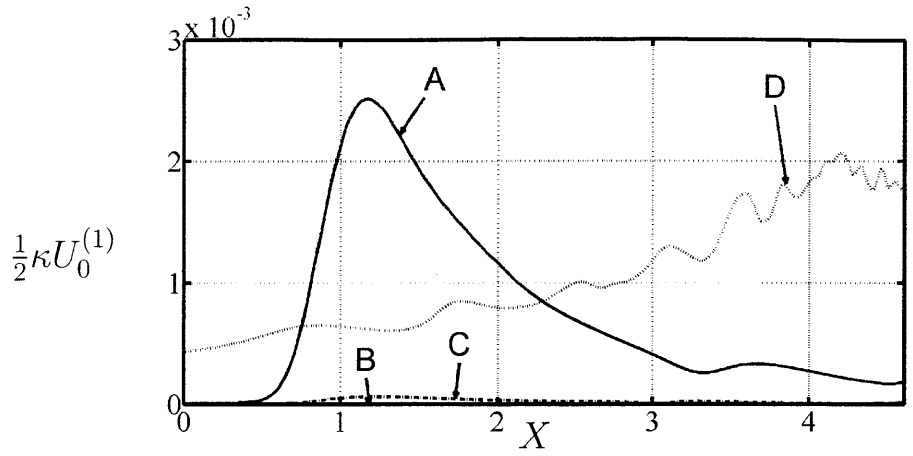

Figure 6-9: Drift velocity $\frac{1}{2}\kappa U_0^{(1)}$. Mud A is Gulf of Mexico mud, mud B is Mobile Bay mud, mud C is Lianyungang mud and mud D is Hangzhou Bay mud. $\kappa = 0.22$.

increases until $X = 4.6$.

We only show the plot up to $X = 4.6$ because strong oscillations appear after that in the Mobile Bay drift current. However, figure 6-10 offers a zoom-in of the drift currents near the shore for each mud. This important figure shows that all drift current eventually reach a zero-value. Since this is what we analytically predicted in section 6.6.4, we obtain that numerical and analytical results agree.

Energy variation

We numerically represented the total first-order energies in figure 6-11. This figure shows that the total energy logically decreases, to reach a zero-value at the shore ($X = 5$). However, we observe once again that dissipation is slower to occur in the Mobile Bay mud (B).

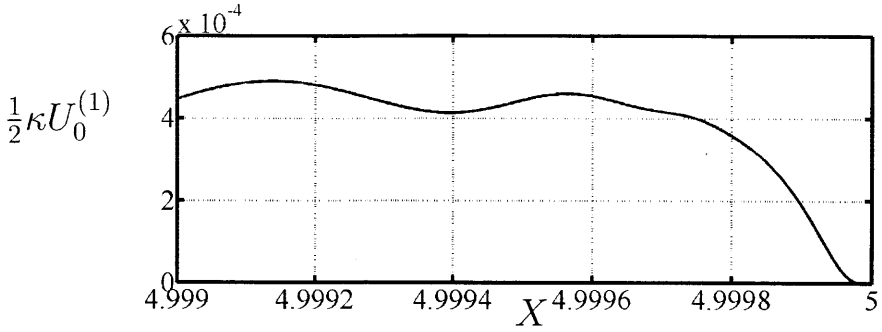

(a) Gulf of Mexico mud

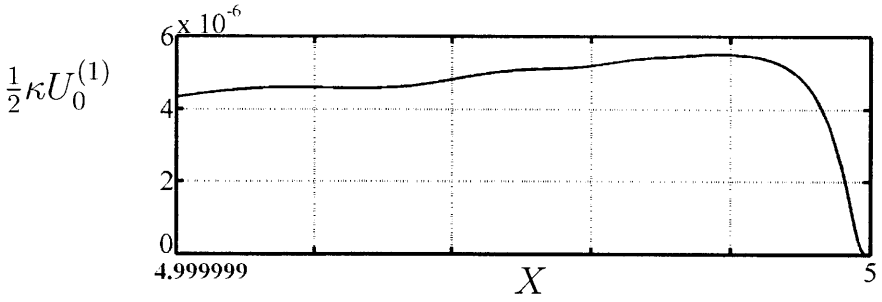

(b) Mobile Bay mud

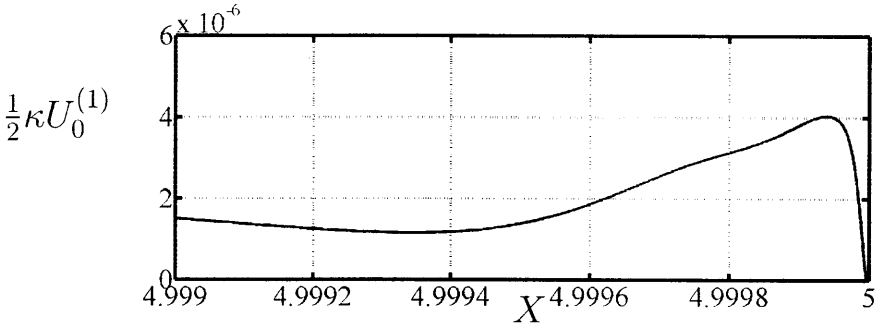

(c) Lianyungang mud

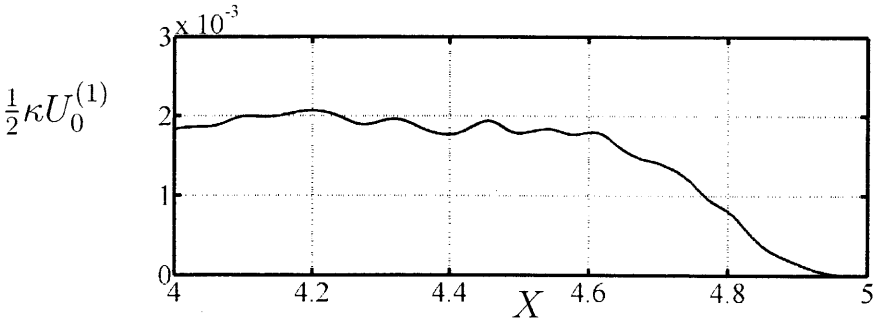

(d) Hangzhou Bay mud

Figure 6-10: Zoom-in of the drift velocity $\frac{1}{2}\kappa U_0^{(1)}$ next to the shore for all muds. $\kappa = 0.22$.

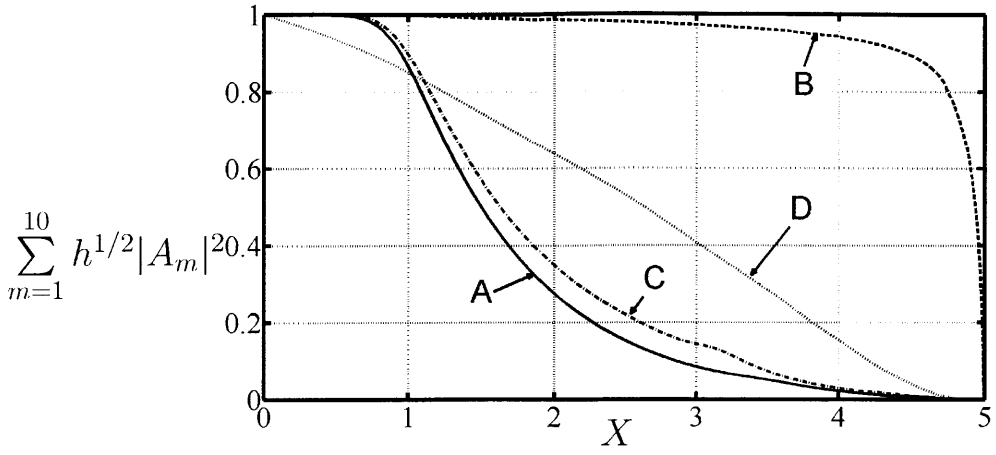

Figure 6-11: Wave energy over a flat thick muddy seabed. Mud A is Gulf of Mexico mud, mud B is Mobile Bay mud, mud C is Lianyungang mud and mud D is Hangzhou Bay mud.

6.7.2 Influence of the slope s'

We now focus on the influence of the slope. We look at the slope values $s' = 0.048$, $s' = 0.024$, $s' = 0.012$, $s' = 0.008$, $s' = 0.0048$ and $s' = 0.0024$, respectively corresponding the non dimensional slope values:

$$\boxed{s = 1,\ s = 1/2,\ s = 1/4,\ s = 1/6,\ s = 1/10,\ s = 1/20} \tag{6.7.2.1}$$

We still have $\bar{h} = 2\text{m}$, $A = 0.4\text{m}$, $d = 0.2\text{m}$ and $\omega = 0.5\text{rad/s}$. These values still correspond to:

$$\boxed{\epsilon = 0.2,\ \kappa = 0.22,\ \kappa_d = 0.1} \tag{6.7.2.2}$$

We particularly focus on the Gulf of Mexico mud (A) and the Hangzhou Bay mud (D), because they respectively correspond to the most elastic and the most Newtonian muds we have data for.

Surface and interface

Figures 6-12, 6-13 and 6-14 show the variation of the surface for different slopes for the Gulf of Mexico and the Hangzhou Bay muds.

We note that when the slope becomes less steep (like $s = 1/20$), the harmonics have time to be damped out before reaching the shore. On the contrary, when the slope is very steep (like $s = 1$), the harmonics are damped very quickly right before the shore.

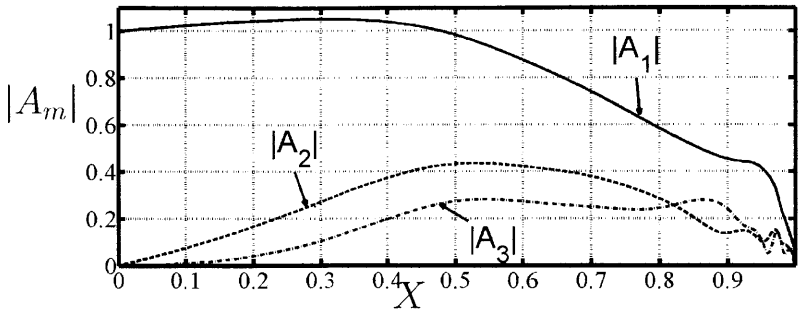

(a) Gulf of Mexico mud, $s = 1$

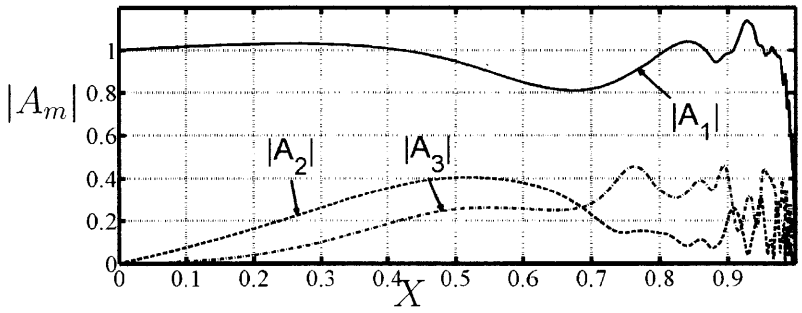

(b) Hangzhou Bay mud, $s = 1$

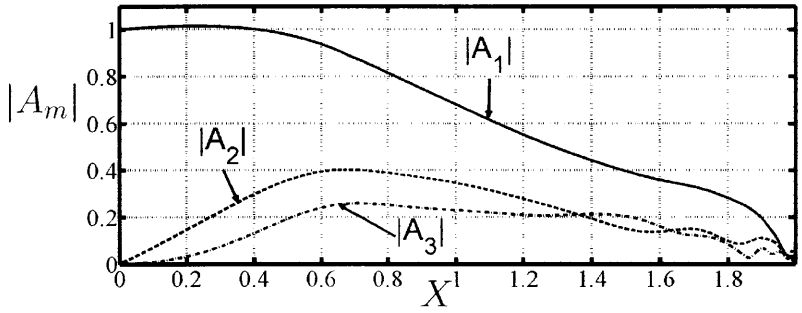

(c) Gulf of Mexico mud, $s = 1/2$

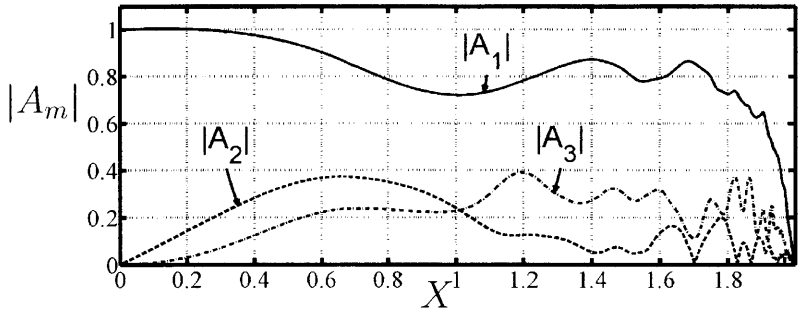

(d) Hangzhou Bay mud, $s = 1/2$

Figure 6-12: Evolution of the first 3 harmonics of the free surface over different types of viscoelastic muddy seabeds, in the cases $s = 1$ and $s = 1/2$. Warning: we use a different scale for the Gulf of Mexico mud, $s = 1$ case.

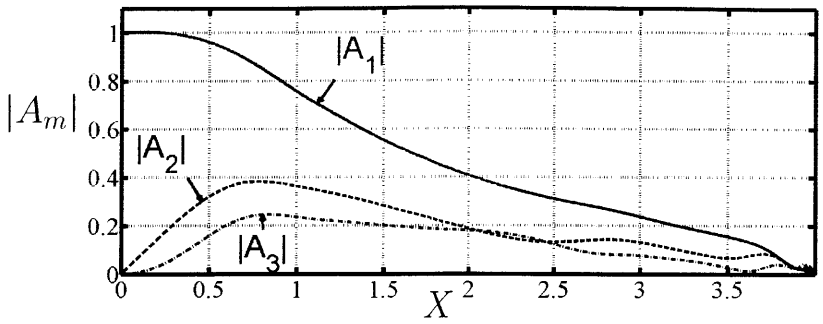

(a) Gulf of Mexico mud, $s = 1/4$

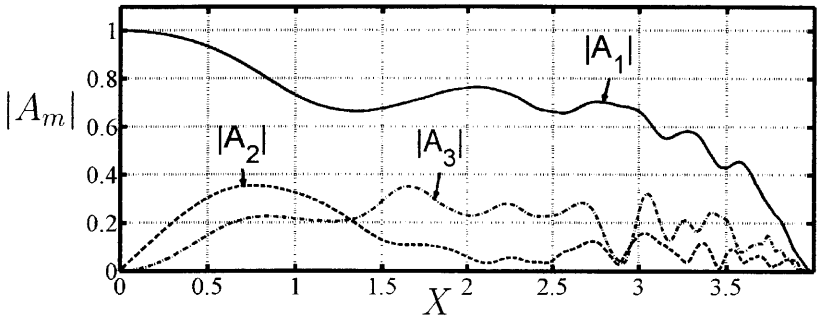

(b) Hangzhou Bay mud, $s = 1/4$

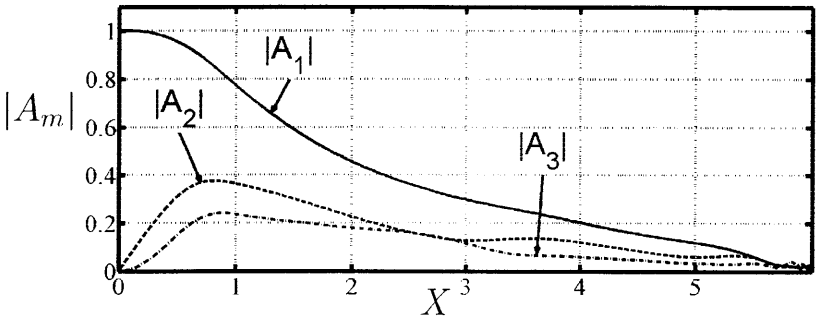

(c) Gulf of Mexico mud, $s = 1/6$

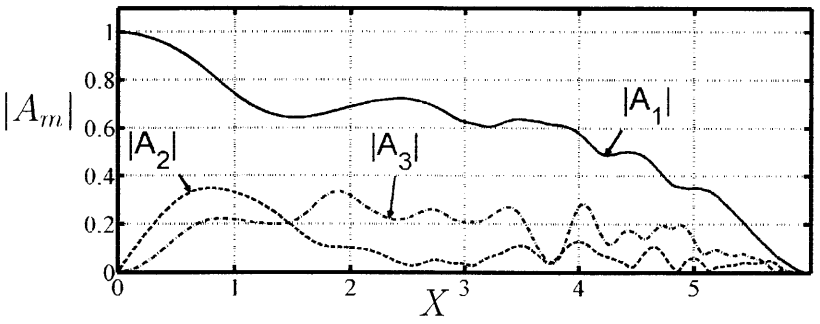

(d) Hangzhou Bay mud, $s = 1/6$

Figure 6-13: Evolution of the first 3 harmonics of the free surface over different types of viscoelastic muddy seabeds, in the cases $s = 1/4$ and $s = 1/6$.

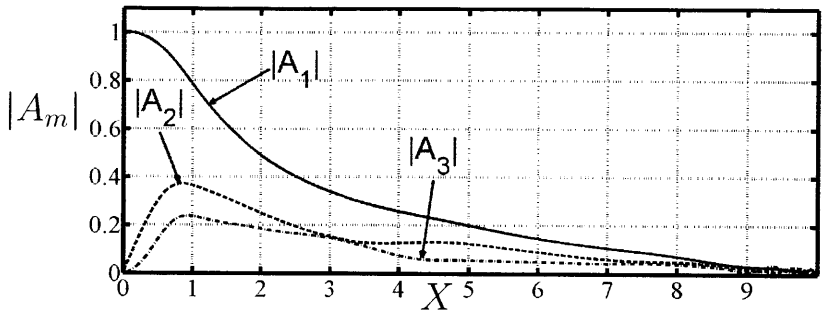

(a) Gulf of Mexico mud, $s = 1/10$

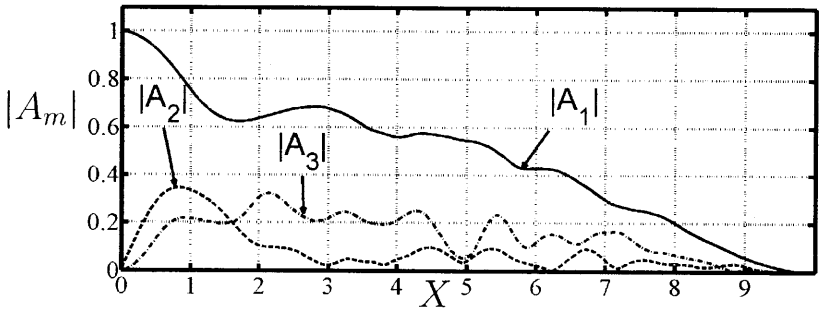

(b) Hangzhou Bay mud, $s = 1/10$

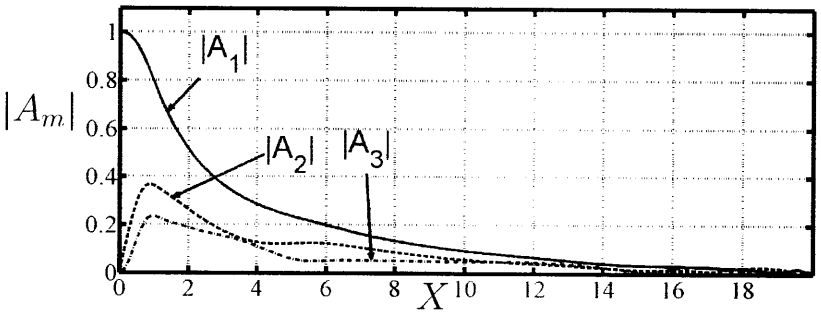

(c) Gulf of Mexico mud, $s = 1/20$

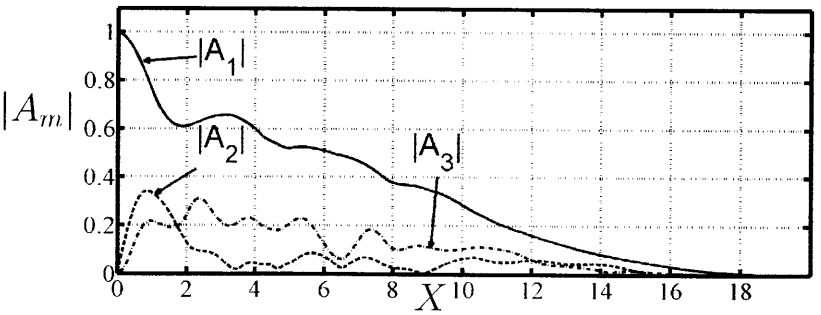

(d) Hangzhou Bay mud, $s = 1/20$

Figure 6-14: Evolution of the first 3 harmonics of the free surface over different types of viscoelastic muddy seabeds, in the cases $s = 1/10$ and $s = 1/20$.

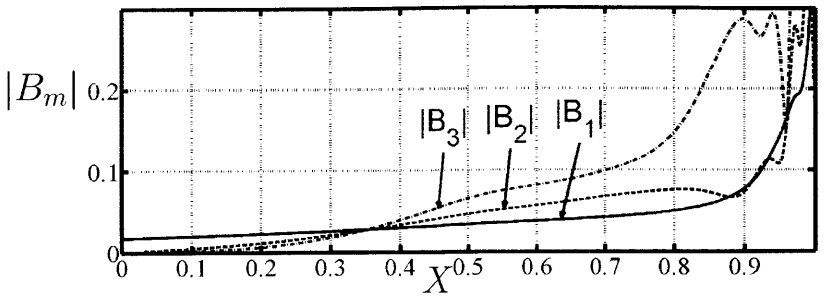

(a) Gulf of Mexico mud, $s = 1$

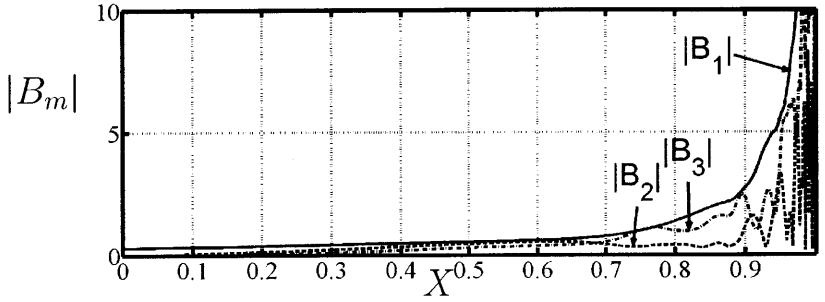

(b) Hangzhou Bay mud, $s = 1$

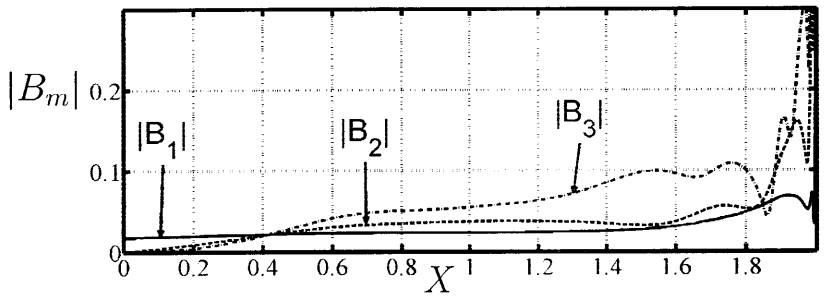

(c) Gulf of Mexico mud, $s = 1/2$

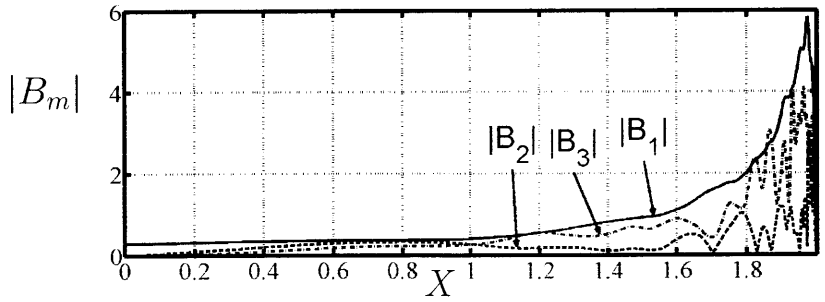

(d) Hangzhou Bay mud, $s = 1/2$

Figure 6-15: Evolution of the first 3 harmonics of the interface between mud and water over different types of viscoelastic muddy seabeds, in the cases $s = 1$ and $s = 1/2$. Warning: we use different scales.

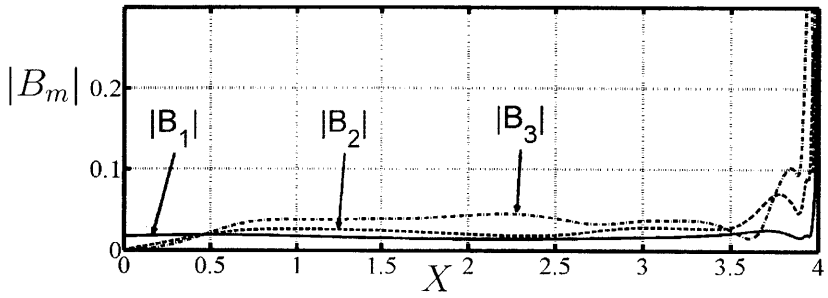

(a) Gulf of Mexico mud, $s = 1/4$

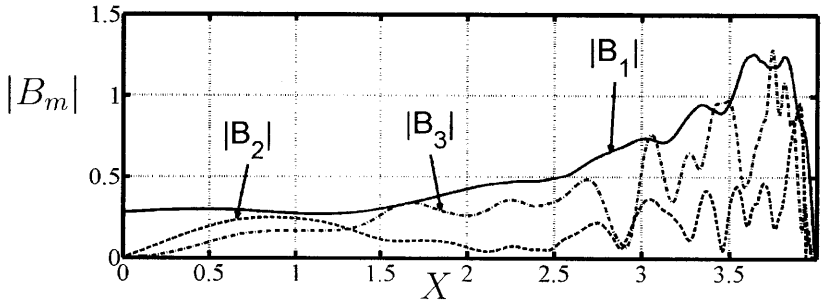

(b) Hangzhou Bay mud, $s = 1/4$

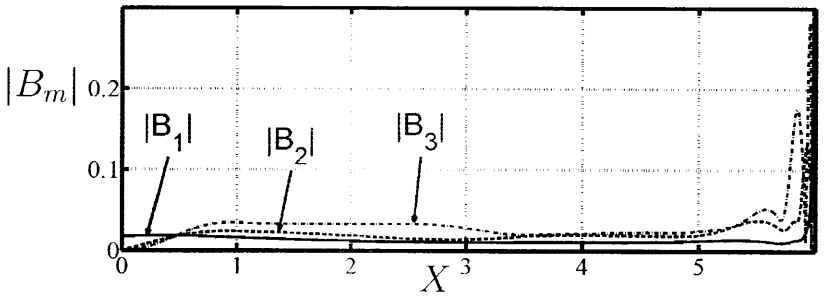

(c) Gulf of Mexico mud, $s = 1/6$

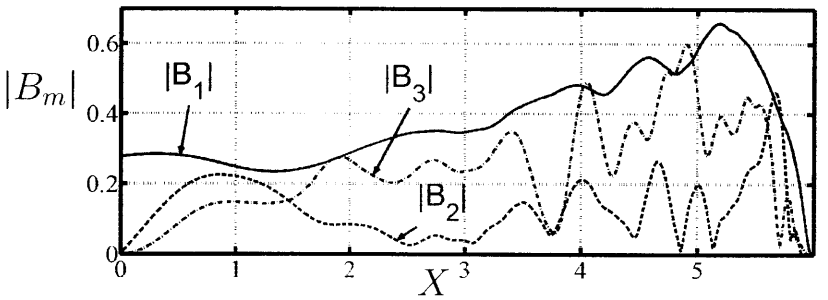

(d) Hangzhou Bay mud, $s = 1/6$

Figure 6-16: Evolution of the first 3 harmonics of the interface between mud and water over different types of viscoelastic muddy seabeds, in the cases $s = 1/4$ and $s = 1/6$. Warning: we use different scales.

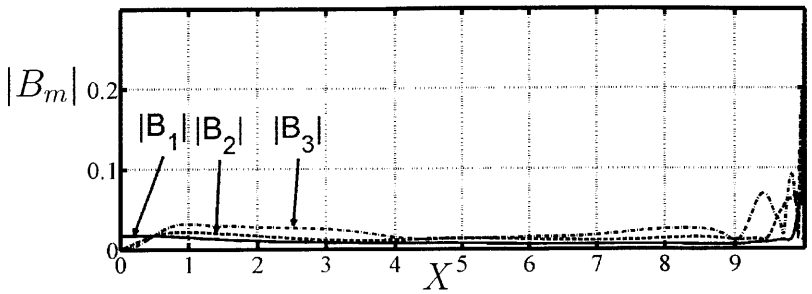

(a) Gulf of Mexico mud, $s = 1/10$

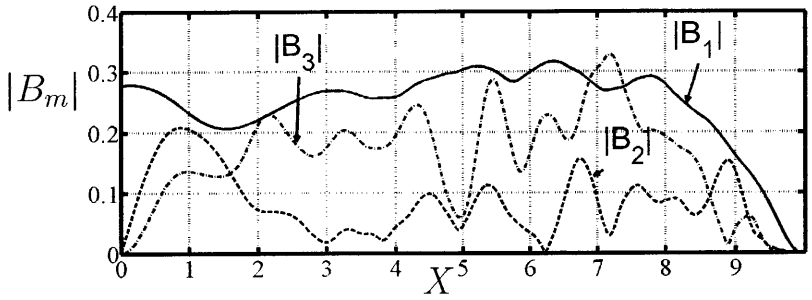

(b) Hangzhou Bay mud, $s = 1/10$

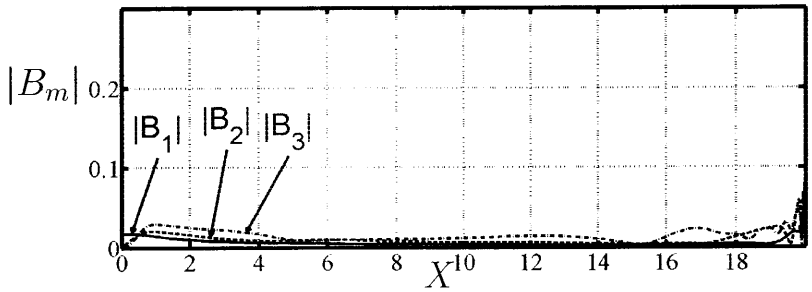

(c) Gulf of Mexico mud, $s = 1/20$

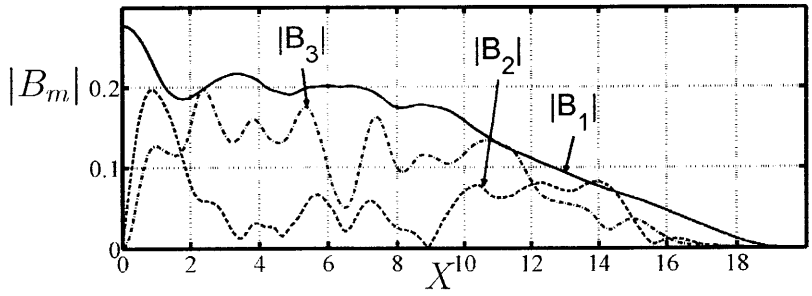

(d) Hangzhou Bay mud, $s = 1/20$

Figure 6-17: Evolution of the first 3 harmonics of the interface between mud and water over different types of viscoelastic muddy seabeds, in the cases $s = 1/10$ and $s = 1/20$. Warning: we use different scales.

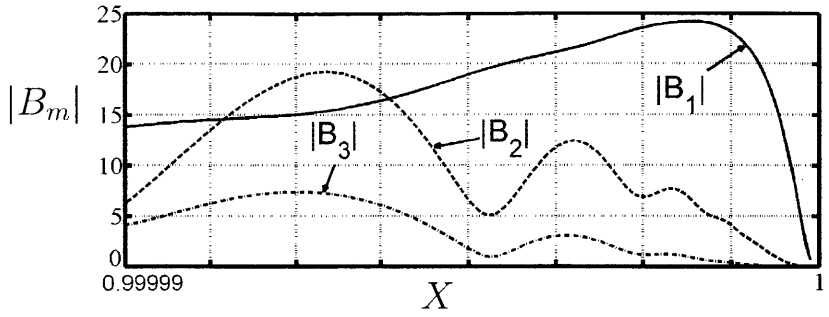

(a) $s = 1$

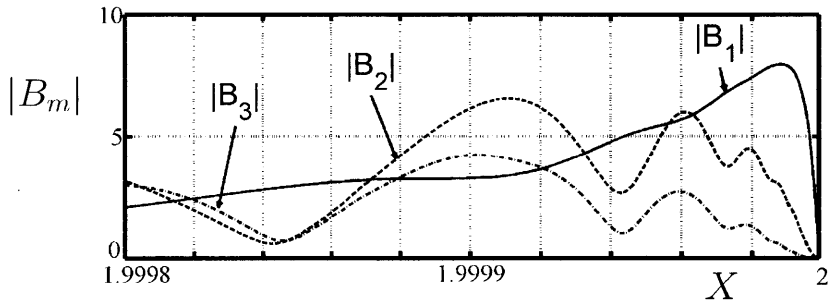

(b) $s = 1/2$

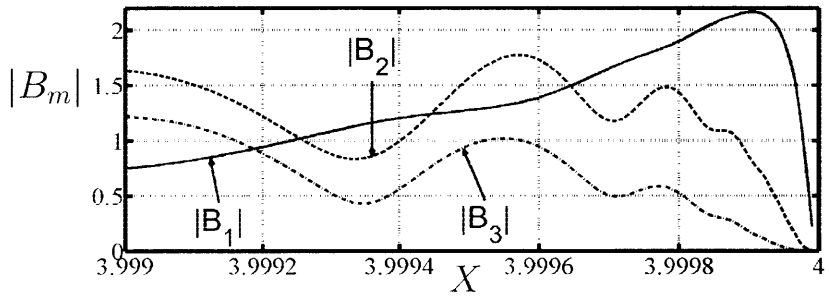

(c) $s = 1/4$

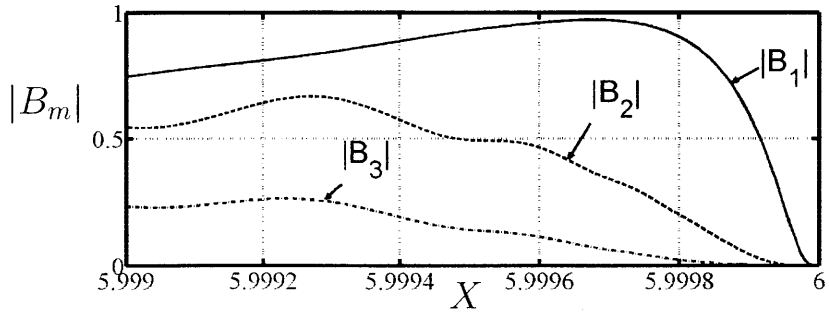

(d) $s = 1/6$

Figure 6-18: Evolution of the first 3 harmonics of the interface near the shore with the Gulf of Mexico mud. The X-scale is from 0.999992 to 1 for $s = 1$.

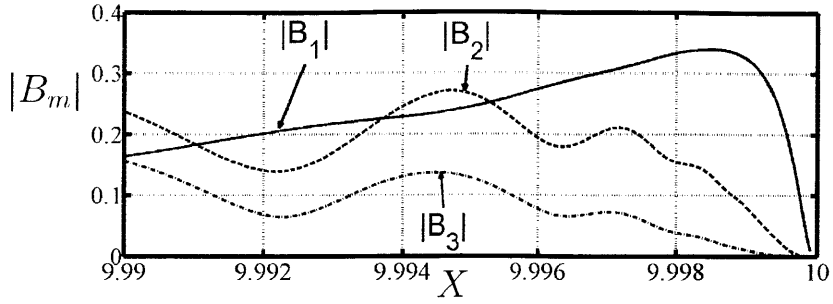

(a) Gulf of Mexico mud, $s = 1/10$

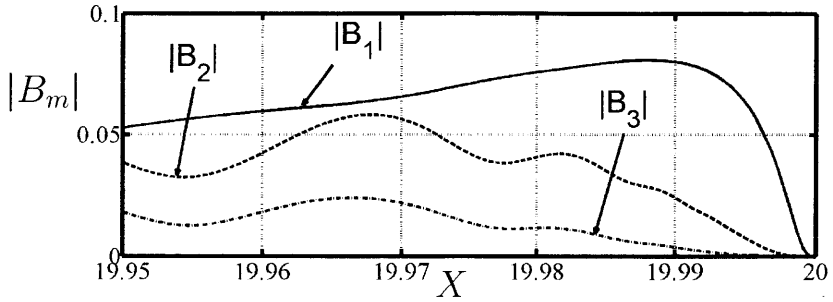

(b) Gulf of Mexico mud, $s = 1/20$

Figure 6-19: Evolution of the first 3 harmonics of the interface bnear the shore with the Gulf of Mexico mud. $s = 1/10$ and $s = 1/20$.

Figures 6-15, 6-16 and 6-17 show the variation of the surface for different slopes for the same muds. As before, the variation of the interface are more important for the Hangzhou Bay mud than for the Gulf of Mexico mud, by a factor of 10.

Figures 6-18 and 6-19 show a zoom-in of the interface motion near the shore for the Gulf of Mexico mud. We can see on these figures that the harmonics ultimately go to zero, which agrees with the analytical predictions.

Drift

We now focus on the drift current at $Z = 1$ and for the different slope steepnesses. The shoreline corresponds to $X = 1$ for $s = 1$, to $X = 2$ in the case $s = 1/2$, to $X = 4$ in the case $s = 1/4$ and so on.

Figures 6-20 and 6-21 show the drift current variation from $X = 0$ to the shore for the different values of slope that we are considering in the case of the Gulf of Mexico mud (A).

Because the behavior at the shore is not easy to see in figure 6-20, figure 6-22 offers a zoom of the drift current at the shore. This figure ashows that the drift current ultimately reaches a zero-value, which is what we were expecting from our analytical study of the behavior at the shore.

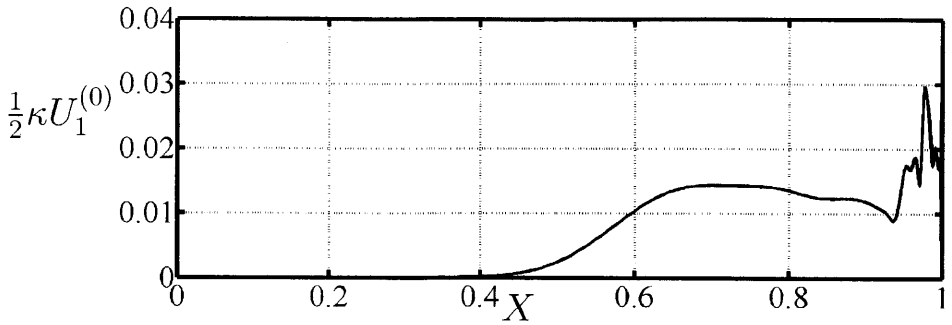

(a) $s = 1$

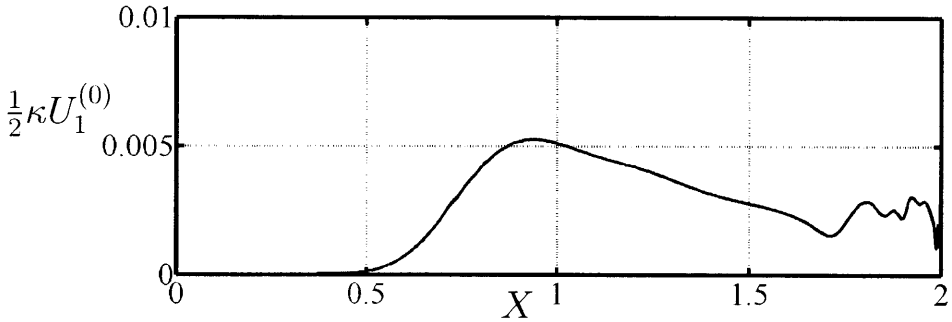

(b) $s = 1/2$

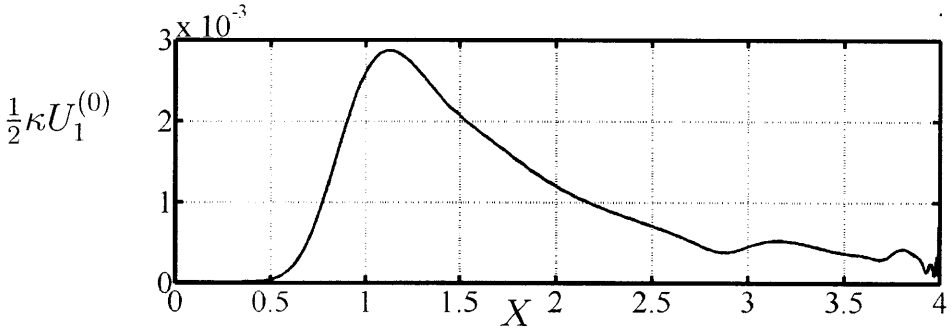

(c) $s = 1/4$

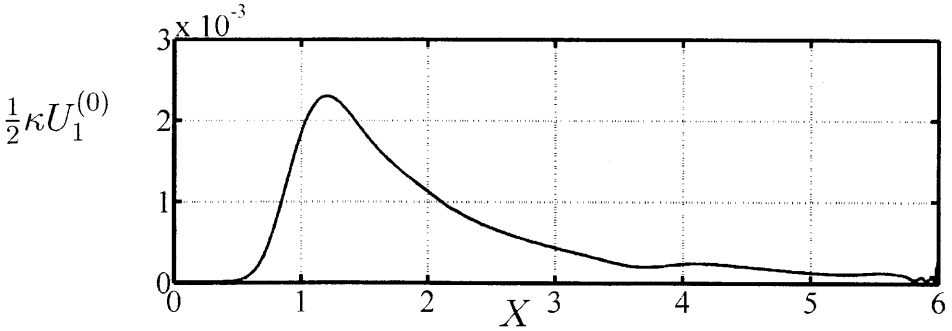

(d) $s = 1/6$

Figure 6-20: Drift velocity $\frac{1}{2}\kappa U_1^{(0)}$ at $Z = 1$ for the Gulf of Mexico mud.

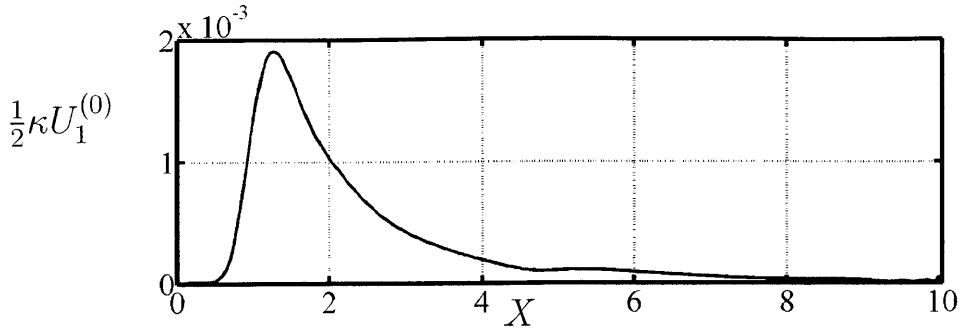

(a) $s = 1/10$

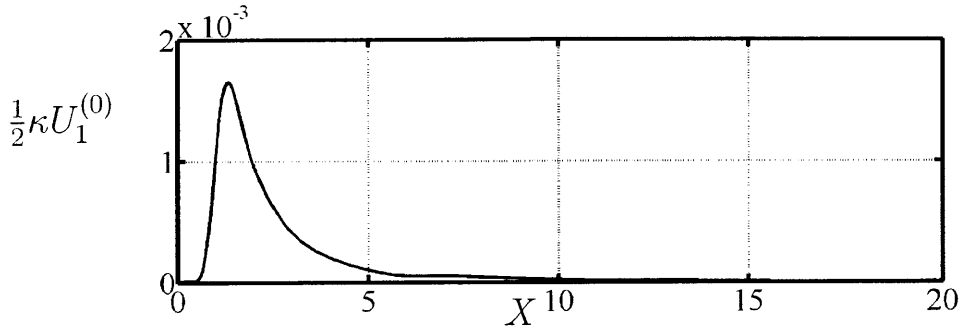

(b) $s = 1/20$

Figure 6-21: Drift velocity $\frac{1}{2}\kappa U_1^{(0)}$ at $Z = 1$ for the Gulf of Mexico mud.

Figures 6-23 and 6-24 show the drift current variation from $X = 0$ to the shore for the different values of slope that we are considering in the case of the Hangzhou Bay mud (D). The drift reaches higher values for the Hangzhou Bay mud than for the Gulf of Mexico mud. This is once again due to the resonance effect happening in the Hangzhou Bay mud.

In particular, we observe that the drift current reaches high values in the case of a very steep slope, $s = 1$. This is because, near the shore, the harmonics are not damped yet (see figure 6-12), but $h(X)$ already is very small. As a consequence, the drift, which is a sum of (Z, m)-dependent coefficients times the $|A_m|^2$, divided by $h(X)^{3/2}$ reaches high values before decreasing exponentially at the shore.

In figure 6-25, we also plot the drift current with the Mobile Bay and the Lianyungang muds. This figure allows us to compare the drift current for very steep and non-steep slopes (respectively $s = 1$ and $s = 1/20$). As before, the graphs corresponding to the Mobile Bay mud are cut before the shore because of oscillations appearing.

For the steep slope ($s = 1$), we observe that the drift current is smaller for the Mobile Bay and Lianyungang muds than for the Gulf of Mexico and Hangzhou Bay muds. Especially, the drift current is 10^{-5} times smaller with the Mobile Bay mud than with the Hangzhou Bay mud.

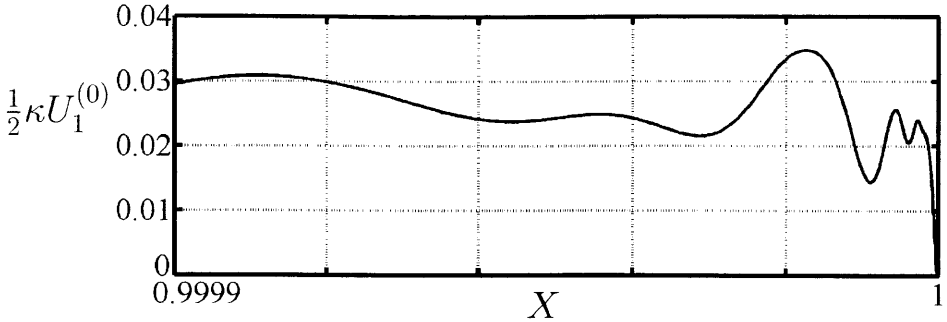

(a) $s = 1$

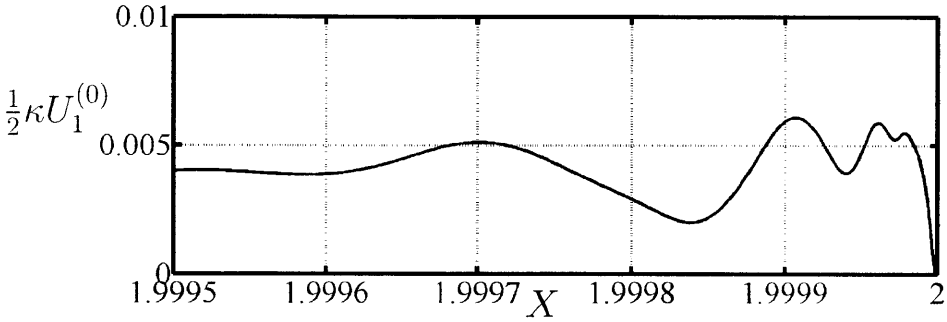

(b) $s = 1/2$

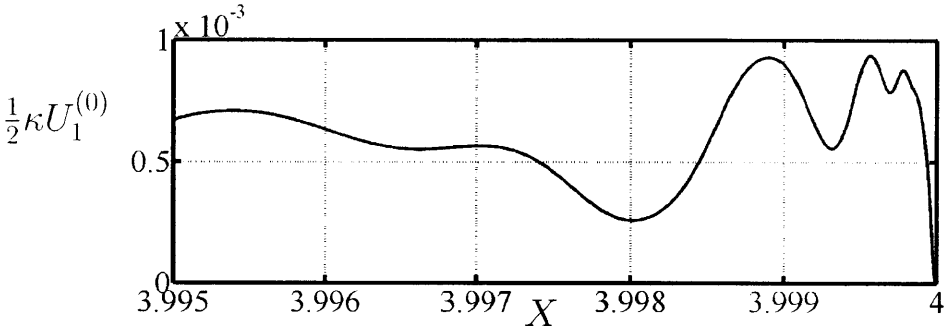

(c) $s = 1/4$

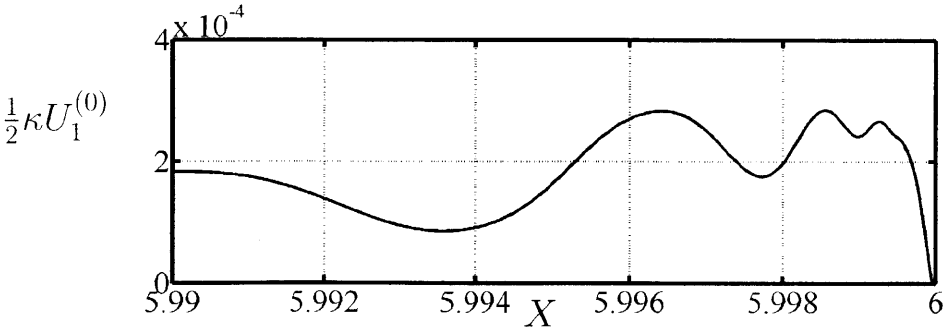

(d) $s = 1/6$

Figure 6-22: Zoom-in at the shore of the drift velocity $\frac{1}{2}\kappa U_1^{(0)}$ at $Z = 1$ for the Gulf of Mexico mud.

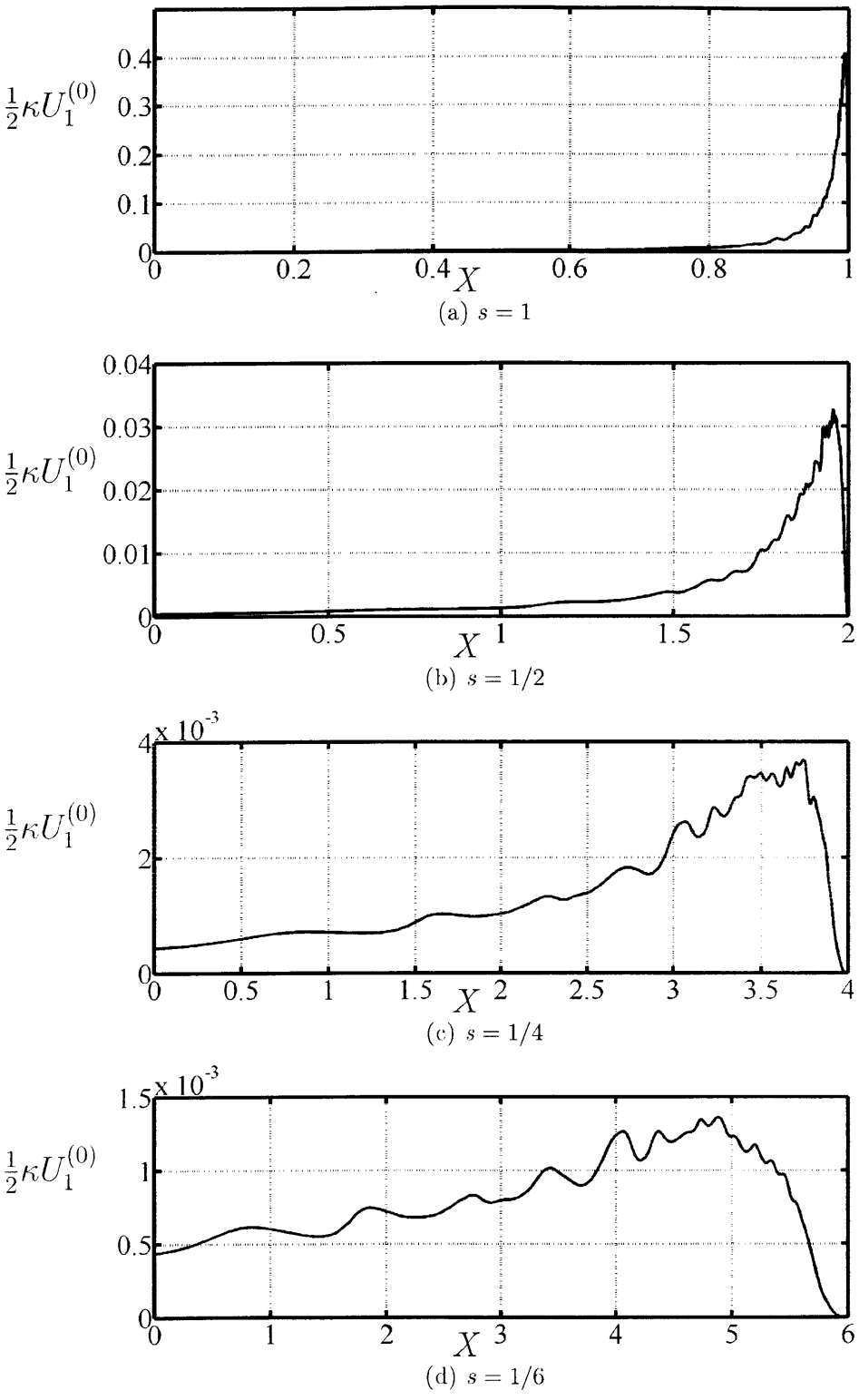

Figure 6-23: Drift velocity $\frac{1}{2}\kappa U_1^{(0)}$ at $Z = 1$ for the Hangzhou Bay mud.

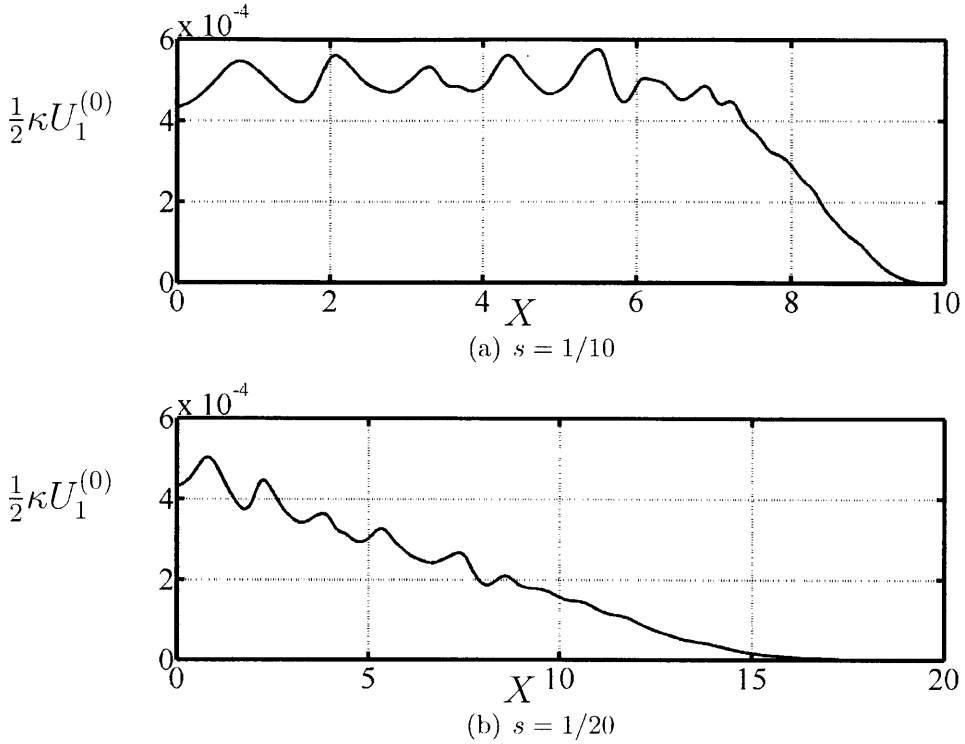

(a) $s = 1/10$

(b) $s = 1/20$

Figure 6-24: Drift velocity $\frac{1}{2}\kappa U_1^{(0)}$ at $Z = 1$ for the Hangzhou Bay mud.

For the non-steep slope ($s = 1/20$), these muds have very different behaviors. The result for the Lianyungang mud is like the results we obtained with the Gulf of Mexico and the Hangzhou Bay muds: since the harmonics $|A_m|$ are damped by the mud long before the shore, the exponential decay of these harmonics appear long before the shore as well, and there is no increase of the drift current near the shore due to the shallow water (ie small value of $h(X)$). On the contrary, since the mud-induced damping is very slow to happen with the Mobile Bay mud, the exponential decay of the harmonics $|A_m|$ does not occur long before $X = 20$. As a consequence, the harmonics are not damped and the effect of the $h^{-3/2}$ in the drift current is visible: the drift current increases with X.

As always, we show in figure 6-26 a zoom of figure 6-25 at the shore, in order to show that the the drift current decays to zero at the shore.

Energy variation

We numerically represented the total first-order energies in figure 6-27 for the different slopes. This figure shows that the total energy logically decreases, to reach a zero-value at the shore ($X = 5$). However, we observe once again that dissipation is slower

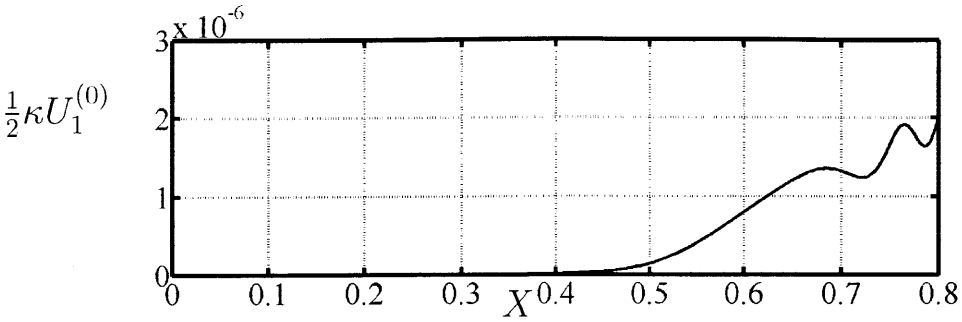

(a) Mobile Bay mud, $s = 1$

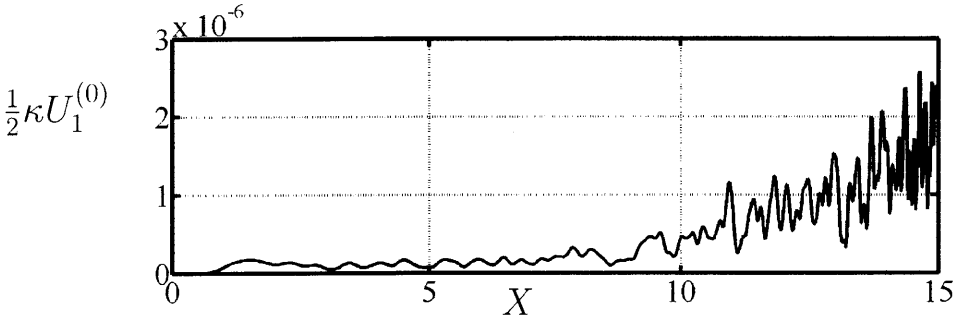

(b) Mobile Bay mud, $s = 1/20$

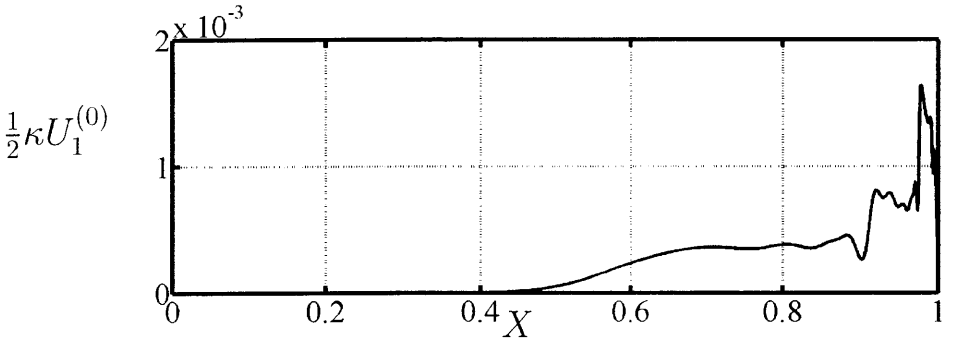

(c) Lianyungang mud, $s = 1$

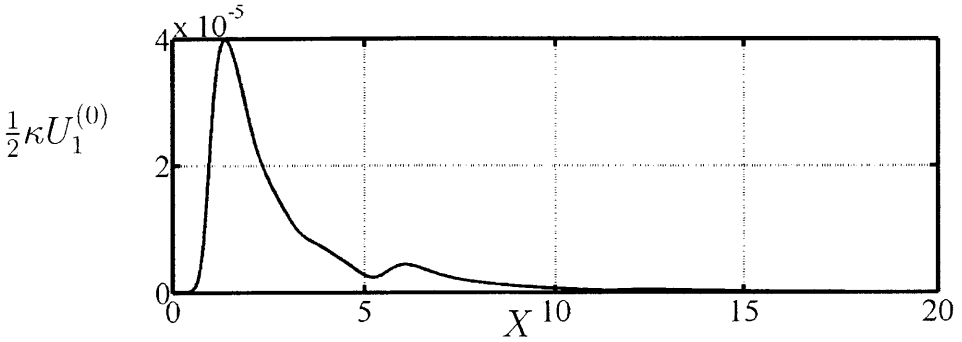

(d) Lianyungang mud, $s = 1/20$

Figure 6-25: Drift velocity $\frac{1}{2}\kappa U_1^{(0)}$ at $Z = 1$ for the Mobile Bay and the Lianyungang muds.

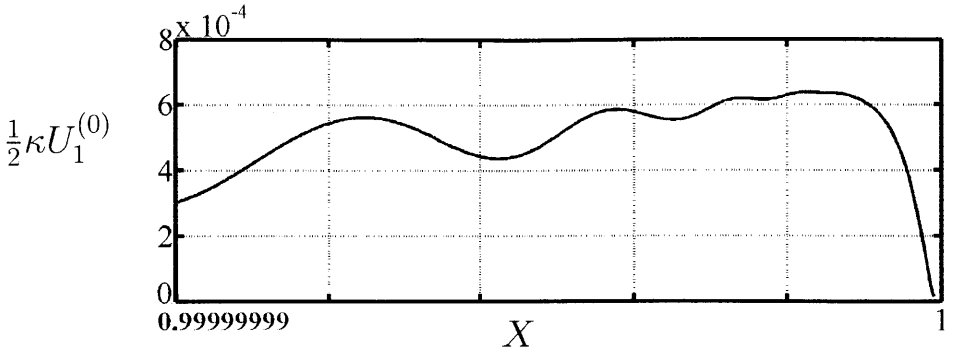

$\frac{1}{2}\kappa U_1^{(0)}$

(a) Mobile Bay mud, $s = 1$

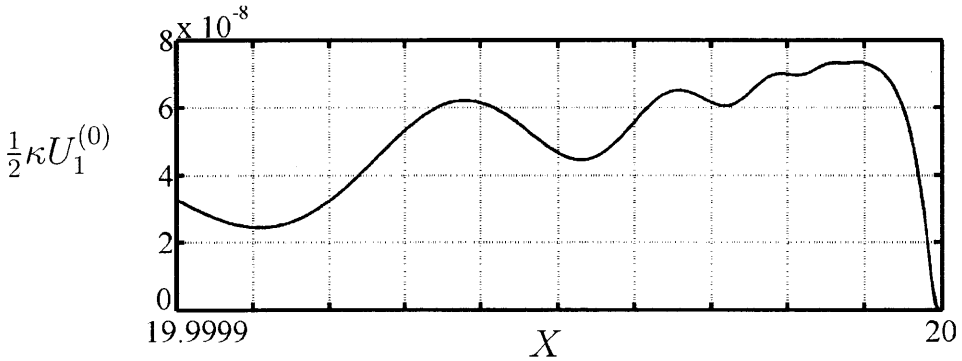

$\frac{1}{2}\kappa U_1^{(0)}$

(b) Mobile Bay mud, $s = 1/20$

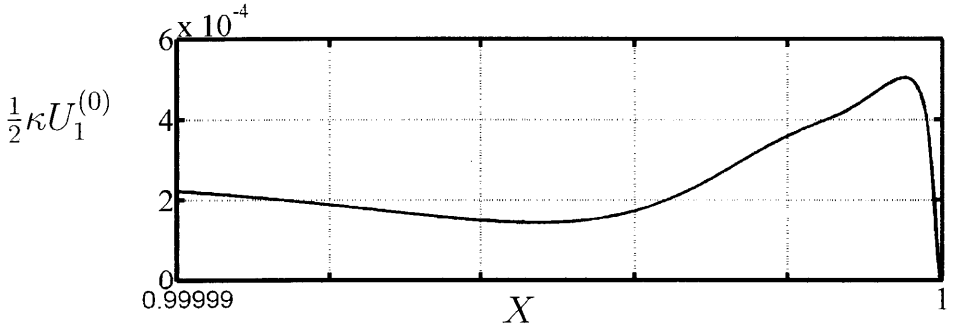

$\frac{1}{2}\kappa U_1^{(0)}$

(c) Lianyungang mud, $s = 1$

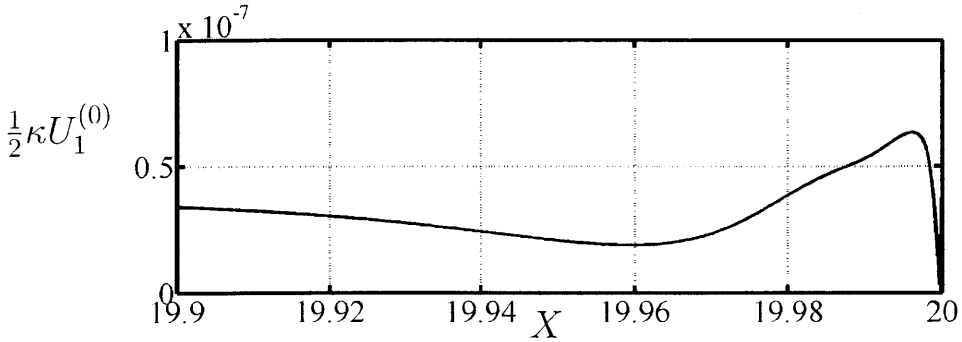

$\frac{1}{2}\kappa U_1^{(0)}$

(d) Lianyungang mud, $s = 1/20$

Figure 6-26: Zoom-in of the drift velocity $\frac{1}{2}\kappa U_1^{(0)}$ at $Z = 1$ for the Mobile Bay and the Lianyungang muds, at the shore.

to occur in the Gulf of Mexico mud (A). The shore is reached for $X = 1$ for $s = 1$, for $X = 2$ for $s = 1/2$ and so on.

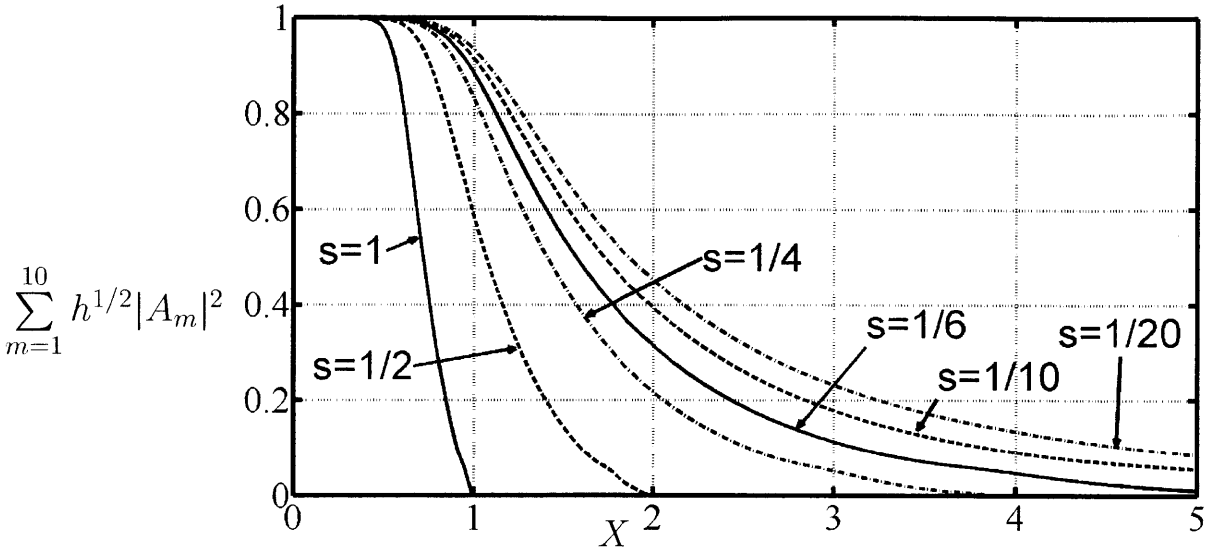

(a) Gulf of Mexico mud

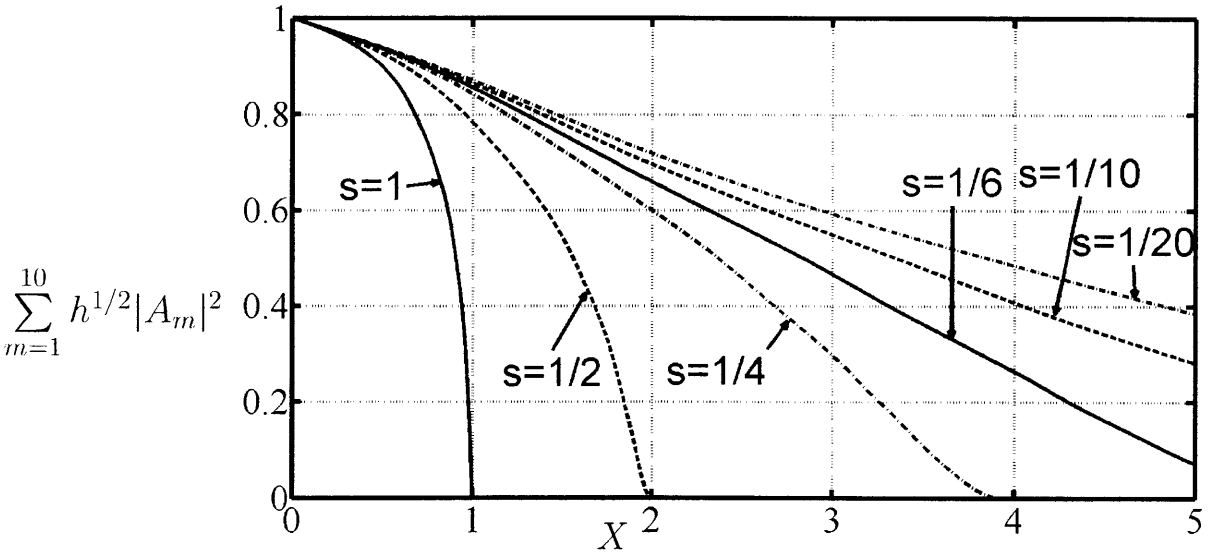

(b) Hangzhou Bay mud

Figure 6-27: Wave energy over a flat thick muddy seabed for the Gulf of Mexico and the Hangzhou Bay muds. Comparison between $s = 1$, $s = 1/2$, $s = 1/4$, $s = 1/6$, $s = 1/10$ and $s = 1/20$.

6.8 Horizontal bottom without mud

6.8.1 Governing equations

From the study we just led in the particular case of viscoelastic mud, it is very easy to deduce the surface waves behavior in the absence of mud. Indeed, the absence of mud simply mean that $B_m = 0$ in equation 6.5.1.12.

As a consequence, the governing equation 6.6.1.4 for the surface waves become:

$$\frac{d(h^{1/4}A_m)}{dX} + \frac{\epsilon}{\kappa}\frac{3i}{8h^{5/4}}m\left[\sum_{l=1}^{n-m} 2A_l^* A_{m+l} + \sum_{l=1}^{[m/2]} \alpha_l A_l A_{m-l}\right] = 0 \qquad (6.8.1.1)$$

The same way, the energy variation can be deduced from equation 6.6.3.4, that becomes:

$$\boxed{\frac{d}{dX}\left[\sqrt{h}\sum_{m=1}^{n}|A_m|^2\right] = 0} \qquad (6.8.1.2)$$

This result looks very logical, since it means that in the absence of mud, there is no energy dissipation in water.

6.8.2 Numerical results by using the first ten harmonics

Since we don't consider mud anymore, there are only four parameters remaining: $\bar{h}$, A, ω' and s'. We already studied the influence of dispersion and non-linearity in chapter 3, by playing on the ratio ϵ/κ.

Let us now study the influence of different slopes. We look at the slope values $s' = 0.048$, $s' = 0.012$ and $s' = 0.0024$, respectively corresponding the non dimensional slope values:

$$\boxed{s = 1,\ s = 1/4,\ s = 1/20} \qquad (6.8.2.1)$$

We still have $\bar{h} = 2\text{m}$, $A = 0.4\text{m}$, and $\omega = 0.5\text{rad/s}$. These values still correspond to:

$$\boxed{\epsilon = 0.2,\ \kappa = 0.22} \qquad (6.8.2.2)$$

The results are shown in figure 6-28 for the three different slopes. Once again, even though we carried the numerical resolution with ten harmonics, we choose to only display the first three harmonics.

The main result is that, in the absence of mud, the harmonics keep growing toward an infinite value at the shore. This result is a very well known phenomenon: wave

height increases as water depth decreases toward the shore.

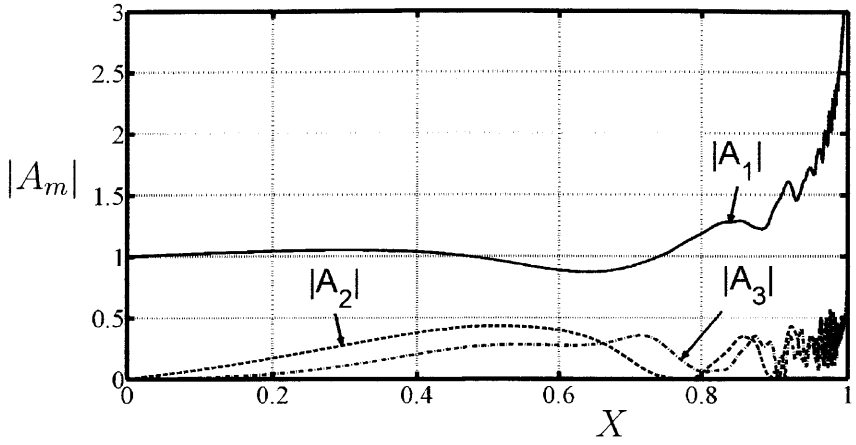

(a) $s = 1$

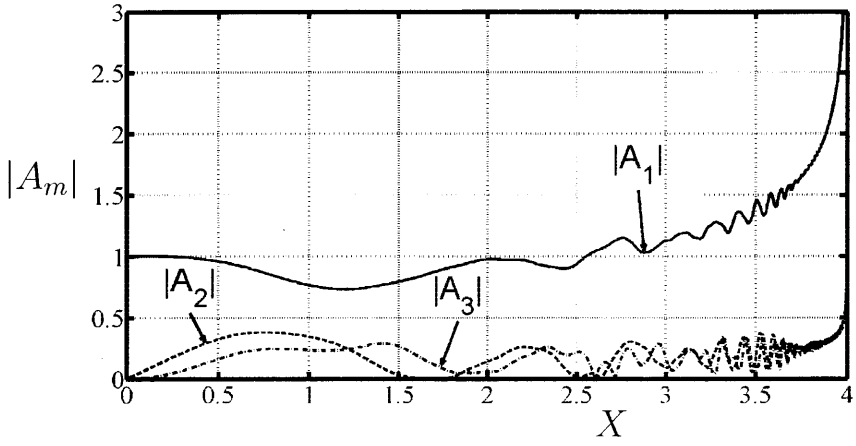

(b) $s = 1/4$

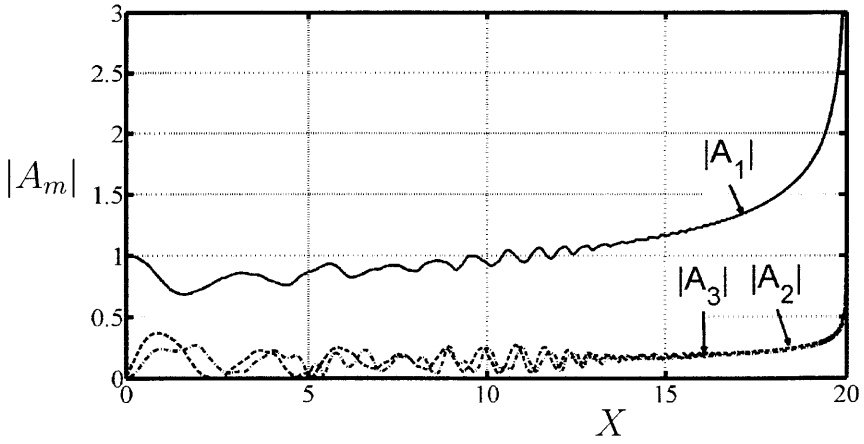

(c) $s = 1/20$

Figure 6-28: Effects of the slope on the evolution of the first 3 harmonics of the free surface on a solid seabed.

Chapter 7

Sloping bottom, with very shallow viscoelastic mud

In this chapter, we still consider the bottom of the ocean to have a gentle slope, as shown on figure 7-1.

However, we now consider that non-linearity ϵ is small compared to dispersion, that is to say ϵ small compared to κ:

$$\boxed{O(\epsilon) = O(\kappa^2)} \tag{7.0.2.1}$$

In order to see the effect of non-linearity on mud-induced damping, we consider the mud layer to be thiner than in the previous chapters:

$$\boxed{\frac{d}{\bar{h}} = \kappa_d = O(\kappa^2)} \tag{7.0.2.2}$$

so that non-linearity and mud-induced damping act at the same order.

The same way, we now consider the slope to be of order $O(\kappa^2)$, so that it is comparable to the damping order we previously found in a flat bottom case. This means that in this entire study, we will consider:

$$\boxed{\frac{dh'}{dx'} = O(\kappa^2)}, \quad \frac{d^2h}{dx^2} = O(\kappa^4) \tag{7.0.2.3}$$

For the same reason as in the previous chapter, we will not study the more simple case of a Newtonian mud because this type of mud would result in a flow down the slope in the static case.

This is why we consider the mud to be viscoelastic. We already demonstrated that

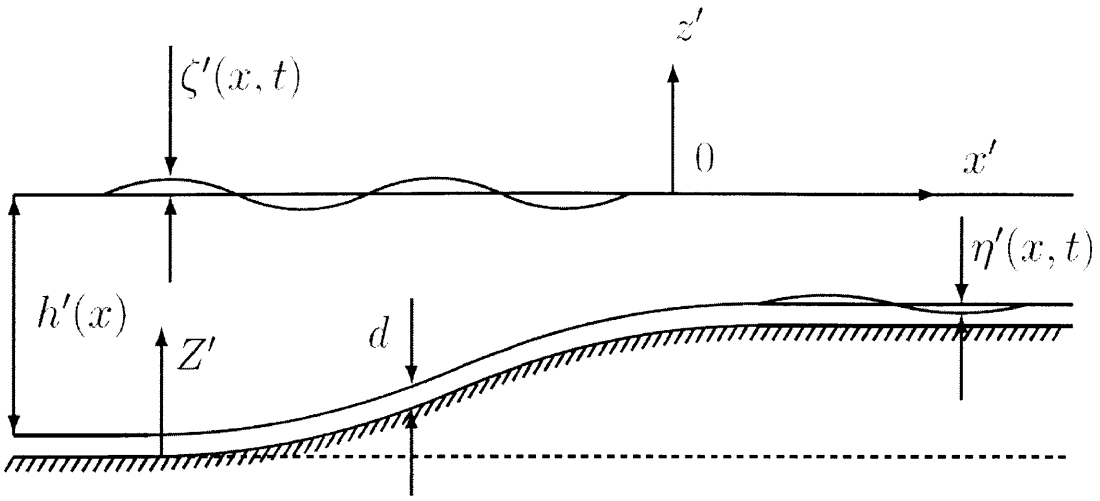

Figure 7-1: Sketch of the studied case. d is the mud layer depth measured vertically.

viscoelastic mud was not flowing down the slope in the static case, and that there is only a displacement of the mud down the slope.

7.1 Scaling

As before, we define a dimensionless complex viscosity:

$$\mu = \frac{\mu'}{\mu_s} \tag{7.1.0.4}$$

We will use the same scaling in water as in the flat bottom case (chapter 5) :

$$\tau_{ij} = \frac{d}{\epsilon \mu_s \sqrt{g\bar{h}}} \tau'_{ij} \tag{7.1.0.5}$$

where μ_s is the characteristic viscosity deduced from the different sets of experiments. Because of calculation simplifications, I still do not need to assign a particular for μ_s for the different muds. Indeed, every time the viscosity appears in the final results, it appears as $\mu\mu_s$, and I could thus use the dimensional value of the viscosity: $\mu' = \mu\mu_s$.

To sum up the scaling in water and mud are:

$$\begin{array}{lll} x = kx' & z = \frac{z'}{\bar{h}}b & t = k(g\bar{h})^{1/2}t' \\ p = \frac{p'}{\rho_W g A} & u = \frac{1}{\epsilon\sqrt{g\bar{h}}}u' & v = \frac{\kappa}{\epsilon\sqrt{g\bar{h}}}v' \\ \zeta = \frac{\zeta'}{A} & \phi = \phi'\left[\frac{A}{k\bar{h}}(g\bar{h})^{1/2}\right]^{-1} & \omega = \frac{\omega'}{k(g\bar{h})^{1/2}} \end{array} \tag{7.1.0.6}$$

and:

$$\begin{array}{lll} x = kx' & Z = \frac{Z'}{d} & t = k(g\bar{h})^{1/2}t' \\ P = \frac{P'}{\rho_W g A} & U = \frac{1}{\epsilon\sqrt{g\bar{h}}}U' & V = \frac{1}{\epsilon\kappa\kappa_d\sqrt{g\bar{h}}}V' \\ \eta = \frac{\eta'}{\kappa_d A} & \mathcal{U} = \frac{k}{\epsilon}\mathcal{U}' & \mathcal{V} = \frac{k}{\epsilon\kappa\kappa_d}\mathcal{V}' \\ T_{ij} = \frac{T'_{ij}}{\rho_W g A} & E_{ij,t} = \frac{d}{\epsilon\sqrt{g\bar{h}}}E'_{ij,t'} & \tau_{ij} = \frac{d}{\epsilon\mu_s\sqrt{g\bar{h}}}\tau'_{ij} \end{array} \tag{7.1.0.7}$$

with Z' in mud as shown in figure 7-1:

$$Z' = z' - h(x') - d \tag{7.1.0.8}$$

Let us compare our new coordinates in mud with the ones we had in the flat bottom case. Now, the axes follow the slope. This fact brings a correction in the differentiations, that become:

$$\begin{array}{l} \frac{\partial}{\partial z} \rightarrow \frac{\partial}{\partial Z} \\ \frac{\partial}{\partial x} \rightarrow \frac{\partial}{\partial x} - \frac{1}{\kappa_d}\frac{dh}{dx}\frac{\partial}{\partial Z} \end{array} \tag{7.1.0.9}$$

In order to emphasize the fact that $\frac{dh}{dx}$ is small, let us introduce

$$X = \kappa^2 x \tag{7.1.0.10}$$

This way, let us write:

$$\begin{array}{l} \frac{dh}{dx} \rightarrow \kappa^2\frac{dh}{dX} \\ \frac{d^2h}{dx^2} \rightarrow \kappa^4\frac{d^2h}{dX^2} \end{array} \tag{7.1.0.11}$$

We can now rewrite relation 7.1.0.9:

$$\begin{array}{l} \frac{\partial}{\partial z} \rightarrow \frac{\partial}{\partial Z} \\ \frac{\partial}{\partial x} \rightarrow \frac{\partial}{\partial x} - \frac{\kappa^2}{\kappa_d}\frac{dh}{dX}\frac{\partial}{\partial Z} \end{array} \tag{7.1.0.12}$$

7.2 Equations in water to order $O(\kappa^4)$

We want to obtain the governing equation of the surface and interface in water to order $O(\kappa^2)$, which is the order we will need later in this thesis. However, since this may be useful for later studies, we will carry the calculation up to order $O(\kappa^4)$.

We will show the parts of the results that will be used in the rest of this thesis by highlighting them.

Let us express the velocity potential in the water as a power series:

$$\boxed{\phi(x,z,t) = \sum_{n=0}^{\infty} \frac{(z+h(x))^n}{n!}\phi^{(n)}(x,t)} \tag{7.2.0.13}$$

where $z = -h(x) + \epsilon\kappa_d\eta$ corresponds to the mud-water interface. We then obtain

$$\frac{\partial\phi}{\partial x} = \sum_{n=0}^{\infty} \frac{(z+h(x))^n}{n!}\left[\frac{\partial\phi^{(n)}}{\partial x} + \frac{dh}{dx}\phi^{(n+1)}\right] \tag{7.2.0.14}$$

And thus:

$$\frac{\partial^2\phi}{\partial x^2} = \sum_{n=0}^{\infty} \frac{(z+h)^n}{n!}\left[\frac{\partial^2\phi^{(n)}}{\partial x^2}(x,t) + 2\kappa^2\frac{dh}{dX}\frac{\partial\phi^{(n+1)}}{\partial x} + \kappa^4\left(\frac{dh}{dX}\right)^2\phi^{(n+2)} + \kappa^4\frac{d^2h}{dX^2}\phi^{(n+1)}\right] \tag{7.2.0.15}$$

and

$$\phi_{zz} = \sum_{n=0}^{\infty} \frac{(z+h)^n}{n!}\phi^{(n+2)}(x,t) \tag{7.2.0.16}$$

7.2.1 Laplace equation

From the Laplace equation in dimensionless variables, we know:

$$\kappa^2\frac{\partial^2\phi}{\partial x^2} + \frac{\partial^2\phi}{\partial z^2} = 0 \tag{7.2.1.1}$$

and from 7.2.0.15 and 7.2.0.16 we deduce:

$$\forall n,\quad \phi^{(n)} = -\kappa^2\left(\frac{\partial^2\phi^{(n-2)}}{\partial x^2} + 2\kappa^2\frac{dh}{dX}\frac{\partial\phi^{(n-1)}}{\partial x} + \kappa^4\frac{d^2h}{dX^2}\phi^{(n-1)} + \kappa^4\left(\frac{dh}{dX}\right)^2\phi^{(n)}\right) \tag{7.2.1.2}$$

7.2.2 Kinematic Boundary condition at the interface

In dimensional form, the interface kinematic boundary condition is:

$$\frac{\partial \phi'}{\partial z'} = -\frac{\partial [h'(x') - \eta'(x,t)]}{\partial t'} - \frac{\partial [h'(x') - \eta'(x,t)]}{\partial x'} \frac{\partial \phi'}{\partial x'}, \quad z = -h'(x') + \eta'(x',t') \tag{7.2.2.1}$$

In dimensionless form we obtain:

$$\frac{\partial \phi}{\partial z} = \kappa^2 \kappa_d \frac{\partial \eta}{\partial t} - \kappa^4 \frac{\partial \phi}{\partial x} \frac{dh}{dX} + \epsilon \kappa^2 \kappa_d \frac{\partial \phi}{\partial x} \frac{\partial \eta}{\partial x}, \quad z = -h(x) + \epsilon \kappa_d \eta(x,t) \tag{7.2.2.2}$$

We use a Taylor series expansion of this equation:

$$\frac{\partial \phi}{\partial z} + \epsilon \kappa_d \eta \frac{\partial^2 \phi}{\partial z^2} = \kappa^2 \kappa_d \frac{\partial \eta}{\partial t} + \kappa^2 \left(-\kappa^2 \frac{dh}{dX} + \epsilon \kappa_d \frac{\partial \eta}{\partial x} \right) \frac{\partial \phi}{\partial x} + O(\kappa^7), \quad z = -h \tag{7.2.2.3}$$

As a consequence, from the series of equation 7.2.0.13 we obtain:

$$\phi^{(1)} + \epsilon \kappa_d \eta \phi^{(2)} = \kappa^2 \kappa_d \frac{\partial \eta}{\partial t} + \kappa^2 \left(-\kappa^2 \frac{dh}{dX} + \epsilon \kappa_d \frac{\partial \eta}{\partial x} \right) \frac{\partial \phi^{(0)}}{\partial x} + O(\kappa^7), \quad z = -h \tag{7.2.2.4}$$

From the relationship 7.2.1.2 and knowing that $\phi(z = -h) = \phi^{(0)}$, $\frac{\partial^n \phi}{\partial z^n}(z = -h) = \phi^{(n)}$, we deduce:

$$\phi^{(1)} = \kappa^2 \kappa_d \frac{\partial \eta}{\partial t} - \kappa^4 \frac{dh}{dX} \frac{\partial \phi^{(0)}}{\partial x} + \epsilon \kappa^2 \kappa_d \frac{\partial \eta}{\partial x} \frac{\partial \phi^{(0)}}{\partial x} + \epsilon \kappa^2 \kappa_d \eta \frac{\partial^2 \phi^{(0)}}{\partial x^2} + O(\kappa^7) \tag{7.2.2.5}$$

and as a consequence:

$$\phi^{(1)} = \kappa^2 \kappa_d \frac{\partial \eta}{\partial t} - \kappa^4 \frac{dh}{dX} \frac{\partial \phi^{(0)}}{\partial x} + \epsilon \kappa^2 \kappa_d \frac{\partial}{\partial x} \left(\eta \frac{\partial \phi^{(0)}}{\partial x} \right) + O(\kappa^7) \tag{7.2.2.6}$$

As a consequence, from equation 7.2.2.6, we can deduce an explicit expression of all the $\phi^{(n)}$:

$$\begin{aligned} \phi^{(2)} &= -\kappa^2 \left(\frac{\partial^2 \phi^{(0)}}{\partial x^2} + 2\kappa^2 \frac{dh}{dX} \frac{\partial \phi^{(1)}}{\partial x} + \kappa^4 \frac{d^2 h}{dX^2} \phi^{(1)} + \kappa^4 \left(\frac{dh}{dX} \right)^2 \phi^{(2)} \right) \\ &= -\kappa^2 \frac{\partial^2 \phi_0}{\partial x^2} + O(\kappa^7) \end{aligned} \tag{7.2.2.7}$$

$$\begin{aligned}\phi^{(3)} &= -\kappa^2\left(\frac{\partial^2\phi^{(1)}}{\partial x^2} + 2\kappa^2\frac{dh}{dX}\frac{\partial\phi^{(2)}}{\partial x} + \kappa^4\frac{d^2h}{dX^2}\phi^{(2)} + \kappa^4\left(\frac{dh}{dX}\right)^2\phi^{(3)}\right)\\ &= -\kappa^2\left(\kappa^2\kappa_d\frac{\partial\eta}{\partial t} - \kappa^4\frac{dh}{dX}\frac{\partial\phi^{(0)}}{\partial x}\right) + 2\kappa^6\frac{dh}{dX}\frac{\partial^3\phi^{(0)}}{\partial x^3} + O(\kappa^7)\\ &= -\kappa^4\kappa_d\left(\frac{\partial\eta}{\partial t} - 3\frac{dh}{dX}\frac{\partial\phi^{(0)}}{\partial x}\right) + O(\kappa^7)\end{aligned} \tag{7.2.2.8}$$

Combining all these equations together, the final expression of ϕ becomes:

$$\begin{aligned}\phi =&\phi^{(0)} + \kappa^2(z+h)\left[\kappa_d\frac{\partial\eta}{\partial t} - \kappa^2\frac{dh}{dX}\frac{\partial\phi^{(0)}}{\partial x} + \epsilon\kappa_d\frac{\partial}{\partial x}\left(\eta\frac{\partial\phi^{(0)}}{\partial x}\right)\right] - \kappa^2\frac{(z+h)^2}{2}\frac{\partial^2\phi^{(0)}}{\partial x^2}\\ &- \kappa^4\frac{(z+h)^3}{3!}\left[\kappa_d\frac{\partial^3\eta}{\partial t\partial x^2} - 3\kappa^2\frac{dh}{dX}\frac{\partial^3\phi^{(0)}}{\partial x^3}\right] + \kappa^4\frac{(z+h)^4}{4!}\frac{\partial^4\phi^{(0)}}{\partial x^4}\\ &- \kappa^6\frac{(z+h)^6}{6!}\frac{\partial^6\phi^{(0)}}{\partial x^6} + O(\kappa^7)\end{aligned} \tag{7.2.2.9}$$

7.2.3 Kinematic Boundary condition at the free surface

The kinematic boundary condition at the surface can be written as:

$$\kappa^2\left(\zeta_t + \epsilon\frac{\partial\phi}{\partial x}\frac{\partial\zeta}{\partial x}\right) = \phi_z, \quad z = \epsilon\zeta \tag{7.2.3.1}$$

Knowing from equation 7.2.2.9 that:

$$\begin{aligned}\phi_z =&\kappa^2\left[\kappa_d\frac{\partial\eta}{\partial t} - \kappa^2\frac{dh}{dX}\frac{\partial\phi^{(0)}}{\partial x} + \epsilon\kappa_d\frac{\partial}{\partial x}\left(\eta\frac{\partial\phi^{(0)}}{\partial x}\right)\right] - \kappa^2(z+h)\frac{\partial^2\phi^{(0)}}{\partial x^2}\\ &- \kappa^4\frac{(z+h)^2}{2!}\left[\kappa_d\frac{\partial^3\eta}{\partial t\partial x^2} - 3\kappa^2\frac{dh}{dX}\frac{\partial^3\phi^{(0)}}{\partial x^3}\right]\\ &+ \kappa^4\frac{(z+h)^3}{6}\frac{\partial^4\phi^{(0)}}{\partial x^4} - \kappa^6\frac{(z+h)^5}{5!}\frac{\partial^6\phi^{(0)}}{\partial x^6} + O(\kappa^7)\end{aligned} \tag{7.2.3.2}$$

we obtain:

$$\begin{aligned}\zeta_t + \epsilon\frac{\partial\zeta}{\partial x}\left(\frac{\partial\phi^{(0)}}{\partial x} - \kappa^2\frac{h^2}{2}\frac{\partial^3\phi^{(0)}}{\partial x^3}\right) =& \kappa_d\frac{\partial\eta}{\partial t} - \kappa^2\frac{dh}{dX}\frac{\partial\phi^{(0)}}{\partial x} + \epsilon\kappa_d\frac{\partial}{\partial x}\left(\eta\frac{\partial\phi^{(0)}}{\partial x}\right)\\ &- (h+\epsilon\zeta)\frac{\partial^2\phi^{(0)}}{\partial x^2}\\ &- \frac{\kappa^2h^2}{2}\left[\kappa_d\frac{\partial^3\eta}{\partial t\partial x^2} - 3\kappa^2\frac{dh}{dX}\frac{\partial^3\phi^{(0)}}{\partial x^3}\right]\\ &+ \frac{\kappa^2}{6}(h^3+3h^2\epsilon\zeta)\frac{\partial^4\phi^{(0)}}{\partial x^4} - \kappa^4\frac{h^5}{5!}\frac{\partial^6\phi^{(0)}}{\partial x^6} + O(\kappa^5)\end{aligned} \tag{7.2.3.3}$$

and thus:

$$\begin{aligned}\zeta_t + \frac{\partial}{\partial x}\left[(h+\epsilon\zeta-\epsilon\kappa_d\eta)\frac{\partial\phi^{(0)}}{\partial x}\right] =& \kappa_d\eta_t + \kappa^2\frac{h^3}{3!}\frac{\partial^4\phi^{(0)}}{\partial x^4}\\ &- \kappa^2\frac{h^2}{2}\left[\kappa_d\frac{\partial^3\eta}{\partial t\partial x^2} - 3\kappa^2\frac{dh}{dX}\frac{\partial^3\phi^{(0)}}{\partial x^3}\right]\\ &+ \epsilon\kappa^2\frac{h^2}{2}\frac{\partial\zeta}{\partial x}\frac{\partial^3\phi^{(0)}}{\partial x^3} + \epsilon\kappa^2\frac{h^2\zeta}{2}\frac{\partial^4\phi^{(0)}}{\partial x^4}\\ &- \kappa^4\frac{h^5}{5!}\frac{\partial^6\phi^{(0)}}{\partial x^6} + O(\kappa^5)\end{aligned} \tag{7.2.3.4}$$

Let us now introduce the horizontal velocity at the bottom:

$$u_0 = \frac{\partial\phi^{(0)}}{\partial x}, \quad z + h(x) = 0 \tag{7.2.3.5}$$

$$\begin{aligned}\zeta_t + \frac{\partial}{\partial x}\left[(h+\epsilon\zeta-\epsilon\kappa_d\eta)u^{(0)}\right] =& \kappa_d\eta_t + \kappa^2\frac{h^3}{3!}\frac{\partial^3u^{(0)}}{\partial x^3} - \kappa^2\frac{h^2}{2}\left[\kappa_d\frac{\partial^3\eta}{\partial t\partial x^2} - 3\kappa^2\frac{dh}{dX}\frac{\partial^2u^{(0)}}{\partial x^2}\right]\\ &+ \epsilon\kappa^2\frac{h^2}{2}\frac{\partial\zeta}{\partial x}\frac{\partial^2u^{(0)}}{\partial x^2} + \epsilon\kappa^2\frac{h^2\zeta}{2}\frac{\partial^3u^{(0)}}{\partial x^3}\\ &- \kappa^4\frac{h^5}{5!}\frac{\partial^5u^{(0)}}{\partial x^5} + O(\kappa^5)\end{aligned} \tag{7.2.3.6}$$

Let us now introduce the depth-averaged velocity $\bar{u}$. It is related to $u^{(0)}$ by the

following relation:

$$\begin{aligned}
\bar{u} &= \frac{1}{h+\epsilon\zeta-\epsilon\kappa_d\eta}\int_{-h+\epsilon\kappa_d\eta}^{\epsilon\zeta}\frac{\partial\phi}{\partial x}dz \\
&= \frac{1}{h+\epsilon\zeta-\epsilon\kappa_d\eta}\int_{-h+\epsilon\kappa_d\eta}^{\epsilon\zeta}\Big[u_0+\kappa^2(z+h)\left(\kappa_d\frac{\partial^2\eta}{\partial t\partial x}-\kappa^2\frac{\partial}{\partial x}\left(\frac{dh}{dX}u^{(0)}\right)\right) \\
&- \kappa^2\frac{(z+h)^2}{2}\frac{\partial^2u^{(0)}}{\partial x^2}-\kappa^4\frac{dh}{dX}(z+h)\frac{\partial u^{(0)}}{\partial x}+\kappa^4\frac{(z+h)^4}{4!}\frac{\partial^4u^{(0)}}{\partial x^4}+O(\kappa^5)\Big]dz \\
&= \frac{1}{h+\epsilon\zeta-\epsilon\kappa_d\eta}\int_{-h+\epsilon\kappa_d\eta}^{\epsilon\zeta}\Big[u^{(0)}-\kappa^2\frac{(z+h)^2}{2}\frac{\partial^2u^{(0)}}{\partial x^2} \\
&+ \kappa^2(z+h)\left(\kappa_d\frac{\partial^2\eta}{\partial t\partial x}-2\kappa^2\frac{dh}{dX}\frac{\partial u^{(0)}}{\partial x}\right)+\kappa^4\frac{(z+h)^4}{4!}\frac{\partial^4u^{(0)}}{\partial x^4}+O(\kappa^5)\Big]dz \\
&= u^{(0)}+\frac{1}{H}\Big[-\frac{\kappa^2}{6}(h^3+3\epsilon\zeta h^2)\frac{\partial^2u^{(0)}}{\partial x^2}+\frac{\kappa^2}{2}h^2\left(\kappa_d\frac{\partial^2\eta}{\partial t\partial x}-2\kappa^2\frac{dh}{dX}\frac{\partial u^{(0)}}{\partial x}\right) \\
&+ \kappa^4\frac{h^5}{5!}\frac{\partial^4u^{(0)}}{\partial x^4}+O(\kappa^5)\Big] \\
&= u^{(0)}-\frac{\kappa^2}{6}(h^2+2\epsilon\zeta h)\frac{\partial^2u^{(0)}}{\partial x^2}+\frac{\kappa^2}{2}h\left(\kappa_d\frac{\partial^2\eta}{\partial t\partial x}-2\kappa^2\frac{dh}{dX}\frac{\partial u^{(0)}}{\partial x}\right) \\
&+ \kappa^4\frac{h^4}{5!}\frac{\partial^4u^{(0)}}{\partial x^4}+O(\kappa^5)
\end{aligned} \tag{7.2.3.7}$$

because:

$$\begin{aligned}
\frac{h^3+3\epsilon\zeta h^2}{h+\epsilon\zeta-\epsilon\kappa_d\eta} &= \frac{h^3+3\epsilon\zeta h^2}{h(1+\frac{\epsilon\zeta}{h}+O(\epsilon^2))} \\
&= \frac{h^2+3\epsilon\zeta h}{1+\frac{\epsilon\zeta}{h}+O(\epsilon^2)} \\
&= (h^2+3\epsilon\zeta h)(1-\frac{\epsilon\zeta}{h}+O(\epsilon^2)) \\
&= h^2+2\epsilon\zeta h+O(\epsilon^2)
\end{aligned} \tag{7.2.3.8}$$

$$\begin{aligned}
\frac{h^2}{h+\epsilon\zeta-\epsilon\kappa_d\eta} &= \frac{h^2}{h(1+\frac{\epsilon\zeta}{h}+O(\epsilon^2))} \\
&= h(1-\frac{\epsilon\zeta}{h}+O(\epsilon^2)) \\
&= h+O(\epsilon)
\end{aligned} \tag{7.2.3.9}$$

and:

$$\begin{aligned}\frac{h^5}{h+\epsilon\zeta-\epsilon\kappa_d\eta} &= \frac{h^5}{h(1+\frac{\epsilon\zeta}{h}+O(\epsilon^2))} \\ &= h^4(1-\frac{\epsilon\zeta}{h}+O(\epsilon^2)) \\ &= h^4+O(\epsilon)\end{aligned} \tag{7.2.3.10}$$

Turning this last result around, we obtain the relation:

$$\begin{aligned}u^{(0)} = \bar{u} &+ \kappa^2\frac{h^2}{3!}\frac{\partial^2\bar{u}}{\partial x^2} + \kappa^4\frac{h^4}{(3!)^2}\frac{\partial^4\bar{u}}{\partial x^4} - \frac{\kappa^2}{2}h\left(\kappa_d\frac{\partial^2\eta}{\partial t\partial x} - 2\kappa^2\frac{dh}{dX}\frac{\partial\bar{u}}{\partial x}\right) + \epsilon\kappa^2\frac{h\zeta}{3}\frac{\partial^2\bar{u}}{\partial x^2} \\ &- \kappa^4\frac{h^4}{5!}\frac{\partial^4\bar{u}}{\partial x^4} + O(\kappa^5)\end{aligned} \tag{7.2.3.11}$$

Using this relationship, we obtain equation 7.2.3.6 in terms of $\bar{u}$ instead of $u^{(0)}$:

$$\begin{aligned}\zeta_t + \frac{\partial}{\partial x}\left[(h+\epsilon\zeta-\epsilon\kappa_d\eta)\bar{u}\right] = &-\frac{\partial}{\partial x}\Big[h\Big(\kappa^2\frac{h^2}{3!}\frac{\partial^2\bar{u}}{\partial x^2} + \kappa^4\frac{h^4}{(3!)^2}\frac{\partial^4\bar{u}}{\partial x^4} \\ &- \frac{\kappa^2}{2}h\left(\kappa_d\frac{\partial^2\eta}{\partial t\partial x} - 2\kappa^2\frac{dh}{dX}\frac{\partial\bar{u}}{\partial x}\right) \\ &+ \epsilon\kappa^2\frac{h\zeta}{3}\frac{\partial^2\bar{u}}{\partial x^2} - \kappa^4\frac{h^4}{5!}\frac{\partial^4\bar{u}}{\partial x^4}\Big) + \epsilon\zeta\Big(\kappa^2\frac{h^2}{3!}\frac{\partial^2\bar{u}}{\partial x^2}\Big)\Big] + \kappa_d\eta_t \\ &+ \kappa^2\frac{h^3}{3!}\frac{\partial^3\bar{u}}{\partial x^3} + \kappa^4\frac{h^5}{(3!)^2}\frac{\partial^3}{\partial x^3}\left(\frac{\partial^2\bar{u}}{\partial x^2}\right) \\ &- \kappa^2\frac{h^2}{2}\left[\kappa_d\frac{\partial^3\eta}{\partial t\partial x^2} - 3\kappa^2\frac{dh}{dX}\frac{\partial^2\bar{u}}{\partial x^2}\right] \\ &+ \epsilon\kappa^2\frac{h^2}{2}\frac{\partial\zeta}{\partial x}\frac{\partial^2\bar{u}}{\partial x^2} + \epsilon\kappa^2\frac{h^2\zeta}{2}\frac{\partial^3\bar{u}}{\partial x^3} - \kappa^4\frac{h^5}{5!}\frac{\partial^5\bar{u}}{\partial x^5} + O(\kappa^5)\end{aligned} \tag{7.2.3.12}$$

We can rewrite this equation:

$$\begin{aligned}\zeta_t + \frac{\partial}{\partial x}\left[(h+\epsilon\zeta-\epsilon\kappa_d\eta)\bar{u}\right] = &-\kappa^2\frac{h^3}{3!}\frac{\partial^3\bar{u}}{\partial x^3} - \kappa^4\frac{h^2}{2}\frac{dh}{dX}\frac{\partial^2\bar{u}}{\partial x^2} - \kappa^4\frac{h^5}{(3!)^2}\frac{\partial^5\bar{u}}{\partial x^5} + \frac{\kappa^2\kappa_d}{2}h^2\frac{\partial^3\eta}{\partial t\partial x^2}\\ &- \kappa^4h^2\frac{dh}{dX}\frac{\partial^2\bar{u}}{\partial x^2} - \epsilon\kappa^2\frac{h^2\zeta}{3}\frac{\partial^3\bar{u}}{\partial x^3} - \epsilon\kappa^2\frac{h^2}{3}\frac{\partial^2\bar{u}}{\partial x^2}\frac{\partial\zeta}{\partial x} + \kappa^4\frac{h^5}{5!}\frac{\partial^5\bar{u}}{\partial x^5}\\ &- \epsilon\kappa^2\zeta\frac{h^2}{3!}\frac{\partial^3\bar{u}}{\partial x^3} - \epsilon\kappa^2\frac{\partial\zeta}{\partial x}\frac{h^2}{3!}\frac{\partial^2\bar{u}}{\partial x^2} + \kappa_d\eta_t\\ &+ \kappa^2\frac{h^3}{3!}\frac{\partial^3\bar{u}}{\partial x^3} + \kappa^4\frac{h^5}{(3!)^2}\frac{\partial^5\bar{u}}{\partial x^5} - \kappa^2\kappa_d\frac{h^2}{2}\frac{\partial^3\eta}{\partial t\partial x^2}\\ &+ \kappa^4\frac{3h^2}{2}\frac{dh}{dX}\frac{\partial^2\bar{u}}{\partial x^2} + \epsilon\kappa^2\frac{h^2}{2}\frac{\partial\zeta}{\partial x}\frac{\partial^2\bar{u}}{\partial x^2} + \epsilon\kappa^2\frac{h^2\zeta}{2}\frac{\partial^3\bar{u}}{\partial x^3}\\ &- \kappa^4\frac{h^5}{5!}\frac{\partial^5\bar{u}}{\partial x^5} + O(\kappa^5)\end{aligned} \tag{7.2.3.13}$$

And finally:

$$\begin{aligned}\zeta_t + \frac{\partial}{\partial x}\left[(h+\epsilon\zeta-\epsilon\kappa_d\eta)\bar{u}\right] = &-\kappa^2\frac{h^3}{3!}\frac{\partial^3\bar{u}}{\partial x^3} + \kappa^2\frac{h^3}{3!}\frac{\partial^3\bar{u}}{\partial x^3}\\ &- \kappa^4\frac{h^2}{2}\frac{dh}{dX}\frac{\partial^2\bar{u}}{\partial x^2} + \kappa^4\frac{3h^2}{2}\frac{dh}{dX}\frac{\partial^2\bar{u}}{\partial x^2} - \kappa^4h^2\frac{dh}{dX}\frac{\partial^2\bar{u}}{\partial x^2}\\ &- \kappa^4\frac{h^5}{(3!)^2}\frac{\partial^5\bar{u}}{\partial x^5} + \kappa^4\frac{h^5}{(3!)^2}\frac{\partial^5\bar{u}}{\partial x^5}\\ &+ \kappa^4\frac{h^5}{5!}\frac{\partial^5\bar{u}}{\partial x^5} - \kappa^4\frac{h^5}{5!}\frac{\partial^5\bar{u}}{\partial x^5}\\ &+ \frac{\kappa^2\kappa_d}{2}h^2\frac{\partial^3\eta}{\partial t\partial x^2} - \kappa^2\kappa_d\frac{h^2}{2}\frac{\partial^3\eta}{\partial t\partial x^2}\\ &- \epsilon\kappa^2\frac{h^2\zeta}{3}\frac{\partial^3\bar{u}}{\partial x^3} + \epsilon\kappa^2\frac{h^2\zeta}{2}\frac{\partial^3\bar{u}}{\partial x^3} - \epsilon\kappa^2\zeta\frac{h^2}{3!}\frac{\partial^3\bar{u}}{\partial x^3}\\ &- \epsilon\kappa^2\frac{h^2}{3}\frac{\partial^2\bar{u}}{\partial x^2}\frac{\partial\zeta}{\partial x} - \epsilon\kappa^2\frac{\partial\zeta}{\partial x}\frac{h^2}{3!}\frac{\partial^2\bar{u}}{\partial x^2} + \epsilon\kappa^2\frac{h^2}{2}\frac{\partial\zeta}{\partial x}\frac{\partial^2\bar{u}}{\partial x^2}\\ &+ \kappa_d\eta_t + O(\kappa^5)\end{aligned} \tag{7.2.3.14}$$

Since most of the right hand terms disappear, we obtain the simplified form of the kinematic boundary condition:

$$\zeta_t - \kappa_d\eta_t + \frac{\partial}{\partial x}\left[(h+\epsilon\zeta-\epsilon\kappa_d\eta)\bar{u}\right] = O(\kappa^5) \tag{7.2.3.15}$$

In the rest of this thesis, we will only make use of this equation up to order $O(\kappa^2)$:

$$\boxed{\zeta_t - \kappa_d\eta_t + \frac{\partial}{\partial x}\left[(h+\epsilon\zeta)\bar{u}\right] = O(\kappa^3)} \tag{7.2.3.16}$$

This result agrees with the equation we obtained in the flat bottom case. Indeed, equation 7.2.3.16 reduces to equation 4.2.3.8 in the case $h(x,t) = 1$, and this allows us to check the long calculations.

7.2.4 Dynamic boundary condition at the free surface

From the dynamic boundary condition at the surface we know:

$$\kappa^2(\phi_t + \zeta) + \frac{1}{2}\epsilon[\kappa^2\phi_x^2 + \phi_z^2] = 0, \quad z = \epsilon\zeta(x,t) \tag{7.2.4.1}$$

From the development of ϕ of the equation 7.2.2.9, we know that:

$$\frac{\partial\phi}{\partial t} = \frac{\partial\phi^{(0)}}{\partial t} + \kappa^2 h\left[\kappa^2\frac{\partial^2\eta}{\partial t^2} - \kappa^2\frac{dh}{dX}\frac{\partial^2\phi^{(0)}}{\partial t\partial x}\right] - \frac{\kappa^2}{2}(h^2 + 2\epsilon\zeta h)\frac{\partial^3\phi^{(0)}}{\partial x^2\partial t} + \kappa^4\frac{h^4}{4!}\frac{\partial^5\phi^{(0)}}{\partial^4 x\partial t} + O(\kappa^6) \tag{7.2.4.2}$$

$$\left(\frac{\partial\phi}{\partial x}\right)^2 = \left(\frac{\partial\phi^{(0)}}{\partial x}\right)^2 - \kappa^2 h^2\frac{\partial\phi^{(0)}}{\partial x}\frac{\partial^3\phi^{(0)}}{\partial x^3} + O(\kappa^4) \tag{7.2.4.3}$$

and:

$$\left(\frac{\partial\phi}{\partial z}\right)^2 = \kappa^4 h^2\left(\frac{\partial^2\phi^{(0)}}{\partial x^2}\right)^2 + O(\kappa^6) \tag{7.2.4.4}$$

So we can deduce:

$$\begin{aligned}\frac{\partial\phi^{(0)}}{\partial t} + \kappa^2 h\left[\kappa_d\frac{\partial^2\eta}{\partial t^2} - \kappa^2\frac{dh}{dX}\frac{\partial^2\phi^{(0)}}{\partial t\partial x}\right] - \frac{\kappa^2}{2}(h^2 + 2\epsilon\zeta h)\frac{\partial^3\phi^{(0)}}{\partial x^2\partial t} + \kappa^4\frac{h^4}{4!}\frac{\partial^5\phi^{(0)}}{\partial x^4\partial t} + \zeta \\ + \frac{1}{2}\epsilon\left(\frac{\partial\phi^{(0)}}{\partial x}\right)^2 - \frac{1}{2}\epsilon\kappa^2 h^2\frac{\partial\phi^{(0)}}{\partial x}\frac{\partial^3\phi^{(0)}}{\partial x^3} + \frac{1}{2}\epsilon\kappa^2 h^2\left(\frac{\partial^2\phi^{(0)}}{\partial x^2}\right)^2 = O(\kappa^6)\end{aligned} \tag{7.2.4.5}$$

Let us derive this expression with respect to x:

$$\begin{aligned}\frac{\partial^2\phi^{(0)}}{\partial t\partial x} + \kappa^2\kappa_d h\frac{\partial^3\eta}{\partial t^2\partial x} - \kappa^4 h\frac{dh}{dX}\frac{\partial^3\phi^{(0)}}{\partial t\partial x^2} - \frac{\kappa^2}{2}h^2\frac{\partial^4\phi^{(0)}}{\partial x^3\partial t} - \kappa^4 h\frac{dh}{dX}\frac{\partial^3\phi^{(0)}}{\partial x^2\partial t} - \epsilon\kappa^2\zeta h\frac{\partial^4\phi^{(0)}}{\partial x^3\partial t} \\ - \epsilon\kappa^2\frac{\partial\zeta}{\partial x}h\frac{\partial^3\phi^{(0)}}{\partial x^2\partial t} + \kappa^4\frac{h^4}{4!}\frac{\partial^6\phi^{(0)}}{\partial x^5\partial t} + \frac{\partial\zeta}{\partial x} + \frac{1}{2}\epsilon\frac{\partial}{\partial x}\left(\frac{\partial\phi^{(0)}}{\partial x}\right)^2 \\ - \frac{1}{2}\epsilon\kappa^2 h^2\frac{\partial}{\partial x}\left(\frac{\partial\phi^{(0)}}{\partial x}\frac{\partial^3\phi^{(0)}}{\partial x^3}\right) + \frac{1}{2}\epsilon\kappa^2 h^2\frac{\partial}{\partial x}\left[\left(\frac{\partial^2\phi^{(0)}}{\partial x^2}\right)^2\right] = O(\kappa^6)\end{aligned} \tag{7.2.4.6}$$

and we can now introduce the horizontal velocity at the bottom $u^{(0)} = \frac{\partial \phi^{(0)}}{\partial x}$

$$\frac{\partial u^{(0)}}{\partial t} + \kappa^2 \kappa_d h \frac{\partial^3 \eta}{\partial t^2 \partial x} - \kappa^4 h \frac{dh}{d} \frac{\partial^2 u^{(0)}}{\partial t \partial x} - \frac{\kappa^2}{2} h^2 \frac{\partial^3 u^{(0)}}{\partial x^2 \partial t} - \kappa^4 h \frac{dh}{dX} \frac{\partial^2 u^{(0)}}{\partial x \partial t} - \epsilon \kappa^2 \zeta h \frac{\partial^3 u^{(0)}}{\partial x^2 \partial t}$$
$$- \epsilon \kappa^2 \frac{\partial \zeta}{\partial x} h \frac{\partial^2 u^{(0)}}{\partial x \partial t} + \kappa^4 \frac{h^4}{4!} \frac{\partial^5 u^{(0)}}{\partial x^4 \partial t} + \frac{\partial \zeta}{\partial x} + \frac{1}{2} \epsilon \frac{\partial}{\partial x} (u^{(0)})^2 - \frac{1}{2} \epsilon \kappa^2 h^2 \frac{\partial}{\partial x} \left(u^{(0)} \frac{\partial^2 u^{(0)}}{\partial x^2} \right)$$
$$+ \frac{1}{2} \epsilon \kappa^2 h^2 \frac{\partial}{\partial x} \left[\left(\frac{\partial u^{(0)}}{\partial x} \right)^2 \right] = O(\kappa^6) \tag{7.2.4.7}$$

As done for the kinematic boundary condition case, we write this equation as a function of the depth-averaged velocity $\bar{u}$, using the relation between $u^{(0)}$ and $\bar{u}$ of the equation 7.2.3.11:

$$\frac{\partial}{\partial t} \left(\bar{u} + \kappa^2 \frac{h^2}{3!} \frac{\partial^2 \bar{u}}{\partial x^2} + \kappa^4 \frac{h^4}{(3!)^2} \frac{\partial^4 \bar{u}}{\partial x^4} - \frac{\kappa^4}{2} h \left(\frac{\partial^2 \eta}{\partial t \partial x} - 2 \frac{dh}{dX} \frac{\partial \bar{u}}{\partial x} \right) + \epsilon \kappa^2 \frac{h\zeta}{3} \frac{\partial^2 \bar{u}}{\partial x^2} - \kappa^4 \frac{h^4}{5!} \frac{\partial^4 \bar{u}}{\partial x^4} \right)$$
$$+ \kappa^2 \kappa_d h \frac{\partial^3 \eta}{\partial t^2 \partial x} - \kappa^4 h \frac{dh}{d} \frac{\partial^2 \bar{u}}{\partial t \partial x} - \frac{\kappa^2}{2} h^2 \frac{\partial^3}{\partial x^2 \partial t} \left(\bar{u} + \kappa^2 \frac{h^2}{3!} \frac{\partial^2 \bar{u}}{\partial x^2} \right) - \kappa^4 h \frac{dh}{dX} \frac{\partial^2 \bar{u}}{\partial x \partial t}$$
$$- \epsilon \kappa^2 \zeta h \frac{\partial^3 \bar{u}}{\partial x^2 \partial t} - \epsilon \kappa^2 \frac{\partial \zeta}{\partial x} h \frac{\partial^2 \bar{u}}{\partial x \partial t} + \kappa^4 \frac{h^4}{4!} \frac{\partial^5 \bar{u}}{\partial^4 x \partial t} + \frac{\partial \zeta}{\partial x} + \frac{1}{2} \epsilon \frac{\partial}{\partial x} \left(\bar{u}^2 + 2\kappa^2 \frac{h^2}{3!} \bar{u} \frac{\partial^2 \bar{u}}{\partial x^2} \right)$$
$$- \frac{1}{2} \epsilon \kappa^2 h^2 \frac{\partial}{\partial x} \left(\bar{u} \frac{\partial^2 \bar{u}}{\partial x^2} \right) + \frac{1}{2} \epsilon \kappa^2 h^2 \frac{\partial}{\partial x} \left(\frac{\partial \bar{u}}{\partial x} \right)^2 = O(\kappa^6) \tag{7.2.4.8}$$

that can be rewritten:

$$\frac{\partial \bar{u}}{\partial t} + \kappa^2 \frac{h^2}{3!} \frac{\partial^3 \bar{u}}{\partial x^2 \partial t} + \kappa^4 \frac{h^4}{(3!)^2} \frac{\partial^5 \bar{u}}{\partial x^4 \partial t} - \frac{\kappa^2 \kappa_d}{2} h \frac{\partial^3 \eta}{\partial t^2 \partial x} + \kappa^4 h \frac{dh}{dX} \frac{\partial^2 \bar{u}}{\partial x \partial t} + \epsilon \kappa^2 \frac{h\zeta}{3} \frac{\partial^3 \bar{u}}{\partial x^2 \partial t}$$
$$+ \epsilon \kappa^2 \frac{h}{3} \frac{\partial \zeta}{\partial t} \frac{\partial^2 \bar{u}}{\partial x^2} - \kappa^4 \frac{h^4}{5!} \frac{\partial^5 \bar{u}}{\partial x^4 \partial t} + \kappa^2 \kappa_d h \frac{\partial^3 \eta}{\partial t^2 \partial x} - \kappa^4 h \frac{dh}{dX} \frac{\partial^2 \bar{u}}{\partial t \partial x} - \frac{\kappa^2}{2} h^2 \frac{\partial^3 \bar{u}}{\partial x^2 \partial t}$$
$$- \frac{\kappa^4}{2} \frac{h^4}{3!} \frac{\partial^5 \bar{u}}{\partial x^4 \partial t} - \kappa^4 h \frac{dh}{dX} \frac{\partial^2 \bar{u}}{\partial x \partial t} - \epsilon \kappa^2 \zeta h \frac{\partial^3 \bar{u}}{\partial x^2 \partial t} - \epsilon \kappa^2 \frac{\partial \zeta}{\partial x} h \frac{\partial^2 \bar{u}}{\partial x \partial t} + \kappa^4 \frac{h^4}{4!} \frac{\partial^5 \bar{u}}{\partial^4 x \partial t}$$
$$+ \frac{\partial \zeta}{\partial x} + \frac{1}{2} \epsilon \frac{\partial}{\partial x} (\bar{u})^2 + \epsilon \kappa^2 \frac{h^2}{3!} \frac{\partial}{\partial x} \left(\bar{u} \frac{\partial^2 \bar{u}}{\partial x^2} \right)$$
$$- \frac{1}{2} \epsilon \kappa^2 h^2 \frac{\partial}{\partial x} \left(\bar{u} \frac{\partial^2 \bar{u}}{\partial x^2} \right) + \frac{1}{2} \epsilon \kappa^2 h^2 \frac{\partial}{\partial x} \left(\frac{\partial \bar{u}}{\partial x} \right)^2 = O(\kappa^6) \tag{7.2.4.9}$$

Let us rewrite this equation:

$$\begin{aligned}\frac{\partial \bar{u}}{\partial t}+\epsilon\bar{u}\frac{\partial \bar{u}}{\partial x}+\frac{\partial \zeta}{\partial x}=&-\kappa^2\frac{h^2}{3!}\frac{\partial^3\bar{u}}{\partial x^2\partial t}-\kappa^4\frac{h^4}{(3!)^2}\frac{\partial^5\bar{u}}{\partial x^4\partial t}+\frac{\kappa^2\kappa_d}{2}h\frac{\partial^3\eta}{\partial t^2\partial x}-\kappa^4 h\frac{dh}{dX}\frac{\partial^2\bar{u}}{\partial x\partial t}\\&-\epsilon\kappa^2\frac{h\zeta}{3}\frac{\partial^3\bar{u}}{\partial x^2\partial t}-\epsilon\kappa^2\frac{h}{3}\frac{\partial\zeta}{\partial t}\frac{\partial^2\bar{u}}{\partial x^2}+\kappa^4\frac{h^4}{5!}\frac{\partial^5\bar{u}}{\partial x^4\partial t}-\kappa^2\kappa_d h\frac{\partial^3\eta}{\partial t^2\partial x}\\&+\kappa^4 h\frac{dh}{dX}\frac{\partial^2\bar{u}}{\partial t\partial x}+\frac{\kappa^2}{2}h^2\frac{\partial^3\bar{u}}{\partial x^2\partial t}+\frac{\kappa^4}{2}\frac{h^4}{3!}\frac{\partial^5\bar{u}}{\partial x^4\partial t}+\kappa^4 h\frac{dh}{dX}\frac{\partial^2\bar{u}}{\partial x\partial t}\\&+\epsilon\kappa^2\zeta h\frac{\partial^3\bar{u}}{\partial x^2\partial t}+\epsilon\kappa^2\frac{\partial\zeta}{\partial x}h\frac{\partial^2\bar{u}}{\partial x\partial t}\\&-\kappa^4\frac{h^4}{4!}\frac{\partial^5\bar{u}}{\partial^4 x\partial t}-\epsilon\kappa^2\frac{h^2}{3!}\frac{\partial}{\partial x}\left(\bar{u}\frac{\partial^2\bar{u}}{\partial x^2}\right)\\&+\frac{1}{2}\epsilon\kappa^2h^2\frac{\partial}{\partial x}\left(\bar{u}\frac{\partial\bar{u}}{\partial x}\right)-\frac{1}{2}\epsilon\kappa^2h^2\frac{\partial}{\partial x}\left(\frac{\partial\bar{u}}{\partial x}\right)^2+O(\kappa^6)\end{aligned}\tag{7.2.4.10}$$

By grouping the right hand side terms that look the same together, we obtain:

$$\begin{aligned}\frac{\partial \bar{u}}{\partial t}+\epsilon\bar{u}\frac{\partial \bar{u}}{\partial x}+\frac{\partial \zeta}{\partial x}=&\kappa^2\frac{h^2}{3}\frac{\partial^3\bar{u}}{\partial x^2\partial t}+\kappa^4\frac{h^4}{12}\frac{\partial^5\bar{u}}{\partial x^4\partial t}-\frac{\kappa^2\kappa_d}{2}h\frac{\partial^3\eta}{\partial t^2\partial x}\\&+\kappa^4 h\frac{dh}{dX}\frac{\partial^2\bar{u}}{\partial t\partial x}+\epsilon\kappa^2\frac{2h\zeta}{3}\frac{\partial^3\bar{u}}{\partial x^2\partial t}-\epsilon\kappa^2\frac{h}{3}\frac{\partial\zeta}{\partial t}\frac{\partial^2\bar{u}}{\partial x^2}+\epsilon\kappa^2\frac{\partial\zeta}{\partial x}h\frac{\partial^2\bar{u}}{\partial x\partial t}\\&+\frac{1}{3}\epsilon\kappa^2h^2\frac{\partial}{\partial x}\left(\bar{u}\frac{\partial^2\bar{u}}{\partial x^2}\right)-\frac{1}{2}\epsilon\kappa^2h^2\frac{\partial}{\partial x}\left(\frac{\partial\bar{u}}{\partial x}\right)^2+O(\kappa^6)\end{aligned}\tag{7.2.4.11}$$

And we finally get the simplified form of the dynamic boundary condition at the surface:

$$\begin{aligned}\frac{\partial \bar{u}}{\partial t}+\epsilon\bar{u}\frac{\partial \bar{u}}{\partial x}+\frac{\partial \zeta}{\partial x}=&\frac{\kappa^2}{3}h^2\frac{\partial^3\bar{u}}{\partial x^2\partial t}-\frac{\kappa^2\kappa_d}{2}h\frac{\partial^3\eta}{\partial t^2\partial x}+\frac{\kappa^4}{12}h^4\frac{\partial^5\bar{u}}{\partial x^4\partial t}+\frac{2}{3}\epsilon\kappa^2h\zeta\frac{\partial^3\bar{u}}{\partial x^2\partial t}\\&-\frac{1}{3}\epsilon\kappa^2h\frac{\partial\zeta}{\partial t}\frac{\partial^2\bar{u}}{\partial x^2}+\epsilon\kappa^2h\frac{\partial\zeta}{\partial x}\frac{\partial^2\bar{u}}{\partial x\partial t}+\frac{1}{3}\epsilon\kappa^2h^2\frac{\partial}{\partial x}\left(\bar{u}\frac{\partial^2\bar{u}}{\partial x^2}\right)\\&-\frac{1}{2}\epsilon\kappa^2h^2\frac{\partial}{\partial x}\left(\frac{\partial\bar{u}}{\partial x}\right)^2+\kappa^4h\frac{dh}{dX}\frac{\partial^2\bar{u}}{\partial t\partial x}+O(\kappa^6)\end{aligned}\tag{7.2.4.12}$$

Once again, we will only need this result up to order $O(\kappa^2)$ for the rest of this thesis:

$$\boxed{\frac{\partial \bar{u}}{\partial t}+\epsilon\bar{u}\frac{\partial \bar{u}}{\partial x}+\frac{\partial \zeta}{\partial x}=\frac{\kappa^2}{3}h^2\frac{\partial^3\bar{u}}{\partial x^2\partial t}+O(\kappa^3)}\tag{7.2.4.13}$$

This result agrees with the equation we obtained in the flat bottom case. Indeed, by replacing the varying depth $h(x)$ by 1, equation 7.2.4.13 reduces to equation 4.2.4.12. This equality confirms the long calculations.

7.2.5 Equation of the total pressure in water

From the Bernoulli equation, we can deduce the total pressure (sum of the static and the dynamic pressure) in the water as a function of the potential:

$$\begin{aligned} p' &= p'_s + p'_d \\ &= -\rho_W \left(\frac{\partial \phi'}{\partial t'} + \frac{1}{2}(\nabla' \phi')^2 + g z' \right) \end{aligned} \tag{7.2.5.1}$$

In dimensionless form, this last equation becomes:

$$p = -\phi_t - \frac{\epsilon}{2}\left[(\phi_x)^2 + \frac{1}{\kappa^2}(\phi_z)^2\right] - \frac{z}{\epsilon}, \quad -h(x) + \epsilon\kappa_d\eta < z < \zeta \tag{7.2.5.2}$$

In particular, we obtain the pressure in water at the interface $z = -h + \epsilon\kappa_d\eta$:

$$p = \frac{h}{\epsilon} - \phi_t - \frac{\epsilon}{2}\left[(\phi_x)^2 + \frac{1}{\kappa^2}(\phi_z)^2\right] - \kappa_d\eta, \quad z = -h(x) + \epsilon\kappa_d\eta \tag{7.2.5.3}$$

And since we know from 7.2.3.2 that:

$$(\phi_z)(z = -h(x) + \epsilon\kappa_d\eta) = O(\kappa^4) \tag{7.2.5.4}$$

we deduce:

$$(\phi_z)^2(z = -h(x) + \epsilon\kappa_d\eta) = O(\kappa^8) \tag{7.2.5.5}$$

and equation 7.2.5.3 can be reduced to:

$$p = \frac{h}{\epsilon} - \phi_t - \frac{\epsilon}{2}(\phi_x)^2 - \kappa_d\eta + O(\kappa^6), \quad z = -h(x) + \epsilon\kappa_d\eta \tag{7.2.5.6}$$

By Taylor expansion, we know that:

$$\phi(z = -h + \epsilon\kappa_d\eta) = \phi(z = -h) + O(\kappa^4) = \phi_0 + O(\kappa^4) \tag{7.2.5.7}$$

As a consequence, 7.2.5.6 becomes:

$$\boxed{p = \frac{h(x)}{\epsilon} - (\phi_0)_t - \kappa_d\eta - \frac{\epsilon}{2}((\phi_0)_x)^2 + O(\kappa^4)}, \quad z = -h(x) + \epsilon\kappa_d\eta \tag{7.2.5.8}$$

7.3 Equations in mud at the first order

We now want to study the mud layer in the dynamic case. Since the static case has already been studied, we only focus on the wave-induced phenomenon. In other words, we only consider the effects of the dynamic pressure, since the static pressure has already been taken into account.

As in the flat bottom case (chapter 5), we only need the terms of the first order ($O(1)$) in order to solve the surface and interface governing equations. We will not go to higher order in this thesis.

7.3.1 Interface kinematic boundary condition in mud

The instantaneous equation of the interface is:

$$F'(x', Z', t') = Z' - (d + \eta') = 0 \tag{7.3.1.1}$$

The assumption of tangential motion then requires that:

$$\frac{\partial F'}{\partial t'} + U' \left(\frac{\partial}{\partial x'} - \frac{dh'}{dx'} \frac{\partial}{\partial Z'} \right) F' + V' \frac{\partial F'}{\partial Z'} = 0, \quad Z' = d + \eta' \tag{7.3.1.2}$$

which means, using equation 7.3.1.1:

$$-\frac{\partial \eta'}{\partial t'} - U' \frac{\partial \eta'}{\partial x'} - U' \frac{dh'}{dx'} + V' = 0, \quad Z' = d + \eta' \tag{7.3.1.3}$$

or in dimensionless form:

$$-\frac{\partial \eta}{\partial t} - \epsilon U \frac{\partial \eta}{\partial x} - \frac{\kappa^2}{\kappa_d} U \frac{dh}{dX} + V = 0, \quad Z = 1 + \epsilon\eta \tag{7.3.1.4}$$

As a consequence we obtain the following equation:

$$\frac{\partial \eta}{\partial t} = V - \frac{\kappa^2}{\kappa_d} U \frac{dh}{dX} + O(\kappa^2), \quad Z = 1 + \epsilon\eta \tag{7.3.1.5}$$

By Taylor expansion around $Z = 1$, we obtain:

$$\boxed{\frac{\partial \eta}{\partial t} = V - \frac{\kappa^2}{\kappa_d} U \frac{dh}{dX} + O(\kappa^2), \quad Z = 1+} \tag{7.3.1.6}$$

7.3.2 Conservation of mass in the mud

$$\left(\frac{\partial}{\partial x}-\frac{\kappa^2}{\kappa_d}\frac{dh}{dX}\frac{\partial}{\partial Z}\right)U+\frac{\partial V}{\partial Z}=0,\quad 0<Z<1+\epsilon\eta \tag{7.3.2.1}$$

By keeping only the first order, this means:

$$\boxed{\frac{\partial U}{\partial x}-\frac{\kappa^2}{\kappa_d}\frac{dh}{dX}\frac{\partial U}{\partial Z}+\frac{\partial V}{\partial Z}=0},\quad 0<Z<1+\epsilon\eta \tag{7.3.2.2}$$

7.3.3 Horizontal momentum in mud

The equation of momentum in mud, projected on the x-axis, gives:

$$\begin{aligned}\frac{\partial U}{\partial t}+\epsilon\left[U\left(\frac{\partial}{\partial x}-\frac{\kappa^2}{\kappa_d}\frac{dh}{dX}\frac{\partial}{\partial Z}\right)U+V\frac{\partial U}{\partial Z}\right]&=-\gamma\left(\frac{\partial}{\partial x}-\frac{\kappa^2}{\kappa_d}\frac{dh}{dX}\frac{\partial}{\partial Z}\right)P_d\\&+\frac{A}{Re*d}\left[\frac{\partial\tau_{xZ}}{\partial Z}+\kappa\kappa_d\left(\frac{\partial}{\partial x}-\frac{\kappa^2}{\kappa_d}\frac{dh}{dX}\frac{\partial}{\partial Z}\right)\tau_{xx}\right]\end{aligned} \tag{7.3.3.1}$$

From this equation we simplify:

$$\frac{\partial U}{\partial t}-\frac{1}{Re^{(2)}}\frac{A}{d}\frac{\partial\tau_{xZ}}{\partial Z}=-\gamma\frac{\partial P_d}{\partial x}+\frac{\kappa^2}{\kappa_d}\frac{dh}{dX}\frac{\partial P_d}{\partial Z}+O(\kappa^2) \tag{7.3.3.2}$$

where U is the horizontal velocity of mud, P_d the hydrodynamic pressure, A the amplitude of the free surface, γ the ratio of densities $\gamma=\rho_W/\rho_M$, d the mud depth and $Re^{(2)}$ the Reynolds number that is still:

$$\boxed{Re^{(2)}=\frac{\rho_M A dk\sqrt{gh}}{\mu_s}} \tag{7.3.3.3}$$

7.3.4 Vertical momentum in mud

The dimensional equation of vertical momentum is:

$$\rho_M\left[\frac{\partial V'}{\partial t'}+U'\left(\frac{\partial}{\partial x'}-\frac{dh'}{dx'}\frac{\partial}{\partial Z'}\right)V'+V'\frac{\partial V'}{\partial Z'}\right]=-\frac{\partial P'_d}{\partial Z'}+\left[\frac{\partial\tau'_{ZZ}}{\partial Z'}+\left(\frac{\partial}{\partial x'}-\frac{dh'}{dx'}\frac{\partial}{\partial Z'}\right)\tau'_{xZ}\right] \tag{7.3.4.1}$$

and becomes, in dimensionless variables:

$$\begin{aligned}\frac{\partial V}{\partial t}+\epsilon\left[U\left(\frac{\partial}{\partial x}-\frac{\kappa^2}{\kappa_d}\frac{dh}{dX}\frac{\partial}{\partial Z}\right)V+V\frac{\partial V}{\partial Z}\right]&=-\frac{\gamma}{\kappa^2\kappa_d^2}\frac{\partial P_d}{\partial Z}\\&+\frac{\epsilon}{Re\kappa^2\kappa_d}\left[\frac{\partial\tau_{ZZ}}{\partial Z}+\kappa\kappa_d\left(\frac{\partial}{\partial x}-\frac{\kappa^2}{\kappa_d}\frac{dh}{dX}\frac{\partial}{\partial Z}\right)\tau_{xZ}\right]\end{aligned} \tag{7.3.4.2}$$

So, in the end,

$$\boxed{\frac{\partial P_d}{\partial Z} = O(\epsilon\kappa)} \quad 0 < Z < 1 + \epsilon\eta \tag{7.3.4.3}$$

We can then simplify the horizontal momentum equation 7.3.3.2:

$$\frac{\partial U}{\partial t} - \frac{1}{Re^{(2)}}\frac{A}{d}\frac{\partial \tau_{xZ}}{\partial Z} = -\gamma\frac{\partial P_d}{\partial x} + O(\kappa^2) \tag{7.3.4.4}$$

7.3.5 Interface dynamic boundary condition

Let us call $\underline{n} = (n_x, n_Z)$ the vector normal to the interface. In dimensional notations, we know that the components of $\underline{n}$ are:

$$\begin{aligned} n_x &= \frac{\frac{d(-h'+\eta')}{dx'}}{\sqrt{1+\left(\frac{d(-h'+\eta')}{dx'}\right)^2}} \\ n_z &= \frac{1}{\sqrt{1+\left(\frac{d(-h'+\eta')}{dx'}\right)^2}} \end{aligned} \tag{7.3.5.1}$$

since $h'(x')$ and η' do not depend on Z. In dimensionless variables, we obtain:

$$\begin{aligned} n_x &= \frac{-\kappa^3\frac{dh}{dX} + \epsilon\kappa\kappa_d\frac{\partial\eta}{\partial x}}{\sqrt{1+\kappa^2\left(-\kappa^2\frac{dh}{dX} + \epsilon\kappa_d\frac{\partial\eta}{\partial x}\right)^2}} \\ &= -\kappa^3\frac{dh}{dX} + O(\kappa^5) \\ n_z &= \frac{1}{\sqrt{1+\kappa^2\left(-\kappa^2\frac{dh}{dX} + \epsilon\kappa_d\frac{\partial\eta}{\partial x}\right)^2}} \\ &= 1 + O(\kappa^6) \end{aligned} \tag{7.3.5.2}$$

Continuity of total (hydrodynamic and dynamic) stress on the mud-water interface then requires:

$$\begin{aligned} T_{xx}n_x + T_{xZ}n_Z &= -pn_x, \quad Z = 1+\epsilon\eta \\ T_{xZ}n_x + T_{ZZ}n_Z &= -pn_Z, \quad Z = 1+\epsilon\eta \end{aligned} \tag{7.3.5.3}$$

Total stress in mud is the sum of hydrostatic and dynamic pressure:

$$T_{ij} = -P\delta_{ij} + \frac{\epsilon\kappa}{\gamma Re^{(2)}}\tau_{ij}, \tag{7.3.5.4}$$

Introducing this sum in equation 6.4.5.3, we obtain:

$$\begin{aligned}\left(-P+\frac{\epsilon\kappa}{\gamma Re^{(2)}}\tau_{xx}\right)n_x+\frac{\epsilon\kappa}{\gamma Re^{(2)}}\tau_{xZ}n_Z&=-pn_x,\quad Z=1+\epsilon\eta\\ \frac{\epsilon\kappa}{\gamma Re^{(2)}}\tau_{xZ}n_x+\left(-P+\frac{\epsilon\kappa}{\gamma Re^{(2)}}\tau_{ZZ}\right)n_Z&=-pn_Z,\quad Z=1+\epsilon\eta\end{aligned}\tag{7.3.5.5}$$

From the approximations of n_x and n_Z that we demonstrated in 7.3.5.1, equations 7.3.5.5 become:

$$\begin{aligned}-\left(-P+\frac{\epsilon\kappa}{\gamma Re^{(2)}}\tau_{xx}\right)\kappa^3\frac{dh}{dX}+\frac{\epsilon\kappa}{\gamma Re^{(2)}}\tau_{xZ}&=p\kappa^3\frac{dh}{dX}+O(\kappa^5),\quad Z=1+\epsilon\eta\\ -\frac{\epsilon\kappa}{\gamma Re^{(2)}}\tau_{xZ}\kappa^3\frac{dh}{dX}+\left(-P+\frac{\epsilon\kappa}{\gamma Re^{(2)}}\tau_{ZZ}\right)&=-p+O(\kappa^4),\quad Z=1+\epsilon\eta\end{aligned}\tag{7.3.5.6}$$

These last equations can easily be simplified to:

$$\begin{aligned}\tau_{xZ}&=-\gamma Re^{(2)}(P-p)\frac{\kappa^2}{\epsilon}\frac{dh}{dX}+O(\kappa^2),\quad Z=1+\epsilon\eta\\ P-p&=O(\kappa^3),\quad Z=1+\epsilon\eta\end{aligned}\tag{7.3.5.7}$$

Let us now make use of the second equation (corresponding to normal stress condition) to simplify the first one (corresponding to tangential stress condition). Since $P-p=O(\kappa^3)$, we obtain:

$$\begin{aligned}\tau_{xZ}&=O(\kappa^2),\quad Z=1+\epsilon\eta\\ P-p&=O(\kappa^3),\quad Z=1+\epsilon\eta\end{aligned}\tag{7.3.5.8}$$

We now focus on the first part of equation 7.3.5.8. Through a Taylor expansion, we can approximate this equation around $Z=1$:

$$\tau_{xZ}(Z=1+\epsilon\eta)=\tau_{xZ}(Z=1)+O(\epsilon)\tag{7.3.5.9}$$

Hence, we obtain an interface boundary condition that we will use later to find the drift in mud:

$$\boxed{\tau_{xZ}(Z=1)=O(\kappa^2)}\tag{7.3.5.10}$$

Let us now focus on the second part of equation 7.3.5.8. From this equation we know that:

$$P=p+O(\kappa^3),\quad Z=1+\epsilon\eta\tag{7.3.5.11}$$

From 6.4.4.3, we know that the vertical gradient of mud dynamic pressure is of order

$O(\kappa^2)$. As a consequence, we have:

$$P = p(Z = 1 + \epsilon\eta) + O(\kappa^3), \quad 0 < Z < 1 + \epsilon\eta \tag{7.3.5.12}$$

Water pressure p is known in any point of the water layer thanks to the Bernouilli equation. In particular, we know from 7.2.5.8 the water pressure at the interface ($z = -h + \epsilon\kappa_d\eta$):

$$p = \frac{h(x)}{\epsilon} - (\phi_0)_t + O(\kappa^2) \tag{7.3.5.13}$$

So we conclude from 7.3.5.12:

$$P = \frac{h(x)}{\epsilon} - (\phi_0)_t + O(\kappa^2), \quad 0 < Z < 1 + \epsilon\eta \tag{7.3.5.14}$$

and we obtain in particular the dynamic pressure in mud:

$$P_d = -(\phi_0)_t + O(\kappa^2), \quad 0 < Z < 1 + \epsilon\eta \tag{7.3.5.15}$$

From equation 7.2.4.5, we also know:

$$\frac{\partial\phi^{(0)}}{\partial t} = -\zeta + O(\kappa^2) \tag{7.3.5.16}$$

which is valid for all z since $\phi^{(0)}$ and ζ do not depend on the vertical coordinate. Combining equations 7.3.5.15 and 7.3.5.16, we get the dynamic pressure in mud:

$$P_d = \zeta + O(\kappa^2), \quad 0 < Z < 1 + \epsilon\eta \tag{7.3.5.17}$$

and the dynamic pressure gradient in mud:

$$\frac{\partial P_d}{\partial x} = \frac{\partial\zeta}{\partial x} + O(\kappa^2), \quad 0 < Z < 1 + \epsilon\eta \tag{7.3.5.18}$$

As a consequence, we can now substitute the dynamic mud pressure P_d from the horizontal momentum equation 7.3.4.4, for $0 < Z < 1 + \epsilon\eta$:

$$\boxed{\frac{\partial U}{\partial t} - \frac{1}{Re^{(2)}}\frac{A}{d}\frac{\partial\tau_{xZ}}{\partial Z} = -\gamma\frac{\partial\zeta}{\partial x} + O(\kappa^2)} \tag{7.3.5.19}$$

7.3.6 Bottom kinematic boundary conditions

At the bottom of the mud layer, we impose the no-slip boundary condition:

$$\boxed{U = V = 0}, \quad Z = 0 \tag{7.3.6.1}$$

7.4 Asymptotic equations in water and viscoelastic mud

7.4.1 Surface and interface

Water equations

We decide to consider that the wavenumber changes with s, because of the bottom slope. As a consequence, we introduce the variables:

$$X = \kappa^2 x, \quad \xi = \frac{1}{\kappa^2}\int^X h^{-1/2} dX - t \tag{7.4.1.1}$$

and the derivatives are:

$$\begin{aligned} \frac{\partial}{\partial t} &\to -\frac{\partial}{\partial \xi} \\ \frac{\partial}{\partial x} &\to \kappa^2 \frac{\partial}{\partial X} + \frac{1}{\sqrt{h}}\frac{\partial}{\partial \xi} \end{aligned} \tag{7.4.1.2}$$

With these new variables, equations 7.2.3.16 and 7.2.4.13 become:

$$-\zeta_\xi + \kappa_d \eta_\xi + \kappa^2 h_X \bar{u} + \kappa^2 h \bar{u}_X + \epsilon \zeta_\xi h^{-1/2} \bar{u} + \epsilon \zeta h^{-1/2} \bar{u}_\xi + h^{1/2} \bar{u}_\xi = O(\kappa^4) \tag{7.4.1.3}$$

$$-\bar{u}_\xi + \epsilon h^{-1/2} \bar{u} \bar{u}_\xi + \kappa^2 \zeta_X + h^{-1/2} \zeta_\xi + \frac{\kappa^2}{3} h \bar{u}_{\xi\xi\xi} = O(\kappa^4) \tag{7.4.1.4}$$

From equation 7.4.1.3 at the first order, we deduce:

$$\begin{aligned} \bar{u}_\xi &= h^{-1/2}\zeta_\xi + O(\kappa^2) \\ \bar{u} &= h^{-1/2}\zeta + O(\kappa^2) \\ \bar{u}_X &= h^{-1/2}\zeta_X - \frac{h_X}{2h^{3/2}}\zeta + O(\kappa^2) \end{aligned} \tag{7.4.1.5}$$

We now consider (equation 7.4.1.3 $+h^{1/2}*$ equation 7.4.1.4) at the second order and we obtain:

$$\begin{aligned}\kappa_d\eta_\xi+\kappa^2 h_X\bar{u}+\kappa^2 h\bar{u}_X+\epsilon\zeta_\xi h^{-1/2}\bar{u}+\epsilon\zeta h^{-1/2}\bar{u}_\xi \\ +h^{1/2}\left(\epsilon h^{-1/2}\bar{u}\bar{u}_\xi+\kappa^2\zeta_X+\frac{\kappa^2}{3}h\bar{u}_{\xi\xi\xi}\right)=O(\kappa^2)\end{aligned} \tag{7.4.1.6}$$

Using the relations 7.4.1.5, equation 7.4.1.6 becomes:

$$\begin{aligned}\frac{\kappa_d}{\kappa^2}\eta_\xi+h_X h^{-1/2}\zeta+h\left(h^{-1/2}\zeta_X-\frac{h_X}{2h^{3/2}}\zeta\right)+\frac{\epsilon}{\kappa^2}\zeta_\xi h^{-1}\zeta+\frac{\epsilon}{\kappa^2}\zeta h^{-1}\zeta_\xi \\ +h^{1/2}\left(\frac{\epsilon}{\kappa^2}h^{-1/2}h^{-1/2}\zeta h^{-1/2}\zeta_\xi+\zeta_X+\frac{1}{3}hh^{-1/2}\zeta_{\xi\xi\xi}\right)=O(\kappa^2)\end{aligned} \tag{7.4.1.7}$$

and equation 7.4.1.7 finally becomes:

$$\boxed{2h^{1/2}\zeta_X+\frac{h_X}{2h^{1/2}}\zeta+\frac{3}{2h}\frac{\epsilon}{\kappa^2}(\zeta^2)_\xi+\frac{h^{1/2}}{3}\zeta_{\xi\xi\xi}=-\frac{\kappa_d}{\kappa^2}\eta_\xi+O(\kappa^2)} \tag{7.4.1.8}$$

Let us compare this result with what we obtained in the case where non-linearity was more important than dispersion (chapter 6). Indeed, equations 6.5.1.8 and 7.4.1.8 differ. A new term appears in equation 7.4.1.8, namely $\frac{h^{1/2}}{3}\zeta_{\xi\xi\xi}$, which is due to dispersion. This term did not appear before because dispersion was less important compared to non-linearity.

Now let us expand the functions ζ, η and $\bar{u}$ as power series:

$$\begin{aligned}\zeta&=\zeta^{(0)}+\kappa^2\zeta^{(1)}+\kappa^4\zeta^{(2)}+\ldots \\ \eta&=\eta^{(0)}+\kappa^2\eta^{(1)}+\kappa^4\eta^{(2)}+\ldots \\ \bar{u}&=\bar{u}^{(0)}+\kappa^2\bar{u}^{(1)}+\kappa^4\bar{u}^{(2)}+\ldots\end{aligned} \tag{7.4.1.9}$$

Because we expect the typical distance of the mud induced damping to be $\kappa^2 x$, let us also introduce the slow coordinate X:

$$X=\kappa^2 x \tag{7.4.1.10}$$

Because this last equation is non-linear, we decide to adopt the following form for $\zeta^{(0)}$ and $\eta^{(0)}$:

$$\zeta^{(0)}=\frac{1}{2}\sum_{m=-\infty}^{+\infty}A_m(X)e^{im\xi}\quad \eta^{(0)}=\frac{1}{2}\sum_{m=-\infty}^{+\infty}B_m(X)e^{im\xi} \tag{7.4.1.11}$$

Then we know that:

$$\begin{aligned}
\frac{\partial \zeta^{(0)}}{\partial X} &= \frac{1}{2}\sum_{m=1}^{\infty}\frac{dA_m}{dX}e^{im\xi} + cc. \\
\frac{3}{2h}\frac{\partial(\zeta^{(0)})^2}{\partial \xi} &= \sum_{m=1}^{\infty}\frac{3}{8h}ime^{im\xi}\left[\sum_{l=1}^{\infty}2A_l^*A_{m+l} + \sum_{l=1}^{[m/2]}\alpha_l A_l A_{m-l}\right] + cc. \\
\frac{\partial^3 \zeta^{(0)}}{\partial \xi^3} &= \frac{1}{2}\sum_{m=1}^{\infty}(-im^3)A_m e^{im\xi} + cc.
\end{aligned} \tag{7.4.1.12}$$

Then, from equation 7.4.1.8, we deduce $\forall m$:

$$\begin{aligned}
\sqrt{h}\frac{dA_m}{dX} + \frac{h_X}{4\sqrt{h}}A_m + \frac{\epsilon}{\kappa^2}\frac{3i}{8h}m\left[\sum_{l=1}^{\infty}2A_l^*A_{m+1l} + \sum_{l=1}^{[m/2]}\alpha_l A_l A_{m-l}\right] - \frac{im^3}{6}hA_m \\
+ \frac{\kappa_d}{\kappa^2}\frac{im}{2}B_m = 0
\end{aligned} \tag{7.4.1.13}$$

where $[m/2]$ is the integer part of $m/2$ and α_l is a coefficient equal to 1 for $l = [m/2]$ and equal to 2 otherwise.

Compared to equation 6.5.1.12 where dispersion was less important than nonlinearity, we have one more term in equation 7.4.1.13, namely $-\frac{im^3}{6}hA_m$, that represents the effects of wave dispersion.

Mud equations

Let us find a new relationship between A_m and B_m in order to solve equation 7.4.1.13

Equation 7.3.5.19 gives:

$$\frac{\partial U}{\partial t} - \alpha^{(2)}\frac{\partial \tau_{xZ}}{\partial Z} = -\gamma\frac{\partial \zeta}{\partial x} + O(\epsilon), \quad 0 < Z < 1 + \epsilon\eta(x) \tag{7.4.1.14}$$

with:

$$\alpha^{(2)} = \frac{\epsilon}{\kappa_d Re^{(2)}} = O(1) \tag{7.4.1.15}$$

From the change of variables defined in 7.4.1.1, we convert equations 7.4.1.14, 7.3.2.2

and 7.3.1.6 in:

$$\begin{aligned}
\alpha^{(2)}\frac{\partial(\tau_{xZ})^{(0)}}{\partial Z}+\frac{\partial U^{(0)}}{\partial \xi}&=\gamma h^{-1/2}\frac{\partial \zeta^{(0)}}{\partial \xi}+O(\epsilon),\quad 0<Z<1+\epsilon\eta(x)\\
h^{-1/2}\frac{\partial U^{(0)}}{\partial \xi}-\frac{\kappa^2}{\kappa_d}\frac{dh}{dX}\frac{\partial U^{(0)}}{\partial Z}+\frac{\partial V^{(0)}}{\partial Z}&=0,\quad 0<Z<1+\epsilon\eta(x)\\
-\frac{\partial \eta^{(0)}}{\partial \xi}&=V-\frac{\kappa^2}{\kappa_d}\frac{dh}{dX}\frac{\partial U^{(0)}}{\partial Z},\quad 0<Z<1+\epsilon\eta(x)
\end{aligned}\tag{7.4.1.16}$$

Since the water equations are not linear, we consider several harmonics and write:

$$\begin{aligned}
U^{(0)}=\frac{1}{2}\sum_{m=-\infty}^{\infty}U_m^{(0)}(Z)e^{im\xi}\quad V^{(0)}=\frac{1}{2}\sum_{m=-\infty}^{\infty}V_m^{(0)}(Z)e^{im\xi}\\
(\tau_{xZ})^{(0)}=\frac{1}{2}\sum_{m=-\infty}^{\infty}(\tau_{xZ})_m^{(0)}(Z)e^{im\xi}
\end{aligned}\tag{7.4.1.17}$$

Let us find an equation between A_m and B_m from the mud equations. From the first equation of 7.4.1.16, we know:

$$\alpha^{(2)}\frac{d(\tau_{xZ})_m^{(0)}}{dZ}+imU_m^{(0)}=h^{-1/2}im\gamma A_m \tag{7.4.1.18}$$

From equation 6.2.0.14, which only applies to simple harmonic waves, we deduce:

$$(\tau_{xZ})_m^{(0)}=\mu_m\frac{dU_m^{(0)}}{dZ}+O(\kappa^4) \tag{7.4.1.19}$$

As a consequence, equation 7.4.1.18 becomes:

$$\frac{d^2U_m^{(0)}}{dZ^2}+\frac{im}{\alpha^{(2)}\mu_m}U_m^{(0)}=h^{-1/2}\frac{im}{\alpha^{(2)}\mu_m}\gamma A_m \tag{7.4.1.20}$$

which can be simplified as:

$$\frac{d^2U_m^{(0)}}{dZ^2}-\tilde{\sigma}_m^2U_m^{(0)}=-h^{-1/2}\tilde{\sigma}_m^2\gamma A_m \tag{7.4.1.21}$$

where $\tilde{\sigma}_m^2$ is as in the flat bottom case (chapter 5):

$$\tilde{\sigma}_m^2=-i\frac{m}{\alpha^{(2)}\mu_m} \tag{7.4.1.22}$$

Knowing the value of $\alpha^{(2)}$, we deduce:

$$\boxed{\tilde{\sigma}_m^2 = -i\frac{m\kappa_d \rho_M A dk\sqrt{g\bar{h}}}{\epsilon\mu'_m}} \tag{7.4.1.23}$$

Let us note that the value of $\tilde{\sigma}_m$ does not depend on μ_s, since $\mu_s\mu_m = \mu'_m$ is the dimensional viscosity. As $\alpha^{(2)}$ and $Re^{(2)}$ do not appear in equation 7.4.1.21, we deduce that we will not need the value of μ_s to solve it.

We also know the boundary conditions:

$$\begin{aligned} U^{(0)} &= 0, \quad Z = 0 \\ \frac{dU^{(0)}}{dZ} &= O(\epsilon), \quad Z = 1 \end{aligned} \tag{7.4.1.24}$$

and thus, $\forall m$:

$$\begin{aligned} U_m^{(0)} &= 0, \quad Z = 0 \\ \frac{dU_m^{(0)}}{dZ} &= 0, \quad Z = 1 \end{aligned} \tag{7.4.1.25}$$

We obtain the value of the horizontal velocity:

$$\begin{aligned} U_m^{(0)} = &\frac{\gamma A_m}{\sqrt{h}}\Big[1 - [1 + \tanh(\tilde{\sigma}_m)]\cosh(\tilde{\sigma}_m Z) \\ &+ [\tanh(\tilde{\sigma}_m)]\sinh(\tilde{\sigma}_m Z)\Big] \end{aligned} \tag{7.4.1.26}$$

From 7.4.1.16, we also know:

$$\forall m, \quad \frac{dV_m^{(0)}}{dZ} = -\frac{im}{\sqrt{h}}U_m^{(0)} + \frac{\kappa^2}{\kappa_d}\frac{dh}{dX}\frac{\partial U_m^{(0)}}{\partial Z} \tag{7.4.1.27}$$

Using the boundary condition:

$$V_m^{(0)}(Z = 0) = 0 \tag{7.4.1.28}$$

we obtain:

$$\begin{aligned} V_m^{(0)} = &- im\frac{\gamma A_m}{\tilde{\sigma}_m h}\Big[\tilde{\sigma}_m Z - [1 + \tanh(\tilde{\sigma}_m)]\sinh(\tilde{\sigma}_m Z) \\ &+ [\tanh(\tilde{\sigma}_m)]\cosh(\tilde{\sigma}_m Z) - \tanh(\tilde{\sigma}_m)\Big] \\ &+ \frac{\kappa^2}{\kappa_d}\frac{dh}{dX}U_m^{(0)} \end{aligned} \tag{7.4.1.29}$$

It is interesting to note that there is a new term in the expression of $V_m^{(0)}$ compared to the flat bottom case (chapter 5). This is due to the fact that we are not considering the sane axes anymore. as a consequence, the vertical velocity must be corrected with a term proportional to the horizontal velocity and the slope $\frac{dh}{dX}$. Now, still from equation 7.4.1.16, we have:

$$\forall m, B_m(X) = -\frac{1}{im}\left(V_m^{(0)}(Z=1) - \frac{\kappa^2}{\kappa_d}\frac{dh}{dX}U_m^{(0)}(Z=1)\right) \tag{7.4.1.30}$$

After calculation, we obtain:

$$\forall m, \quad \boxed{B_m(X) = \frac{\gamma A_m}{h}\left[1 - \frac{\tanh\tilde{\sigma}_m}{\tilde{\sigma}_m}\right]} \tag{7.4.1.31}$$

Combining equations 7.4.1.13 and 7.4.1.31, we naturally obtain:

$$\begin{aligned}\sqrt{h}\frac{dA_m}{dX} + \frac{h_X}{4\sqrt{h}}A_m + \frac{\epsilon}{\kappa^2}\frac{3i}{8h}m\left[\sum_{l=1}^{\infty} 2A_l^* A_{m+1l} + \sum_{l=1}^{[m/2]} \alpha_l A_l A_{m-l}\right] - \frac{im^3}{6}hA_m \\ + \frac{\kappa_d}{\kappa^2}\frac{im}{2}\frac{\gamma A_m}{h}\left[1 - \frac{\tanh\tilde{\sigma}_m}{\tilde{\sigma}_m}\right] = 0\end{aligned} \tag{7.4.1.32}$$

where $[m/2]$ is the integer part of $m/2$ and α_l is a coefficient equal to 1 for $l = [m/2]$ and equal to 2 otherwise.

Let us compare this equation to what we found in the case where non-linearity was more important than dispersion (chapter 6). We observe that equations 6.5.1.31 and 7.4.1.32 only differ by one term, which is due to dispersion, namely $\frac{im^3}{6}A_m$.

As we already pointed out, this term did not appear before because dispersion was less important compared to non-linearity.

7.5 Further details

7.5.1 Surface and the interface

By truncating the infinite series, equation 7.4.1.32 becomes:

$$\forall m,\quad \sqrt{h}\frac{dA_m}{dX}+\frac{h_X}{4\sqrt{h}}A_m+\frac{\epsilon}{\kappa^2}\frac{3i}{8h}m\left[\sum_{l=1}^{n-m}2A_l^*A_{m+1l}+\sum_{l=1}^{[m/2]}\alpha_l A_l A_{m-l}\right]-\frac{im^3}{6}hA_m + \frac{\kappa_d}{\kappa^2}\frac{im}{2}\frac{\gamma A_m}{h}\left[1-\frac{\tanh\tilde{\sigma}_m}{\tilde{\sigma}_m}\right]=0 \tag{7.5.1.1}$$

The truncated differential system is true for $0<m\leq n$.

7.5.2 Energy variation

We found the partial differential equation 7.5.1.1:

$$\frac{d(h^{1/4}A_m)}{dX}-\frac{im^3}{6}h^{3/4}A_m+\frac{3i}{8}\beta m\frac{1}{h^{5/4}}\left(\sum_{l=1}^{\infty}2A_l^*A_{m+1l}+\sum_{l=1}^{[m/2]}\alpha_l A_l A_{m-l}\right) + h^{-5/4}\frac{\kappa_d}{\kappa^2}\frac{i\gamma}{2}m\left(1-\frac{\tanh(\tilde{\sigma}_m)}{\tilde{\sigma}_m}\right)A_m=0 \tag{7.5.2.1}$$

We introduce $\tilde{A}_m=h^{1/4}A_m$, and modify equation 7.5.2.1 as:

$$\frac{d\tilde{A}_m}{dX}-\frac{im^3}{6}h^{1/2}\tilde{A}_m+\frac{3i}{8}\beta m\frac{1}{h^{7/4}}\left(\sum_{l=1}^{\infty}2\tilde{A}_l^*\tilde{A}_{m+1l}+\sum_{l=1}^{[m/2]}\alpha_l\tilde{A}_l\tilde{A}_{m-l}\right) + \frac{\kappa_d}{\kappa^2}h^{-3/2}\frac{i\gamma}{2}m\left(1-\frac{\tanh(\tilde{\sigma}_m)}{\tilde{\sigma}_m}\right)\tilde{A}_m=0 \tag{7.5.2.2}$$

Using the same demonstration than in the flat case, we easily deduce the variation law:

$$\frac{d}{dX}\left[\sum_{m=1}^{n}|\tilde{A}_m|^2\right]=-2h^{-3/2}\frac{\kappa_d}{\kappa^2}\sum_{m=1}^{n}Re\left[\frac{i\gamma}{2}m\left(1-\frac{\tanh(\tilde{\sigma}_m)}{\tilde{\sigma}_m}\right)\right]|\tilde{A}_m|^2 \tag{7.5.2.3}$$

and we then obtain the energy variation relation:

$$\boxed{\frac{d}{dX}\left[\sqrt{h}\sum_{m=1}^{n}|A_m|^2\right]=-\frac{\gamma}{h}\frac{\kappa_d}{\kappa^2}\sum_{m=1}^{n}Re\left[im\left(1-\frac{\tanh(\tilde{\sigma}_m)}{\tilde{\sigma}_m}\right)\right]|A_m|^2} \tag{7.5.2.4}$$

7.5.3 Behavior at the shore

Let us study the evolution of $|A_m|$ towards the shore, that is to say towards $h = 0$. Since this study is based on the energy variation equation 7.5.2.4, which is very similar to the result we previously obtained (equation 6.6.3.4), this demonstration will be similar to the one made in the previous chapter.

We will here consider that the water depth decreases as X increases. In other words $h_X < 0$.

As demonstrated before, we know that there is always one harmonic $|A_m|$ that decays last. Let us prove that this harmonic decays to zero, and we will have proven that all harmonics decay to zero at the shore. Let us call A_{dom} this harmonic.

Let us consider X_0 such as $\forall X > X_0$, all the A_m are negligible compared to A_{dom}. Such an X_0 exists because the attenuation rate of A_{dom} is the smallest.

Ignoring all modes $m \neq dom$, let us rewrite equation 7.5.2.4 for $|A_{dom}|^2$ only:

$$\frac{d}{dX}\left[\sqrt{h}|A_{dom}|^2\right] = -\frac{1}{h}\frac{|A_{dom}|^2}{L_{dom}} \tag{7.5.3.1}$$

Let us write $\tilde{A}_{dom}$ such as:

$$\tilde{A}_{dom} = h^{1/4}A_{dom} \tag{7.5.3.2}$$

Then equation 7.5.3.1 becomes:

$$\frac{d|\tilde{A}_{dom}|^2}{dX} = -\frac{1}{h^{3/2}}\frac{|\tilde{A}_{dom}|^2}{L_{dom}} \tag{7.5.3.3}$$

Since the aim of this study is to consider the behavior very close to the shore, the beach can be approximated as a plane beach. We choose s such as $h(X) = 1 - sX$, and thus $h_X = -s$. The solution of this equation is:

$$|\tilde{A}_{dom}|^2 = \alpha_{dom}\exp\left[-\frac{2}{L_{dom}}\frac{h^{-1/2}}{s}\right] \tag{7.5.3.4}$$

With α_{dom} a real constant. And thus:

$$|A_{dom}|^2 = \frac{\alpha_{dom}}{h^{1/2}}\exp\left[-\frac{2}{L_{dom}}\frac{h^{-1/2}}{s}\right] \tag{7.5.3.5}$$

Since $L_{dom} > 0$ and $h^{-1/2}$ is a growing function of X, we deduce that $|A_{dom}|^2 \to 0$ exponentially as $h \to 0$.

Since A_{dom} is the dominant harmonic, and all the others are negligible, we deduce

that: $\boxed{\text{all harmonics } |A_m|^2 \to 0 \text{ exponentially as } h \to 0}$.

Let us now study the interface harmonics B_m. From equation 7.4.1.31, we know that:

$$\forall m, \quad B_m(X) = \frac{\gamma A_m}{h}\left[1 - \frac{\tanh(\tilde{\sigma}_m)}{\tilde{\sigma}_m}\right] \tag{7.5.3.6}$$

As a consequence, by multiplying 7.5.3.6 to its complex conjugate:

$$\forall m, \quad |B_m|^2 = \frac{\gamma |A_m|^2}{h^2}\left|1 - \frac{\tanh(\tilde{\sigma}_m)}{\tilde{\sigma}_m}\right|^2 \tag{7.5.3.7}$$

And we deduce from the previous result on the $|A_m|^2$ that $|B_m|^2 \to 0$ exponentially as $h \to 0$.

7.6 Numerical results by using the first ten harmonics

We now solve this equation in the particular case:

$$\begin{aligned} &h'(x') = \bar{h}, \quad 0 < X \\ &h'(x') = \bar{h} - s'x', \quad 0 < X < 1/s \\ &h'(x') = 0, \quad X \geq 1/s \end{aligned} \tag{7.6.0.8}$$

In dimensionless form, writing

$$s' = \kappa^3 s, \tag{7.6.0.9}$$

equation 7.6.0.8 becomes:

$$\begin{aligned} &h(X) = 1, \quad 0 < X \\ &h(X) = 1 - sX, \quad 0 < X < 1/s \\ &h(X) = 0, \quad X \geq 1/s \end{aligned} \tag{7.6.0.10}$$

corresponding to:

$$\begin{aligned} &h_X = 0, \quad 0 < X \\ &h_X = -s, \quad 0 < X < 1/s \\ &h_X = 0, \quad X > 1/s \end{aligned} \tag{7.6.0.11}$$

We are going to plot these results for the viscoelastic muds we previously studied.

Let us sum up the different muds we have:

- Case A: Gulf of Mexico mud. This mud is rather elastic.
- Case B: Mobile Bay mud. This mud is rather elastic as well
- Case C: Lianyungang mud. This mud complex viscosity's phase is around $\frac{\pi}{4}$ so it is as elastic as viscous.
- Case D: Hangzhou Bay mud. This mud is rather viscous, its complex viscosity's phase being close to zero.

7.6.1 Comparison of the different types of mud

We first look at the results for four types of mud in the case $\bar{h} = 5m$, $T = 18s$ (which means $\omega' = 1/3rad/s$), $A = 40cm$ and $d = 25$cm. As in the previous chapter, we first decide to set the slope such as $s = 1/5$. So in the end, and for this entire section, the parameters are:

$$\boxed{\kappa = 0.24,\ \epsilon = 0.08,\ \kappa_d = 0.05,\ s = 1/5} \tag{7.6.1.1}$$

Surface and interface

Computations have been carried out for 10 harmonics. In figures 7-2 and 7-4, we present the variation of the first three harmonics of the surface and the interface. Warning: the scales are not the same for every mud.

In figure 7-2, it can be observed that damping is stronger for the Gulf of Mexico, Lianyungang and Hangzhou Bay (A, C, D) than for the Mobile Bay mud (B). This result is consistent with the previous chapter for horizontal sea bed.

We only plot the surface motion up to $X = 4.6$ for the Mobile Bay mud, because strong oscillations appear for X higher. However, we show in figure 7-3 a zoom-in of the interface variation for this mud at the shore. This figure allows us to see that the surface motion eventually reaches a zero-value at the shore.

The fastest damping occurs with the Hangzhou Bay mud, as we already noted over a flat bottom (chapter 5).

Figure 7-4 shows the variation of the interface. For the Mobile Bay mud, the interface displacement is very small compared to the other muds. We already observed before that the interface displacement was small for this mud, because the mud-induced damping is less significant than with the other muds.

For the Gulf of Mexico, Mobile Bay and Lianyungang muds (A, B, C), the harmonics increase next to the shore. Figure 7-5 gives a zoom of the interface motion for these muds. These zoomed figures allow us to see that the $|B_m|$ go to zero extremely quickly right before the shore, which is what we expected from the analytic study we carried in section 7.5.3.

Energy variation

We numerically represented the total first-order energies in figure 7-6. This figure shows that the total energy logically decreases, to reach a zero-value at the shore ($X = 5$). However, we observe once again that dissipation is slower to occur in the Mobile Bay mud (B).

On the contrary, we note that energy decays more quickly with the Hangzhou Bay mud, where mud-induced damping leads to energy losses before the shore.

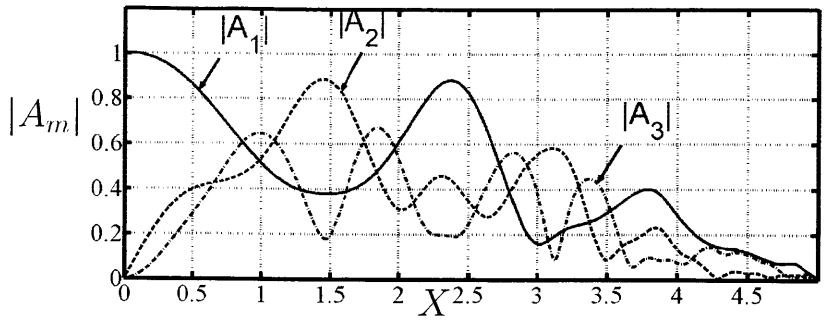

(a) Gulf of Mexico mud

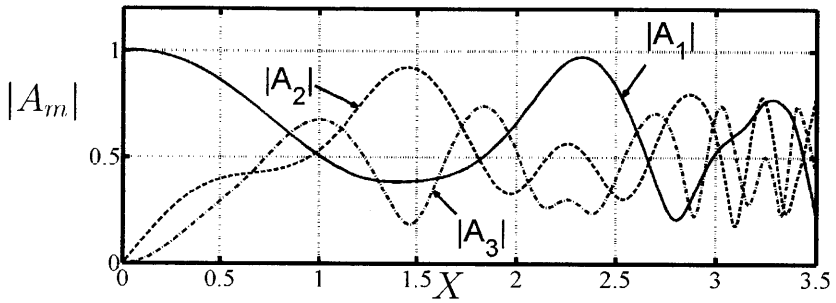

(b) Mobile Bay mud

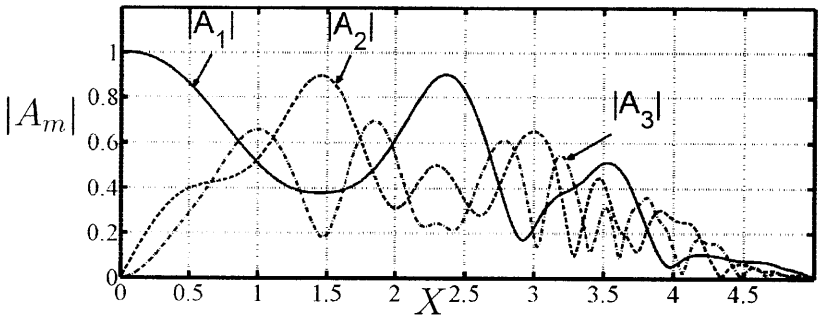

(c) Lianyungang mud

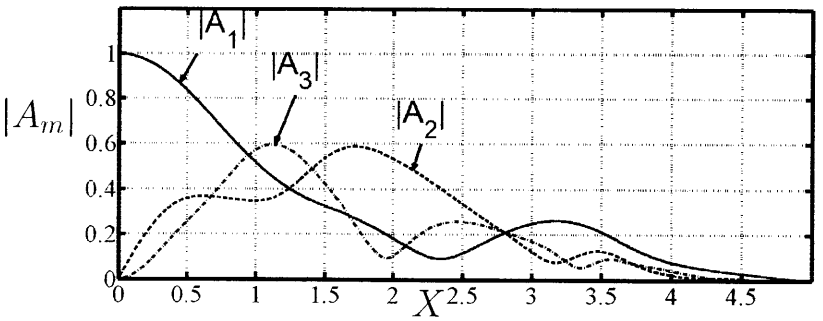

(d) Hangzhou Bay mud

Figure 7-2: Evolution of the first 3 harmonics of the free surface over different types of viscoelastic muddy seabeds. Warning: the horizontal and vertical scales are different for mud B.

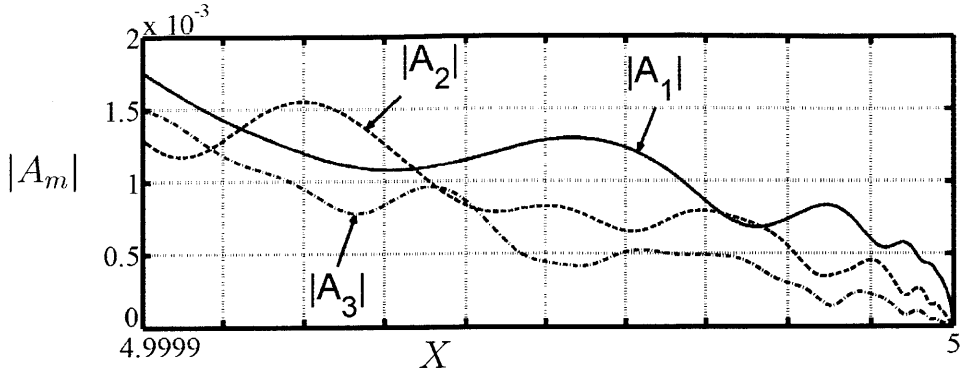

Figure 7-3: Zoom-in of the surface motion for the Mobile Bay mud.

7.6.2 Influence of the slope s'

We now focus on the influence of the slope. We look at the slope values $s' = 0.014$, $s' = 0.0069$, $s' = 0.0035$, $s' = 0.0023$, $s' = 0.0014$ and $s' = 0.00069$, respectively corresponding the non-dimensional slope values:

$$\boxed{s = 1,\ s = 1/2,\ s = 1/4,\ s = 1/6,\ s = 1/10,\ s = 1/20} \tag{7.6.2.1}$$

We still have $\bar{h} = 5m$, $T = 18s$ (which means $\omega' = 1/3rad/s$), $A = 40cm$ and $d = 25$cm, corresponding to the parameters values:

$$\boxed{\kappa = 0.24,\ \epsilon = 0.08,\ \kappa_d = 0.05} \tag{7.6.2.2}$$

We only focus on the Gulf of Mexico mud (A) and the Hangzhou Bay mud (D), because they respectively correspond to the most elastic and the most Newtonian muds we have data for.

Surface and interface

Figures 7-7, 7-8 and 7-9 show the variation of the surface for different slopes for the Gulf of Mexico and the Hangzhou Bay muds.

We obtained in the flat bottom case of chapter 5 (figure 5-1), that the harmonics $|A_m|$ were not even damped at $X = 40$ with the Gulf of Mexico mud and are damped after $X = 20$ with the Hangzhou Bay mud.

Now, with a sloping bottom, we observe that the harmonics are always damped before the shore, to reach a zero value at $X = 5$. In particular, when the slope is steep with $s = 1$, the harmonics are all damped at $X = 1$. This result agrees to what we analytically demonstrated in section 7.5.3.

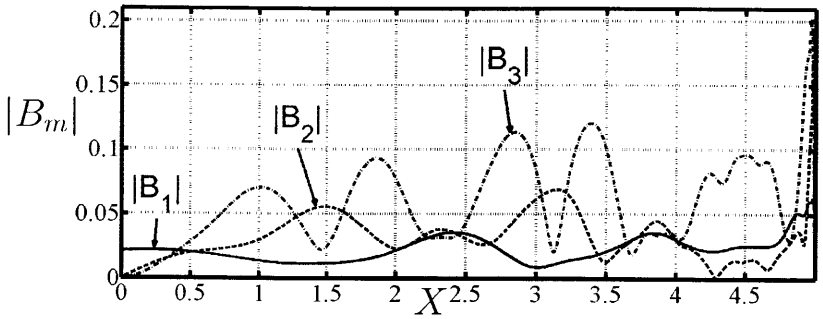

(a) Gulf of Mexico mud

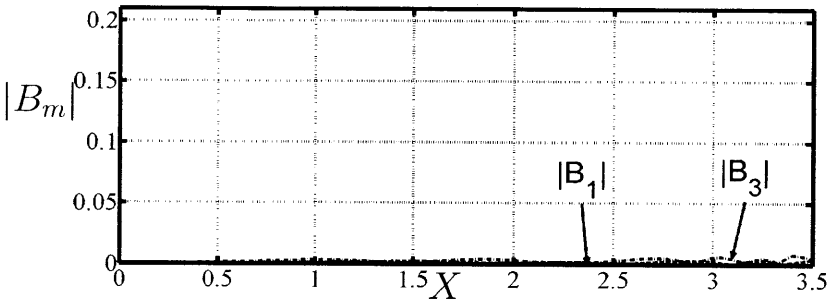

(b) Mobile Bay mud

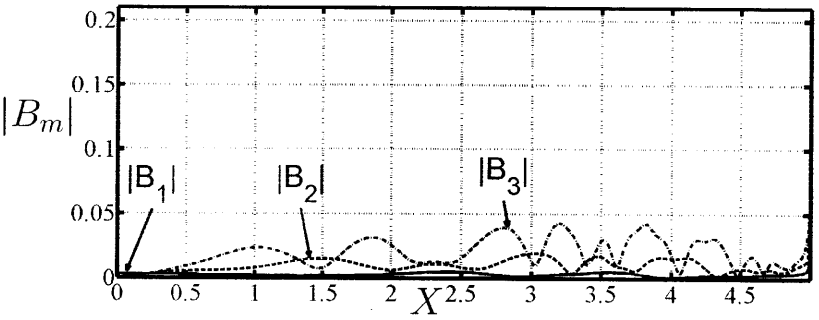

(c) Lianyungang mud

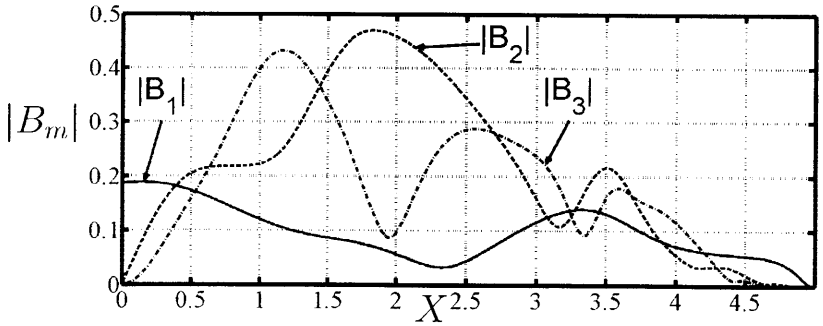

(d) Hangzhou Bay mud

Figure 7-4: Evolution of the first 3 harmonics of the interface over different types of viscoelastic muddy seabeds. Warning: the scale is different for mud D.

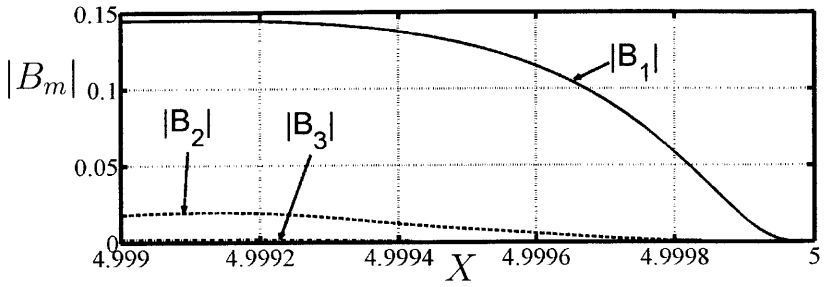

(a) Gulf of Mexico mud

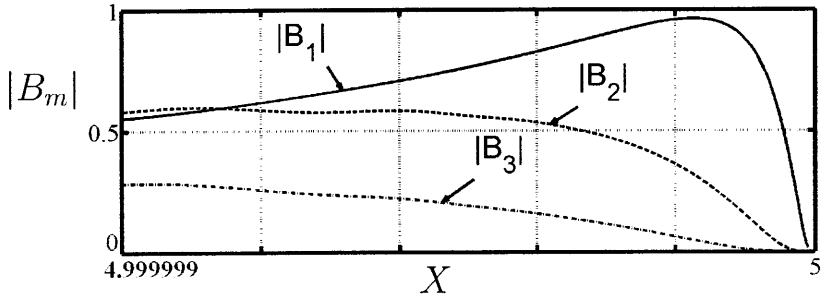

(b) Mobile Bay mud

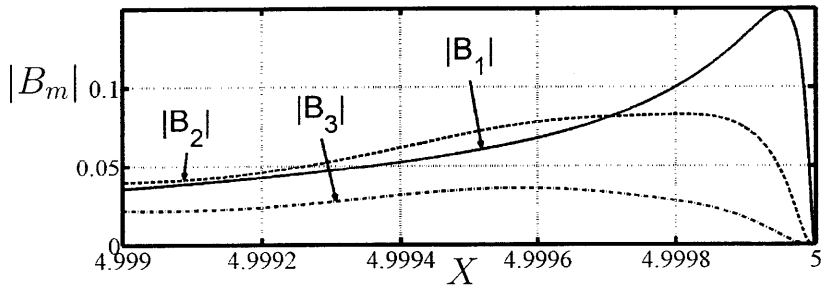

(c) Lianyungang mud

Figure 7-5: Evolution of the first 3 harmonics of the interface near the shore for the Gulf of Mexico, Mobile Bay and the Lianyungang muds.

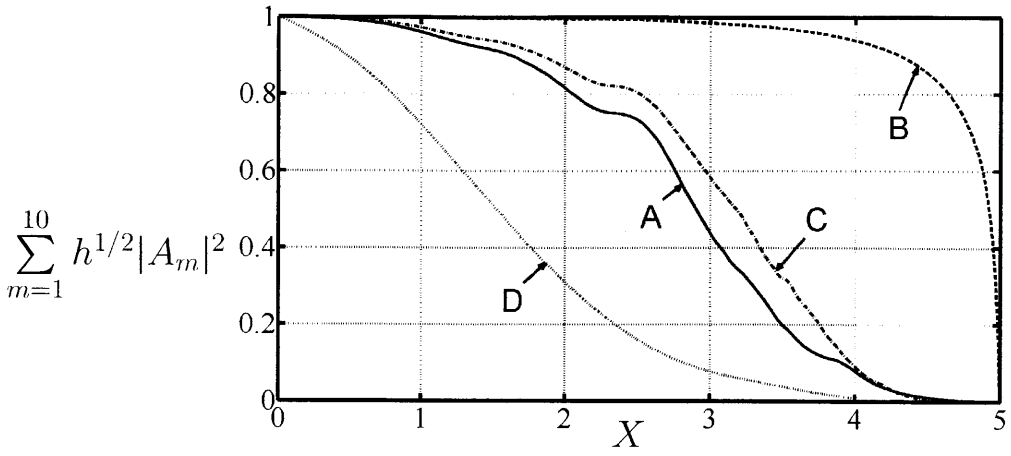

Figure 7-6: Wave energy over a flat thick muddy seabed. Mud A is Gulf of Mexico mud, mud B is Mobile Bay mud, mud C is Lianyungang mud and mud D is Hangzhou Bay mud.

However, when the slope becomes less steep ($s = 1/20$), the harmonics have time to be damped out before reaching the shore for the Hangzhou Bay mud. In this case, the damping is also due to the presence of mud.

Figures 7-10, 7-11 and 7-12 show the variation of the surface for different slopes for the same muds. We observe that the interface displacement is always stronger with the Hangzhou Bay mud, where the damping is the most significant.

Figures 7-13 and 7-14 show a zoom-in of the interface motion near the shore for the Gulf of Mexico mud. We see on these figures that the harmonics $|B_m|$ ultimately go to zero, which agrees with the analytical predictions.

Energy variation

We numerically represent the total first-order energies in figure 7-15 for the different slopes. This figure shows that the total energy logically decreases, to reach a zero-value at the shore ($X = 5$). The shore is reached for $X = 1$ for $s = 1$, for $X = 2$ for $s = 1/2$ and so on ...

We observe once again that dissipation is slower to occur in the Gulf of Mexico mud (A). For instance, for $s = 1/20$ and at at $X = 10$ the total energy is already nearly zero with the Hangzhou Bay mud, when it still represents more than 30% of its initial value with the Gulf of Mexico mud.

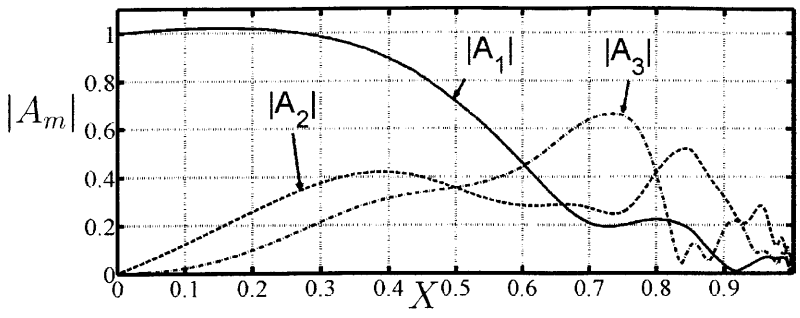

(a) Gulf of Mexico mud, $s = 1$

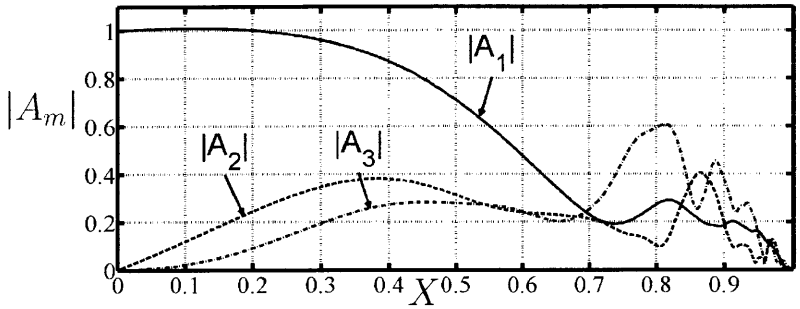

(b) Hangzhou Bay mud, $s = 1$

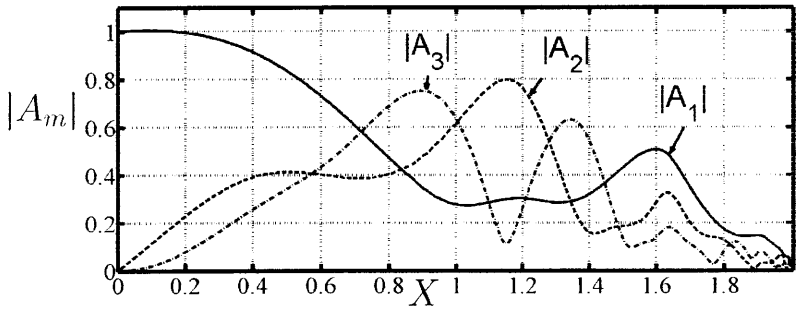

(c) Gulf of Mexico mud, $s = 1/2$

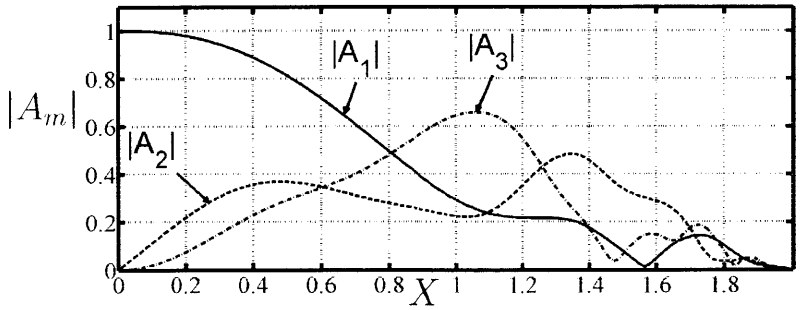

(d) Hangzhou Bay mud, $s = 1/2$

Figure 7-7: Evolution of the first 3 harmonics of the free surface over different types of viscoelastic muddy seabeds, in the cases $s = 1$ and $s = 1/2$. Warning: we use a different scale for the Gulf of Mexico mud, $s = 1$ case.

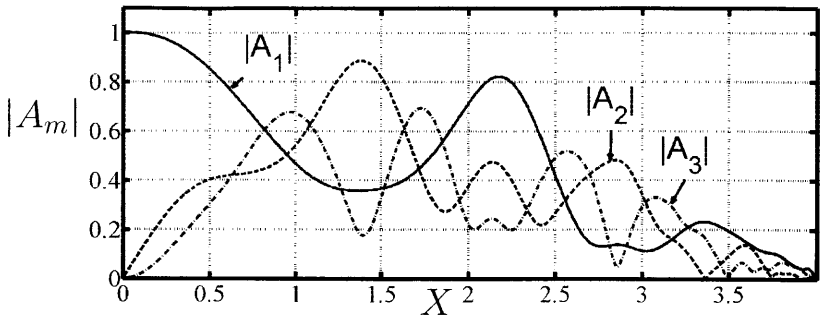

(a) Gulf of Mexico mud, $s = 1/4$

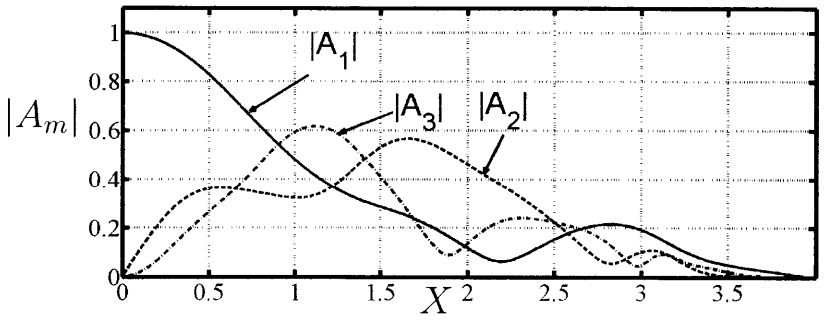

(b) Hangzhou Bay mud, $s = 1/4$

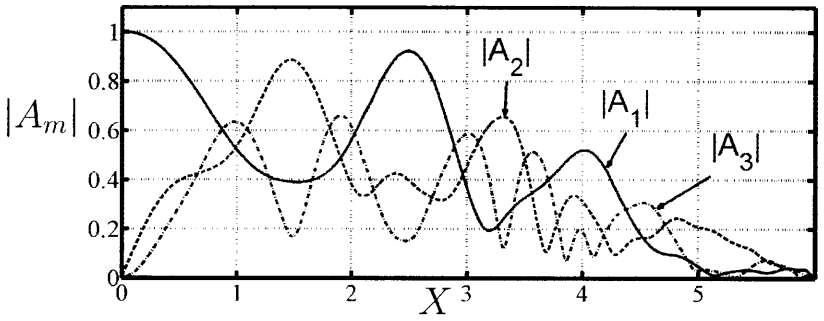

(c) Gulf of Mexico mud, $s = 1/6$

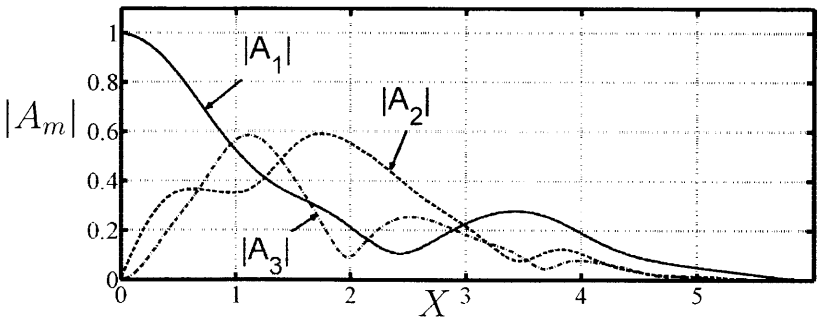

(d) Hangzhou Bay mud, $s = 1/6$

Figure 7-8: Evolution of the first 3 harmonics of the free surface over different types of viscoelastic muddy seabeds, in the cases $s = 1/4$ and $s = 1/6$.

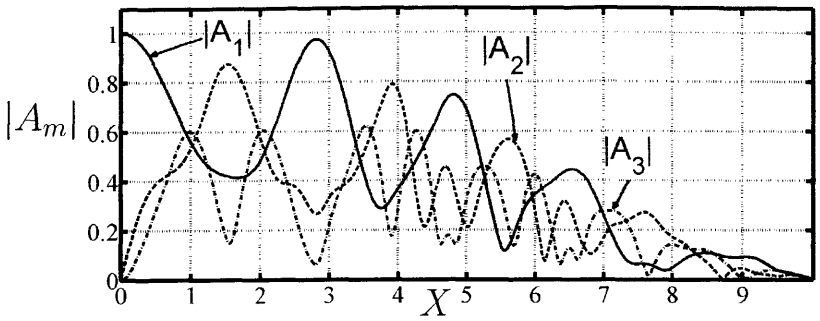

(a) Gulf of Mexico mud, $s = 1/10$

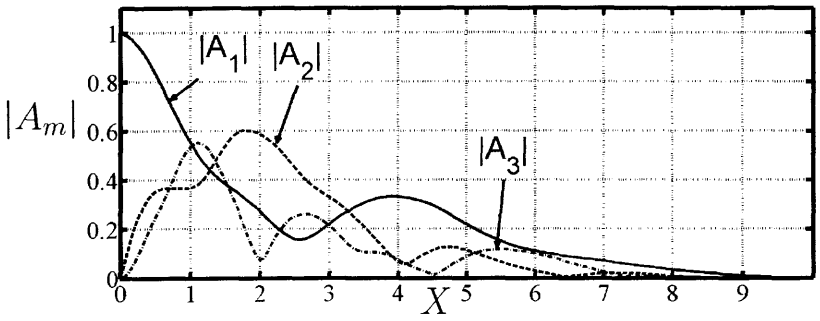

(b) Hangzhou Bay mud, $s = 1/10$

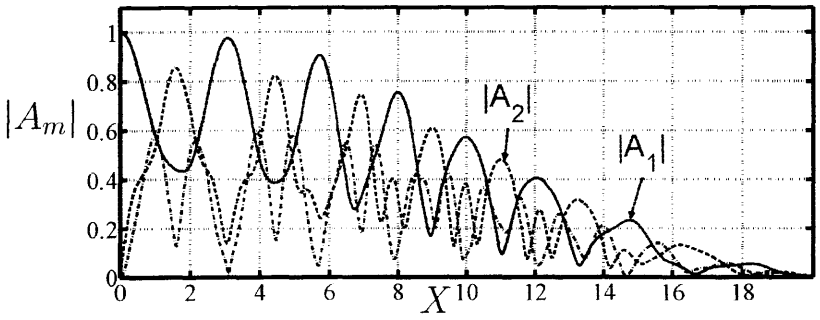

(c) Gulf of Mexico mud, $s = 1/20$

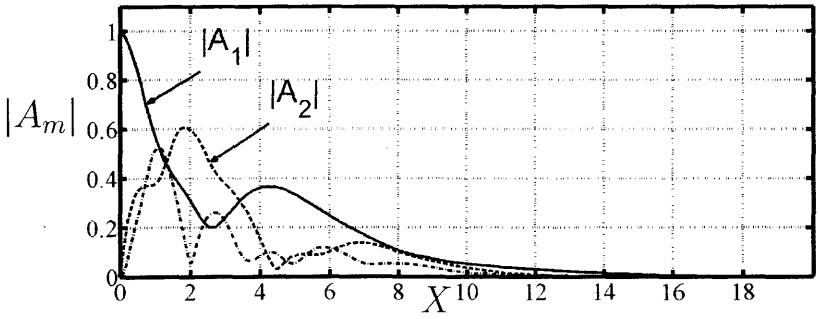

(d) Hangzhou Bay mud, $s = 1/20$

Figure 7-9: Evolution of the first 3 harmonics of the free surface over different types of viscoelastic muddy seabeds, in the cases $s = 1/10$ and $s = 1/20$.

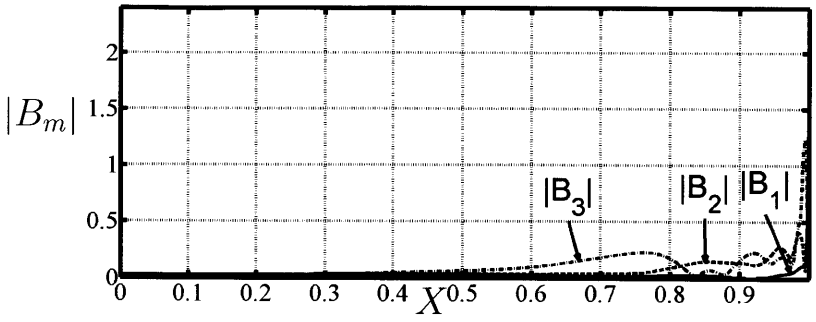

(a) Gulf of Mexico mud, $s = 1$

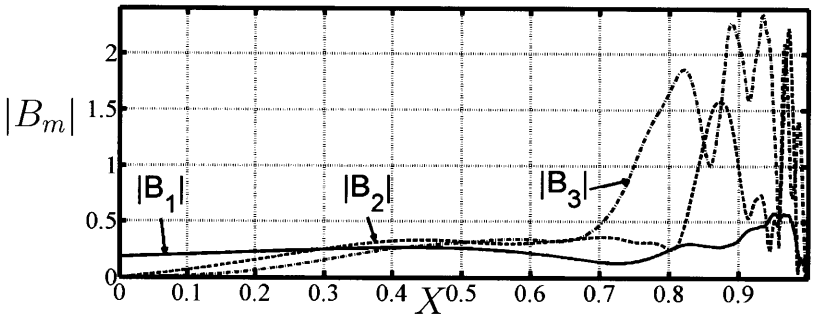

(b) Hangzhou Bay mud, $s = 1$

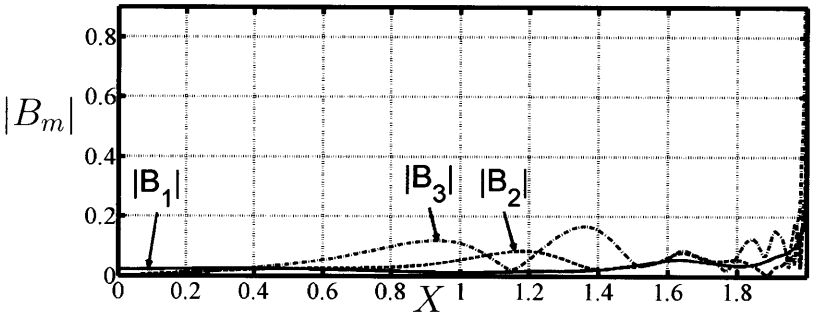

(c) Gulf of Mexico mud, $s = 1/2$

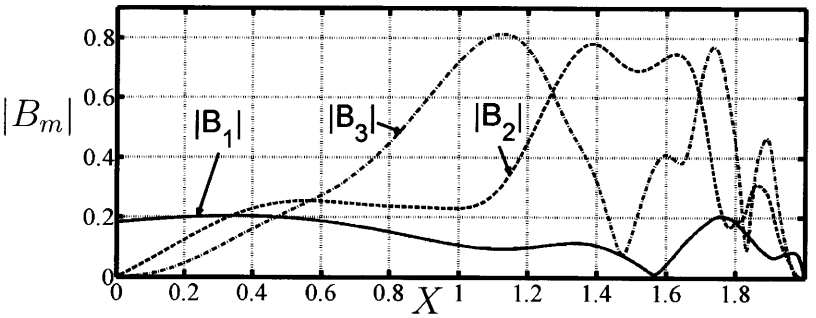

(d) Hangzhou Bay mud, $s = 1/2$

Figure 7-10: Evolution of the first 3 harmonics of the interface between mud and water over different types of viscoelastic muddy seabeds, in the cases $s = 1$ and $s = 1/2$.

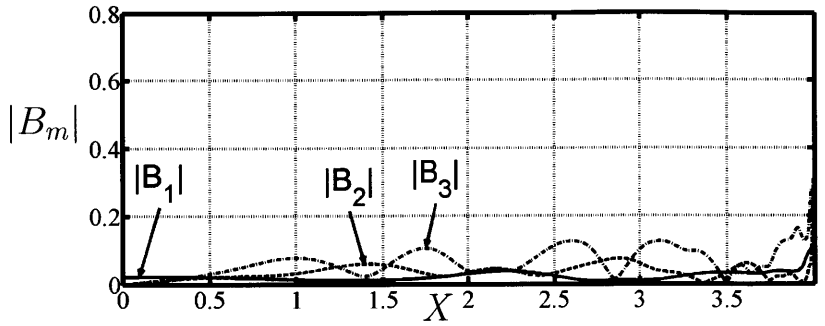

(a) Gulf of Mexico mud, $s = 1/4$

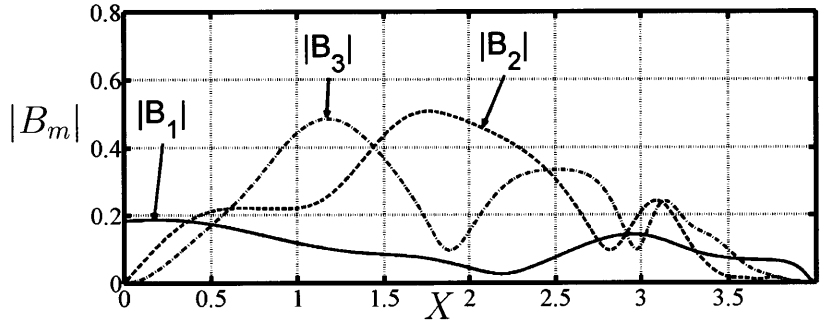

(b) Hangzhou Bay mud, $s = 1/4$

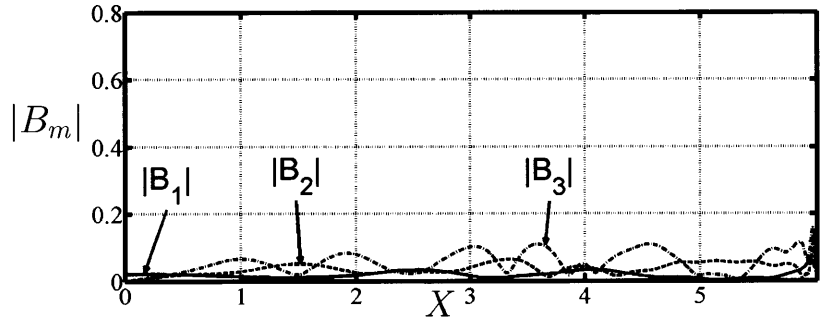

(c) Gulf of Mexico mud, $s = 1/6$

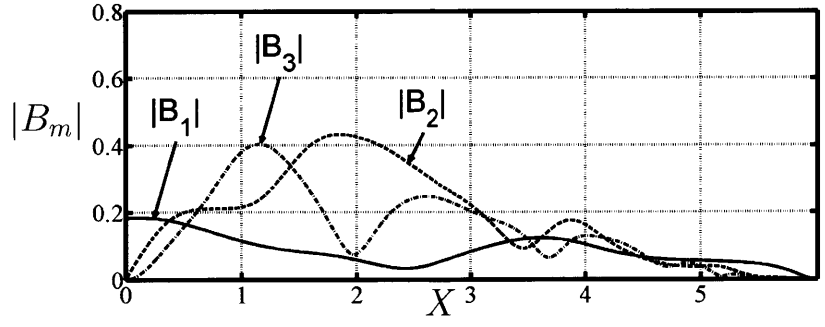

(d) Hangzhou Bay mud, $s = 1/6$

Figure 7-11: Evolution of the first 3 harmonics of the interface between mud and water over different types of viscoelastic muddy seabeds, in the cases $s = 1/4$ and $s = 1/6$.

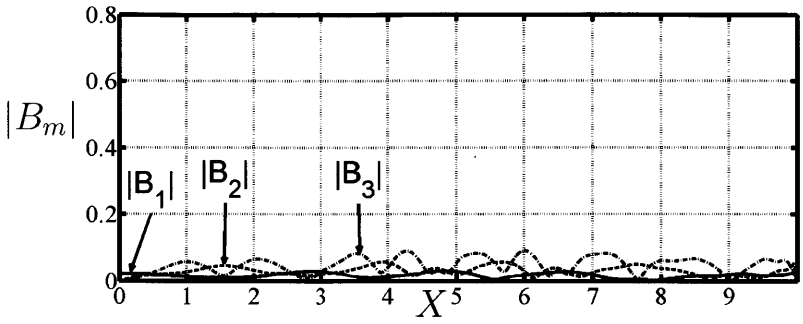

(a) Gulf of Mexico mud, $s = 1/10$

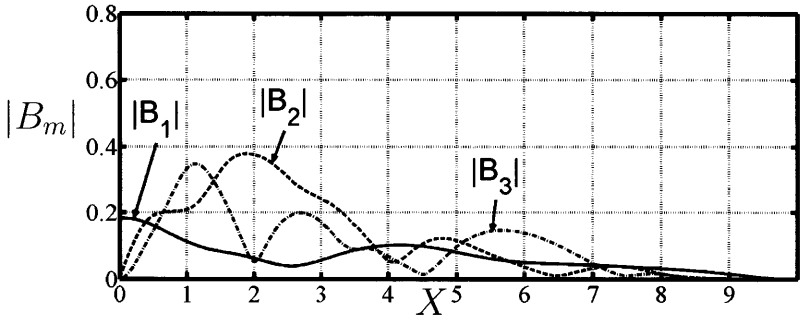

(b) Hangzhou Bay mud, $s = 1/10$

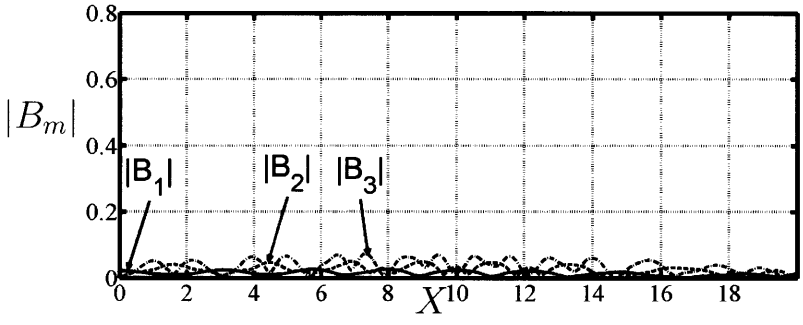

(c) Gulf of Mexico mud, $s = 1/20$

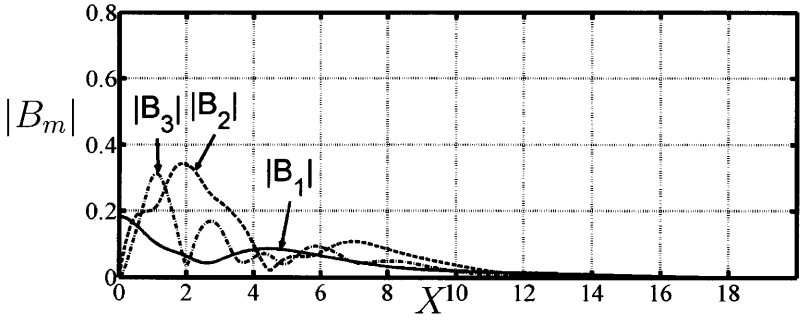

(d) Hangzhou Bay mud, $s = 1/20$

Figure 7-12: Evolution of the first 3 harmonics of the interface between mud and water over different types of viscoelastic muddy seabeds, in the cases $s = 1/10$ and $s = 1/20$.

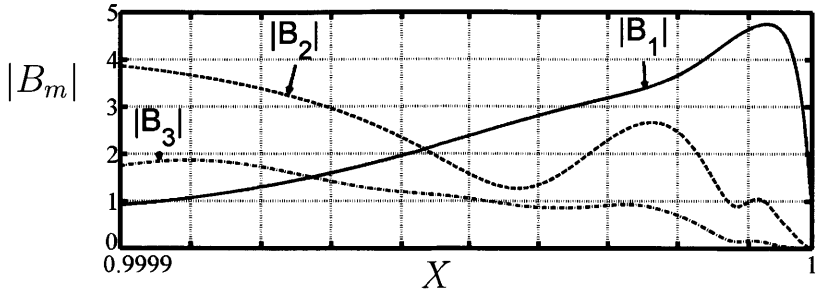

(a) $s = 1$

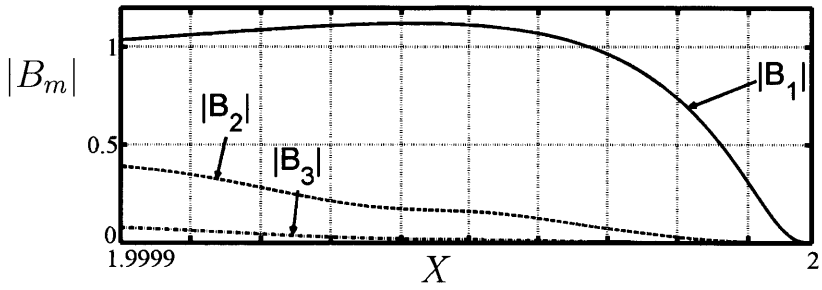

(b) $s = 1/2$

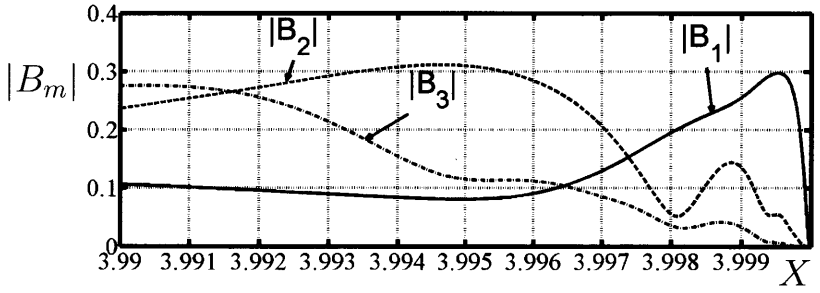

(c) $s = 1/4$

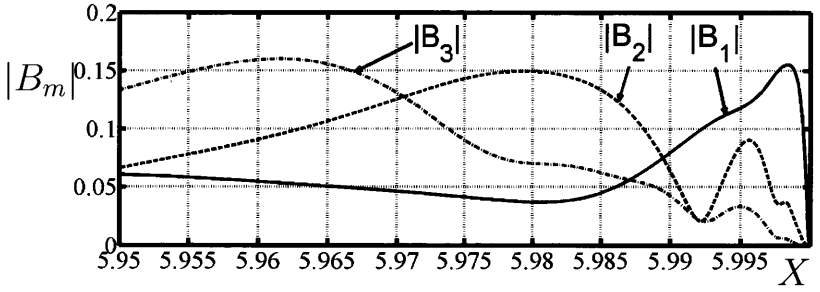

(d) $s = 1/6$

Figure 7-13: Zoom-in of the first 3 harmonics of the interface near the shore with the Gulf of Mexico mud.

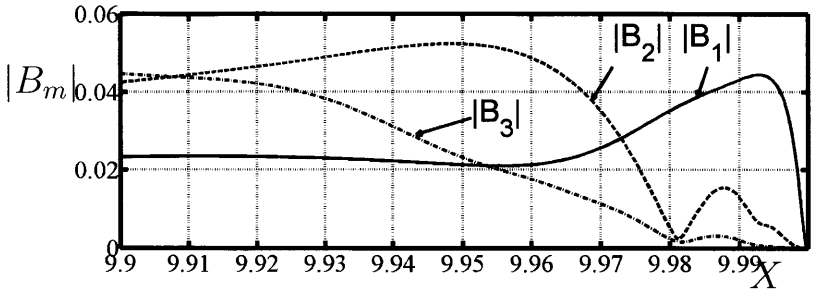

(a) Gulf of Mexico mud, $s = 1/10$

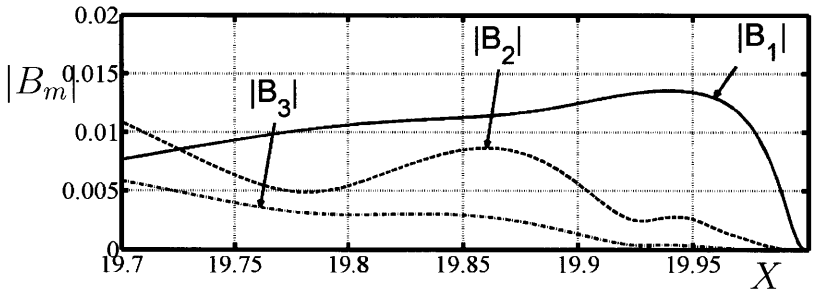

(b) Gulf of Mexico mud, $s = 1/20$

Figure 7-14: Zoom-in of the first 3 harmonics of the interface near the shore with the Gulf of Mexico mud. $s = 1/10$ and $s = 1/20$.

7.7 Sloping bottom without mud

7.7.1 Governing equations

From the study we just led in the particular case of viscoelastic mud, it is very easy to deduce the surface waves behavior in the absence of mud. Indeed, the absence of mud simply means that $B_m = 0$ in equation 7.4.1.13.

As a consequence, the governing equation 7.5.1.1 for the surface waves become $\forall m$:

$$\boxed{\sqrt{h}\frac{dA_m}{dX} + \frac{h_X}{4\sqrt{h}}A_m + \frac{\epsilon}{\kappa^2}\frac{3i}{8h}m\left[\sum_{l=1}^{n-m} 2A_l^* A_{m+1l} + \sum_{l=1}^{[m/2]} \alpha_l A_l A_{m-l}\right] - \frac{im^3}{6}hA_m = 0} \tag{7.7.1.1}$$

Once again, the difference between this equation and the result we obtained in the previous chapter (equation 6.8.1.1), where non-linearity was more important than dispersion is the dispersion term proportional to m^3 that appears here. As we already pointed out, this term did not appear before because dispersion was less important compared to non-linearity.

The same way, the energy variation can be deduced from equation 7.5.2.4, that

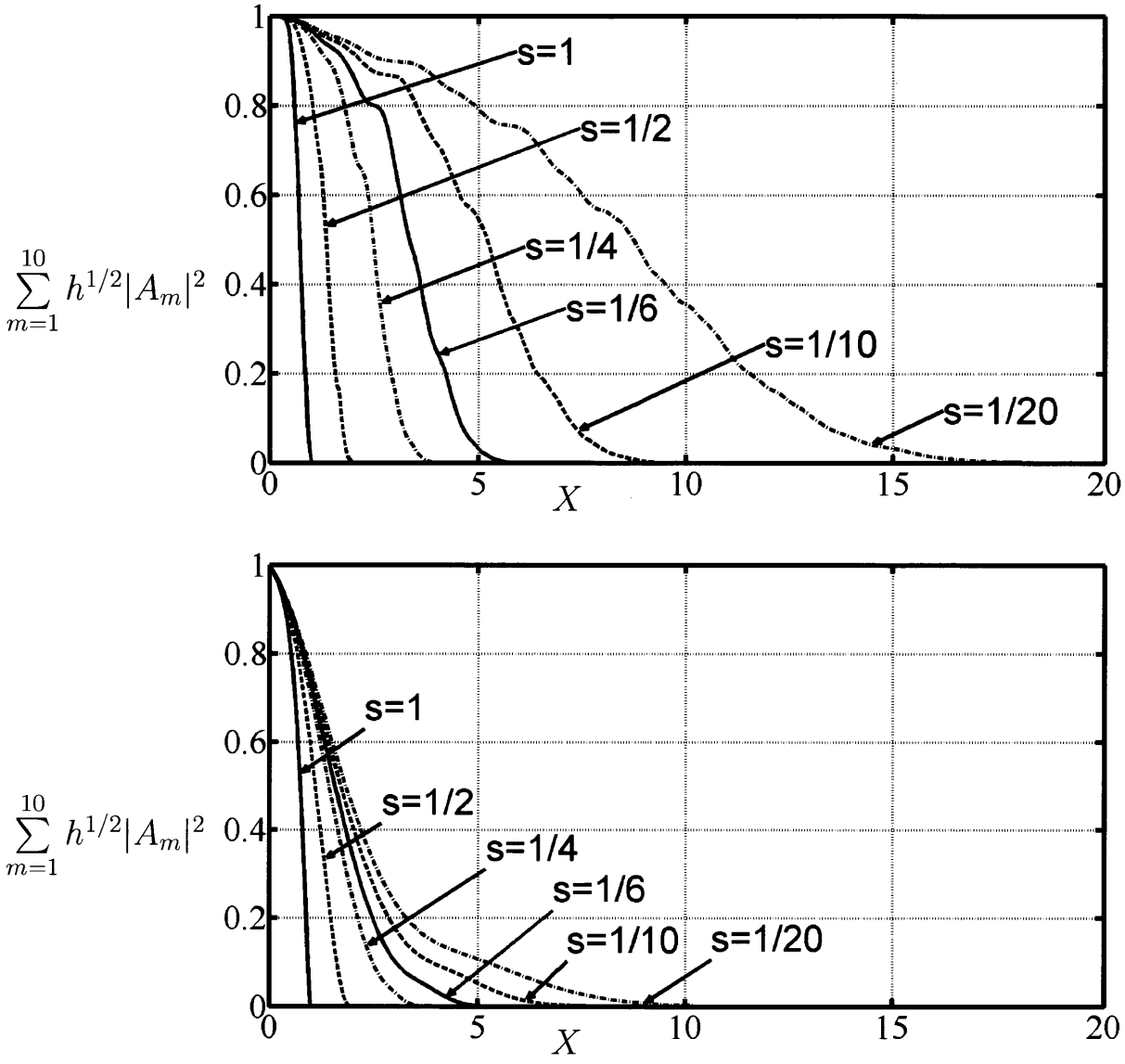

Figure 7-15: Wave energy over a flat thick muddy seabed. Comparison between $s = 1$, $s = 1/2$, $s = 1/4$, $s = 1/6$, $s = 1/10$ and $s = 1/20$.

becomes:

$$\boxed{\frac{d}{dX}\left[\sqrt{h}\sum_{m=1}^{n}|A_m|^2\right]=0} \tag{7.7.1.2}$$

This result looks very logical: in the absence of mud, there is no energy dissipation in water.

7.7.2 Numerical results by using the first ten harmonics

Since we don't consider mud anymore, there are only four parameters remaining: $\bar{h}$, A, ω' and s'. We already studied the influence of dispersion and non-linearity in chapter 5, by playing on the ratio ϵ/κ^2.

Let us now study the influence of different slopes. We look at the slope values $s' = 0.014$, $s' = 0.0035$ and $s' = 0.00069$, respectively corresponding the non-dimensional slope values:

$$\boxed{s=1,\ s=1/4,\ s=1/20} \tag{7.7.2.1}$$

We still have $\bar{h} = 5m$, $T = 18s$ (which means $\omega' = 1/3rad/s$) and $A = 40cm$, corresponding to the parameters values:

$$\boxed{\kappa=0.24,\ \epsilon=0.08} \tag{7.7.2.2}$$

The results are shown in figure 7-16 for the three different slopes. Once again, even though we carried the numerical resolution with ten harmonics, we choose to only display the first three harmonics. As always, even though we carried the numerical resolution with ten harmonics, we only display the first three harmonics.

We observe that these results are significantly different from the results of the previous chapter. This means that the dispersion term in equation 7.7.1.1 actually has an important influence. The harmonics oscillates more widely towards the shore than in figure 6-28.

The main result is that, in the absence of mud, the harmonics keep growing toward an infinite value at the shore. This result is a very well known phenomenon: wave height increases as water depth decreases toward the shore.

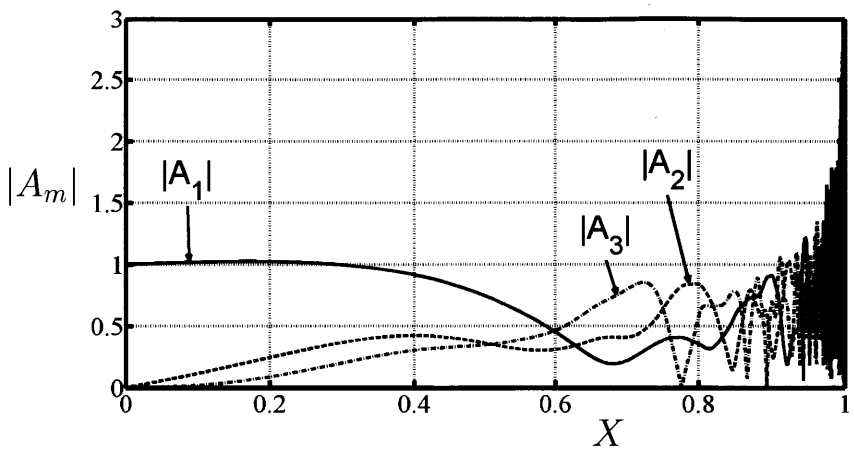

(a) $s = 1$

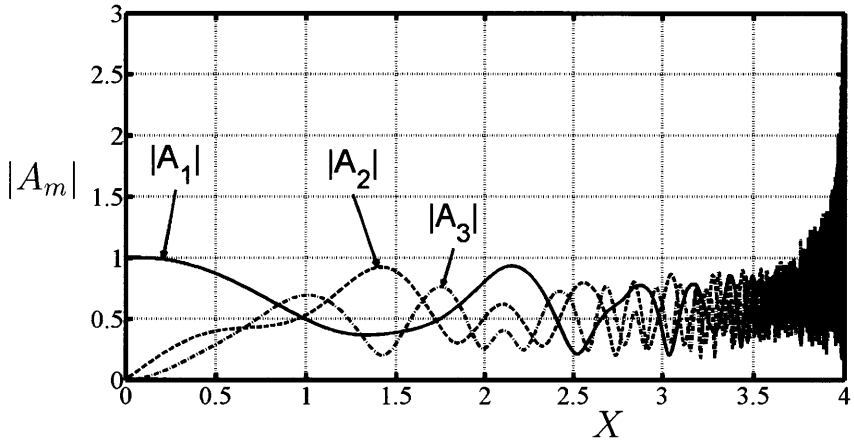

(b) $s = 1/4$

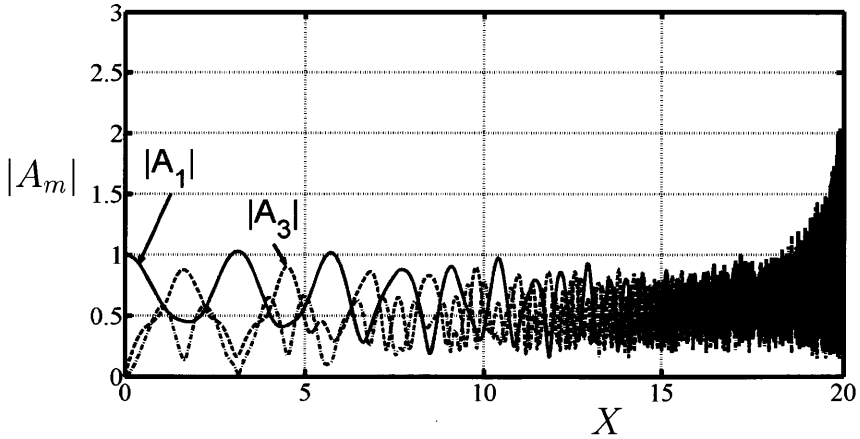

(c) $s = 1/20$

Figure 7-16: Effects of the slope on the evolution of the first 3 harmonics of the free surface on a solid seabed.

Chapter 8

Conclusion

We have first studied the propagation of surface and interface waves in the case of a flat muddy seabed, considering the mud as a Newtonian fluid. Considering that non-linearity is more important than dispersion, and by the method of multiple scales, we have proved the existence of a drift current in mud at the second order. Through numerical simulations, we found that the drift current in mud was the most significant in the case of high non-linearity, high dispersion or thick mud layer. The analytic expression for the evolution of the wave energy allowed us to verify the numerical simulations run for 10 harmonics.

We then studied the same setting with viscoelastic mud instead of Newtonian mud. Governing equations have once again been found for the surface, interface and drift current variations. Four different muds have been studied, some rather elastic and others more viscous. The attenuation rates were plotted as a function of the dispersion for the different muds. We found that the attenuation rates did not have any peak for long waves in the muds where the viscosity modulus was high (Gulf of Mexico, Mobile Bay and Lianyungang). On the other hand, we found that, for given values of the water depth, the attenuation rate had a peak for long waves in the Hangzhou Bay mud, whose viscosity modulus is smaller. We then plotted the surface, interface and drift current variations. We showed that the mud-induced damping was very slow with the Mobile Bay mud, and faster with the three other muds. We showed that the Hangzhou mud had the strongest interface displacement because of its small viscosity modulus and that the drift current was the strongest in the Gulf of Mexico and the Hangzhou Bay muds.

The same pattern has then be followed with a Boussinesq class case (where dispersion is comparable to nonlinearity). We showed that dispersion and non-linearity were now appearing at the same order, allowing to compare both influences. We

observed that mud-induced damping was the most significant in the case of high non-linearity, small dispersion or thick mud layer. We then compared the results between the viscoelastic muds and showed that, with the chosen parameters, the mud-induced damping was the strongest for the Hangzhou Bay mud.

Finally, we studied the effect of a sloping muddy seabed. We demonstrated that, with viscoelastic mud, the static problem only induced a displacement in the mud layer. We demonstrated analytically that all harmonics of the surface, interface and the drift current were decaying exponentially to a zero-value at the shore. Different slope steepnesses were studied. We showed that, if the slope was to steep to allow mud-induced damping before the shore, harmonics were decaying sharply to zero at the end. However, we showed that in the case of gentle slopes and for muds with sufficient attenuation rates, mud-induced damping appeared before the wave could reach the shore. The drift current was plotted for different slope steepnesses, emphasizing the fact that the highest currents are obtained at the shore with steep slopes.

Bibliography

[1] Shibayama T . and An N . N . A visco-elastic-plastic model for wave mud interaction. *Coastal Eng . in Japan*, 36(1):67, 1993.

[2] Ng C. and Zhang X. Mass transport in water waves over a thin layer of soft viscoelastic mud. *Journal of Fluid Mechanics*, 573:105–130, 2007.

[3] Mei C.C. and K.-F. Liu. The attenuation of water waves over a non-rigid bed. *Journal of Fluid Mechanics*, 97:721742, 1980.

[4] Mei C.C. and K.-F. Liu. A bingham-plastic model for a muddy seabed under long waves. *J. Geophys. Res.*, 92:14581–14594, 1987.

[5] I-Chi CHAN and Philip L.-F. LIU. Responses of bingham-plastic muddy seabed to a surface solitary wave. *Journal of Fluid Mechanics*, 618:155–180, 2009.

[6] Michael Stiassnie Chiang C. Mei and Dick K.-P. Yue. *Theory and Applications of ocean surface waves.* World Scientific, 2005.

[7] R.A. Dalrymple and P. L.-F. Liu. Water waves over soft muds: a two-layer fluid model. *J. Phys. Ocean.*, 8:1121–1131, 1978.

[8] Geraldine L. Grataloup and Chiang C. Mei. Localization of harmonics generated in nonlinear shallow water waves. *Physical review*, 68, 2003.

[9] Garcia M. H. Huang X. A herschel-bulkley model for mud flow down a slope. *J. Fluid Mech.*, 374:305–333, 1998.

[10] O. D. Huhe and Huang. An experimental study of fluid mud rheology - mud properties in hangchow bay navigation channel. part ii. *Institute of Mechanics Report*, pages 34–56, 1994.

[11] Feng Jiang and Ashish J. Mehta. Mudbanks of the southwest coast of india iv: Mud viscoelastic properties. *Journal of Coastal research*, 11:918–926, 1995.

[12] Krotov. Water Waves Over a Muddy Seabed. Massachusetts Institute of Technology thesis, 2008.

[13] Jiang L. and Leblond P.H. Numerical modeling of an underwater bingham plastic which it generates. *J Geophys Res*, 98(C6):10303–10317, 1993.

[14] Philip L.-F. Liu and I-Chi Chan. On long-wave propagation over a fluid-mud seabed. *Journal of Fluid Mechanics*, 579:467–480, 2006.

[15] Chiang C. Mei, Mikhael Krotov, Zhenhua Huang, and Huhe Aode. Short and long waves over a muddy seabed. *Journal of Fluid Mechanics*, 643:33–58, 2009.

[16] D.H. Peregrine. Equations for water waves and the approximations behind them. *Waves on Beaches and Resulting Sediment Transport*, page 95122, 1972.

[17] Okuno M. Shibayama T. and Sato S. Mud transport rate in mud layer due to wave action. *Proceedings of the 22nd Conference on Coastal Engineering*, page 30373048, 1990.

[18] Shibayama T. Soltanpour M. and Noma T. Cross-shore mud transport and beach deformation model. *Coastal Engineering Journal*, 45(3):363387, 2003.

[19] Sakakiyama T. and Bijker E.W. Mass transport velocity in mud layer due to progressive waves. *Journal of Waterway, Port, Coastal and Ocean Engineering*, 115:614–633, 1989.

[20] H. Sellmeigher T. Yamamoto, H.L. Koning and E.V. Hijum. On the response of a poro-elastic bed to water waves. *J. Fluid Mech.*, 87:193–206, 1978.

[21] J. Wen and P.L.-F. Liu. Effects of seafloor conditions on water wave damping. *Free-Surface Flows with Viscosity*, 1998.